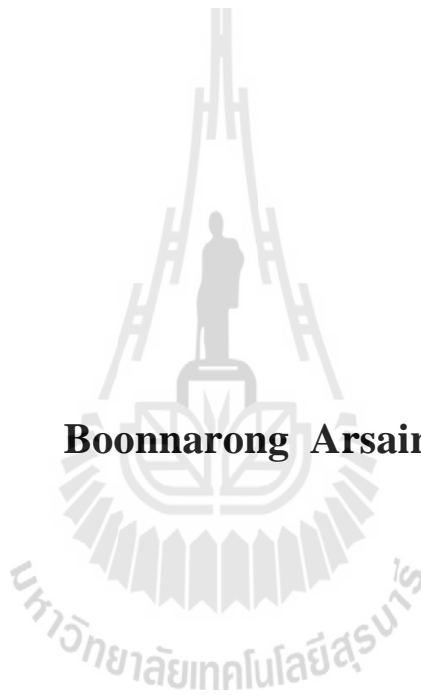


**DEPOSITIONAL ENVIRONMENT AND PETROLEUM
SOURCE ROCK POTENTIAL OF THE LATE
TRIASSIC HUAI HIN LAT FORMATION,
NORTHEASTERN THAILAND**

Boonnarong Arsairai



**A Thesis Submitted in Partial Fulfillment of the Requirements for the
Degree of Doctor of Engineering in Geotechnology**

Suranaree University of Technology

Academic Year 2014

สภาพแวดล้อมการสะสมตัวและศักยภาพการเป็นหินต้นกำเนิดปิโตรเลียมของ
หมวดหินห้วยหินลาดยุคไทรแอสซิกตอนปลาย
ภาคตะวันออกเฉียงเหนือ ประเทศไทย



นายบุญณรงค์ อาศัยไร่

วิทยานิพนธ์นี้เป็นส่วนหนึ่งของการศึกษาตามหลักสูตรปริญญาวิศวกรรมศาสตรดุษฎีบัณฑิต

สาขาวิชาเทคโนโลยีธรณี

มหาวิทยาลัยเทคโนโลยีสุรนารี

ปีการศึกษา 2557

**DEPOSITIONAL ENVIRONMENT AND PETROLEUM SOURCE
ROCK POTENTIAL OF THE LATE TRIASSIC HUAI HIN LAT
FORMATION, NORTHEASTERN THAILAND**

Suranaree University of Technology has approved this thesis submitted in partial fulfillment of the requirements for the Degree of Doctor of Philosophy.

Thesis Examining Committee

(Prof. Dr. Kittitep Fuenkajorn)

Chairperson

(Asst. Prof. Dr. Akkhapun Wannakomol)

Member (Thesis Advisor)

(Dr. Chongpan Chonglakmani)

Member

(Assoc. Prof. Dr. Benjavun Ratanasthien)

Member

(Dr. Assanee Meesook)

Member

(Dr. Kruawun Jankaew)

Member

(Prof. Dr. Sukit Limpijumnong)

Vice Rector for Academic Affairs
and Innovation

(Assoc. Prof. Flt. Lt. Dr. Kontorn Chamniprasart)

Dean of Institute of Engineering

บุญณรงค์ อาศัยไร่ : สภาพแวดล้อมการสะสมตัวและศักยภาพการเป็นหินต้นกำเนิด
ปิโตรเลียมของหมวดหินห้วยหินลาดยุคไทรแอสซิกตอนปลาย ภาคตะวันออกเฉียงเหนือ
ประเทศไทย (DEPOSITIONAL ENVIRONMENT AND PETROLEUM SOURCE
ROCK POTENTIAL OF THE LATE TRIASSIC HUAI HIN LAT FORMATION,
NORTHEASTERN THAILAND) อาจารย์ที่ปรึกษา : ผู้ช่วยศาสตราจารย์ ดร.อัมพรศักดิ์
วรรณโกมล, 311 หน้า.

หินดินดานที่อุดมด้วยสารอินทรีย์ของหมวดหินห้วยหินลาดในแอ่งชับลพ (ภาคตัดบ้าน
หนองไทร) และแอ่งนาพอสอง (ภาคตัดตาดใหญ่) ได้ถูกเลือกเพื่อทำการศึกษาเชิงรายละเอียด
เกี่ยวกับสภาพแวดล้อมการสะสมตัวและศักยภาพด้านปิโตรเลียม เนื่องด้วยมีการเปิดเผยที่ดิของหิน
ต้นกำเนิดปิโตรเลียม การวิเคราะห์ธรณีเคมีและการวิเคราะห์สัณฐานวิทยาของหินตัวอย่างได้ถูก
ดำเนินการเพื่อใช้ในการประเมินคุณสมบัติของหินต้นกำเนิดปิโตรเลียมและหินกักเก็บปิโตรเลียม

จากผลการศึกษาของการผลิตในอดีตและสภาวะรีดอกซ์ในอดีต ชนิดของสารอินทรีย์
ความสมบูรณ์และคุณภาพของสารอินทรีย์ ภาวะได้ที่ของหินต้นกำเนิดปิโตรเลียมและสาร
ไฮโดรคาร์บอนที่เกิดขึ้น ได้ใช้เพื่อการประเมินศักยภาพของหินต้นกำเนิดปิโตรเลียม ซึ่งการผลิตใน
อดีตสามารถจำแนกได้จากค่าตัวแปรของ AOM, acritarchs, phytoclasts, TOC, excess SiO₂, Ba/Al
และ P/Al โดยจะแสดงค่าสูงในชั้น 1, 7, 9, 10, 13, 15-16 และ 19 (ภาคตัดบ้านหนองไทร) และชั้น
1, 3, 9, 12, 14, 16, 17, 22, 27, 30 และ 32 (ภาคตัดตาดใหญ่) ซึ่งแสดงถึงการผลิตในอดีตแบบขั้นสูง
โดยชั้นที่ 3 และชั้นที่วางตัวอยู่ล่างของชั้น 13 (ภาคตัดบ้านหนองไทร) และชั้นที่ 18 (ภาคตัดตาด
ใหญ่) จะแสดงการผลิตในอดีตแบบขั้นต่ำ แต่ปริมาณคาร์บอนอินทรีย์ทั้งหมดสูง ซึ่งแสดงถึง
สภาวะการเก็บรักษาสารอินทรีย์ที่ดี สภาวะรีดอกซ์ในอดีตสามารถจำแนกได้จากค่าของ Ni/Co,
U/Th, V/Cr, V/(V+Ni), Ni/V, (Cu+Mo)/Zn และ Ce anomaly โดยค่าสูงของทั้งสองภาคตัดจะแสดง
ถึงสภาวะรีดอกซ์ขั้นสูง โดยภาคตัดบ้านหนองไทรจะมีลำดับชั้นที่ต่ำกว่าเล็กน้อย ส่วนหินดินดาน
ของภาคตัดบ้านหนองไทรและภาคตัดตาดใหญ่จะแสดงค่าปริมาณคาร์บอนอินทรีย์ทั้งหมดจาก 1.9-
7.1 % และ 4.7-10.1 % ซึ่งแสดงถึงเป็นหินต้นกำเนิดปิโตรเลียมชนิดยอดเยี่ยม จากผลการวิเคราะห์
ชนิดของมาซีรอลของภาคตัดทั้งสองจะแสดงถึงคีโรเจนชนิดที่หนึ่งเป็นส่วนใหญ่ จากค่า R₀ และ
T_{max} ของภาคตัดบ้านหนองไทร คือ 0.91 %R₀ และ 445.7 °C และภาคตัดตาดใหญ่ คือ 1.71 %R₀
และ 602.8 °C ซึ่งสามารถประเมินค่าได้ระดับขั้นภาวะได้ที่สูงสุดและภาวะหลังการได้ที่ โดย
สอดคล้องกับค่าดัชนีการเปลี่ยนแปลงที่แสดงค่าจาก 69.0-99.6 % และ 99.8-99.9 % ซึ่งผลจะแสดง
ถึงก๊าซขึ้นและก๊าซแห้งจะกำเนิดมาจากภาคตัดบ้านหนองไทรและก๊าซแห้งเป็นส่วนใหญ่จะมาจาก

ภาคตัดตาดใหญ่ โดยปริมาณคาร์บอนอินทรีย์ดั้งเดิมจะมีค่าจาก 5.1-10.7 % และ 7.8-14.9 % ของภาคตัดบ้านหนองไทรและภาคตัดตาดใหญ่ตามลำดับ โดยสารไฮโดรคาร์บอนที่เกิดขึ้นทั้งหมดของทั้งสองภาคตัด คือ 16,914.4 mcf/ac-ft ดังนั้นภาคตัดทั้งสองของหมวดหินห้วยหินลาดจึงมีศักยภาพสูงที่จะให้กำเนิดก๊าซสำหรับการสะสมตัวในแอ่งโคราช

หมวดหินห้วยหินลาดมีศักยภาพสูงสำหรับเป็นแหล่งก๊าซธรรมชาติในชั้นหินดินดาน โดยมีการศึกษาแร่ประกอบหินกักเก็บก๊าซธรรมชาติและแหล่งเก็บรักษาก๊าซธรรมชาติ เพื่อใช้ในการประเมินคุณสมบัติของหินดินดานสำหรับเป็นหินกักเก็บก๊าซธรรมชาติ ซึ่งปริมาณของแร่เปราะและแร่ดินเหนียวจะมีค่าโดยเฉลี่ย 45.9 % และ 42.6 % (ภาคตัดบ้านหนองไทร) และ 50.7 % และ 23.6 % (ภาคตัดบ้านตาดใหญ่) โดยภาคตัดทั้งสองจะมีศักยภาพเป็นแหล่งเก็บก๊าซธรรมชาติโดยตัวของมันเองภายใต้สภาวะการฝังตัวที่เหมาะสม ส่วนช่องว่างขนาดไมโครเมตรเป็นลักษณะที่ดีสำหรับเป็นความสามารถในการจัดเก็บและเป็นเส้นทางสำหรับการซึมผ่านของก๊าซธรรมชาติ ซึ่งความพรุนสูงของหินดินดานที่เป็นสาเหตุมาจากช่องว่างขนาดไมโครเมตรจะแสดงค่าจาก 6.7-6.9 % (ภาคตัดบ้านหนองไทร) และ 8.6-14.7 % (ภาคตัดตาดใหญ่) เมื่อก้าวถึงการประเมินความเสี่ยงของก๊าซธรรมชาติในชั้นหินดินดานแบบไม่ปกติ จะพบว่าค่าดัชนีการผลิตของภาคตัดทั้งสองจะแสดงค่าที่ต่ำกว่าค่าเกณฑ์ความเสี่ยงที่ดีสำหรับแหล่งก๊าซธรรมชาติในชั้นหินดินดาน

สาขาวิชา เทคโนโลยีธรณี

ปีการศึกษา 2557

ลายมือชื่อนักศึกษา _____

ลายมือชื่ออาจารย์ที่ปรึกษา _____

ลายมือชื่ออาจารย์ที่ปรึกษาร่วม _____

BOONNARONG ARSAIRAI : DEPOSITIONAL ENVIRONMENT AND
PETROLEUM SOURCE ROCK POTENTIAL OF THE LATE TRIASSIC
HUI HIN LAT FORMATION, NORTHEASTERN THAILAND.

THESIS ADVISOR : ASST. PROF. AKKHAPUN WANNAKOMOL, Ph.D.,
311 PP.

SAP PHLU BASIN/NA PHO SONG BASIN/PALAEOPRODUCTIVITY/
PALAEOREDOX CONDITION/SHALE GAS/MATURITY/RESERVOIR

The organic rich shales of the Huai Hin Lat Formation in the Sap Phlu (Ban Nong Sai section) and Na Pho Song Basins (Dat Yai section) are selected for detailed study in term of depositional environment and petroleum potential due to good exposures of source rock. Geochemical and petrographic analyses of rock samples are carried out for evaluation of petroleum source rock and reservoir rock properties.

The results of palaeoproductivity and palaeoredox condition, organic matter type, organic richness and quality, thermal maturity, and generated hydrocarbon studies are used for evaluation of source rock potential. The palaeoproductivity can be distinguished by values of AOM, acritarchs, phytoclasts, TOC, excess SiO₂, Ba/Al, and P/Al proxies. They are high in Beds 1, 7, 9, 10, 13, 15-16, and 19 (Ban Nong Sai section) and Beds 1, 3, 9, 12, 14, 16, 17, 22, 27, 30, and 32 (Dat Yai section) which indicate a high palaeoproductivity. The Bed 3 and lower Bed 13 (Ban Nong Sai section) and Bed 18 (Dat Yai section) are low palaeoproductivity but high in TOC indicating a high preservation. The palaeoredox condition is distinguished by values of Ni/Co, U/Th, V/Cr, V/(V+Ni), Ni/V, (Cu+Mo)/Zn, and Ce anomaly. High values of both sections indicate a high reducing condition, although the Ban Nong Sai section is slightly lower. The shales of the Ban Nong Sai and Dat Yai sections show

TOC values ranging from 1.9-7.1 % and 4.7-10.1 % which indicate an excellent source rock. The analyzed result of maceral type of both sections shows that they belong mainly to Type I kerogen. R_o and T_{max} values of the Ban Nong Sai section are 0.91 % R_o and 445.7 °C and the Dat Yai section are 1.71 % R_o and 602.8 °C. They indicate the peak mature and the postmature levels of thermal maturity which are conformable to the transformation ratios of 69.0-99.6 % and 99.8-99.9 %. The result shows that wet and dry gases were generated from the Ban Nong Sai section and mainly dry gases from the Dat Yai section. TOC_o values range from 5.1-10.7 % and 7.8-14.9 % for the Ban Nong Sai and Dat Yai sections respectively. The total generated hydrocarbon of both sections is 16,914.4 mcf/ac-ft. Therefore, both sections of the Huai Hin Lat Formation are high potential to generate gas for accumulation in the Khorat Basin.

The Huai Hin Lat Formation is evaluated for potential of shale gas resource. The study of reservoir-forming minerals and hydrocarbon storages are used for evaluation the property of shale for reservoir rocks. The average content of brittle and clay minerals are 45.9 % and 42.6 % (Ban Nong Sai section) and 50.7% and 23.6 % (Dat Yai section). Both sections have the potential to host gas under proper burial condition. The micropore types are good for both storage capacities and permeability pathways of gases. The high porosity of shales estimated from micropores ranges from 6.7-6.9 % (Ban Nong Sai section) and 8.6-14.7 % (Dat Yai section). According to risk evaluation of unconventional shale gas, the production index of both sections shows lower value than the good risk criteria for shale gas resource.

School of Geotechnology

Academic Year 2014

Student's Signature _____

Advisor's Signature _____

Co-Advisor's Signature _____

ACKNOWLEDGEMENTS

I would like to express my sincere appreciation to everyone who involved with this thesis.

First and foremost, I would like to express my gratitude to all those who gave me the possibility to complete this thesis. With a deep sense of gratitude, I wish to express my sincere thanks to my supervisors Dr. Chongpan Chonglakmani (SUT), Prof. Dr. Feng Qinglai (CUG), and Asst. Prof. Dr. Akkhapun Wannakomol (SUT) for their immense help in planning and executing the works.

Special thanks to Dr. Chongpan Chonglakmani and Asst. Prof. Dr. Akkhapun Wannakomol who encouraged me to learn geology and provided me the opportunity for work and study on an integrated multidisciplinary topic in geosciences. This includes five years for field works in Thailand and visits various schools of geosciences in China.

I express my indebtedness to Prof. Dr. Feng Qinglai who advised and stimulated me on petroleum, element, and petrographic laboratories and supported me during my stay in China. He conducted me this thesis under his supervision with was a great pleasure. The special field works and journeys in China also let me got the valuable experiences.

The thesis would not be completed without the mentions and comments of my thesis committee Prof. Dr. Kittitep Fuenkajorn from the school of Geotechnology, Institute of Engineering, Suranaree University of Technology, Assoc. Prof. Dr. Benjavun Ratanasthien from the department of Geological Sciences, faculty of

Chiang Mai University, Dr. Assanee Meesook is a former geologist from the department of Mineral Resources, and Dr. Kruawun Jankaew from the department of Geology, faculty of Science, Chulalongkorn University. They advised me immensely by giving me encouragement and would also like to gratefully acknowledge the support of some very special individuals.

Special thanks are for three scholarships supported and granted by the Royal Golden Jubilee (RGJ) No. PHD/0155/2551, the National Natural Science Foundation of China (NSFC) project No. 41172202, and the China Geological Survey Program (No. 1212011121256) of China University of Geosciences (Wuhan), which have made my stay, study, and research in China possible.

Many thanks are conveyed to the officials at the State Key Laboratory of Geological Processes and Mineral Resources and State Key Laboratory of Biology and Environmental Geology, China University of Geosciences, Wuhan and are also conveyed to Miss Hathaichanok Vattanasak, Mr. Pradit Nulay, Miss Krongkaew Jenchitpibul, Mr. Peerawat Kongurai, Miss Namporn Wattanaton, Mr. Warut Sirichoat, and Mr. Pornchai Kamhom who assisted me on field works.

Finally, I am grateful to thank my parent as my first teacher and rendered me enormous supports during my research.

Boonnarong Arsairai

TABLE OF CONTENTS

	Page
ABSTRACT (THAI)	I
ABSTRACT (ENGLISH)	III
ACKNOWLEDGEMENTS	V
TABLE OF CONTENTS	VII
LIST OF TABLES	XV
LIST OF FIGURES	XIX
CHAPTER	
I INTRODUCTION	1
1.1 Petroleum exploration in the Khorat Plateau of NE Thailand ...	1
1.2 Petroleum system of NE Thailand	3
1.2.1 Source rocks	4
1.2.2 Reservoir rocks	5
1.2.3 Seal	6
1.2.4 Maturation	6
1.3 Natural gas	7
1.3.1 Conventional natural gas	8
1.3.2 Unconventional natural gas	9
1.3.2.1 Unconventional shale gas	11

TABLE OF CONTENTS (Continued)

	Page
1.3.2.2 Shale gas in the United States	13
1.3.2.3 Shale gas in Thailand	14
1.4 Research objectives.....	15
1.5 Scope and limitations of the study	15
1.5.1 Outcrop study	16
1.5.2 Laboratory study.....	16
1.6 Research methodology.....	17
II LITERATURE REVIEW	19
2.1 Geologic setting of Thailand.....	19
2.2 Geologic setting of NE Thailand	25
2.2.1 Na Mo and Pak Chom Group	26
2.2.2 Mid-Carboniferous event	26
2.2.3 Saraburi Group in Middle Carboniferous- Upper Permian.....	26
2.2.4 Indosinian I Event	28
2.2.5 Huai Hin Lat Formation (Kuchinarai Group).....	28
2.2.6 Indosinian II Event (Latest Triassic)	29
2.2.7 Khorat Basin.....	29
2.2.8 Middle Cretaceous Event	32
2.2.9 Maha Sarakham Formation	32

TABLE OF CONTENTS (Continued)

	Page
2.2.10 Phu Tok Formation.....	33
2.2.11 Tertiary uplift and folding	33
2.3 Geologic setting of the Huai Hin Lat Formation	33
III METHODOLOGY	39
3.1 Fieldwork for measured stratigraphic sections	39
3.2 Microfossil extraction	43
3.2.1 Microfossil extraction processes	43
3.2.2 Configured solution preparations	44
3.3 Geochemical analysis.....	45
3.3.1 Elemental analysis.....	46
3.3.1.1 Major elements	47
3.3.1.2 Trace elements and rare earth elements.....	48
3.3.2 Mineralogical analysis.....	50
3.3.3 Hydrocarbon analysis	53
3.3.3.1 Total organic carbon (TOC).....	53
3.3.3.2 Vitrinite reflectance (R_o).....	56
3.3.3.3 Rock-Eval pyrolysis.....	59
3.4 Physical property analysis.....	62
3.4.1 Scanning Electron Microscope (SEM).....	62
3.4.2 Micro computed tomography (Micro-CT)	65

TABLE OF CONTENTS (Continued)

	Page
3.5 Visual petrographic analysis for kerogen types.....	67
IV STRATIGRAPHIC RESULTS.....	68
4.1 Measured stratigraphic sections.....	68
4.1.1 Sap Phlu Basin area.....	68
4.1.1.1 Ban Nong Sai section.....	68
4.1.1.2 Southern Sap Phlu section	74
4.1.1.3 Northern Sap Pulu section	78
4.1.1.4 Khao E-Dang section and Wat Tham Nong Sai section	82
4.1.2 Na Pho Song Basin area	87
4.1.2.1 Sila section.....	87
4.1.2.2 Dat Syo section	92
4.1.2.3 Dat Kloi Nuea section.....	96
4.1.2.4 Lak Dan section	99
4.1.2.5 Sarn Chaopoh Hin Tang section	102
4.1.2.6 Dat Yai section.....	109
4.1.2.7 Ban Huai Sai Thong section	113
4.2 Establish sequence for source rock evaluation	117
4.2.1 Stratigraphic correlation.....	117
4.2.1.1 Correlation of the Sap Phlu Basin.....	120

TABLE OF CONTENTS (Continued)

	Page
4.2.1.2	Correlation of the Na Pho Song Basin.....123
4.2.2	Selected sections for source rock evaluation.....126
V	PETROGRAPHIC AND GEOCHEMICAL RESULTS127
5.1	Palaeoproductivity and palaeoredox analysis127
5.1.1	Palaeoproductivity and palaeoredox proxies.....127
5.1.1.1	Palaeoproductivity proxies127
5.1.1.2	Palaeoredox proxies132
5.1.2	Palaeoproductivity and palaeoredox analysis.....135
5.1.2.1	Evaluation of the Ban Nong Sai Section (Sap Phlu Basin).....135
5.1.2.1.1	Petrographic analysis135
5.1.2.1.2	Geochemical analysis.....140
5.1.2.2	Evaluation of the Dat Yai section (Na Pho Song Basin)148
5.1.2.2.1	Petrographic analysis 148
5.1.2.2.2	Geochemical analysis 152
5.1.3	Palynofacies analysis159
5.2	Hydrocarbon analysis.....162
5.2.1	Source rock analysis.....162
5.2.1.1	Visual petrographic analysis.....162

TABLE OF CONTENTS (Continued)

	Page
6.1.1.2 Palaeoredox conditions.....	210
6.1.2 Palaeodepositional model.....	213
6.1.3 Organic matter quality of kerogen types	215
6.1.4 Organic matter quantity and quality	225
6.1.4.1 Present-day total organic carbon	226
6.1.4.2 Original total organic carbon.....	227
6.1.5 Thermal maturity	235
6.1.5.1 Vitrinite reflectance (R_o)	236
6.1.5.2 Maximum temperature (T_{max}).....	238
6.1.5.3 Production index (PI)	239
6.1.5.4 Kerogen transformation ratio (TR).....	239
6.1.6 Volume of generated hydrocarbon in source rocks	246
6.1.7 Evaluation of conventional gas potential	249
6.2 Shale gas evaluation.....	250
6.2.1 Risk evaluation of source rock data	251
6.2.2 Reservoir-forming minerals	254
6.2.3 Hydrocarbon storages.....	258
6.2.3.1 Micropores.....	258
6.2.3.2 Porosity network and distribution	260

TABLE OF CONTENTS (Continued)

	Page
6.2.4 Risk evaluation of reservoir condition data.....	262
6.2.5 Zone of shale gas accumulation	267
6.2.6 Evaluation of unconventional shale gas potential	268
VII CONCLUSIONS AND RECOMMENDATIONS	271
7.1 Conclusions.....	271
7.2 Recommendations.....	273
REFERENCES	274
BIOGRAPHY	311

LIST OF FIGURES

Figure	Page
1.1 The natural gas production by source (tcf/year) (EIA, 2008)	10
1.2 The United States unconventional gas outlook (bcf/day) (American Clean Skies, 2008)	11
1.3 Map showing the studied areas	18
2.1 Principal structure elements of Thailand including the two principal blocks or terranes which comprised the country (Ridd et al., 2011)	21
2.2 Sections across Northern and NE Thailand showing the narrowing of Palaetethys Ocean in the earliest Triassic and the final collision of the Sibumasu block with the Sukhothai Arc and Indochina block in the Late Triassic (Sone and Metcalfe, 2008; Ridd et al., 2011)	25
2.3 Evolution of the Huai Hin Lat Formation in northeastern Thailand (Cooper et al., 1989)	35
2.4 Isochronopatch of the Huai Hin Lat Formation or the Kuchinarai Group showing distribution of the major half-graben basins (Booth and Sattayarak, 2011)	37
3.1 Flow chart showing the methods of study for shale gas evaluation on the Ban Nong Sai and Dat Yai sections of the Huai Hin Lat Formation	41

LIST OF FIGURES (Continued)

Figure	Page
3.2 Examples of the relationship of the true and apparent thicknesses of stratigraphic units (Lewis and McConchie, 1937).....	42
3.3 Leica DM550 B microscope is using for microfossil identification.....	45
3.4 XRF-1800 based on wavelength-dispersive X-ray fluorescence (XRF) analysis for measured element abundances on fused glass beads.....	48
3.5 X’Pert PRO Dy 2198 basis on X-ray diffraction analysis for measurement the mineral results.....	52
3.6 Liqui TOC instrument based on thermal inductivity method for TOC identification	55
3.7 Reflectance microscope and the description of its implements to identify the vitrinite reflectance of rock samples (Matchette-Downes, 2009)	58
3.8 General diagram showing the different fractions of the total organic matter of analyzed rocks, the corresponding parameters and their recordings (after Tissot and Welte, 1978; Khashayar, 2010)	61
3.9 Quanta 200 is using for identification the microscopic images.....	64
3.10 Micro-CT (micro computed tomography) Skyscan 1172 is applied for performance of closed and open porosities.....	66

LIST OF FIGURES (Continued)

Figure	Page
4.1 The locations of the studied sections in the area of the Sup Phlu Basin in Pak Chong district, Nakhon Ratchasima province, including the Ban Nong Sai section (1), the Southern Sup Phlu section (2), the Northern Sap Phlu section (3), the Khao E-Dang section (4), and the Wat Tham Nong Sai section (5).....	71
4.2 Field investigation of the Ban Nong Sai section (47P 785346 N and 1619790 E) showing the lower (top left), middle (top right), and upper sections (bottom). Men as scale were looking east.....	72
4.3 Stratigraphic column of the Ban Nong Sai section of the Huai Hin Lat Formation in the Sap Phlu Basin area	73
4.4 Field investigation of the Southern Sup Phlu section (47P 779126 N and 1618940 E) showing the poorly preserved outcrop. Man as scale was looking the northwest	76
4.5 Stratigraphic column of the Southern Ban Sap Phlu section of the Huai Hin Lat Formation in the Sap Phlu Basin area.....	77
4.6 Field investigation of the Northern Sap Phlu section (47P 779011 N and 1619179 E) showing the poorly preserved outcrop along hill. Hammer handles are in the NW direction.....	80
4.7 Stratigraphic column of the Northern Ban Sap Phlu section of the Huai Hin Lat Formation in the Sap Phlu Basin area.....	81

LIST OF FIGURES (Continued)

Figure	Page
4.8 Field investigation of the Khao E-Dang section (47P 779982 N and 1618739 E) showing a contact (b) between the Permian silicified rocks (a) and Triassic basal conglomerate rocks (c and d)	84
4.9 Field investigation of the Wat Tham Nong Sai section (47P 785052 N and 1618816 E) showing a contact between the Permian massive limestone and Triassic basal conglomerates (a and b) oriented in the NW direction (c and d)	85
4.10 Stratigraphic columns of the Khao E-Dang section (A) and the Wat Tham Nong Sai section (B) of the Sap Phlu Basin	86
4.11 The locations of studied sections in the Na Pho Song Basin along road No. 2216 (Nam Nao district, Petchabun province- Dan Sai district, Loei province comprising the Sila section (1), the Dat Syo section (2), the Dat Kloi Nuea section (3), the Lak Dan section (4), the Sarn Chaopor Hin Tang section (5), the Dat Yai section (6), the Ban Huai Sai Thong section (7)	89
4.12 Field investigation of the Sila section (47Q 742210 N and 1884191 E) showing the road cut outcrop along the local road No. 2016 at Ban Song Pluei, Lom Kao district, Petchabun province. Man as scale is looking south	90

LIST OF FIGURES (Continued)

Figure	Page
4.13 Stratigraphic column of the Sila section of the Huai Hin Lat Formation in the Na Pho Song Basin area	91
4.14 Field investigation of the Dat Syo section (47Q 736501 N and 1895756 E) which (a) to (f) show the lower to upper sections and the uppermost section shows a contact between the Huai Hin Lat Formation and the overlying Nam Phong Formation in the NW direction.....	94
4.15 Stratigraphic column of the Dat Syo section of the Huai Hin Lat Formation in the Na Pho Song Basin.....	95
4.16 Field investigation of the Dat Kloi Nuea section (47Q 754714 N and 1880033 E) showing the rock exposure of volcanic, pyroclastic, and fine-grained rocks which their bedding attitude is in the E direction	97
4.17 Stratigraphic column of the Dat Kloi Nuea section of the Huai Hin Lat Formation in the Na Pho Song Basin	98
4.18 Field investigation of the Lak Dan section (47Q 760707 N and 1880500 E) showing mainly calcareous shale and overlying calcareous sandstone which (a) and (b) are in left and right of the outcrop respectively	100
4.19 Stratigraphic column of the Lak Dan section of the Huai Hin Lat Formation in the Na Pho Song Basin.....	101

LIST OF FIGURES (Continued)

Figure	Page
4.20 Field investigation of the Sarn Chaopoh Hin Tang section (47Q 792362 N and 1845710 E) showing thick beds of coal similar to the nearby Ban Huai Sanam Sai, Nam Nao district, Petchabun province which (a) and (b) are in left and right of the outcrop respectively	105
4.21 Stratigraphic column of the Sarn Chaopoh Hin Tang section of the Huai Hin Lat Formation in the Na Pho Song Basin area	106
4.22 Slumped structures which associated with penecontemporaneous faulting and low angle of slide planes.....	107
4.23 Moor types and resulting brown coal lithotypes and petrographic composition of the Miocene Rhenish coals (Teichmüller et al., 1982) as indicated to swarm sub-facies of Na Pho Song Basin	108
4.24 Field investigation of the Dat Yai section (47Q 796604 N and 1850718 E) showing a natural outcrop exposed along the flow directions of the Dat Yai water fall and (a) to (f) show lower to upper sections respectively	111
4.25 Stratigraphic column of the Dat Yai section of the Huai Hin Lat Formation in the Na Pho Song Basin.....	112

LIST OF FIGURES (Continued)

Figure	Page
4.26 Field investigation of the Ban Huai Sai Thong section (47Q 793057 N and 1843768 E) showing a contact (b) between overlying sandstone (a) and basal conglomerate (c-d) containing crinoid and fusulinid faunas.....	115
4.27 Stratigraphic column of the Ban Huai Sai Thong section of the Huai Hin Lat Formation in the Na Pho Song Basin.....	116
4.28 Succession of the Huai Hin Lat Formation showing classification and facies relation of the various members from Ban Dat Fa to Lom Kao district (Chonglakmani and Sattayarak, 1978).....	120
4.29 Measured stratigraphic sections showing classification and members of the Huai Hin Lat Formation along rural road No. 2048 from Ban Sap Phlu to Ban Nong Sai, Pak Chong district, Nakhon Ratchasima province.....	122
4.30 Measured stratigraphic sections showing classification and members of the Huai Hin Lat Formation along rural road No. 2216 from Ban Dong Maphai, Nam Nao district to Ban Songplueai, Lom Kao district, Petchabun province and Dan Sai district, Loei province.....	125
5.1 Al-Fe-Mn ternary diagrams of fine-grained rocks of the Ban Nong Sai section (A) and the Dat Yai section (B) (after Adachi et al., 1986)	130

LIST OF FIGURES (Continued)

Figure	Page
5.2 Photomicrographs of palynological assemblage of the Ban Nong Sai section consisting of palynomorphs (A-G), opaque biostructured phytoclasts (H-I), non-opaque biostructured phytoclast as stripe (J) and cuticle (K), non-opaque biostructured phytoclast (L), and non-opaque biostructured phytoclasts as striped elongate shape with AOM (M).....	138
5.3 Bio- and chemostratigraphic data: (A) Palynofacies (AOM, acritarchs, and phytoclast fraction); (B) AOM; (C) Acritarch concentration; (D) Phytoclast particle concentration; (E) Total organic carbon (TOC); (F) Excess SiO ₂ ; (G) The normalized Ba/Al trend; and (H) The normalized P/Al trend.....	142
5.4 Crossplots of palaeoproductivity proxies; (A) Normalize P/Al (10 ⁻⁴) and Ba/Al (10 ⁻⁴), (B) Acritarchs (particles/g) and TOC (%), (C) Phytoclasts (particles/g) and Acritarchs (particles/g).....	143
5.5 Chemostratigraphic data: (A) U/Th relationship; (B) V/Cr relationship; (C) Ni/Co relationship; (D) (Cu+Mo)/Zn relationship; (E) Ni/V relationship; (F) Ce/Ce* relationship.....	147

LIST OF FIGURES (Continued)

Figure	Page
5.6 Photomicrographs of particulate organic components of selected samples under transmitted light; (A) Phytoclasts performed mainly of opaque biostructured as pitted and elongated in shape of fragments; (B) Phytoclasts are mainly of non-opaque biostructured as pitted and elongated in shape of fragments; (C) Phytoclasts and structureless palynology are amorphous organic matter (AOM) as illustrated in cluster in the uppermost Dat Yai section	150
5.7 Bio- and chemostratigraphic data: (A) Palynofacies (AOM, and phytoclast) fraction; (B) AOM; (C) Phytoclast abundance; (D) Total organic carbon (TOC); (E) The normalize Ba/Al trend; and (F) The normalize P/Al trend	157
5.8 Chemostratigraphic data: (A) U/Th relationship; (B) U/Th relationship; (C) V/Cr relationship; (D) V/(V+Ni) relationship; (E) Ni/V relationship; (F) (Cu+Mo)/Zn relationship	158
5.9 Kerogen plot AOM-Phytoclast-Palynomorph (APP) of Ban Nong Sai section (pink) and Dat Yai section (orange). In the APP diagram it is possible to define nine fields using the percentages of the 3 main kerogen groups. These fields represent different environmental conditions (Tyson, 1995; Suarez-Ruiz et al., 2012).....	161

LIST OF FIGURES (Continued)

Figure	Page
5.10 Region of interest (ROI) is used to interpret the characteristics and distributions both porous media and pyrite which observed in the Ban Nong Sai section of the Huai Hin Lat Formation, the Sap Phlu Basin.....	182
5.11 Region of interest (ROI) is used to interpret the characteristics and distributions both porous media and pyrite which observed in the Dat Yai section of the Huai Hin Lat Formation, the Na Pho Song Basin	183
5.12 Pore type classifications of the Ban Nong Sai (Sap Phlu Basin) and the Dat Yai sections (Na Pho Song Basin) including pores of organic matter, interparticle, intraparticle, and microfractures and microchannels (after slat and O'Brien, 2011; Loucks et al., 2012)	190
5.13 (A, B) Different forms of organic matter pores, (C) typical flocculated clay microfabric, random edge-face (yellow arrows) and edge-edge (white arrows) clay flake orientations, (D) intergranular pores, (E) rigid individual pyrite crystal pores (white arrows) and covering pyrite crystalpores (yellow arrows), (F) pores along rim of rigid solitary quartz	197
5.14 (A) Interparticle pores between crystals of minerals, (B) intercrystalline pores, (C, D) different forms of intraplatelet pores cause clay types, (E) internal chamber of fossil fragment pores, (F) complex interparticle pores	198

LIST OF FIGURES (Continued)

Figure	Page
5.15 (A) Irregular microfractures (yellow arrows) and neighboring micropores, (B) microfracture related-pores (yellow arrows) and microjoints, (C) artificial fractures along changed compositions, (D) interparticle platelets of rock matrix are forming the microchannel related-pores, (E) carbonate minerals, (F) phosphate minerals	199
5.16 (A) Organic matter is dispersed with small organic matter pores, (B) typical flocculated clay microfabric, random edge-face (yellow circle) and edge-edge (white circle) clay flake orientations, (C) other forms of clay aggregates as produced elongate pores, (D, E) intergranular pores in rigid grain, (F) the soluble composition is dissolved as produced intergranular pores	204
5.17 (A, B) Intergranular pores along rim of rigid solitary grain crystal, (C, D) intercrystalline pores are produced by growth of micro-pellet pyrite and irregular-shaped mineral, (E, F) different forms of intraplatelet pores as elongate and irregular lath shape cause other clay types	205

LIST OF FIGURES (Continued)

Figure	Page
5.18 (A, C) Micropores of internal chamber of fossil fragment as multi-long strip length, (B) round pores are dispersed in fossil texture, (D, E) microfracture related-pores are produced from the external forces, (F) micropores among the bedding planes in rock matrix are forming the microchannel related-pores	206
6.1 Schematic chemical structures of oil-generating sapropelic kerogen and gas generating humic kerogens (Hunt, 1996)	220
6.2 Modified van Krevelen diagram for identifying the kerogen types of the Ban Nong Sai samples (purple solid circles) and the Dat Yai samples (orange solid circles) of the Huai Hin Lat Formation	223
6.3 Hydrogen index versus Tmax temperature for kerogen type of the Ban Nong Sai samples (purple solid circles) and the Dat Yai samples (orange solid circles) of the Huai Hin Lat Formation	224
6.4 Classification of potential source rocks of the Ban Nong Sai section based on total organic carbon content (TOC)	231
6.5 Classification of potential source rocks of the Dat Yai section based on total organic carbon content (TOC)	232
6.6 Thermal maturity stages of source rocks of the Ban Nong Sai section, Sap Phlu Basin that evaluated by (A) vitrinite reflectance (R_o) of visual analysis (purple) and calculation from T_{max} (black) and (B) T_{max} ($^{\circ}C$)	242

LIST OF FIGURES (Continued)

Figure	Page
6.7 Thermal maturity stages of source rocks of the Ban Nong Sai section, Sap Phlu Basin that evaluated by (A) production index (PI) and (B) transformation ratio (TR).....	243
6.8 Thermal maturity stages of source rocks of the Dat Yai section, the Na Pho Song Basin that evaluated by (A) vitrinite reflectance (R_o) of visual analysis (orange) and calculation from T_{max} (black) and (B) T_{max} ($^{\circ}C$)	244
6.9 Thermal maturity stages of source rocks of the Dat Yai section, the Na Pho Song Basin that evaluated by (A) production index (PI) and (B) transformation ratio (TR).....	245
6.10 Polar shale-gas risk plot with various visual and chemical assessments; (A) Good conditions for comprehensive evaluation (yellow), (B) Polar shale-gas risk plot of the Ban Nong Sai section, (C) Polar shale-gas risk plot of the Dat Yai section.....	253
6.11 The correlation between clay and carbonate minerals as shown a strong relationship of the Ban Nong Sai section (A) and the Dat Yai section (B)	256
6.12 Ternary diagrams of quartz, carbonate, and clay minerals of the Ban Nong Sai section (A) and the Dat Yai section (B)	257

LIST OF TABLES

Table	Page
1.1 Source rock qualities of the Khorat Group, Huai Hin Lat Formation, and Permian rocks (Sattayarak et al., 1996)	5
1.2 The combustion by products of other fossil fuels (EIA, 1999).....	8
5.1 Palynofacies point count (particles/g) and fraction in a cumulative percentage of AOM, acritarchs, and phytoclasts as compared with TOC data of the Ban Nong Sai section of the Sap Phlu Basin.....	139
5.2 Palynofacies point count (particles/g) and fraction in a cumulative percentage of phytoclasts, AOM, and palynomorphs as compared with TOC data of the Dat Yai section of the Na Pho Song Basin.....	151
5.3 Maceral types determined by visual petrographic analysis of the Ban Nong Sai section of the Huai Hin Lat Formation	166
5.4 Maceral types determined by visual petrographic analysis of the Dat Yai section of Huai Hin Lat Formation	167
5.5 Vitrinite reflectance (R_o) testing by using optical method of the Ban Nong Sai section of the Huai Hin Lat Formation	171
5.6 Vitrinite reflectance (R_o) testing by using optical method of the Dat Yai section of the Huai Hin Lat Formation	172

LIST OF TABLES (Continued)

Table	Page
5.7	T_{max} , S_1 , S_2 , and S_3 testing by Rock-Eval pyrolysis of the Ban Nong Sai section (Sap Phlu Basin) and the Dat Yai section (Na Pho Song Basin) of the Huai Hin Lat Formation175
5.8	Mineralogic and clay fraction XRD data of the Ban Nong Sai section177
5.9	Mineralogic and clay fraction XRD data of the Dat Yai section178
5.10	Description of collected samples of the Ban Nong Sai and the Dat Yai sections of the Huai Hin Lat Formation which were scanned by Micro-CT instrument. They show the concentrations of object volume, porosity both closed and opened pores, and connectivity181
5.11	Comparison of pore characteristics among the various types of rocks in the Dat Yai section of the Sap Phlu Basin.....195
5.12	Comparison of pore characteristics among the various types of rocks in the Dat Yai section of the Sap Phlu Basin (Continued)196
6.1	Average TOC, rock-Eval, and vitrinite reflectance values and computations of the Ban Nong Sai section, the Sap Phlu Basin221
6.2	Average TOC, rock-Eval, and vitrinite reflectance values and computations of the Dat Yai section, the Na Pho Song Basin222
6.3	Organic matter type is classified by maceral of kerogen (Dai et al., 2008, Chen et al., 2011).....224

LIST OF TABLES (Continued)

Table	Page
6.4	Type index (TI) and kerogen type classifications of the Ban Nong Sai section and the Dat Yai section225
6.5	Classification of potential source rock in shale and limestone based on TOC values (Gehman, 1962; Peter and Cassa, 1994).....230
6.6	Original hydrogen index (HI _o), transformation or conversion ratio (TR _{HI}), and original total organic carbon (TOC _o) of the Ban Nong Sai section, the Sap Phlu Basin233
6.7	Original hydrogen index (HI _o), transformation or conversion ratio (TR _{HI}), and original total organic carbon (TOC _o) of the Dat Yai section, the Na Pho Song Basin.....234
6.8	Classification of thermal maturity stages by T _{max} , vitrinite reflectance (R _o), production index (PI) (Peters and Cassa, 1994; Espitalié and Bordenave, 1993; Bacon et al., 2000), and transformation ratio (TR) (Jarvie et al., 2005; 2007)241
6.9	Calculated original potential (S _{2o}), generated hydrocarbons, and average hydrocarbon yield of the Ban Nong Sai section, the Sap Phlu Basin.....248
6.10	Calculated original potential (S _{2o}), generated hydrocarbons, and average hydrocarbon yield of the Dat Yai section, the Na Pho Song Basin248

LIST OF TABLES (Continued)

Table	Page
6.11 The criteria of source rock evaluation show the seven excellent parameters of T_{\max} , vitrinite reflectance (R_o), production index (PI) (Peters and Cassa, 1994; Espitalié and Bordenave, 1993; Bacon et al., 2000), transformation ratio (TR), TOC, thickness (Jarvie et al., 2005; Jarvie et al., 2007), and organic matter type.....	252
6.12 The criteria of reservoir rock evaluation as shown the four excellent parameters of porosity, brittle minerals, clay minerals (Passey et al., 2010), and thickness (Jarvie et al., 2005; Jarvie et al., 2007).....	264
6.13 The main features of the U.S. gas shale (Curtis, 2002).....	270

CHAPTER I

INTRODUCTION

In recent year, the fossil fuel especially oil and gas are used and distributed across several sectors of the economy. It is an important energy source for the industrial, commercial, and electrical generation sectors and also serves in the residential heating. But it produces many problems such as air and water pollutions. The march towards sustainable renewable energy sources such as wind and solar are a better ways. However, they are still in the development stage. Therefore, the fossil fuels are still an integral facet of moving forward with energy options. With the current emphasis on the potential effects of air emissions on global climate change, air quality, and visibility, the fossil fuel is still an important energy source of the world and Thailand today and the near future.

1.1 Petroleum exploration in the Khorat Plateau of NE Thailand

The petroleum fields in the Khorat Plateau were explored following the authorization by the Thai government. Thai government realized that the petroleum exploration and production have high investment cost and risk. Thailand has been importing oil in increasingly high volume. The Khorat Plateau is an energy starved region with a large population providing a ready market for any gas. Despite past disappointments, this basin will continue to attract exploration (Booth, 1998). As the results, Thai government lets the international companies to bid for the petroleum exploration concession to reduce the volume of imported petroleum.

The exploration stages in NE Thailand can be classified into four stages (Booth, 1998) as follows:

1) First stage: The Khorat Plateau has been explored for petroleum by private companies since 1971 of the Thai 1st Licensing Round. The Union Oil Company explored and drilled the first well (Kuchinarai-1) in NE Thailand (Kuchinarai district, Kalasin province) but potential for petroleum were not found.

2) Second stage: This stage is during the Thai 6th, 7th, and 8th Bidding Round in period of 1979-1990. Esso Khorat Company found natural gas in 4 wells that Nam Phong-A1 well (1981) and Nam Phong-A2 well (1983) are commercial production as located in Block E5. And other two of uneconomic wells are Chonabot-1 well and Dong Mun-1 well. Esso Udon Company explored and drilled 3 exploration wells and only one of Phu Horm-1 well that the natural gas was found in Block EU1. Then Phillip Company explored in Block P2 and drilled a Non Sung-1 well that was non potential.

3) Third stage: This stage is in period of 1990-2000 as during the Thai 13th and 15th Bidding Round. In this stage there were several companies attending for bidding e.g., Unocal, Thai Shell, Texaco, Total Khorat, and Amerada Hess. Only two of Dao Ruang-1 well (Texaco, 1993) and Mukdahan-1 well (Unocal, 1994) have found natural gas in minor amount. Huai Muk-1 well (Unocal, 1994) and Phu Wiang-1 well (Booth, 1998) have shown petroleum traces but the other 6 wells were unsuccessful.

4) Fourth stage: This stage is during the Thai 18th, 19th, and 20th Licensing Round in period of 2000 to present day. In 2002, Amerada Hess continued drilling in Block E5 that natural gas was found in Phu Horm-3st well. The wells in Block E5

were combined with the wells in Block EU1 and developed as Sin Phu Horm gas field in 2006. Subsequently, several companies have also interested in the Khorat Plateau e.g., Apico Khorat, Tatex, Salamander, and PTT Exploration and Production Company. TEW-E, TEW-EST wells discovered natural gas but cannot be developed due to minor tested gas. In 2011, PTT Exploration and Production Company also found minor amount of natural gas in Rattana-1 well. In 2013, PTTEP continued to drill Rattana-2 well and natural gas was found but cannot be developed due to quite low flow rate of hydrocarbon. In 2012, Apico Company continued to explore Block L27/43. Dong Mun-3st well was drilled and natural gas was found in high amount for commercial production.

From the first stage to the present day, there are 49 wells were drilled in the Khorat Plateau including exploration, appraisal, and production wells. All wells do not show significant amount of tested oil. Natural gas was discovered as three commercial gas fields of Nam Phong, Sin Phu Horm, and Dong Mun gas fields but only in the former two fields can be produced recently (DMF, 2014).

1.2 Petroleum system of NE Thailand

For oilmen, the three most important parameters for hydrocarbon exploration are source, reservoir, and seal. Two more things normally discussed are maturation and play type. The petroleum potential and the general stratigraphy of the Huai Hin Lat Formation are shown in Table 2.1.

1.2.1 Source rocks

Geochemical data from the Triassic Pre-Khorat sediments, the Permian-Carboniferous carbonates and shale suggest that they contain a good to fair source richness (Sattayarak et al., 1989; Chinoroje and Cole, 1995; Piyasin, 1995). The Huai Hin Lat Formation consists dominantly of lacustrine grey shales, mudstones, and limestones of good source quality. The thickness of this sequence varies from a few hundred meters to over 2,000 meters. Geochemical analyses of these sediments from both surface samples (Unocal, 1990) and exploration well samples in the Khorat Plateau have TOC values from 0.9-2.52% (Sattayarak, 2005). Maturation modeling is based on Lopatin's method at average geothermal gradient 1.2 °F/100 ft and assuming a complete overlying section of the Khorat Group (6-7 km) that suggested oil generation was occurred between 191-109 Ma (Sattayarak et al., 1989). Those geochemical studies indicate that the maturation ranges from 189-62 Ma (Sattayarak et al., 1989).

Although these sediments have frequently exhausted their potential for liquid hydrocarbons, it is inferred that they were originally good and occasionally rich source rock for oil and gas.

The gas samples collected from carbonate reservoirs of Dao Ruang-1 well were studied by Chinoroje and Cole (1995). The methane and ethane carbon isotopes show that gas from Dao Ruang-1 well comes from organic-rich lacustrine shale and coals of the Triassic Pre-Khorat (Chinoroje and Cole, 1995). Besides the source rocks, fluvial sandstones in the upper unit constitute the most likely Pre-Khorat reservoirs. Mainly I and III kerogen types are dominant in the source rock of the group (Sattayarak, 2005) which can be generated both oil and gas.

Table 1.1 Source rock qualities of the Khorat Group, Huai Hin Lat Formation, and Permian rocks (Sattayarak et al., 1996).

Formation/ Group	TOC (%)	R _o (%)	Source rock richness	Maturity	Kerogen type	Proneness
Khorat	0.03-0.35	0.63-1.38	Very poor-poor	Mature	III	Gas
Huai Hin Lat	0.20-5.76	0.90-2.52	Fair-very good	Mature to very mature	I, III	Gas/Liquid
Permian	0.29-1.59	1.02-4.57	Poor-fair	Very mature to over mature	?, II, III	Gas

1.2.2 Reservoir rocks

Permian carbonates are the main gas producing strata in northeastern Thailand (Sattayarak, 2005). However, gas and oil also found in the other types of rocks and ages (Sattayarak, 2005). Existing and potential reservoir rocks of the Triassic are discussed as below.

Fluvial sandstones in the upper unit are the most likely Triassic Pre-Khorat reservoir. The porosity of these sandstones varies from 3-8% (Polachan et al., 1980). The basal conglomerates also have a reservoir potential providing that they have appropriate fractures (Sattayarak, 2005). These types of reservoirs might be encountered in rollover anticline, fault bounded, and stratigraphic pinch out traps (Sattayarak, 2005). A strong evidence to prove its reservoir potential is an amount of about 0.2 million cubic feet of dry gas per day which flow from the Triassic sandstone in Mukdahan-1 well (Sattayarak, 2005).

1.2.3 Seal

Thick sequence of fine-grained and dense rocks on the top of impregnated hydrocarbon beds in northeastern is quite common (Sattayarak, 2005). For example, the lower part of the Khorat Group which contains a thick and monotonous layer of claystone with some intercalations of sandstones and siltstones. These clastics are tightly packed with argillaceous cement thus permeabilities are expected to be very poor (Sattayarak, 2005). They act as excellent seal all over northeastern Thailand for all types of play (Sattayarak, 2005). For those trap types comprising Permian reservoirs and seal apart from Khorat rocks, they could be tight Permian Carbonates and fine sediments of the Permian Upper Clastics and/or Triassic rocks (Sattayarak, 2005). Triassic reservoir could be laterally or vertically sealed by finer sediments of the same age (Sattayarak, 2005).

1.2.4 Maturation

Maturation history modeled by using the burial and heat flow histories indicates that the Permo-Carboniferous sediments first became mature between 197 and 175 million years ago and continued to increase maturity during the rapid burial and heating in the Late Triassic to Early Jurassic (Sattayarak, 2005). Due to the combination of rapid burial and heating, all source rocks encountered in the wells to date are over mature (Sattayarak, 2005). This is meant that petroleum generated from Paleozoic rocks is supposed to be cracked down into dry gas already. The Triassic Pre-Khorat source could initially generated both oil and gas while reaching its window during Late Cretaceous time and just passing the wet gas maturity level (Sattayarak, 2005). The Khorat sediments are still in oil window level (Sattayarak, 2005).

More study will be conducted since crude oil has been found in the Khorat sandstones from the Phu Horm-3 well. It is unlikely that this oil can be generated from Khorat rocks. Moreover, Booth (1998) suggested that the original drilling concept was a Tertiary (Himalayan) anticline coincident with an underlying Permian tilted fault block. The platform carbonates of the Permian Pha Nok Khao Formation have proved to be the productive reservoir. Sandstones and conglomerates of the overlying Lower Huai Hin Lat Formation (Kuchinarai Group) was a secondary target (Booth, 1998). The exact sources of generated gas have not been studied in detail. The organic rich shale of the Huai Hin Lat Formation is, therefore, selected for the study of its potential for hydrocarbon generation. It will provide a comprehensive data which proved the gasses were supplied from. Moreover, the readers can form an objective opinion of the effectiveness of the remaining potential of this basin. They will gain some insights into the shale gas evaluation which are produced and increasingly supplied for all sectors of Thailand.

1.3 Natural gas

EIA (2007) published a key advantage that is efficient and clean burning. The natural gas has gained its popularity as a fossil fuel due to its relatively lower carbon emissions and air pollutants (Figure 1.1) during the combustion process in comparison to oil and coal (EPA, 2012; Paltsev et al., 2013). It emits approximately half the carbon dioxide (CO₂) of coal and quietly lowers oil along with low levels of other air pollutants (EIA, 1999; GWPC, 2009). The byproducts of natural gas combustions are mostly CO₂ and water vapor the same compounds that people exhale when breathing especially its liberates very small amounts of sulfur dioxide (SO₂), nitrogen oxides

(NOX), virtually no ash, lower levels of carbon dioxide (CO₂), carbon monoxide (CO), and other hydrocarbons (GWPC, 2009). The composition of hydrocarbon gases are combined and consists primarily of methane (CH₄) and lesser percentages of butane, ethane, propane and other gases. The natural gas reservoirs are classified into 2 types as follows:

Table 1.2 The combustion by products of other fossil fuels (EIA, 1999).

Air Pollutant	Combusted Source (Pound/billion btu of energy input)		
	Natural Gas	Oil	Coal
Carbon dioxide (CO ₂)	117,000	164,000	208,000
Carbon monoxide (CO)	40	33	208
Nitrogen oxide (NO ₂)	92	448	457
Sulfur dioxide (SO ₂)	0.6	1,122	2,591
Particulates (PM)	7.0	84	2,744
Formaldehyde	0.750	0.220	0.221
Mercury (Hg)	0.000	0.007	0.016

1.3.1 Conventional natural gas

Basically, the conventional reservoir is the meaning of the most of the oil and natural gas produced by using traditional methods are already being accessed. Hydrocarbons can be flown naturally or pumped to the surface which is composed principally of methane. GWPC (2009) published the meaning of the conventional reservoirs produced from sand and carbonates (limestone and dolomites) and contain the gases in interconnected pore spaces that flow to the wellbores. The gases in the pores can move from each pore to another through smaller pore throats that create permeability flow through the reservoir. The sources of gas are often from organic-

rich shale proximal to the more porous and permeable sandstone and carbonate (GWPC, 2009). The possessing is a large resource endowment and the natural gas in a half of them is consumed today. The method is hard to explore and produce due to it lacks of more complex technologies to identify prospective drilling location. The hydrocarbon produced from drilled wells is being consumed at the rate exceeding domestic production and the gap is increasing. It is believed that many unconventional natural gas resources can significantly alter that balance and are prime example of this trend (GWPC, 2009).

1.3.2 Unconventional natural gas

The unconventional natural gases are called the group of gas play systems including tight sands, basin center gas, shallow basin methane, coal bed methane, and shale gas. These types of accumulations may be thermogenic sources, either from primary cracking of organic matter or secondary cracking of bitumen, and oil or mixed thermogenic-biogenic sources. Natural gas may be further categorized as in-situ generated-reservoirs or as migrated gas (Jarvie et al., 2003). Moreover, it is gas that increases due to explore, identify prospective of drilling location, and produce primarily a result of advancements in technology. As a result to an increase of commercially recoverable reservations that were previously thought to be uneconomic but recently thought to be economic already (Navigant Consulting, 2008; GWPC, 2009). According to gas shale resource systems recently are boom, worldwide in any part of the world due to this energy independence is created by the remarkable success achieved by the development of unconventional shale gas resources (Jarvie, 2012). It is proved by this type of natural gas that has evolved into an important resource play, accounting for more than 14% of produced gas in the United States by the end of

2004. In the annual shale gas production and recently projected production of Energy Information Administration (EIA, 2008) and Curtis (2009) show the shale gas accounted is 1.6 % of total US natural gas production in 2000 and had jumped to 4.1 % and 23.1 % in 2005 and 2010 respectively (Wang and Krupnick, 2013) as illustrated in Figure 1.2. In addition, Figure 1.3 is also illustrated the projected contribution of shale gases to overall unconventional gas production in United State in bcf/day. Therefore, this gas shale is interested and needed more understanding.

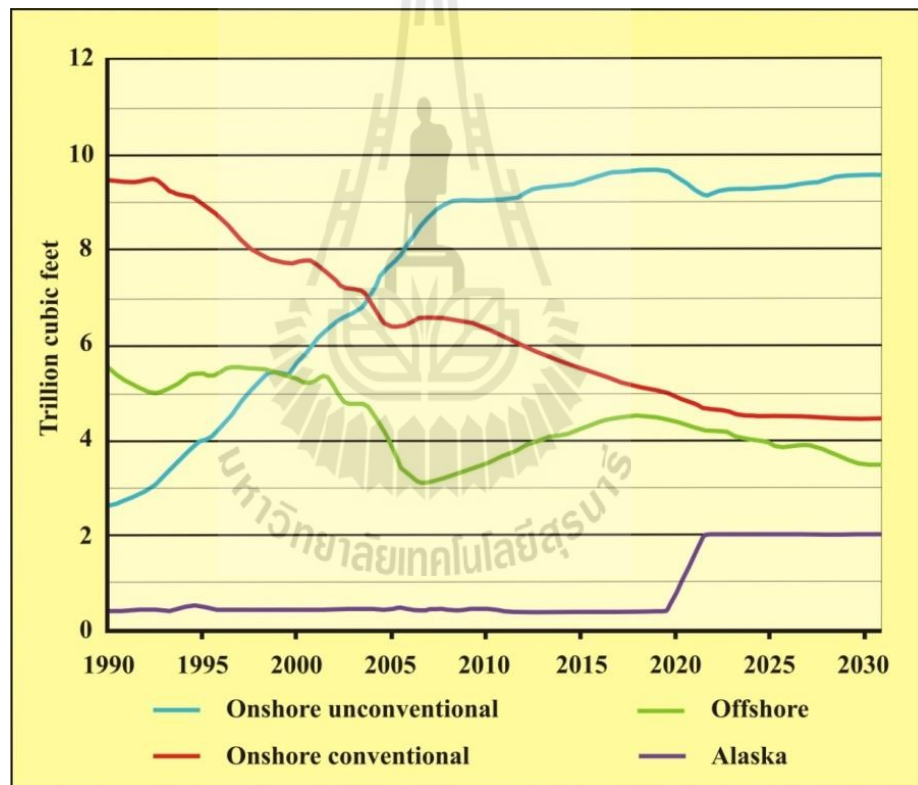


Figure 1.1 The natural gas production by source (tcf/year) (EIA, 2008).

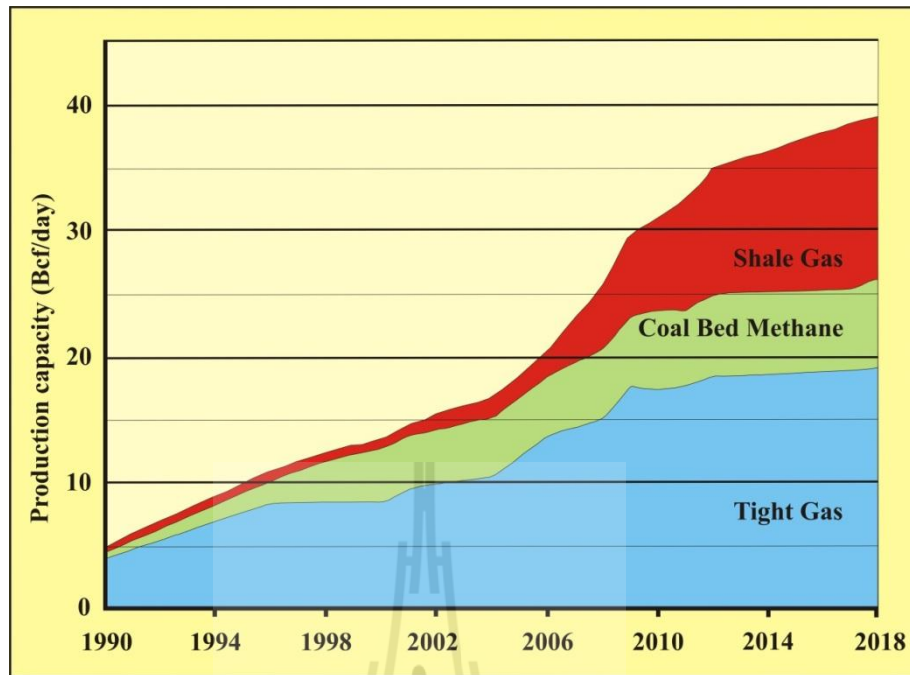


Figure 1.2 The United States unconventional gas outlook (bcf/day) (American Clean Skies, 2008).

1.3.2.1 Unconventional shale gas

Shale gas is a future long-term energy source among the others (Slatt and O'Brien, 2011), becomes an increasingly important source of natural gas in the United States, and interest has spread to potential gas-rich shales in Canada, Europe, Asia, and Australia (Sondergeld et al., 2010; Tian et al., 2011). Shale in gas shale refers to black shale containing organic matters in dark-coloured mudrock, silt- and clay-size mineral grains that accumulated together (Swanson, 1961; Suarez-Ruiz et al., 2012). It is deposited in different environments in low energy anoxic environment with sulfate-reducing (Hallam, 1980; Tourtelot, 1978; Suarez-Ruiz et al., 2012), the organic content is mainly constituted by structureless, carbonized (Chemically inert kerogen) or organic components, and a variable amount of

terrestrially-derived components which can be presented (spores, pollen grain, and wood material) (Suarez-Ruiz et al., 2012). A higher concentration of organic matter can provide excellent original organic richness and high generation potential, resulting in higher gas-in-place volumes (Bowker, 2007). The gas shale systems generated the gas (Suarez-Ruiz et al., 2012) and stored in shale source rocks. The gas is adsorbed within the organic matrix (Jarvie et al., 2007) or function as low matrix-permeability and low porosity reservoir rocks (Suarez-Ruiz et al., 2012) due to the very fine sheet-like clay mineral grains and laminated layers of sediments (GWPC, 2009). Jarvie et al. (2007) classified shale gas systems into five categories as high thermal maturity shales, low thermal maturity shales, mixed lithology intraformational systems, interformational systems (gas is generated in mature shale and stored in lesser mature shale), and combination plays (containing both thermogenic and biogenic gases).

The types of organic petrographic (visual kerogen type, quality, and thermal maturity) and geochemical analyses (TOC and rock-Eval pyrolysis) are the key in identifying the best prospective areas for gas. Moreover, the geochemical modeling of hydrocarbon generation and retention are recognized of gas storage sites and primary migration pathways along the kerogen/bitumen network (Cardott, 2012; Suarez-Ruiz et al., 2012). However, exploration for shale gas requires a somewhat different mindset from that of conventional petroleum exploration, and a completely different technology. The mindset of conventional are described in terms of seismic prospecting, well drilling, completion (Chalmers and Bustin, 2008; Hill et al., 2007; Jarvie et al., 2001, 2003, 2007; Lopatin et al., 2003; Loucks and Ruppel, 2007; Martini et al., 2003; Montgomery et al., 2005; Pollastro, 2003; Pollastro et al., 2003,

2004a,b; Ross and Bustin, 2007, 2009; Schmoker, 1995; Schmoker et al., 1996; Selley, 2005; Smith et al., 2010; Suarez-Ruiz et al., 2012), and application of microseismic survey allowed engineers to map where the stimulation energy was being directed, thereby, allowing adjustments to the stimulation program (Steward, 2007; Jarvie, 2012).

1.3.2.2 Shale gas in the United States

Shale gas in the United States, mentioned to the producible natural gas resource systems provide a mean of energy independence in natural gas for the foreseeable future and independence is created by the remarkable success achieved by the development of unconventional shale gas resources (Jarvie, 2012). The growth of shale gas production in the United States has spurred increasing interest in exploring shale resources in the other areas of the world (Wang and Krupnick, 2013). According to Steward, (2007) and Jarvie (2012) they described the history and development of shale gas in the United State, MEDC (Mitchell Energy and Development Corp.) pursued and developed these unconventional shale gas reservoir systems. Even in 1982, the MEDC 1-Slay well was drilled but it was incredibly difficult resource to exploit, and noncommercial through the 1980s and most of 1990s. In 1991, the first Barnett Shale horizontal well of MEDC 1-Sims was drilled but not an economic or even technical success. For this experience, horizontal drilling is an important part of the equation that has led to the development of shale resource plays to form a series of interlinked controls on obtaining gas flow from shale. Moreover, if without the understanding the importance of rock mechanical properties, stress fields, and stimulation processes affected to the horizontal drilling is not successful as mentioned above. In 1990s, 1-Sims is only horizontal well but

others are vertical and measured 500 mcf/day of gas flow rate. The economics were enhanced when MEDC began using slick-water stimulation to reduce costs with the surprising benefit to improve performance in terms of gas flow rates. The use of technologies such as three-dimensional seismic and microseismic proved highly beneficial in moving the success. In 2002, Devon Energy purchased MEDC and invested in new technologies to evaluate the play with Southwestern Energy that success in the Arkoma Basin. And addition of movement from MEDC of experienced, knowledgeable shale resource, geologists, and engineers to the general E&P pool. These factors led many companies to begin looking at shale resource potential and brought the potential of shale-gas resource systems to national and ultimately global levels.

1.3.2.3 Shale gas in Thailand

Shale gas in Thailand is expected on the onshore of the Khorat Plateau. It is a prospective area of the northeastern part with high potential area 150,000 square kilometers (DMR, 2007). In 2011, PTTEP (PTT Exploration and Production) drilled the Rattana-1 well that the target reached to the Permian Formation for the conventional natural gases. In 2013, PTTEP drilled the Rattana-2 well that reached to the Phu Kradung Formation (approximately 1,000 m). This well discovered for the tight sand gases of unconventional natural gas. It used the high technologies in drilling processes of hydraulic fracturing and microseismic survey but the well was also dry. Although the well was dry, it led us more experience and understanding to pursue the unconventional natural gases for the future. In addition, shale gases are boom now and many independent companies still interested especially the Huai Hin Lat Formation of lacustrine environment is high potential of shale gases.

1.4 Research objective

The objectives of this study are as follows:

- 1) To study the stratigraphy, sedimentology, and geological structures of the Huai Hin Lat Formation at the Sap Phlu Basin and the Na Pho Song Basin that crop out within the rim of the Khorat Plateau.
- 2) To study the geochemistry of the Huai Hin Lat Formation at the Sap Phlu Basin and Na Pho Song Basin.
- 3) To evaluate the palaeoproductivity and palaeoenvironments of deposition based on microfossils, wood materials, and geochemistry analysis of the selected sections at the Sap Phlu and Na Pho Song Basins.
- 4) To evaluate the source rock potential that eventually produced the generated hydrocarbon of the Sap Phlu and Na Pho Song Basins.
- 5) To evaluate unconventional shale gas potential based on source rock data and reservoir condition data of the Sap Phlu and Na Pho Song Basins.

1.5 Scope and limitations of the study

The study area covers the Sap Phlu Basin and the Na Pho Song Basin of the Huai Hin Lat Formation exposed along the N-S elongated mountain belts at the western rim of the Khorat Plateau (Figure 1.4). The Sap Phlu Basin is in Nakhon Ratchasima province. The Na Pho Song Basin covers a part of Petchabun, Khon Khaen, Chaiyaphum, and Loei provinces. This study is divided into 2 parts which worked on outcrop exposures and laboratory as follows:

1.5.1 Outcrop study

The outcrop study is focused mainly on stratigraphy, sedimentology, and geological structures to establish facies and its members. The study areas are divided into 2 parts as follows:

Firstly, the Sap Phlu Basin (Ban Nong Sai, Southern Ban Sap Phlu, Northern Ban Sap Phlu, Khao E-Dang, and Wat Tham Nong Sai sections) is located along the local road (No. 2048) in Nakhon Ratchasima province. Secondly, the five sections of the Na Pho Song Basin (Sila, Dat Kloi, Lak Dan, Sarn Chaopoh Hin Tang, Dat Yai sections) are situated along the road No. 2216. The other two sections of the Dat Syo section is along the road No. 4017, Dan Sai district, Loei province and the Ban Huai Sai Thong section is along the highway No. 12, Khon San district, Chaiyaphum province.

Of these mentioned sections, the Ban Nong Sai section (Sap Phlu Basin) and Dat Yai section (Na Pho Song Basin) are selected for potential evaluation of both conventional and unconventional shale gas resources.

1.5.2 Laboratory study

1) The collected samples are focused mainly on palynology extraction and geochemical data to establish paleaodepositional environments.

2) Stratigraphically, only two available sections (Ban Nong Sai and Dat Yai sections) of high potential as petroleum source rocks are selected for further testing on petroleum geochemistry laboratory. The results from selected sections are the proxies to evaluate the potentials of petroleum source rock and unconventional gas resources.

1.6 Research methodology

Research strategies and activities will be done as follows:

1) The field surveys in central and northeastern Thailand to investigate the stratigraphic sequences and collect rock samples. The selected areas of stratigraphic, structural, and tectonic importance will be examined.

2) The samples are prepared for geochemical analysis and other testing as follows:

2.1) The palaeoenvironment, palaeoproductivity, and palaeoredox will be carried out by XRF, ICP-MS methods, and palynology extraction.

2.2) The mineral compositions in the in-situ reservoir rocks will be carried out by XRD (X-Ray Diffraction) method.

2.3) The quantities of organic matters will be carried out by TOC analysis.

2.4) The qualities of organic matters and types will be carried out by palynology extraction, rock-Eval pyrolysis, maceral type method, and type index.

2.5) The thermal maturation will be carried out by vitrinite reflectance and rock-Eval pyrolysis.

2.6) The porosity and porous media evaluation will be carried out by Micro-CT and SEM viewing machines.

3) All results will be compiled and evaluated for the potential of the petroleum source rock and unconventional shale gas.

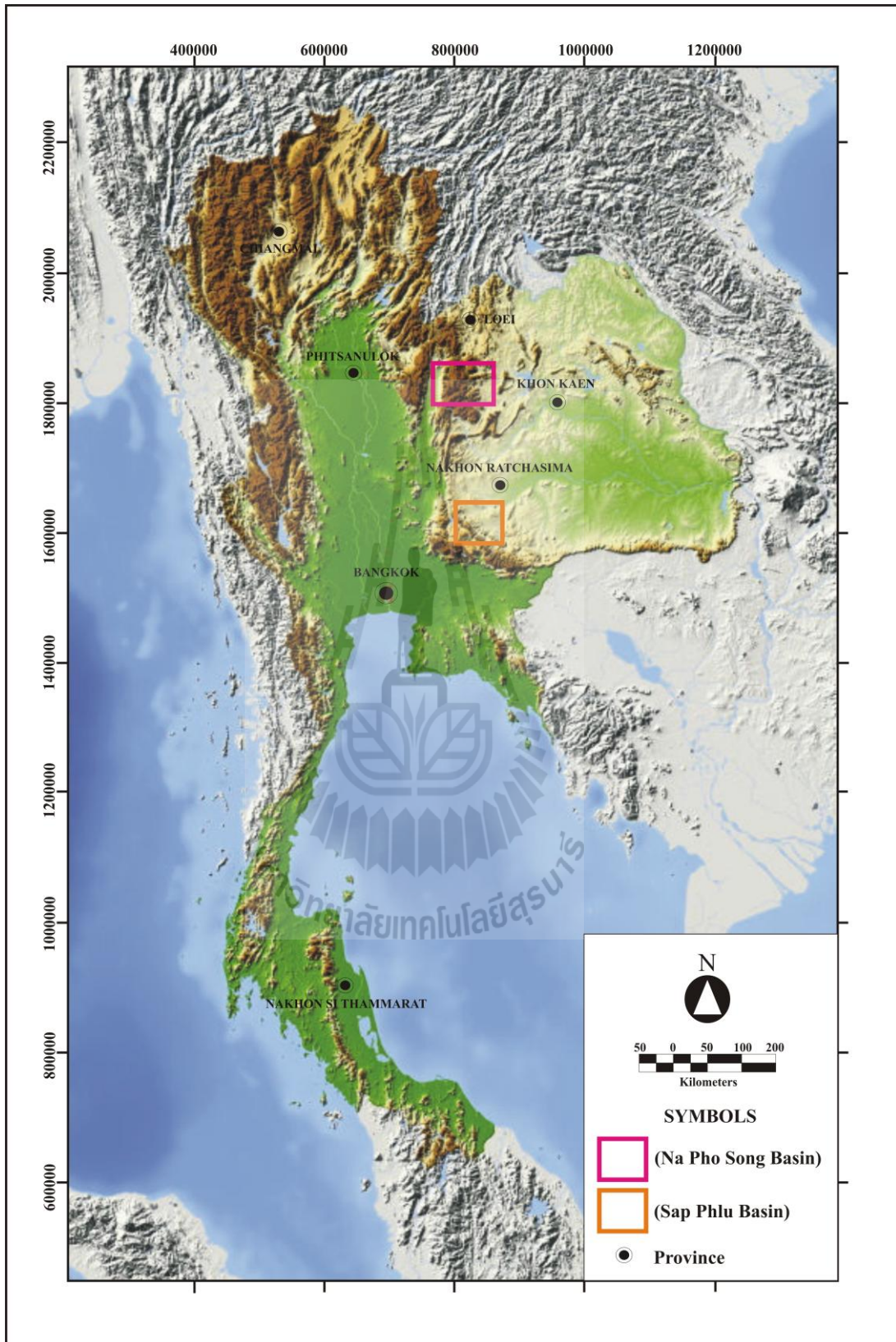


Figure 1.3 Map showing the studied areas.

CHAPTER II

LITERATURE REVIEW

Hydrocarbon resources are the most important energy sources not only for Thailand but in the world. According to Thailand, people need more hydrocarbons to respond their needs. Each year, the demand for hydrocarbon has increased. Their quantity is not enough, hence the budgets to pay for importing are increasing continuously. For energy sustainable of Thailand, alternative energy sources should be pursued, explored, and discovered continuously in order to reduce the need for import especially to have sufficient energy sources for domestic use in the future (Khositchisri, 2012). Therefore, Khorat Plateau in the northeastern part of Thailand has more potential both conventional and unconventional gas sources especially shale gas. The Huai Hin Lat Formation is selected for study and evaluation for gas resources.

2.1 Geologic setting of Thailand

Geological framework of Thailand is described; it lies within a larger geological entity which is widely referred to as Sundaland, the continental core of SE Asia comprising Vietnam, Laos, Cambodia, Thailand, eastern Myanmar, West Malaysia, Sumatra and Java, and Borneo (Ridd et al., 2011). For recent synthesis is thrust in two principle tectonic blocks (also referred to as plates or as plates or terranes) can be identified in Thailand. Indochina Block in the east and the Sibumasu

Block in the west Sibumasu (Metacafe, 1984) are the terms most widely used in recent literature for the plate which includes north-western and Peninsular Thailand (Ridd et al., 2011). Although these terranes had different histories, both had their origins on the margin of Gondwana before drifting north and fusing in the Mesozoic to form the core of Sundaland. The line of collision which marks the site of the former ocean Palaeotethys runs approximately north-south through Thailand. It is clear that the extreme west of the country, including most of the peninsula is part of Sibumasu whereas the NE and narrow strips close to the Cambodia and the eastern part of the Thai-Malaysian border are parts of the Indochina Blocks (Ridd et al., 2011). The southwards continuation of these zones into SE Thailand and continue that far into the Peninsula (Ridd et al., 2011). The every geologic system from Cambrian to Middle Cenozoic is described follows:

Lower Palaeozoic, the term of plate tectonic is used to describe the discontinuous outcrop belt within the Sibumasu Block. It is absent of stratigraphy evidence due to fault-bounded block which recognize that distinctiveness by the term of Phuket Terrane (Figure 2.1). The Cambrian succession is laid down in warm shallow seas, Ordovician is marine limestone, and Silurian is black shale with faunas including trilobite, brachiopods goniatites, nautiloids, crinoids, and conodonts. Therefore, Lower Palaeozoic faunal affinities to both Australia and to the South China have been proposed based on nautiloids and trilobites. However, wider stratigraphic considerations suggest that the Sibumasu was still part of Gondwana at this time when super continent lay to the west of Sibumasu (Ridd et al., 2011).

Devonian, west flank of Indochina Block was not a simple ramp but interrupted by the local ocean basin of thin-bedded chert and black shale with radiolarians in Devonian and Middle Triassic Age. It is widely thought to be remnant of the ocean, Palaeotethys which separated Sibumasu from Indochina Blocks (Ridd et al., 2011).

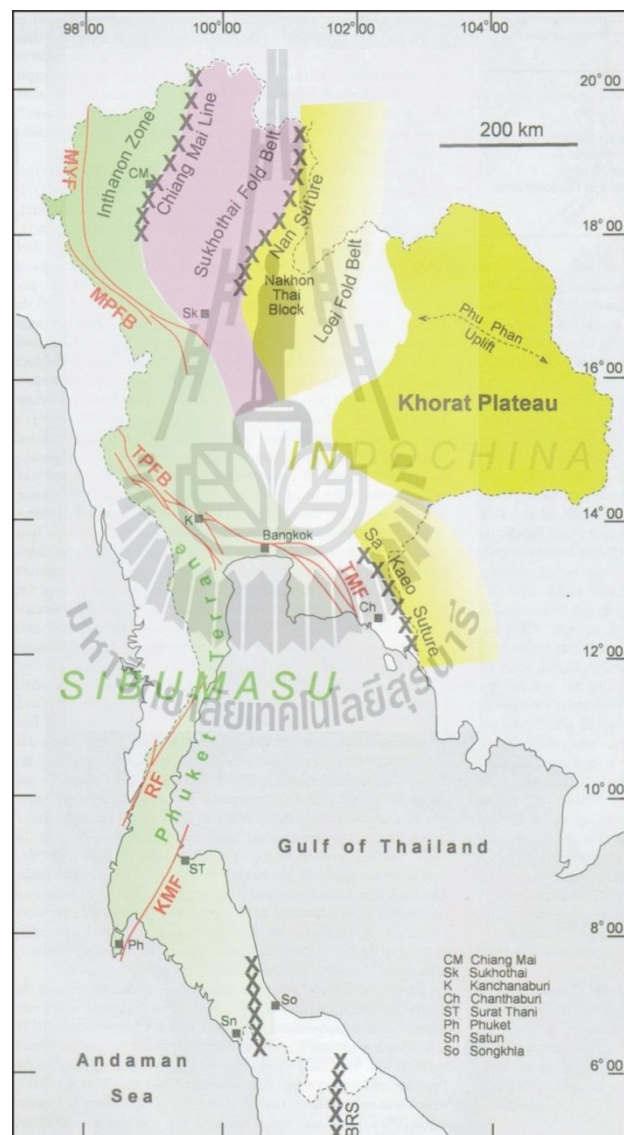


Figure 2.1 Principal structure elements of Thailand including the two principal blocks or terranes which comprised the country (Ridd et al., 2011).

Carboniferous and Permian sedimentary rocks are among the most widespread in Thailand, cropping out or occurring in subsurface in all regions of the country (Ueno and Chareontitirat, 2011; Ridd et al., 2011). They may be divided into mainly 4 interested characteristics as follows:

1) Carboniferous to Permian of active volcanism was named by Barr and Charusiri (2011) as Sukhothai Zone, particularly in the Permian of Northern and NE Thailand and interpreted this zone as a back arc basin separated from the Indosinian Block. Sone and Metacafe (2008) interpreted that this back arc basin was closed at the end of the Permian (Late Triassic?) (Cobbing, 2011) forming the Nan-Uttaradit Suture and presumed southern extension as Sa Kaew Suture.

2) Carboniferous and Permian faunas provide the unraveling the plate tectonic history of the two principle terranes. Indosinian Block is represented by the warm-water Tethyan characteristics with rich and diverse faunas including corals, brachiopods, and foraminifera but Sibumasu Block is represented by the cooler-water Tethyan characteristics with the comparable age and faunas have lesser diversity.

3) Carboniferous to Permian of NE Thailand comprises the Fang Chert (oceanic-floor deposit) and Doi Chang Limestone and was named as Inthanon Zone by Barr and Macdonald (1991). Ueno and Chareontitirat (2011) interpreted these rocks as accretionary complex that thrust westwards onto Sibumasu when Palaeotethys was closed in the Late Triassic.

4) Carboniferous to Permian rocks in the peninsula, unequivocally western part of Sibumasu Block has shown the strong evidence of the former presence of a cratonic block of Gondwana. It lays to the present-day west (Ridd et al., 2011). The Kaeng Krachan Group of Upper Peninsula (Phuket Terrane) is diamictite. Ridd

(2007, 2009a, 2009b) suggested that thick diamictite bearing succession of the Upper Peninsula was deposited in a rift within the Phuket Terrane as Sibumasu split from Gondwana. The rift succession is generally agreed to have been deposited in a glacially influenced environment.

Triassic Period, Chonglakmani (2011) suggested the marine shelf sedimentation over much of Northern, Western, and Peninsular Thailand while chert continued to be deposited on the floor of the progressively closing Palaeotethys Ocean. Subduction of Palaeotethys eastwards beneath the island arc of Sukhothai Zone is the result of the emplacement of I-type granitoids and acid volcanic rocks as associated with marine deep-water sediments (Ridd et al., 2011). Finally, Palaeotethys was closed in Late Triassic (Figure 2.2) with the emplacement of S-type granitoids (Cobbing, 2011; Ridd et al., 2011). This collision is caused by the Indosinian Orogeny in which Bunopas (1981) considered the Nan Uttaradit Suture.

Over the eastern part of the country in the Khorat Plateau of NE Thailand, the collision was followed by continental sedimentation in the half-grabens. The collision was commenced in the Norian (Late Triassic) of the Huai Hin Lat Formation and passing up into the overlying Nam Phong Formation and the other younger Khorat Group. Booth and Sattayarak (2011) studied the subsurface geology of NE Thailand and identified three unconformities. They equate the Indosinian I as presented the largest deformation event as strongest unconformity between the Huai Hin Lat Formation and an eroded surface of Permian and older rocks. Indosinian II is represented the unconformity between the base of the Nam Phong Formation and the underlying Huai Hin Lat Formation of minor basin inversion. Indosinian III separated

the upper and lower Nam Phong Formation by hiatus on seismic data, it appeared to mark the absence much of the Jurassic system.

The major regression which began in the Late Triassic and continued through the Jurassic reached its maximum extent in the Cretaceous. The Cretaceous successions throughout Thailand consist of non-marine red-beds which crop out most extensively in the Khorat Plateau of NE Thailand (Meesook and Saengsrichan, 2011; Ridd et al., 2011). Moreover, the Mid Cretaceous has shown evidences of Phu Phan Uplift that responsible for initiating the line of NW-SE trending anticlines across the plateau. Deformation increased towards the end of the Cretaceous and into the Palaeogene. It coincided with the late stage of the emplacement of the Western Granite Belt which occupies the Upper Peninsula and adjacent parts of Myanmar (Cobbing, 2011; Ridd et al., 2011). In addition, the extent to fault movements can be related to the distant collision of India with Eurasia commenced in the Early Eocene (Ridd et al., 2011).



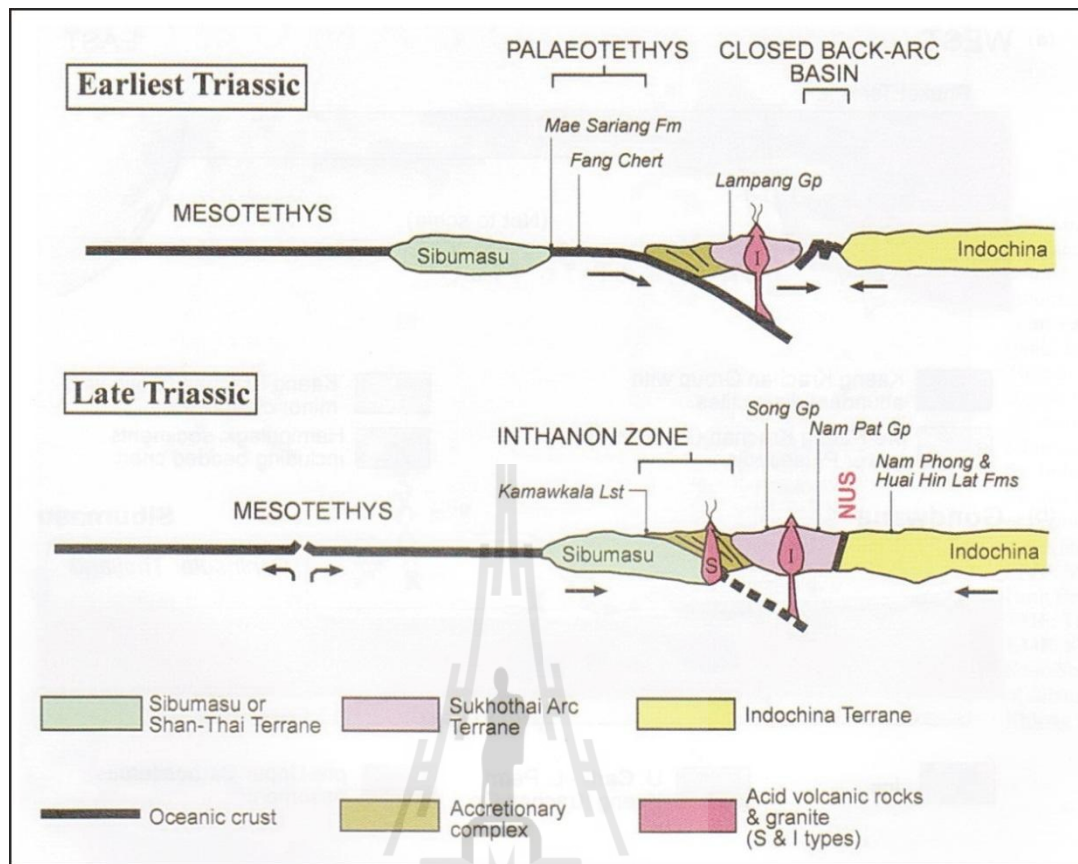


Figure 2.2 Sections across Northern and NE Thailand showing the narrowing of the Palaeotethys Ocean in the earliest Triassic and the final collision of the Sibumasu block with the Sukhothai Arc and Indochina block in the Late Triassic (Sone and Metcalfe, 2008; Ridd et al., 2011).

2.2 Geologic setting of NE Thailand

Thailand shown on the geological map is divided into two distinct parts. Most of NE Thailand is a broad expanse of gently deformed Mesozoic sedimentary rocks which comprise the Khorat Plateau. The rest of the country has a more complex and sinuous outcrop patterns in every geological system (Ridd et al., 2011). According to the Khorat Plateau, it is in reality a relatively flat plain, generally 150-200 m above

sea level, rimmed by low mountains and a distinctive scarp edge. It covers an area of approximately 200,000 square kilometers occupying most of NE Thailand and extending into parts of Laos. The surface geology of NE Thailand consists almost entirely of Jurassic to Mid-Cretaceous Khorat Group red-beds. According to the subsurface data of drilling wells, sedimentary fill in these basins has proved to be similar to the Upper Carboniferous-Triassic strata. It crops out to the west and SW in the Loei-Petchabun Fold Belt (Booth and Sattayarak, 2011). Details of the geological framework in NE Thailand are intensively summarized by Booth and Sattayarak (2011) as follows:

2.2.1 Na Mo and Pak Chom Group

They are the basement rocks in Pre-middle Carboniferous of this stratigraphy containing the metamorphic rocks with brick-red shale and siltstone.

2.2.2 Mid-Carboniferous event

This is the event of uplift on Indochina Block (Ridd et al., 2011) with large scale folding and nappe thrusting as generated the unconformity separating the Upper and Lower eroded Carboniferous. The seismic line across the Khorat Plateau Basin image a complexly foliated and thrust basement with a fabric striking NW-SE and moderate angle dips to NE (Booth and Sattayarak, 2011).

2.2.3 Saraburi Group in Middle Carboniferous-Upper Permian

The extensive outcrops along the western and southwestern margins of the Khorat Plateau are provided by Ueno and Charoentitirat (2011).

1) Si That Formation

The initial stratigraphic scheme is consistent with the ages obtained from outcrops of the Wang Saphung Formation east of Loei province (Ueno and

Charoentitirat, 2011). Their deposition recommenced in shallow-marine to marginal-terrestrial conditions and water depth soon increased but still remained across NE Thailand after Mid-Carboniferous Unconformity. The initial sedimentation was mixed siliciclastics, carbonates, and then turn to shale and sandstone (Booth and Sattayarak, 2011).

2) Pha Nok Khao Formation

The main reservoir targets for gas exploration in NE Thailand yield a variety of age from the latest Carboniferous to Middle Permian. They were deposited in seaways between the platform areas comprising the fusulinid and echinoderm debris of packstone (Booth and Sattayarak, 2011). They crop out to the west of the Khorat Plateau in Loei-Petchabun Fold Belt (Ueno and Chareontitirat, 2011; Booth and Sattayarak, 2011). Volcanic tuffs are interbedded with limestones at the base of this formation that occurs in the quarry at Wat Khao Tham Toh Bon, south of Petchabun which is located on the Khao Khwang platform. This indicates to coincide with volcanic activity along the western edge of Indochina Block. The margin was subsequently uplifted and eroded during the Indosinian I Event (Early-Middle Triassic); an elongate south-facing cuesta and formed by the more resistance of the underlying Si That Formation (Booth and Sattayarak, 2011).

3) Hua Na Kham Formation

It is considered to occur above Middle-Upper Permian boundary to Late Permian or extended into at least the Earliest Triassic with an interval of mixed siliciclastics and carbonates. Ueno and Chareontitirat (2011) regarded this formation to be a lateral equivalent of the Pha Dua Formation. This time, Booth and Sattayarak, (2011) suggested that the large faults are controlled during deposition of the Pha Nok

Khao Formation and remained active during deposition of the Hua Na Kham Formation. Their succession records an upwards transition from marine to coastal environments, as yet there is no indication of the landmass which supplies the siliciclastic sediments was located. It is clear from the seismic lines that a considerable proportion of this formation was also removed by erosion during the Indosinian I Event.

2.2.4 Indosinian I Event

This event is suggested by Booth and Sattayarak (2011) that was clearly formed by the mostly intense uplift of the Indosinian Orogeny. Deep erosion associated with major compressional deformation of the Saraburi Group around the Palaeozoic-Mesozoic boundary as a major regional unconformity. By the end of the Indosinian I Event, almost the whole of NE Thailand had been peneplained. The limited residual topographic highs generally took the form of karst hills of the Pha Nok Khao Formation carbonates or cuesta ridges as formed by tilting of the more resistance of the Si That Formation.

2.2.5 Huai Hin Lat Formation (Kuchinarai Group)

This group is deposited in Late Triassic; they contain a predominantly terrestrial with a mixture of alluvial, fluvial and lacustrine deposits. Distribution of depositional environments in these basins is complex. Moreover, lowermost units predominantly volcanoclastics which indicate basin initiation was associated with volcanic activity elsewhere in the region. This formation located between the Indosinian I and II Unconformities has simply been referred to as Pre-Khorat Triassic (Esso Internal Report; Non Sung-1, 1985; Sattayarak et al., 1989; Booth and Sattayarak, 2011).

2.2.6 Indosinian II Event (Latest Triassic)

This event is suggested by Booth and Sattayarak (2011) that the deformation event produced buttress folding along the basin-bounded faults, minor sediment fill excursion on the dip-slope edge, and occasional minor thrust faults. The subsurface data shown hiatus associated with this unconformity is short and divided the underlying Kuchinarai Group and the overlying Lower Nam Phong Formation. This region is less degree of uplift and erosion except the northern and southern edges as both Indosinian I and II Unconformities coalesce. By the end of Indosinian II Event, the whole of NE Thailand was essentially a peneplain. There were a few low relief topographic highs which were remnant karst hills of the Pha Nok Khao Formation or cuesta scarps formed by the more resistant of the Si That Formation.

2.2.7 Khorat Basin

It contains the succession above the Indosinian II Unconformity including the Cretaceous exposures at the present-day surface of the Khorat Plateau. In general, the Khorat Basin has the appearance of large intra-cratonic sag. At the end of the Indosinian II Event, the sediments comprise even the earliest fill of the Khorat Basin which must have been sourced from the outside the region located on the northern flank of the Phu Phan Uplift to those parts of succession exposure in the core of the uplift. It is a large Tertiary inversion structure in the middle part of the basin and the edge as the cuesta escarpments are surrounding. Mouret et al. (1993) concluded that during the Late Jurassic and Early Cretaceous, these sediments were brought into the basin from the north, east, and south. These sediments were transported across it toward the west. Therefore, the massive volume of sediments contained in the Khorat Basin especially remnants that preserved today have been

sourced by the erosion of a significant mountain belt and prolonged uplift (Booth and Sattayarak, 2011). This basin is divided into subdivision including Indosinian III Unconformity as follows:

1) Nam Phong Formation

It is divided into 2 parts, the Lower and the Upper Nam Phong Formations by the Indosinian III Unconformity as follows:

1.1) Lower Nam Phong Formation

It is composed of the interbedded claystones, siltstones, and sandstones. These sediments are interpreted to have been deposited in alluvial fan and fluvial floodplain environments with limited areas of shallow lakes or swamps. Based on subsurface data, this formation can be distinguished from the Kuchinarai Group by predominant reddish brown colour of its shales and siltstones. On seismic lines, the internal pattern of this formation comprises the semicontinuous to discontinuous parallel reflections with the lowermost onlapping onto the Indosinian II Unconformity (Booth and Sattayarak, 2011).

1.2) Upper Nam Phong Formation

It is a fining-upwards sequence characterized by thick-bedded to massive sandstone with conglomerates. The lower part was deposited in predominantly fluvial environment and upper part was deposited in mixed alluvial-fluvial floodplain environments with meandering-river systems (Booth and Sattayarak, 2011).

2) Indosinian III Unconformity

It is recognized by Racey and Goodall (2009) that a major hiatus between the Upper and Lower Nam Phong Formations is corresponding to the entire

Early and Middle Jurassic. It is an interval of some 45-50 million years in which the relatively low angle unconformity (onlapped by the overlying formation) is referred to Indosinian III Unconformity (Booth and Sattayarak, 2011).

3) Phu Kradung Formation

It is described by Booth and Sattayarak (2011) that the formation has generally formed a coarsening upwards succession and deposited in alluvial and fluvial floodplain environment with meandering systems. They consist of claystones, siltstones, and sandstones especially sandstones having more thickness increasing from the lower to upper.

4) Phra Wihan Formation

It is composed of thick-bedded to massive white sandstones with rare thin beds of reddish-brown to grey claystones. This predominant sandstone formation is interpreted to have been deposited by a stacked series of braided rivers. The palaeocurrent directions are generally westward flows of rivers that enter the basin from the north, east, and south (Booth and Sattayarak, 2011).

5) Sao Khua Formation

It is composed of succession of thin- to thick-bedded, reddish-brown to purple-brown and greenish-grey claystones, siltstones, and sandstones. It is interpreted to deposit in a fluvial floodplain environment with meandering systems (Booth and Sattayarak, 2011).

6) Phu Phan Formation

It comprises a stacked series of thick-bedded to massive white sandstones interbedded with thin red-brown siltstones and claystones of meandering

rivers to locally braided rivers. Palaeocurrent directions indicate westward flows entering the basin from the north, east and south.

7) Khok Kruat Formation

It consists of thin- to thick-bedded sandstones interbedded with purplish red to red-brown claystones and siltstones of meandering-river and floodplain deposits. The patterns show the sharp contrast to the rest of the Khorat Group in which thickness towards a NW-SE trending. Moreover, Sattayarak and Polachan (1990) suggested that it is to be the results of uplift, tilting, and erosional truncation during a Middle Cretaceous deformational event.

2.2.8 Middle Cretaceous Event

It is the deformational event because the Phu Phan Uplift was initiated (Sattayarak et al., 1991) in NW-SE trending anticlinorium following the inversion. These sedimentations began with the evaporitic Maha Sarakham Formation (Cooper et al., 1989). Sattayarak et al. (1991) identified an angular unconformity at the base of the Maha Sarakham Formation and mentioned that these evaporites are in fact of Middle Cretaceous.

2.2.9 Maha Sarakham Formation

It is associated with the uplift of Middle Cretaceous Event, the present-day Khorat Plateau became isolated and drainage was internal leading to the deposition of the evaporitic Maha Sarakham Formation. These evaporites are composed mainly of halite and minor anhydrite in which Utha-Aroon (1991) confirmed that they were deposited in a continental setting.

2.2.10 Phu Tok Formation

Sattayarak (1983) suggested that consistence of a sequence of brick-red to red-brown claystones with minor siltstones and rare fine-grained sandstone beds in lower part. It is interpreted that have been deposited in low-energy fluvial environment. The upper part consists of sandstones with large-scale of high angle cross-bedding of aeolian environment. It may show interfingering and lateral equivalent with the Maha Sarakham Formation.

2.2.11 Tertiary uplift and folding

They are the large-wavelength folds of the Khorat Group that interpreted the notable features of the surface geology of NE Thailand were initiated in Early Tertiary. This event is created the style of Tertiary folding associated with the inversion of the Kuchinarai Group (Late Triassic), the Saraburi Group (Permo-Carboniferous), including some faults that had formed during the Indosinian I Event.

2.3 Geologic setting of the Huai Hin Lat Formation

The rock exposures of the Huai Hin Lat Formation are cropped out at the NW margin of the Khorat Plateau, the west of Loei-Petchabun Fold Belt. Chonglakmani and Sattayarak (1978) identified a non-marine Triassic section. They termed the Huai Hin Lat Formation and placed as the lowermost formation of the Khorat Group. Then Sattayarak et al. (1989) removed the Huai Hin Lat Formation from their definition of the Khorat Group (Booth and Sattayarak, 2011). The present-day Thailand is the result of the collision and fusion of two principle continental blocks or terranes, Sibumasu (also called Shan-Thai) in the west and Indochina in the east (Chonglakmani, 2011). Both blocks had their origins on the margin of the

Gonwana in the Palaeozoic. Chonglakmani (2011) suggested that they broke away from their parent continent at different times and different histories which are drifted north before arriving in tropical latitudes in the Triassic. This collision was probably responsible for the strongest unconformity seen in NE Thailand as the Indosinian I Event (Booth and Sattayarak, 2011; Chonglakmani, 2011). The central Belt S-type granites were emplaced also in the Late Triassic (Cobbing, 2011; Chonglakmani, 2011). This Time, sediments were being deposited in rifted basins on an eroded surface of Permian and older rocks (Figure 2.3) that was applied the name to the Huai Hin Lat Formation. The Huai Hin Lat Formation also called the Kuchinarai Group (Ridd et al., 2011) due to during the phases of exploration drilling in the Khorat Plateau was applied the name to the sequence between the Indosinian I and II Unconformities of Late and Latest Triassic. Chonglakmani (2011) compiled data of this formation and considered it to be of Late Triassic (Norian) age on the basis of its plant remains (Kon'no and Asama, 1973), pollen and spores (Haile, 1973) and conchostracans (Kobayashi, 1975). Haile (1973) recorded the presence of these palynomorph in the Nam Pha Formation which can be correlated to the Huai Hin Lat Formation and assigned a Carnian-Norian age. Racey et al. (1996) recorded taxa and considered it to be older (Carnian-Norian) because lack of Rhetian marker taxa. However, this formation also confirm to Late Triassic (Norian) age by vertebrate faunas of Norian.

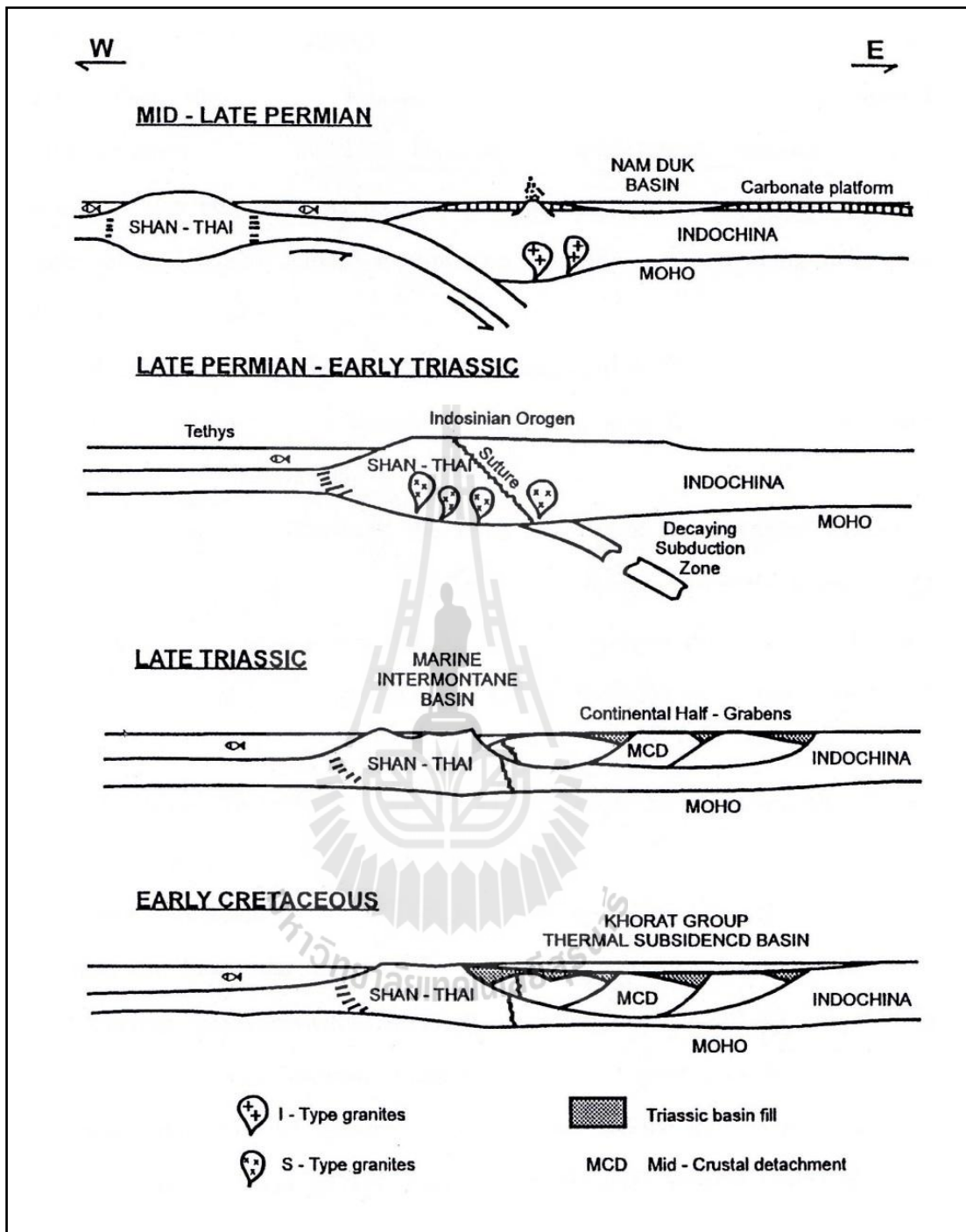


Figure 2.3 Evolution of the Huai Hin Lat Formation in northeastern Thailand (Cooper et al., 1989).

Based on the extensive grid of seismic lines, it is possible to map several separated basins containing this formation (Figure 2.4). These basins comprise a considerable sedimentary fill that ranges from 2.5 km to over 6.5 km in thickness. Almost all of these basins have a simple half-graben shape controlled by a single large fault and most of them trend from NW-SE to west-east. In contrast, the main basins are Phu Kao and Chok Chai Basins which have more complex fault geometries including multiple linked half-grabens with opposing fault polarities. Finally, these faults were reactivated a NE-dipping basement fabric which form during the Middle Carboniferous Event. This fabric is probably pervasive in the basement across most of NE Thailand that may be more weakly developed to the SW. This pre-exist structural grain probably explains why almost all of controlling faults on these half-grabens basins are thrown down to the NE (Booth and Sattayarak, 2011).

The drilling well data and seismic interpretation are contributed to better understanding the subsurface distribution and expansion of the Huai Hin Lat Formation. The largest basin located in northwestern of the Khorat Plateau showing more prospecting basin is being investigated on its potential to be a petroliferous basin. The Norian Triassic crops out along the rim of the Khorat Plateau (Sap Phlu and Na Pho Song Basins) in Figure 2.4 as contacted with Permian Basin. The exposure of Sap Phlu Basin is the combination of two basins of Sap Phlu and Chok Chai Basins in which the uppermost part (the post-rift sequences) may join together. In addition, the upper sequence may represent the deposition in a larger (combined) basin. The stratigraphic classification of the sedimentary sequences is established in relation to their structural styles and tectonic development.

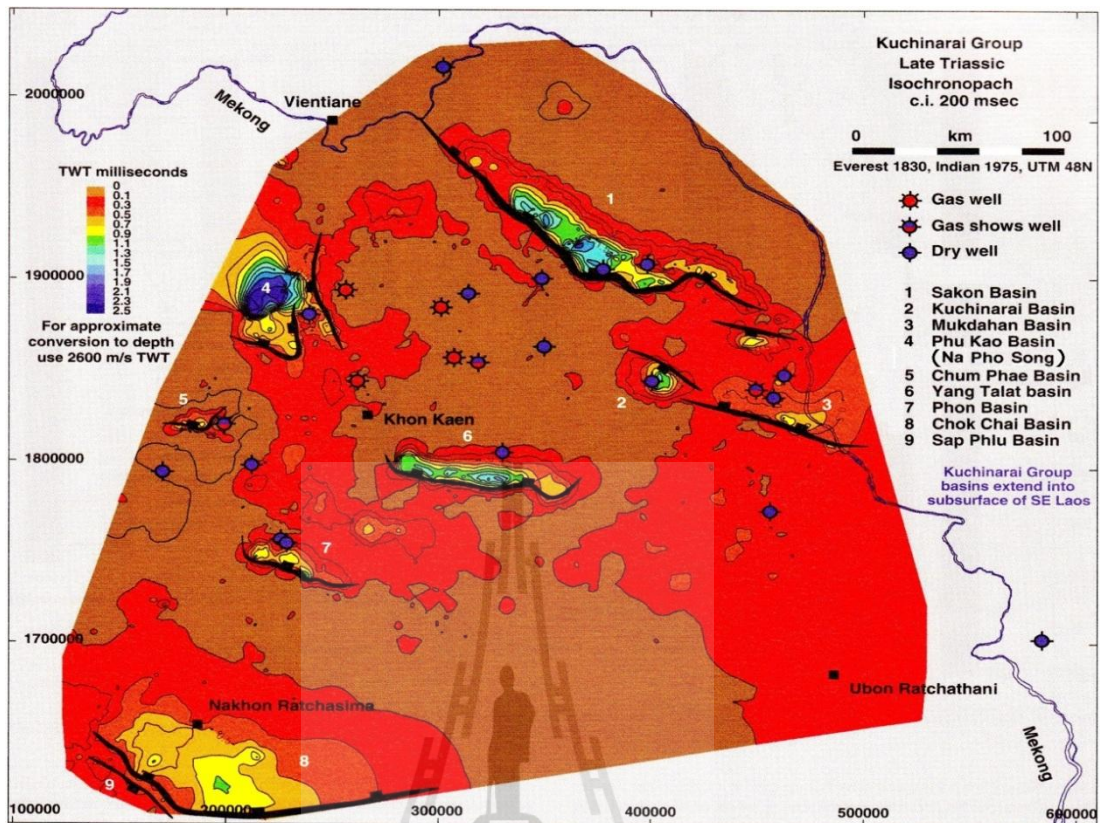


Figure 2.4 Isochronopatch of the Huai Hin Lat Formation or the Kuchinarai Group showing distribution of the major half-graben basins (Booth and Sattayarak, 2011).

The basins are orientated in the NW-SE direction, the active margin was controlled by a west dipping listric normal fault located in the northeastern basin. To the west, a thick sequence of basal conglomerate is found resting unconformably on top of the Permian beds. The sequences were followed by fluvial sandstone which was changed laterally to be fluvio-lacustrine sands with interfingering lacustrine shale. Subsequently, dark gray shale and argillaceous limestone were accumulated as the depositional cycle became regressive. The fluvial sediments which are

unfortunately, not visible in this area, and not believe to cover the dark gray sequences.

The exposure of the Huai Hin Lat Formation at the NW margin of the Khorat Plateau unconformably overlies the Permian and older strata. It is overlain unconformably by the Nam Phong Formation. It is divided into five units of the Pho Hai, Sam Khaen Conglomerate, Dat Fa, Phu Hi, and I Mo Members.



CHAPTER III

METHODOLOGY

In this chapter, the author would describe all methods that use to study for this research that is summarized in flow chart as illustrated in Figure 3.1. According to entire methods, the reviewing methodology of field work for stratigraphic sections, microfossils extraction, geochemical analysis, and physical analysis on the siliciclastic sedimentary rocks and especially shale samples as follows:

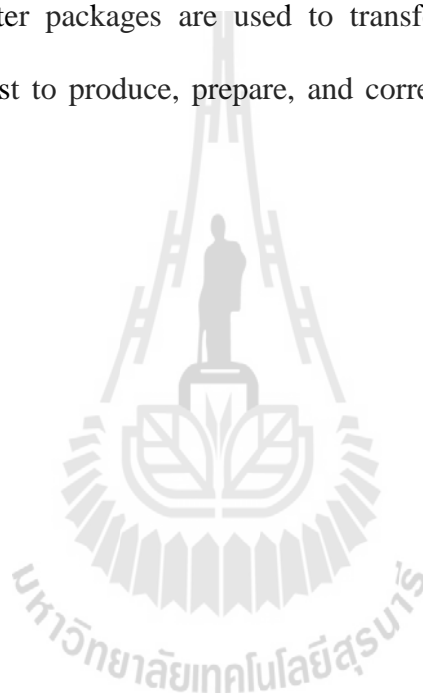
3.1 Fieldwork for measured stratigraphic sections

Successful fieldwork relies heavily on a clear identification of the objective for the fieldwork and efficient planning before departing for the field. Plan operation in the time framework of the project as a whole and allow ample time with pessimistic assumption.

In the field, it is vital to establish a systematic pattern of work for field observations, note taking, and sample collecting. The sample collecting and storage are importance for laboratory work that has to beware of contamination. Moreover, detailed measurements of stratigraphic sections are also considered after areal mapping is almost completed. The measurement of sections by the tape traverse along lines determined by compass bearings is the most widespread and useful technique, wherever sediment variation is rapid and detailed description is necessary. If distances are great, lithological character does not vary greatly over short intervals, units dip more than 10° , and there is little relief along the line of section (Lewis and

McConchie, 1937). Pace and compass measurement are feasible for near approximations to the true values. Where beds are dip less than 10° and there is marked relief along the line of traverse. The plane table surveying and graphical solution for slopes and dips are commonly necessary (Lewis and McConchie, 1937). The trigonometric relationships linking bed thickness, surface topography, dip, and outcrop width are shown in Figure 3.2.

Useful computer packages are used to transfer the field data that can be simplified. They assist to produce, prepare, and correlate the multiple stratigraphic sections.



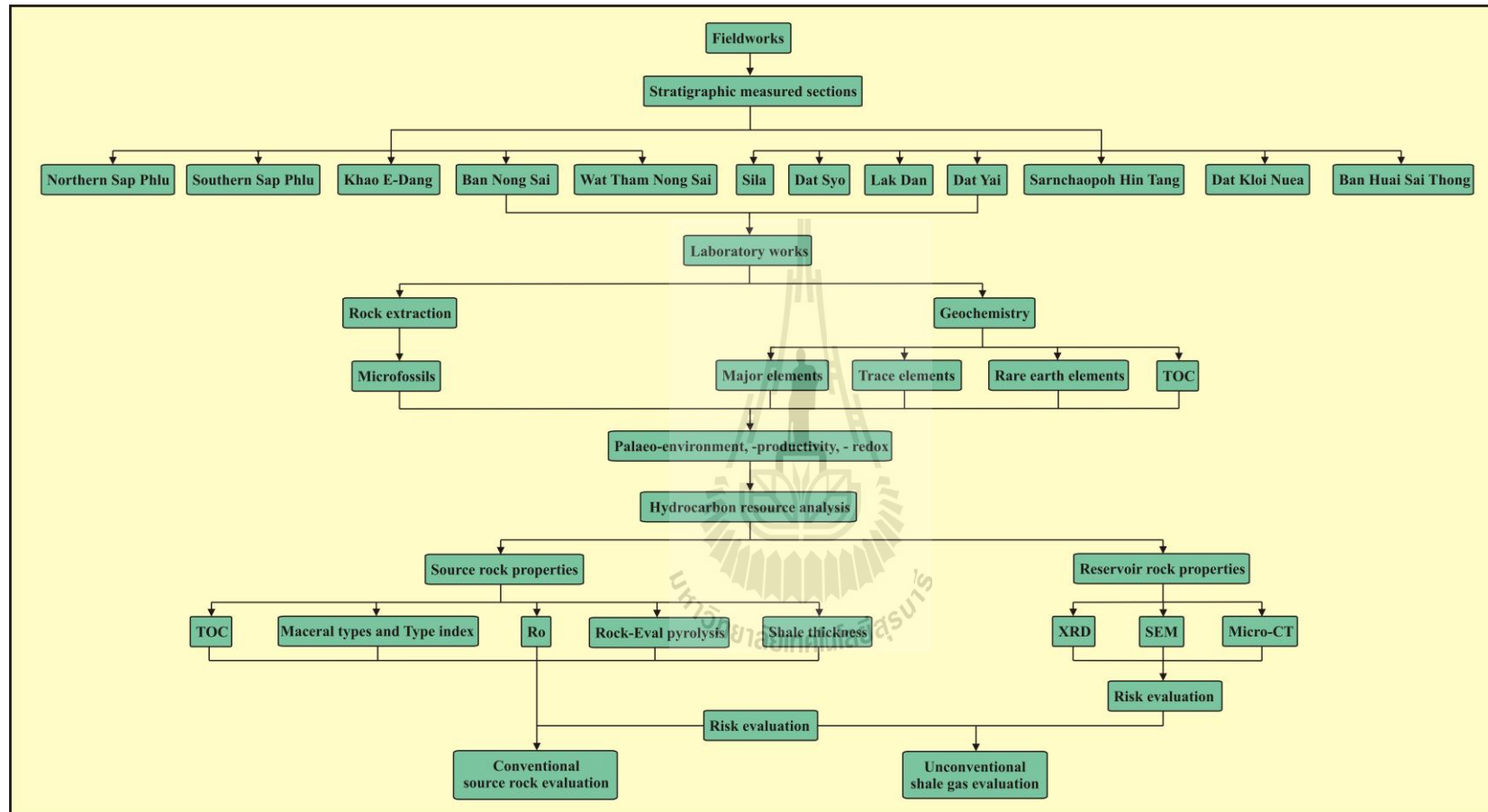


Figure 3.1 Flow chart showing the methods of study for shale gas evaluation on the Ban Nong Sai and Dat Yai sections of the Huai Hin Lat Formation.

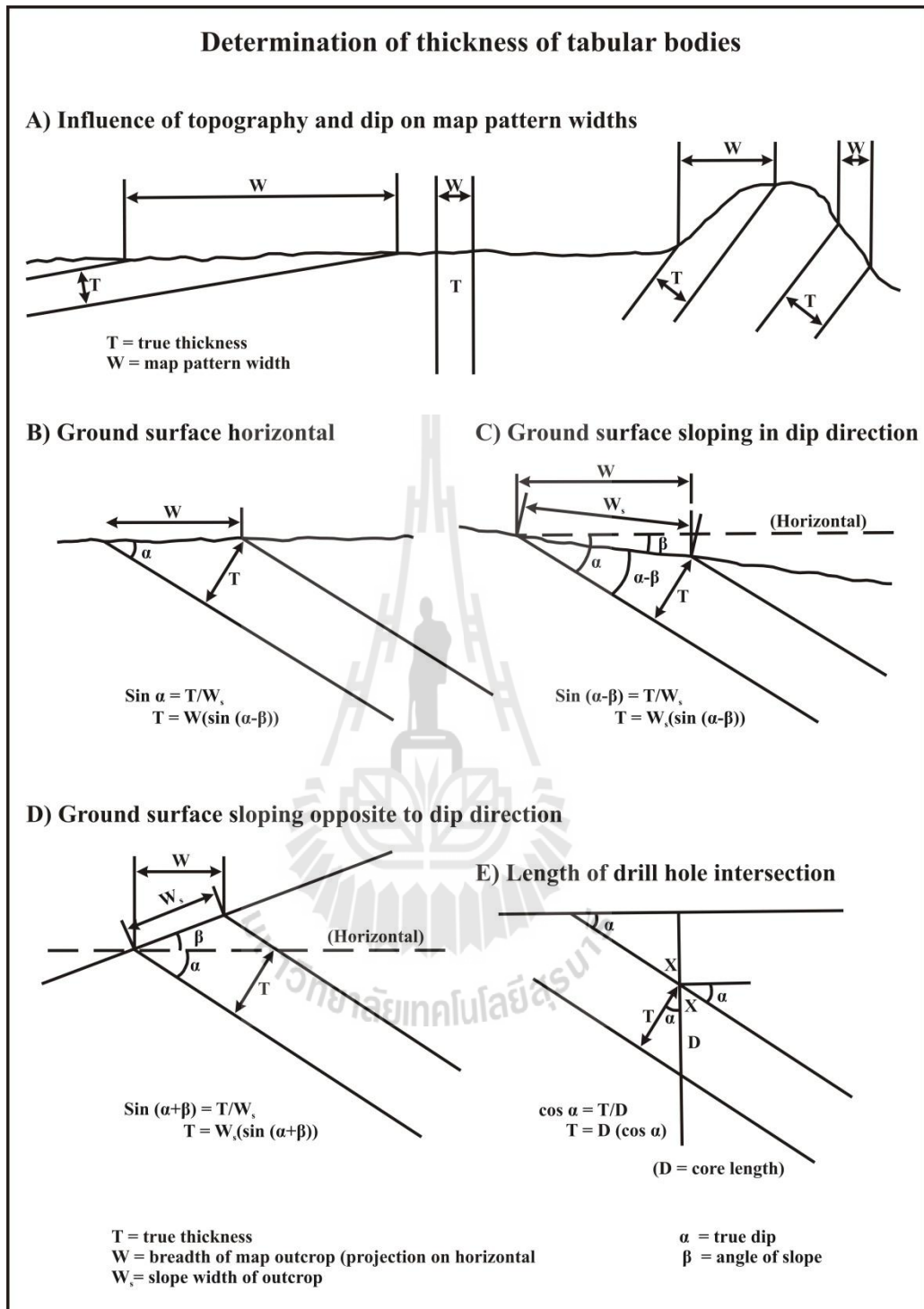


Figure 3.2 Examples of the relationship of the true and apparent thicknesses of stratigraphic units (Lewis and McConchie, 1937).

3.2 Microfossil extraction

The extraction of microfossils was presented the palynology (spores, pollen, acritarchs, and algae etc.) and palynomorph (phytoclast and inertinite). These microfossils were the ancient organic matters preserved in the formation when deposition. Plant and animal microfossils may comprise the substantive quantities of the sand of mud fraction of sediments. They are important indicators of palaeoenvironment (even though the vast majority has been transported from their position in life) and were the predominant indicators of the time of sedimentation (Lewis and McConchie, 1937). These samples were analyzed by using Leica DM550 B microscope (Figure 3.3) at the laboratory of State Key Laboratory of Geological Processes and Mineral Resources, China University of Geosciences (Wuhan).

3.2.1 Microfossil extraction processes

1) Samples were pounded in bean size (high clay content in rock samples can make it thicker), 50 g of each sample was collected and take them to 1000 ml plastic beaker with lycopodium spore tablet for microfossils counting.

2) 500 ml HCl was added with slowly to prevent the acid spilling and stirred. Waited for samples were not dissolved (3-4 days), filled the distilled water and poured out for cleaning (3-4 times and be careful that not to pour the residues out).

3) 500 ml HF was added and stirred every 4-5 hours until the residues is dissolved and after completion should be cleaned with the same as step 2.

4) The residues were taken to big centrifuged tube for first centrifugation about 5-10 minutes. After centrifugation was completed, drain the upper water out, upright tube mouth down on the table, and wait it dry (1 day).

5) The configured solution (specific gravity about 2.2) is added to the big centrifuged tubes, amount of configured solution and residues ratio about 1:1 and stirring. Then centrifuged for 20 minutes, pour the upper part to the small beaker, filled 5% CH_3COOH solution fully and wait for 1 day while suspended remains were settling down.

6) The upper part is poured out, taken all suspended remains into the small centrifuged tubes, and centrifuged again for 5-10 minutes. Then clean them with the same as step 2 also. The last time, the water was drained leaving residue was taken to next step of microscopic analysis.

3.2.2 Configured solution preparations

- 1) Chemical materials are used as HI, Zn, and KI
- 2) Zn is weighed as 80-100 g into the pot and added 500 ml HI. Waiting for 12 hours until the reaction was completed (Zn reaction should not be finished as has a surplus).
- 3) Adding 500 g KI and stirring while dissolved and measuring specific gravity of solution (if greater than 2.0 is available; if only about 1.8, place it on an electrical furnace with slightly heated and measure while KI completely dissolved).
- 4) The solution is filtered and used as the centrifuged solution.

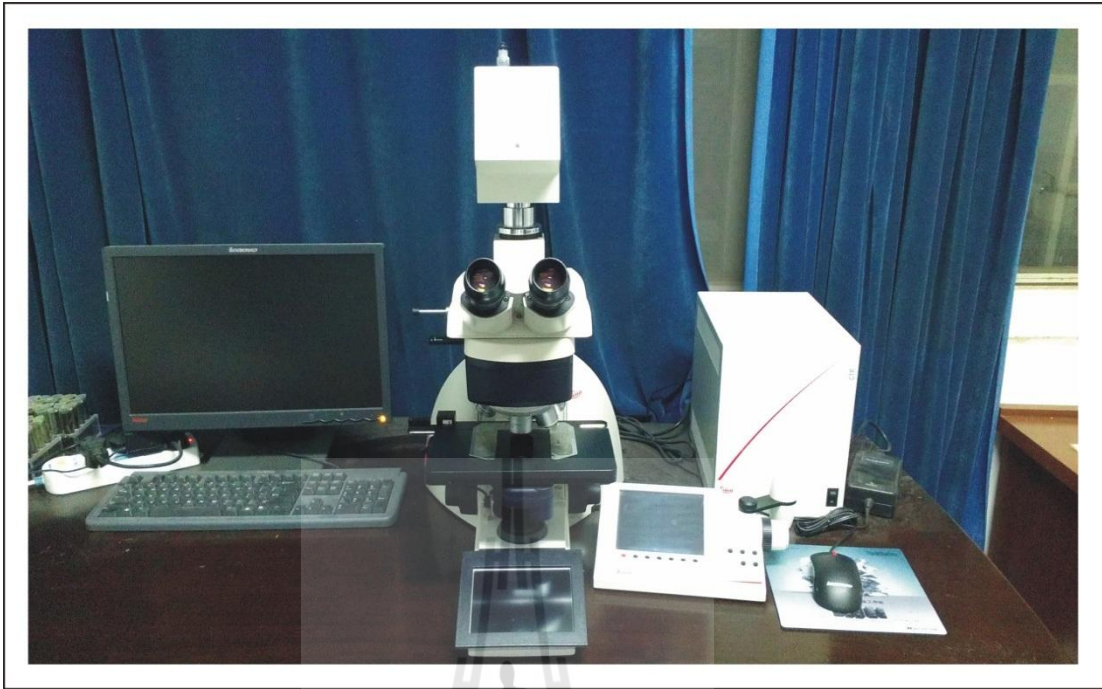


Figure 3.3 Leica DM550 B microscope is using for microfossil identification.

3.3 Geochemical analysis

The geochemical analysis was used to determine the history of rocks especially clastic sedimentary rocks. According to these methods, the author would divide them into 3 parts as elemental, mineral, and hydrocarbon analyses. The composition of clastic sediments is controlled by many complex factors. Although detritus from the sources are rarely interrupted because the path of clastic sediments from the parent rocks to the sedimentary rock basin is composed of several stages, including tectonic movement, weathering, erosion, transportation, and deposition. However, the determination of the palaeoenvironment, palaeoproductivity, palaeoredox, depositional condition, source rock quantity, maturation, and hydrocarbon potential is solved by measurement of the elements that deposited, generated, and recorded in the formation. According to this formation, the

geochemical data is different due to the environment and other factors which have been changed through section. Therefore, these will be made it is clear.

The preparations of samples were trimmed to remove the weathered surface, crushed, and split into small piece of rocks. These rocks were taken to the grinding machine and sieving for powder with 200 mesh sieve. After finish for grinding of each sample, the agate ball mill and agate mortar should be washed before next sample grinding. The washing procedure was started with distilled water and made them dried. Next procedure was cleaned them again with alcohol to prevent the organic matter and microorganism contamination.

3.3.1 Elemental analysis

The certain geochemically immobile major, trace, and rare earth elements were generally accepted as quantitatively transferred into siliciclastic sediments and preserved the record of the average element abundances. According to shale of siliciclastic sediments were concerned and considerable efforts have been made to extract the palaeoenvironment, palaeoproductivity, palaeoredox, and deposited condition information from composition of shale. This information through review of subject was given by Van der Weijden (2002), who suggested identifying the information by using the aluminium normalization. Aluminium normalization of elemental concentrations was useful procedure for the examining the degree of enrichment of an element in sediments and sedimentary rocks. It can be considered as an indicator of the aluminosilicate fraction of the sediments with very little ability to move during diagenesis (Brumsack, 1989; Calvert and Pederson, 1993; Morford and Emerson, 1999; Piper and Perkins, 2004; Tribovillard et al., 2006) as referred to high resistivity. Moreover, these elements should be identified where element source was

forming by Al-Fe-Mn diagram and equivalent to shale standard of PAAS (Post-Archean Australian Shales) by Taylor and McLennan (1985).

3.3.1.1 Major elements

1) Analytical method

Major element was an element in a sample that has an average concentration of greater than 100 parts per million measured in atomic count or greater than 100 micrograms per gram. In other words, it is usually greater than 0.1% of rock composition and mainly consists of SiO₂, TiO₂, Al₂O₃, Fe₂O₃, MnO, MgO, CaO, Na₂O, K₂O, and P₂O₅. These element abundances were measured on fused glass beads by using a XRF-1800 (Figure 3.4) basis on wavelength-dispersive X-ray fluorescence (XRF) analysis at the laboratory of State Key Laboratory of Geological Processes and Mineral Resources, China University of Geosciences (Wuhan) and the laboratory of the 10th fundamental and equipment center, Suranaree University of Technology. The XRF is using the fusion discs as prepared according to the method of Norrish and Hutton (1969).

2) Sample preparation for XRF

2.1) The prepared rock powders were dried by keeping in oven with 105 °C for 4 hours and cleaned the crucibles with pure water and left them dried.

2.2) The samples and compounds were weighed with 0.7000 ± 0.0005 g and 5.0000 ± 0.0005 g respectively, mixed in the ceramic crucible, and placed into Pt-Au crucible with releasing 10 drops of 0.15 g/ml LiBr agent.

2.3) Putting the Pt-Au crucible with the mixture into the high frequency melting furnace to make glass disk. Waiting for completely melt and

placed into the mold and swirled for level off. When it was cool, the flat-surfaced disc will be forming and transfers to the XRF for major element identification.

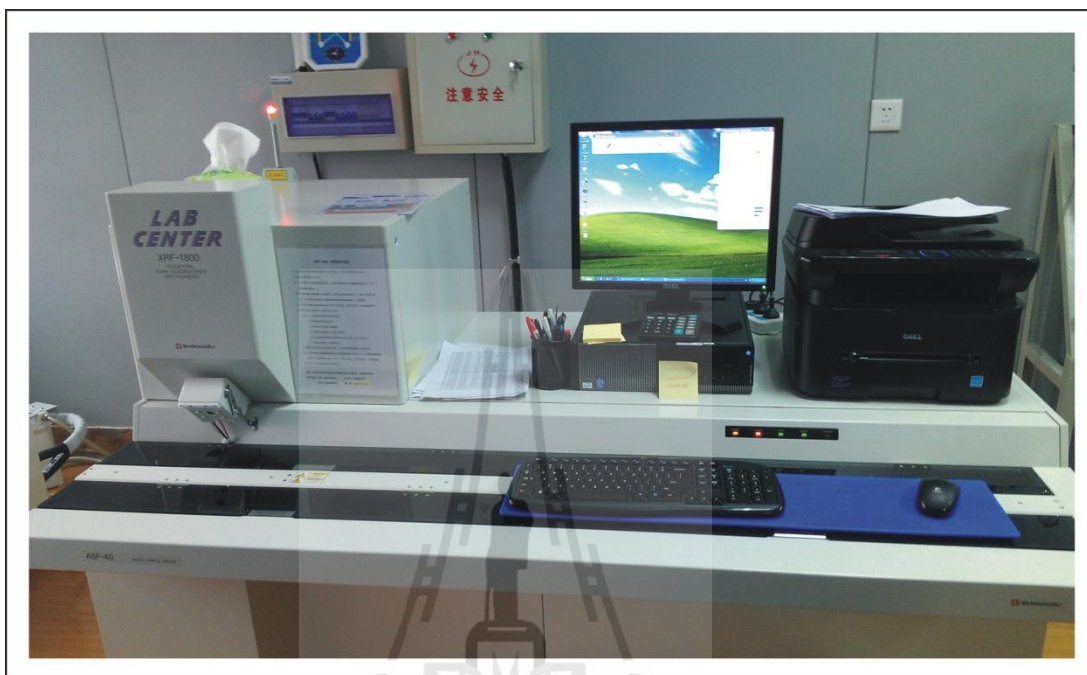


Figure 3.4 XRF-1800 based on wavelength-dispersive X-ray fluorescence (XRF) analysis for measured element abundances on fused glass beads.

3.3.1.2 Trace elements and rare earth elements

1) Analytical method

Trace element was an element in a sample that has an average concentration of less than 100 parts per million measured in atomic count or less than 100 micrograms per gram. In other words, it is usually less than 0.1% of rock composition. Rare earth elements were group of 17 chemical elements in the periodic table, comprising Scandium, Yttrium, and the 15 Lanthanides of Lanthanum, Cerium, Praseodymium, Neodymium, Promethium, Samarium, Europium,

Gadolinium, Terbium, Dysprosium, Holmium, Erbium, Thulium, Ytterbium, and Lutetium which less minor amount percentage of rock composition. Both trace elements and rare earth elements were analyzed by inductively coupled plasma mass spectrometry (ICP-MS) at a Key Laboratory of Biology and Environmental Geology of the Ministry of Education, China University of Geosciences (Wuhan) for the Ban Nong Sai samples. And the Dat Yai samples were tested in laboratory of Wuhan Comprehensive Rock and Mineral Analysis Center, Ministry of Land and Mineral Resources of Wuhan University.

2) Sample preparation for ICP-MS

2.1) The sample is crushed to powder and weighed as 50 mg to a Teflon bomb.

2.2) The sample is moistened with a few drops of ultrapure water and followed by adding of 1 ml HNO₃ and HF.

2.3) The sealed bomb was heated at 190 °C in oven for 48 hours.

2.4) After cooling, the bomb was evaporated at 115 °C to incipient dryness. Then adding 1 ml HNO₃ and evaporating to the second round of incipient dryness.

2.5) The resultant salt was re-dissolved by adding 3 ml of 30% HNO₃, resealed, and heated in the bomb at 190 °C for 12 hours.

2.6) Finally, the final solution was transferred to a polyethylene bottle and diluted to 100 g (corresponding to a dilution factor of 2,000) with mixing with 2 % HNO₃ for ICP-MS analysis.

3.3.2 Mineralogical analysis

1) Analytical method

Apart from the naked eye and the microscope, X-ray diffraction (XRD) was the most widely used technique for mineral identification, particularly for minerals of very small size. In addition to mineral identification, XRD studies can also provide information on the degree of disorder in minerals, crystal size, and other characteristics of mineral crystals. The XRD technique was also used in conjunction with other instruments for determination of multiple properties (Veblen et al., 1990; Lewis and McConchie, 1937). The result of mineral identification was described and determined the rock-forming minerals in samples. The most mineral group will be let us known their physical properties and behaviors. These characteristics can be predicted to the reservoir properties as forming microfractures or microcracks. These features were generated from natural event as tectonic in the region and hydraulic fracturing when well drilling. More minerals of silica group were referred to brittle property as performed more fractures both natural and fracturing process. The samples were identified by using an X'Pert PRO Dy 2198 (Figure 3.5) basis on X-ray diffraction analysis at the laboratory of State Key Laboratory of Geological Processes and Mineral Resources, China University of Geosciences (Wuhan) and Center for Scientific and Technological Equipment, Suranaree University of Technology.

2) Sample preparation for XRD (Lewis and McConchie, 1937)

2.1) Samples for powder diffraction studies must be finely grounded less than 5 μm and completely homogeneous (coarse particles in the sample will be substantially reduce peak-to-background ratios and will produce diffraction patterns with abnormal peak in density ratios).

2.2) The prepared rock powders were usually prepared for analysis either as a thin smear (by mixing the sample with a small volume of alcohol) on the glass slide (half a microscope slide) or by packing the powder into the well about 2 mm deep of sample holder designed to fit into the goniometer. When an autosample changer was used, sample holders compatible with the sample changer must be used.

2.3) The packing samples that may contain the platy minerals (clay) into a sample holder, mineral grains may become preferentially oriented relative to the top of the holder. Whether some grains have a preferred orientation in the sample or the assemblage was randomly oriented was not usually a problem in mineral identification but oriented grains will enhance peak-intensity ratios (the 001, 002, 003, etc. peak for phyllosilicate minerals will be selectively enhance if the grains were oriented with their c axis normal to the surface of the sample).

2.4) For clay minerals studies, there were advantages in deliberately orienting the clay particles (by settling samples from a fluid onto the glass slide). Additional information can be obtained by pretreating samples by examples by exposure to an atmosphere of ethylene glycol and/or firing them to 550 °C. A very readable discussion of sample preparation procedures and problems can be found in Bish and Reynolds (1989).



Figure 3.5 X'Pert PRO Dy 2198 basis on X-ray diffraction analysis for measurement the mineral results.

3.3.3 Hydrocarbon analysis

3.3.3.1 Total organic carbon (TOC)

1) Analytical method

The total organic carbon method was used to determine the concentration of total organic carbon in sediments or in soil samples and the inorganic was removal by digestion in hydrochloric solution. Estimation of the organic carbon content by measuring the weight loss on firing the sample to temperature above 550 °C and the organic will be combusted between 450-550 °C by using combustion in an atmosphere of oxygen in either an induction or an equivalent high-temperature furnace (Lewis and McConchie, 1937). The samples were identified by using a Liqui TOC (Figure 3.6) basis on thermal inductivity method at State Key Laboratory of Biogeology and Environmental Geology of Ministry of Education, China University of Geosciences (Wuhan).

2) Sample preparation for TOC

2.1) Dried powder samples were weighted for 100 mg, taken to 100 ml erlenmeyer flask, and mixed with a few drop of water, 10 ml of 0.1 mol/L hydrochloric acid solution for removal the inorganic carbon especially carbonate from the sample.

2.2) Mixed sample was placed to the 80 °C water bath, heated for 15-20 minutes, removed to the 50 ml centrifuge tube, and centrifugation.

2.3) The completed centrifuge tube was poured the upper liquid out, added 50 ml of water, stirred, and centrifuged. The remaining sediments (after poured out the upper liquid) were heated dry with 80 °C and crushed to powder for next combustion furnace.

2.4) The dried powder sample was taken to the combustion furnace with the temperature about 960-970 °C due to the most organic matter will combust between 450-500 °C. When the standard substance in the organic carbon content is less than 1%, it was measured absolute error of the result to be controlled within 0.2%.

2.5) Measured data of the organic carbon content of the dried powder sample, the detector sensitivity coefficient (KC), the value of detection signal, the weight of the sample, and the calculation as follows:

$$W_{oc} = \frac{S}{K_c \frac{W_1}{1-C} (1 - W_{H_2O})} \times 100 \% \quad (3.1)$$

Where;

- W_{OC} = The organic carbon content of dried powder samples, %
- S = The total value of the signal
(reading value - blank value-zero readings), mV
- K_C = The detector sensitivity coefficient (per mg of the standard substance of organic carbon detector response signal values), mV/mg
- W_1 = The amount of the acid-treated sample, mg
- C = The percentage content of carbonate in the sample, %
- W_{H_2O} = The dried sample moisture content, %



Figure 3.6 Liqui TOC instrument based on thermal inductivity method for TOC identification.

3.3.3.2 Vitrinite reflectance (R_o)

1) Analytical method

Vitrinite reflectance compliments are a means of optically measuring changed in kerogens by using the reflectance microscope (Figure 3.7). It was measured the fraction of incident light reflected from the polished surfaces of woody fragments (vitrinite). This was an optical technique for determining maturity, industry accepted, and generally regarded as the most reliable technique for measuring maturity. However, there were many situations where this technique cannot be used, situations where the data could be unreliable, and there were many pit-falls with the technique. So these reasons are no one technique should be used exclusively. According to vitrinite determination was became a skilled operation to both distinguish maceral of autochthonous and allochthonous vitrinite. It was the autochthonous or primary vitrinite that measurements should be made on and the values were derived from primary vitrinite that should be recorded. False values of maturity will result if unsuitable particles are measured (Matchette-Downes, 2009). The samples were identified by using a Leica MSP200 Light Microscope at the Petroleum Geologic Test Center, Petroleum Exploration and Development Research Institute of Jiangnan Oilfield Company (SINOPEC).

2) Sample preparation for R_o

2.1) The powder samples were sieved to selected particles with the size between 63 μm to 1 mm. Each sample was collected for 2-3 g, taken into the resin mold with epoxide resin, hardener at a ratio of 10:1, and then mixed (Khositchaisri, 2012).

2.2) The mixed sample was left for 24 hours while it settled, moved out the mold. The resin block was polished with fine silicon carbide powder until the surface of the sample became smooth and cleaned with water. Then, the resin block was polished again with finer polishing agent until the sample surface smoother (Khositchaisri, 2013).

2.3) The smooth resin block was checked by using the reflected light of reflectance microscope with appropriated value of standard reflectance calibration value. Typically a geochemist will be looking at vitrinite of reflectances in the range R_o 0.3% to 1.5%. A useful standard might be an artificial Sapphire with a reflectance of R_o 0.504%. Other standards should include glass (various values) or Yttrium Aluminium Garnet (0.917%) or diamond (3.314%) as suggested by (Matchette-Downes, 2009).

2.4) If the signal from the photomultiplier is sent to a chart recorded. Then a series of peaks will be recorded for the sample and the standard corresponding to each measurement (Matchette-Downes, 2009).

$$R_{o_{sample}} (\%) = \frac{D_{sample}}{D_{standard}} \times R_{o_{standard}} \quad (3.2)$$

Where;

R_o (%) = Reflectance in oil

D = Deflectance of pen recorder

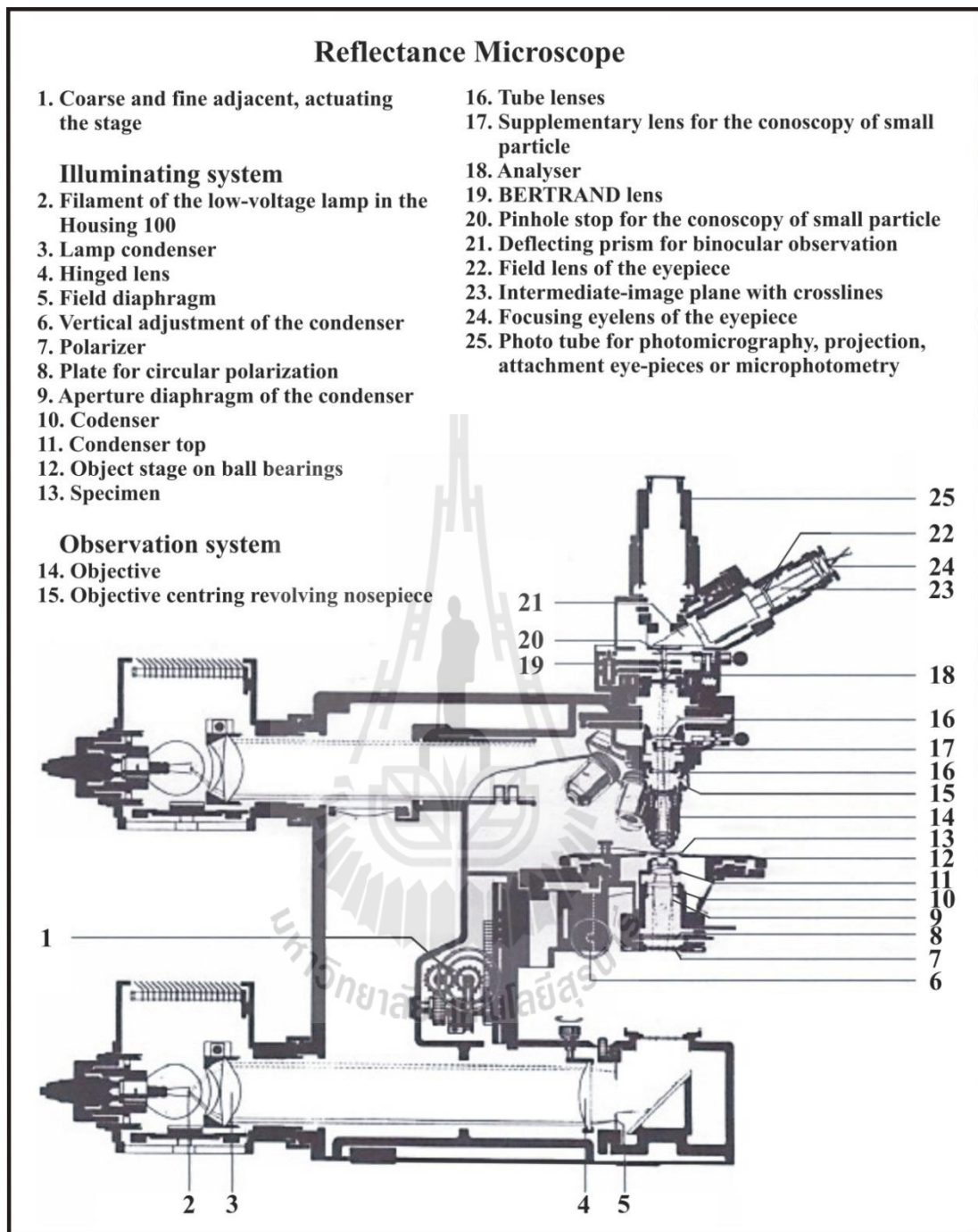


Figure 3.7 Reflectance microscope and the description of its implements to identify the vitrinite reflectance of rock samples (Matchette-Downes, 2009).

3.3.3.3 Rock-Eval pyrolysis

1) Analytical method

This technique evaluates oil and gas shows, oil and gas generation potential, thermal maturity, and identifies the organic matter type (Tissot and Welte, 1978; Peters, 1986; Espitalie et al., 1985; Behar et al., 2001; Unfiled report, 2011), widely used method of rapidly evaluating the quality, and thermal maturity of prospective petroleum source rocks (Espitalie et al., 1977, 1984; Clementz et al., 1979; Tissot and Welte, 1984; Peters, 1986; Stanley et al., 1992). The procedure mimics in some respects, the natural hydrocarbon-generation processes are occurred at much slower rates within the earth when sediments containing kerogen (sedimentary organic matter). Then they were buried progressively deeper and subjected to higher temperatures (Waples, 1985; Stanley et al., 1992). Besides, software was developed for description of pyrolysis kinetics by using the rock-Eval measurements (Johannes et al., 2006). The samples were identified by using a Rock-Eval 6 basis in value of S_1 , S_2 , S_3 , and T_{max} (Figure 3.8) on pyrolysis kinetics method at the Petroleum Geologic Test Center, Petroleum Exploration and Development Research Institute of Jiangnan Oilfield Company (SINOPEC).

2) Sample preparation for rock-Eval pyrolysis

2.1) The samples were crushed in the mortar, weighed 100 mg of crushed sample into a platinum crucible, cover was made from sintered steel, and analysed on a rock-Eval pyrolysis (Krokstad et al., 1986).

2.2) The crushed sample was held at 250 °C for 3 minutes (the isothermal period), the S_1 parameter was measured free or adsorbed hydrocarbons volatilized at 250 °C of moderate temperatures (Stanley et al., 1992).

2.3) Then gradually heated from 250 °C to 600 °C at 25 °C per minute in an oxygen-free atmosphere, S_2 was measured the hydrocarbons liberated during a ramped heating, and S_2 was the amount of hydrocarbons generated by pyrolytic degradation or cracking. The T_{max} is the temperature, generally about 400-500 °C at that S_2 was a maximum and regarded as a rough indicator of thermal maturity (Stanley et al., 1992). The kinetic study based on the temperature pattern, the integration ranks, and the parameters defined for the basic method while different heating rates for pyrolysis (1, 2, 5, 10, 15, 20, 25 °C/min) were programmed. As the results, distribution of activation energies (E_i) for multicomponent parallel reactions and the computed values of frequency factor (A_i) can be obtained (Johannes et al., 2006).

2.4) The S_3 parameter was measured the amount of organic CO_2 and CO . It generated from the kerogen during rapid heating (250-390 °C at 25°C/min) or pyrolysis and was thought to be related to the amount of oxygen in the pyrolyzed organic matter (Stanley et al., 1992).

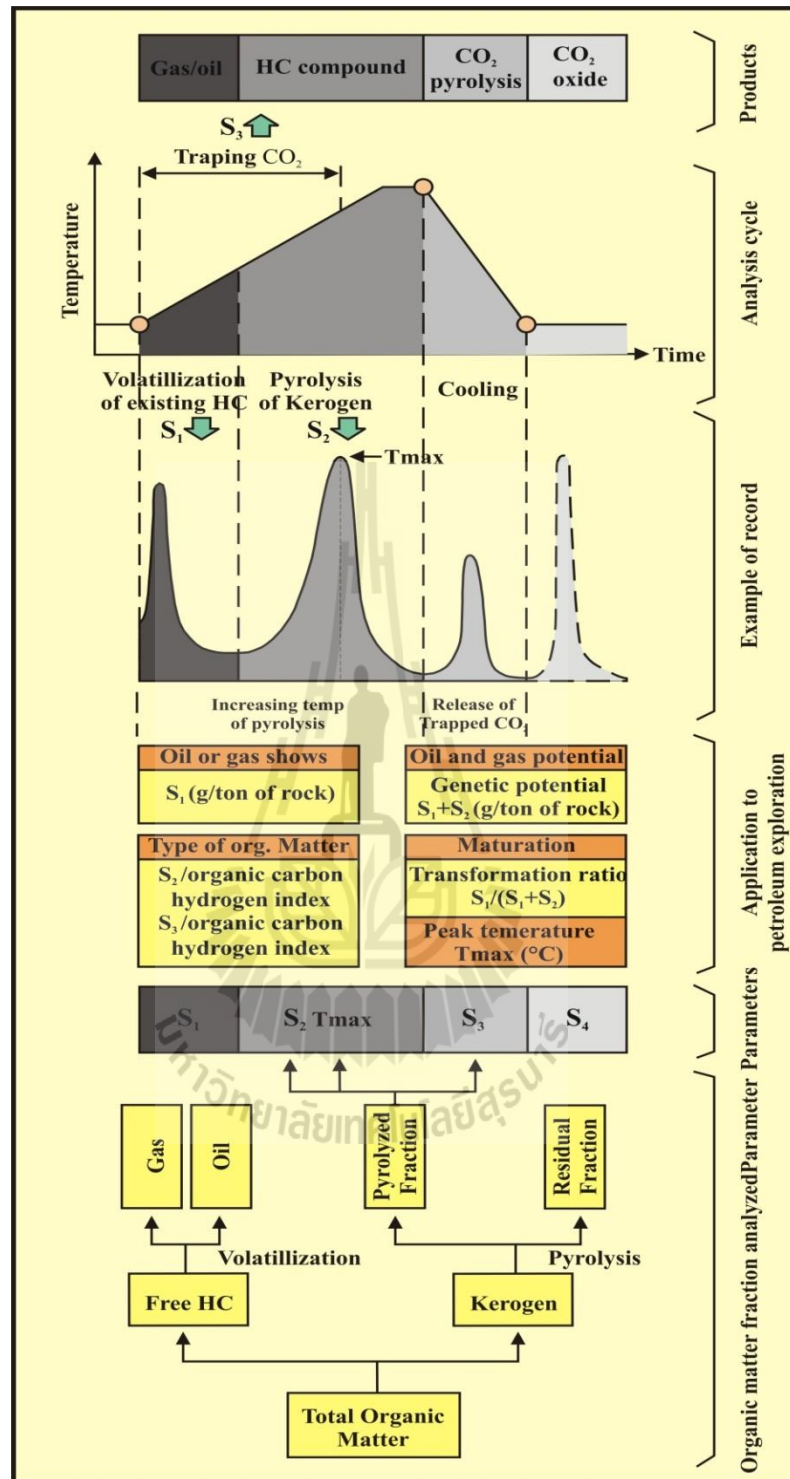


Figure 3.8 General diagram showing the different fractions of the total organic matter of analyzed rocks, the corresponding parameters and their recordings (after Tissot and Welte, 1978; Khashayar, 2010).

3.4 Physical property analysis

3.4.1 Scanning Electron Microscope (SEM)

1) Analytical method

Scanning electron microscopes became available in 1965 because SEM analysis permits nondestructive magnification of surface normally from 50x up to 100,000x or more. It has been applied to a wide variety of studies since that time. SEM principles were well presented in Nixon (1969) and Smart and Tovey (1982). Essentially a metal specimen stub was coated with an adhesive. The samples were mounted on the stub and thinly coated with the conducting metal under vacuum and the stub plus sample was inserted in a vacuum chamber of the SEM and bombarded with electron. SEM studies probably the best known geological application has been in the area of quartz-grain surface texture (Krinaley and Doornkamp, 1973) but there are a magnitude of studies ranging to pores and fractures in rocks. The coating applied to grains and rock surfaces for SEM analysis were generally too thin to interfere with optical microscope analyses (Lewis and McConchie, 1937). Therefore, the same specimen maybe used even with transmitted light petrographic microscopes. The samples were identified by using a Quanta 200 (Figure 3.9) at the laboratory of State Key Laboratory of Geological Processes and Mineral Resources, China University of Geosciences (Wuhan).

2) Sample preparation for SEM (Lewis and McConchie, 1937)

2.1) Samples were prepared in 3-10 mm thick and chipped the surface to be examined; the surface must be cleaned and dried. The initial of preparation should be mind of contamination and preparation-caused development of abnormal relief, tension or compressional fractures.

2.2) Applied glue to stub surface, leaving a small area clear for labeling and having a label on the top of the stub was invaluable when working under SEM. Specimen was placed on the surface, orienting as requiring if it is irregularly shaped. If multiple small specimens were to be viewed and ensure that the adhesive did not cover the upper surfaces.

2.3) Stubs were placed in desiccator with fresh silica gel until ready to view and coated with conducting medium (generally gold or carbon, 100-500 angstrom thick) and examined. The coating was provided a conductive path to the stage and thereby to earth, preventing excessive electron charge buildup. It was assisted secondary electron generation for the improved resolution and provided greater thermal conductivity for preventing uneven heat-generated expansion of the specimen.

2.4) The coating device was a vacuum chamber attached to a nitrogen source, in which high-voltage generates a cloud of the coating substance. Details of the device used and thickness of the coating vary depending on the equipment available, the nature of the specimen, and the method of SEM examination. If the specimen was highly porous, two stages of coating were required on a special stub holder.



Figure 3.9 Quanta 200 is using for identification the microscopic images.

3.4.2 Micro computed tomography (Micro-CT)

1) Analytical method

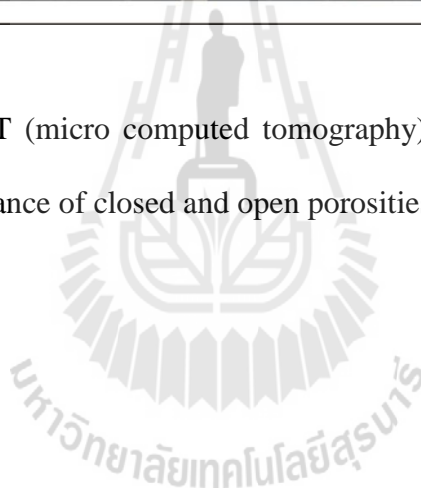
Micro-CT can be applied for the visualization of the inner structure of a material or biological tissue in a non-destructive manner. Besides visualization, image analysis was an important topic in micro-CT to obtain quantitative parameters from scanned datasets. A parameter that was often evaluated was porosity and porosity network especially open and closed porosity were related to number parameters of pores and pore volume. This application was performed by using Micro-CT method of Skyscan 1172 (Figure 3.10) at the State Key Laboratory of Biology and Environmental Geology of the Ministry of Education, China University of Geosciences (Wuhan). For more understanding, the sample reconstruction under instrument is analyzed and generated the precisely performed images of internal features and minerals by DataViewer software.

2) Sample preparation for Micro-CT

Samples were cut where without impurity compositions into sub-cores. The sub-cores were trimmed to a width of 1.0-1.5 mm and 5.0 mm in length. The imperfect cylindrical rock samples were scour by very fine sand paper. The sample size and shape were dictated by the size and limitations of the micro-CT instrument used in this work. The projections are obtained by placing the object. For this research the cylindrical rock samples were lightly coated and putted on a rotating stage between an X-ray point source and a detector. The X-ray source voltage and current settings were at 62 kV and 161 μ A. The optimal choice of current and voltage used were determined from empirical data and calculations based on parameters from the XCOM database (Berger et al., 2010, Agbogun, 2011).



Figure 3.10 Micro-CT (micro computed tomography) Skyscan 1172 is applied for performance of closed and open porosities.



3.5 Visual petrographic analysis for kerogen types

1) Analytical method

The visual kerogen analysis was a basis of identified organic matters that preserved in the formation while deposition. The amount of them was let us known the volume and type of them, depended on their palaeoenvironment. The environment may change or not, it will be identified by using the organic matter recording and their types. According to this analysis, it will separate the kerogen from the rock matrix and identify the kerogen composition which was reported in percentage of contribution. The type of kerogen was performed into 4 mainly in type are amorphinite, exinite, vitrinite, and inertinite. Moreover, oil or gas of hydrocarbon that preserved was depended on each type of kerogen. These types were performed and identified in laboratory of Petroleum Geologic Test Center, Petroleum Exploration and Development Research, Institute of Jiangnan Oilfield Company (SINOPEC).

2) Sample preparation for kerogen types

The organic matters were isolated from the rock sample; these isolated organic matters (kerogen) are put on a glass slide, identified and point counted into percentage of each type under a high powered microscope (Khositchaisri, 2012).

CHAPTER IV

STRATIGRAPHIC RESULTS

The Huai Hin Lat Formation consists mainly of fine-grained clastic rocks which has more potential on petroleum source and reservoir rocks. It should be studied in detail for more understanding in petroleum system. It is recognized appropriated stratigraphic sections for further petroleum evaluation.

4.1 Measured stratigraphic sections

For this study, two areas are selected for detailed study which is located in the Sap Phlu Basin and the Na Pho Song Basin. Details of all studied sections of both areas will be described as follows:

4.1.1 Sap Phlu Basin area

It is composed of the Ban Nong Sai, Southern Sap Phlu, Northern Sap Phlu, Khao E-Dang, and Wat Tham Nong Sai sections. They will be described below.

4.1.1.1 Ban Nong Sai section

This measured stratigraphic section is located between Ban Nong Sai and Ban Khlong Maung, Khlong Maung sub-district, Pak Chong district, Nakhon Ratchasima province at Km 28+050 along the rural road No. 2048 (Pak Chong-Wang Nam Khiao). At the location of 47P 785346 N and 1619790 E on the Royal Thai Survey Department, topographic map sheet WGS 84, series L7018, 5338 III, Ban Sap Noi, scale 1:50,000. The studied location is approximately plotted in Figure 4.1.

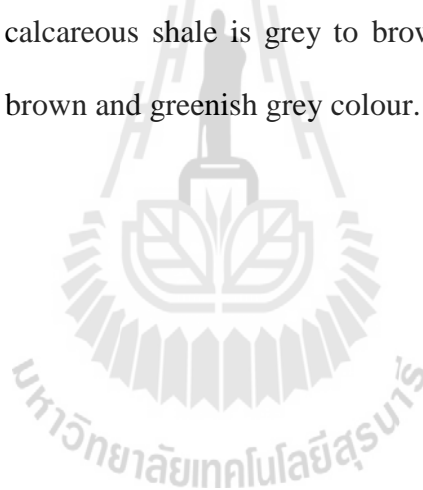
The Huai Hin Lat Formation of the Sap Phlu area has been the subject to the earlier lithostratigraphic study and mapping (DMR, 2007). But it has not previously been investigated geochemically except for a few source rock quality data (Sattayarak et al., 1996). The section (Figures 4.2 and 4.3) is approximately 14 m thick and consists mainly of calcareous shale, calcareous mudstone, marlstone, and limestone. The section can be lithostratigraphically subdivided into 3 parts, i.e. the lower part (Beds 1-7), the middle part (Beds 8-12), and the upper part (Beds 13-20).

The lower part, Beds 1-7, is mainly light grey to black calcareous shale. It is massive and highly resistant beds except Bed 3 which is thin-bedded, approximately 6-10 cm thick, and can be differentiated into 3A-3D. These beds are orientated in the NW-SE direction and have gently dipping approximately 10-15 degrees. They are conformable to the lower part of the Khorat Group. Beds 1, 6, and 7 contain well-preserved *Estheria* sp. Mud cracks can be observed on Beds 1, 3, and 4. They indicate a desiccation in a sunny or an arid condition. The calcareous shale beds are in places characterized by abundant pyrite crystals and spheres. Love (1962) and Vallentyne (1962) concluded that the pyrite spheres in dark colour sediments appear to be the product of early diagenesis in an anaerobic environment. The weathered calcareous black shale is generally grey to brownish grey.

The middle part, Beds 8-12, is composed mainly of light grey to grey marlstone or muddy limestone and dark grey to grey limestone. They are thick-bedded and extremely resistant especially in the limestone beds. They are gently dipping 15-18 degrees and are conformable with the lower part. The calcareous shale and mudstone normally grade into marlstone. Much of the calcite in

these calcareous sediments is extremely fine-grained and there is a few evidence of recrystallization. The limestone is well-bedded, consisting of a high percentage of clay which grades to the argillaceous limestone. Graded-bedding and cracks filled with small calcite crystals have been observed in Bed 9.

The upper part, Beds 13-20, mainly comprises greenish grey to black calcareous mudstones and light grey to black calcareous shale. The beds are also gently dipping (12-13 degrees). The calcareous shale beds are higher resistant than the mudstone beds but they are less resistant than the shale beds of the lower part. Beds 15 and 17 contain *Estheria* sp. The calcareous shale of both lower and upper parts is similar. The calcareous shale is grey to brownish grey and the calcareous mudstone is yellowish brown and greenish grey colour.



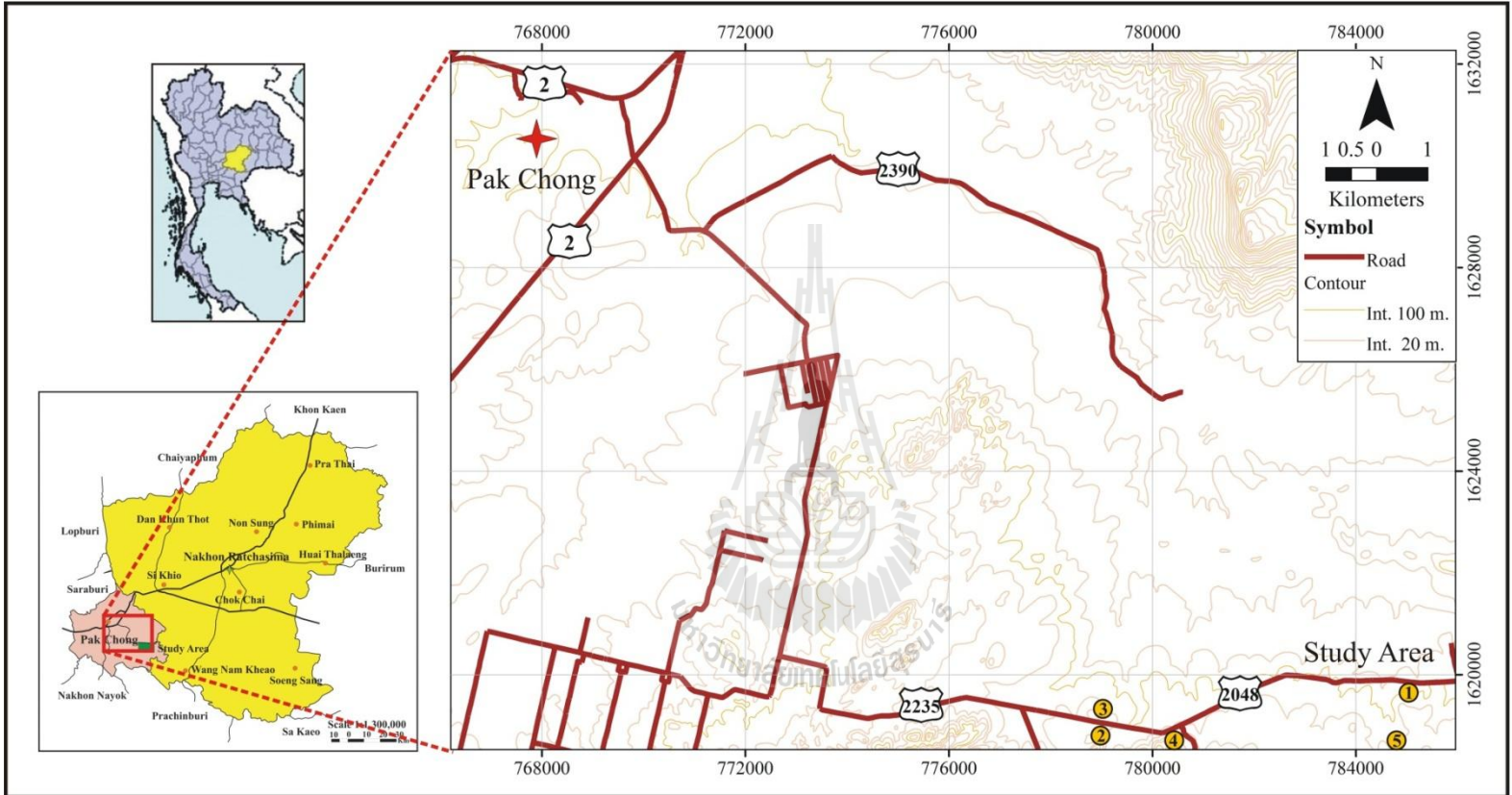


Figure 4.1 The locations of the studied sections in the area of the Sup Phlu Basin in Pak Chong district, Nakhon Ratchasima province, including the Ban Nong Sai section (1), the Southern Sup Phlu section (2), the Northern Sap Phlu section (3), the Khao E-Dang section (4), and the Wat Tham Nong Sai section (5).



Figure 4.2 Field investigation of the Ban Nong Sai section (47P 785346 N and 1619790 E) showing the lower (top left), middle (top right), and upper sections (bottom). Men as scale were looking east.

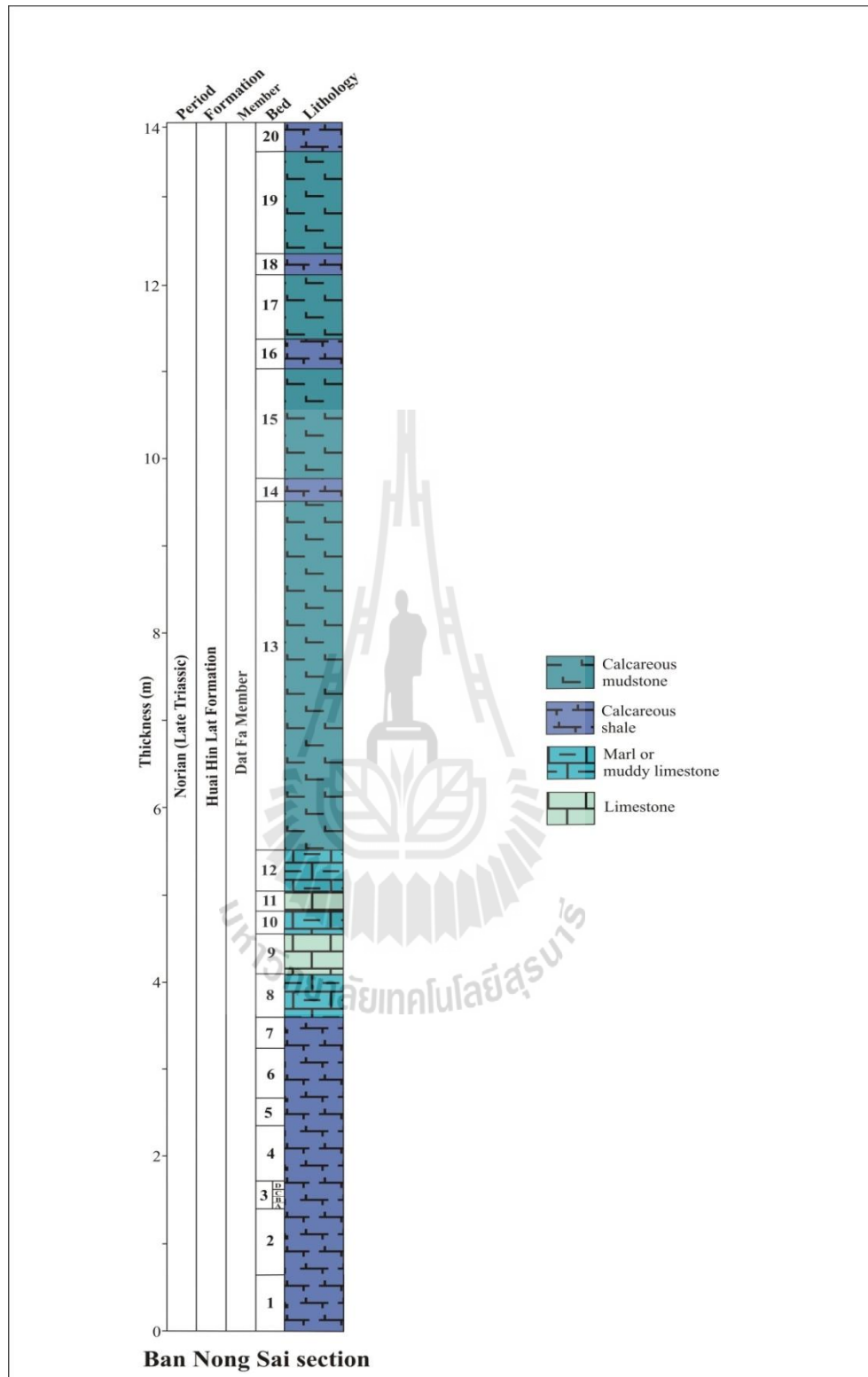


Figure 4.3 Stratigraphic column of the Ban Nong Sai section of the Huai Hin Lat Formation in the Sap Phlu Basin area.

4.1.1.2 Southern Sap Phlu section

This measured stratigraphic section is situated in Ban Sap Phlu, Khlong Maung sub-district, Pak Chong district, Nakhon Ratchasima province at Km 23+400 along the rural road No. 2048. It is located at 47P 779126 N and 1618940 E on the Royal Thai Survey Department, topographic map sheet WGS 84, series L7018, 5338 III, Ban Sap Noi, scale 1:50,000. The studied location is approximately plotted in Figure 4.1.

The Southern Sap Phlu section of the Sup Phlu Basin has also been a subject to earlier lithostratigraphic study and mapping. The section, (Figures 4.4 and 4.5) approximately 24 m thick, consists mainly of calcareous shale interbedded with marlstone and calcareous sandstone. It can be lithostratigraphically subdivided into 3 parts, i.e. the lower part (Beds 1-17), the middle part (Beds 18-19), and the upper part (Bed 20).

The lower part, Beds 1-17, is mainly calcareous shale and marlstone or muddy limestone and some beds comprising calcareous shale as interbedded with marlstone. The calcareous shale beds are light to black in colour. They clearly show laminated beds of 0.5-1.0 cm that are very brittle and very poor preservation. The marlstone beds are light to grey in colour. The calcareous shale normally grade into marlstone in Beds 7 to 8 and Beds 9 to 10. They are tight and highly resistant with thickness from a few centimeters to up to forty centimeters. These beds are orientated in the NW-SE direction and are varying in dipping (approximately 10-70 degrees from the lower to upper parts). They are conformable to the lower part of the Khorat Group. Beds 1-3 contain well-preserved *Estheria* sp.

Mud cracks are observed at the bottom of Bed 1 which indicates a sunny or an arid condition.

The middle part, Beds 18-19, consists mainly of black calcareous shale. They are laminated beds of 0.2-0.5 cm, low resistant, brittle, and very poor preservation. Bed 18 contains sandstone beds of 1.0-1.5 cm thick in the middle part interbedded with calcareous shale. They are well-bedded with high dip of 60-70 degrees that are conformable to the lower part. The upper part, Bed 20, is mainly composed of calcareous shale and calcareous sandstone. The calcareous shale is black in colour and shows laminated beds of 0.2-0.5 cm. The calcareous sandstone is light black in fresh colour and yellowish brown in weathered colour. The calcareous shale beds have lower resistance than the calcareous sandstone which is similar to the middle part. These beds also dip steeply of 70 degrees. The intervals where associated with the calcareous sandstone, they can be indicated to the fluvial sediments of the shallower environment. They mean that the section is became shallower in ascending and became deeper in the uppermost part. However, they are not too thick and interbedded with calcareous shale but less meaning in tectonic event.



Figure 4.4 Field investigation of the Southern Sup Phlu section (47P 779126 N and 1618940 E) showing the poorly preserved outcrop. Man as scale was looking the northwest.

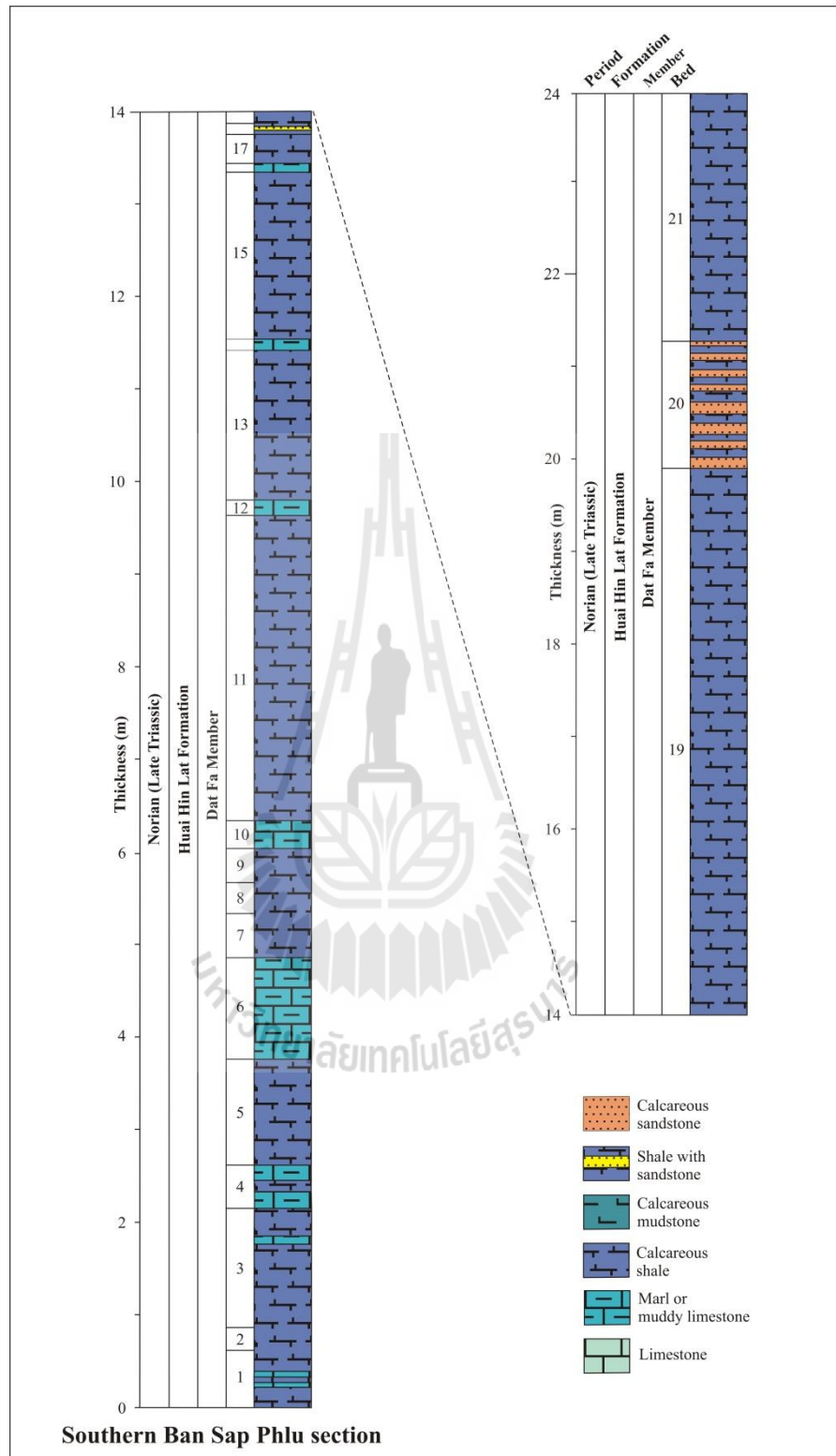


Figure 4.5 Stratigraphic column of the Southern Ban Sap Phlu section of the Huai Hin Lat Formation in the Sap Phlu Basin area.

4.1.1.3 Northern Sap Phlu section

This measured stratigraphic section is located in Ban Sap Phlu, Khlong Maung sub-district, Pak Chong district, Nakhon Ratchasima province at Km 23+400 along the rural road No. 2048. At the location of 47P 779011 N and 1619179 E on the Royal Thai Survey Department, topographic map sheet WGS 84, series L7018, 5338 III, Ban Sap Noi, and 1:50,000 in scale. The studied location is approximately plotted in Figure 4.1.

The section (Figures 4.6 and 4.7) is approximately 10.5 m thick consisting mainly of calcareous mudstone, calcareous shale, and marlstone. The section can be lithostratigraphically subdivided into 3 parts, i.e. the lower part (Beds 1-3), the middle part (Beds 4-12), and the upper part (Beds 13-21).

The lower part, Beds 1-3, is mainly composed of marlstone or muddy limestone. It is massive and highly resistant with light grey in fresh colour and greenish to yellowish brown in weathered colour. They are composed of argillaceous limestone which shows spheroidal weathering and contains wood fragments. Mud cracks are preserved at Bed 3. It indicates a desiccation in a sunny or an arid condition. These beds are orientated in the NW-SE direction with gentle dipping of approximately 20 degrees.

The middle part, Beds 4-12, comprises mainly calcareous shale and calcareous mudstone. It has light grey colour in Beds 4, 11, and 12, while other beds are black to dark black. The calcareous shale is thin beds, approximately 2.5 cm. The bed thickness of calcareous mudstone is thicker. They are gentle dipping of 15-20 degrees and are conformable to the lower part. The upper part, Beds 13-21, is mainly composed of light to dark black calcareous mudstone. The beds are also

gentle dipping (15-25 degrees). Mud cracks are preserved in Bed 15 which also indicates the same condition as the lower part.





Figure 4.6 Field investigation of the Northern Sap Phlu section (47P 779011 N and 1619179 E) showing the poorly preserved outcrop along hill. Hammer handles are in the NW direction.

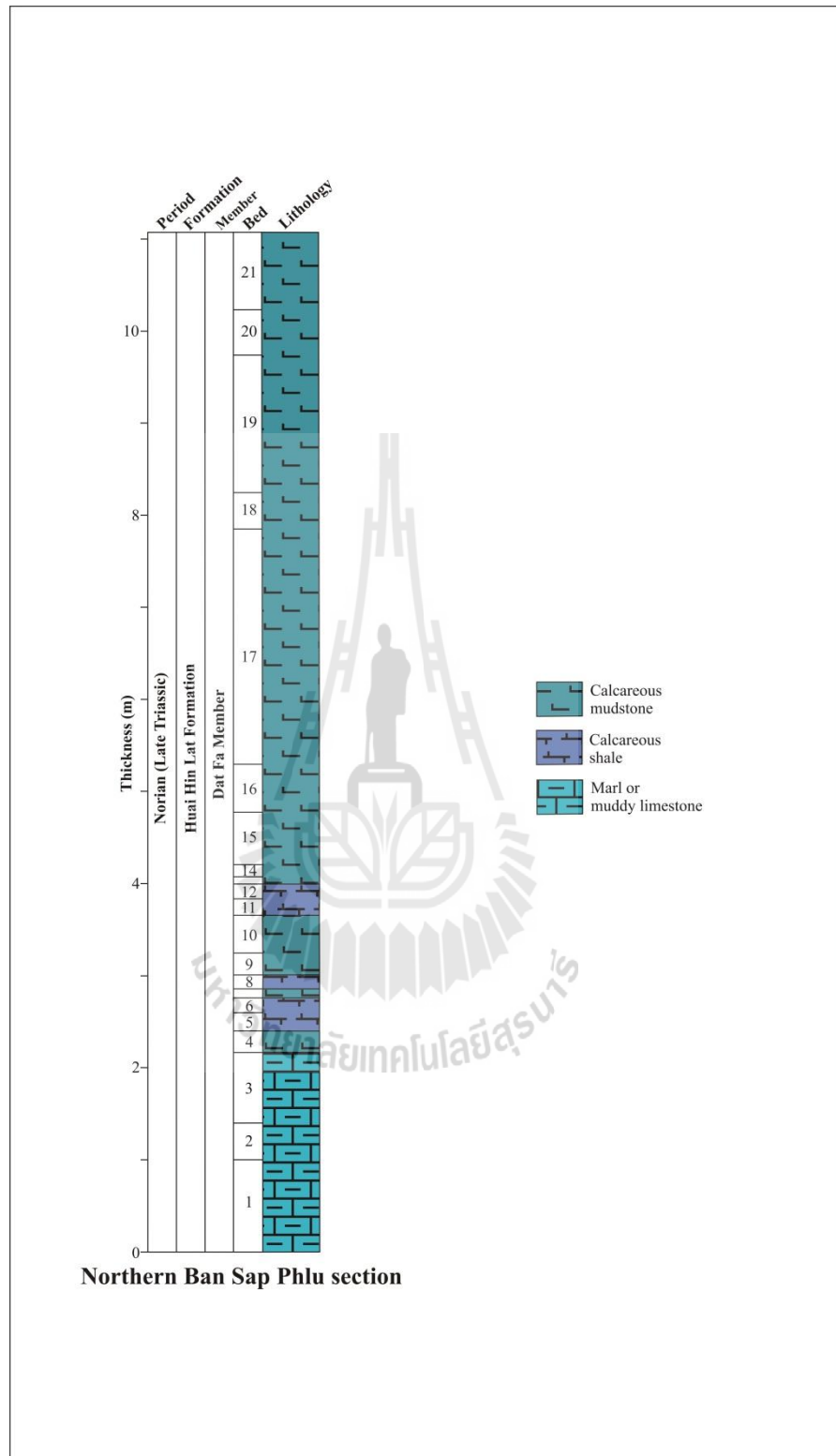


Figure 4.7 Stratigraphic column of the Northern Ban Sap Phlu section of the Huai Hin Lat Formation in the Sap Phlu Basin area.

4.1.1.4 Khao E-Dang section and Wat Tham Nong Sai section

The Khao E-Dang and Wat Tham Nong Sai measured sections are in Ban Sap Phlu and Ban Nong Sai respectively. Both sections are in Khlong Maung sub-district, Pak Chong district, Nakhon Ratchasima province. The Khao E-Dang section is located at Km 24+150 along the rural road No. 2048. The Wat Tham Nong Sai section is located 4 Km south of local road No. 2048 at approximately Km 27+500. They are located at 47P 779982 N, 1618739 E and 47P 785052 N, 1618816 E respectively, on the Royal Thai Survey Department, topographic map sheet WGS 84, series L7018, 5338 III, Ban Sap Noi, and 1:50,000 in scale. The studied locations are plotted in Figure 4.1.

The Khao E-Dang section (Figures 4.8 and 4.10A) contains the siliceous clastic rocks and conglomerate. The Wat Tham Nong Sai section (Figures 4.9 and 4.10B) is composed mainly of limestone and also conglomerate. The conglomerates are preserved in the upper part of both sections and have similar characteristics. They are clast-supported orthoconglomerates and may be divided into lithic conglomerate and polymictic conglomerate. They are composed mainly of limestone, chert, siliceous rock, and volcanic rock fragments. They have moderate sorting with size varies from granule (2-4 mm) up to cobble (64-256 mm). They are rounded to well-rounded with low sphericity and also vary in shapes as sphere, disk, roller, and blade. These limestone pebbles preserved the fusulinid faunas that are probably indicative of Permian age with chert, siliceous rock, and volcanic rock pebbles. The lower part of Khao E-Dang section is thick-bedded siliceous fine-grained rocks. The lower part of the Wat Tham Nong Sai section is massive limestone. Its limestone can be identified as micrite of mud-supported texture.

Moreover, the brachiopods, coral, bryozoa, and fusulinid are preserved in the formation. The outcrops of both sections are not well preserved, however; conglomerates are orientated in the NW-SE direction having gentle dipping, approximately 10 degrees. They are conformable to the other sections.



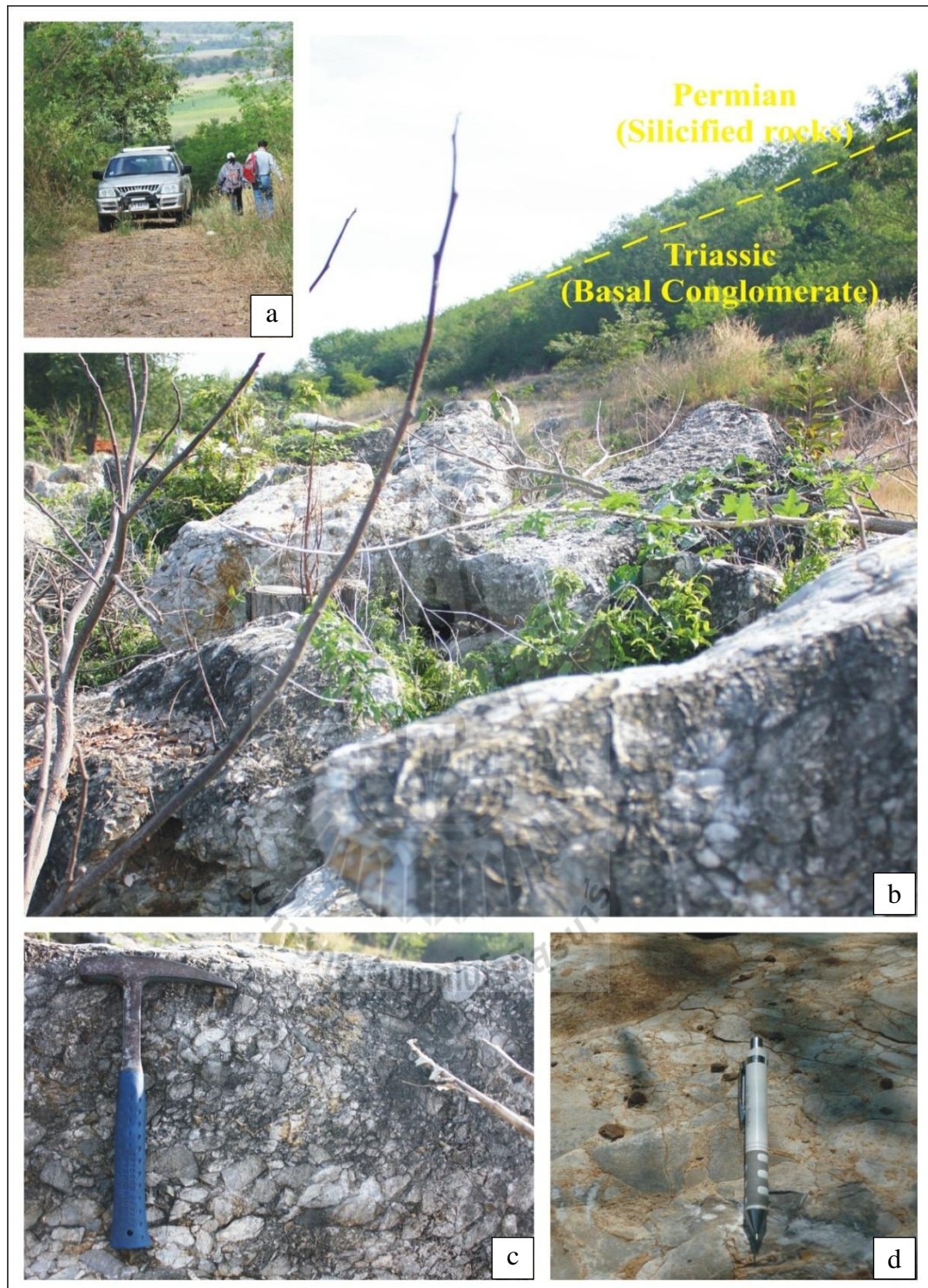


Figure 4.8 Field investigation of the Khao E-Dang section (47P 779982 N and 1618739 E) showing a contact (b) between the Permian silicified rocks (a) and Triassic basal conglomerate rocks (c and d).



Figure 4.9 Field investigation of the Wat Tham Nong Sai section (47P 785052 N and 1618816 E) showing a contact between the Permian massive limestone and Triassic basal conglomerates (a and b) oriented in the NW direction (c and d).

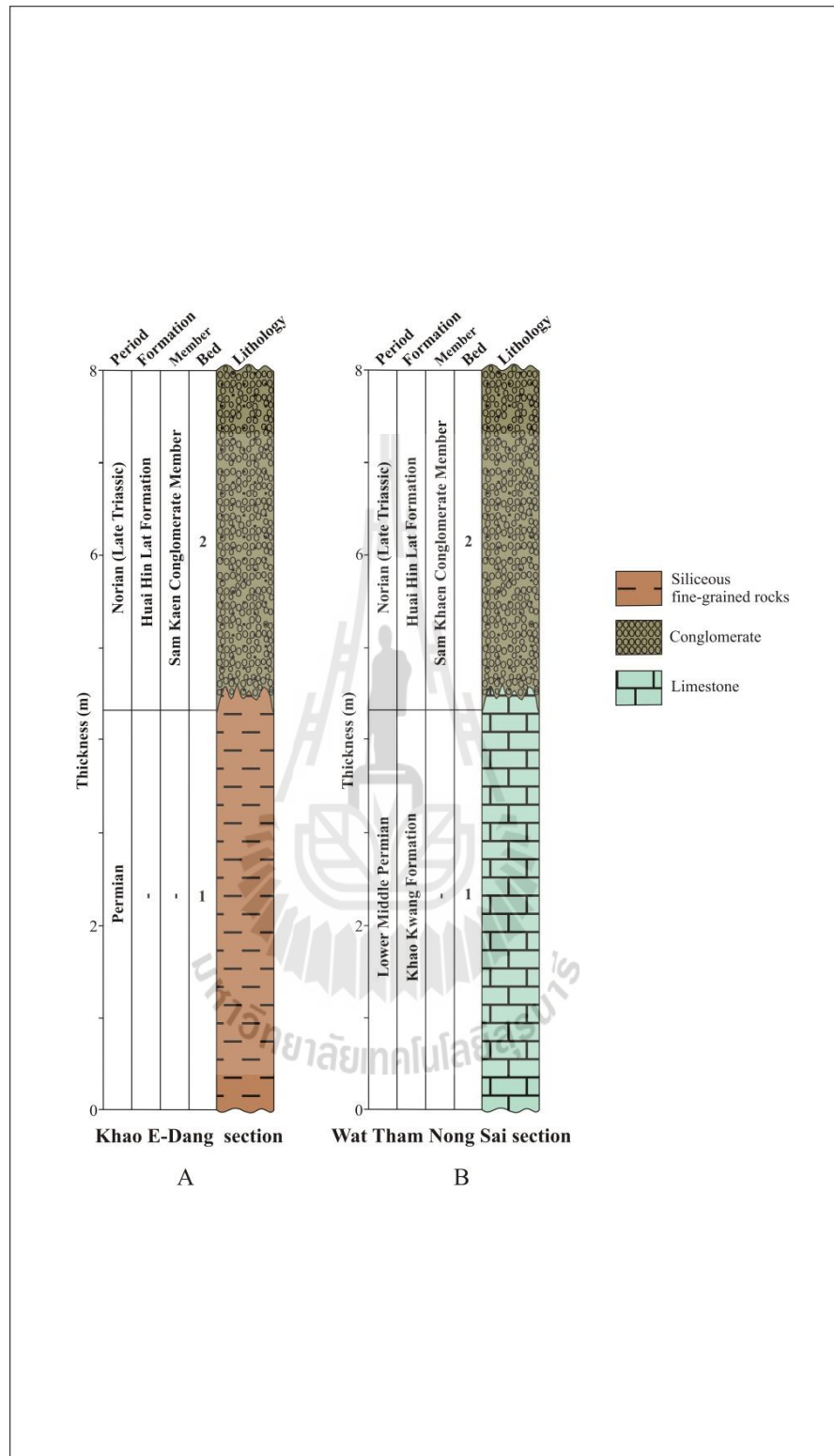


Figure 4.10 Stratigraphic columns of the Khao E-Dang section (A) and the Wat Tham Nong Sai section (B) of the Sap Phlu Basin.

4.1.2 Na Pho Song Basin area

It contains in ascending order of the Sila, Dat Syo, Dat Kloi, Lak Dan, Sarn Chaopoh Hin Tang, Dat Yai, and Ban Huai Sai Thong sections. They will be described below.

4.1.2.1 Sila section

This measured stratigraphic section is located in Ban Song Plueai, Sila sub-district, Lom Kao district, Petchabun province at Km 92+100 along the rural road No. 2216. It is located at 47Q 742210 N and 1884191 E on the Royal Thai Survey Department, topographic map sheet WGS 84, series L7018, 5243 II, Ban Sila, and 1:50,000 in scale. The studied location is plotted in Figure 4.11.

The Sila section (Figures 4.12 and 4.13) contains a variety of rock types and commonly low-lying areas or a lower slope of a mesa-shaped mountain. This section is 41 m thick and composed mainly of fine- to very fine-grained sandstones interbedded with siltstones and mudstones. The sands are 0.06-0.2 mm in grain size and have reddish purple colour. The section is approximately 40-850 cm thick. The rocks are hard due to its cementation of dominantly siliceous but may be calcareous in part. As the result, they are also reacted with acid as well as other fine-grained sediments which are composed in the section. Siltstones are thicker bedds of 10-188 cm. Moreover, fine conglomeratic sandstone comprises small pebbles about 0.1 cm in size. Some conglomerates are diagenesis limestones which formed in semi-arid environment. The calcareous mudstones are greenish grey to light grey colour. These characteristics show the thin to very thick beds, generally 4-240 cm approximately. Middle Bed 13 has gypsum above and below this bed. Gypsum beds suggest arid environment of deposition. The muddy limestone and

marlstone have light grey colour, extremely compacted, and beds are approximately 10-20 cm thick usually interbedded with calcareous mudstones. According to the section, the bedding attitude is approximately 246/37. Plant fragments and common fossils (*Estheria*) are not found in this lithologic unit.

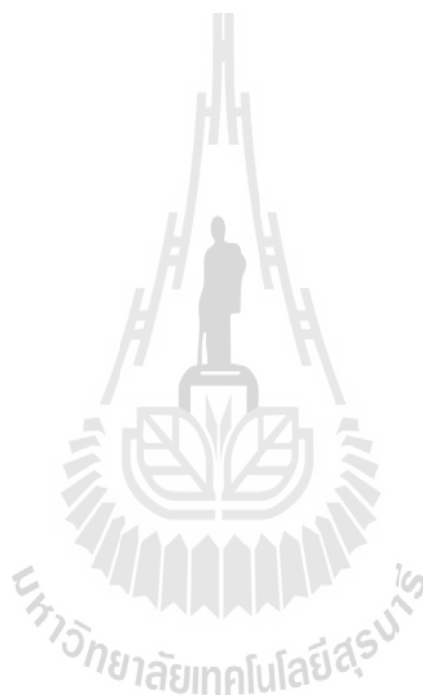
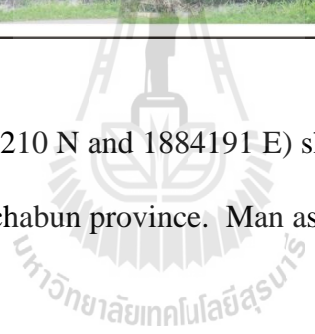




Figure 4.12 Field investigation of the Sila section (47Q 742210 N and 1884191 E) showing the road cut outcrop along the local road No. 2016 at Ban Song Pluei, Lom Kao district, Petchabun province. Man as scale was looking south.



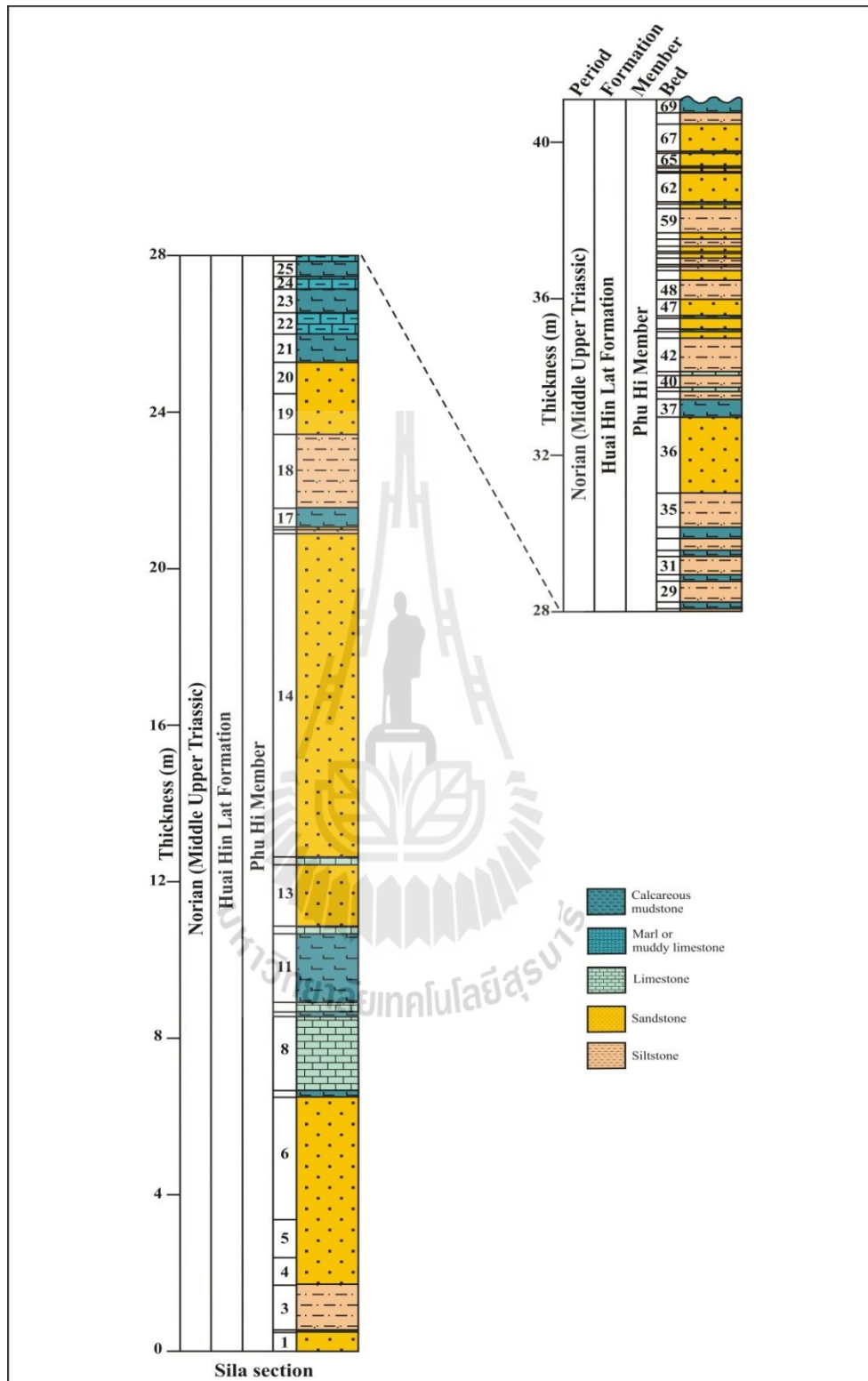


Figure 4.13 Stratigraphic column of the Sila section of the Huai Hin Lat Formation in the Na Pho Song Basin area.

4.1.2.2 Dat Syo section

This measured stratigraphic section is situated in Ban Dat Syo, I Phum sub-district, Dan Sai district, Loei province at approximately Km 14 along the rural road No. 4017 next to the Dat Syo temple. It is located at 47Q 736501 N and 1895756 E on the Royal Thai Survey Department, topographic map sheet WGS 84, series L7018, 5243 III, Ban Dan Du, 1:50,000 in scale. The studied location is performed in Figure 4.11.

The Dat Syo section (Figures 4.14 and 4.15) is 34 m thick. This section is composed mainly of calcareous mudstone, shale, and sandstone. They are thin to thick beds of generally few centimeters to up to 92 cm. They have strong reactions with acid, including laminated sandstone in the upper part. Their bedding attitudes are approximately 290/13, 310/12, 282/14, and 293/12 from beds 1 to 4 respectively. The colour is varied from greenish grey to black through the section except beds 2 and 6 which are typically black and yellowish grey to yellow for weathered colour. The muddy limestone and marlstone are thin to thick beds, generally 2-82 cm. The common fossils are found in the lowest section of beds 1-1, 1-2, 1-14, 1-16, 3-1, 3-3, 4-1, 4-3, 4-4, and 4-10. They are *Estheria mansuryi* that confirm the Norian age of Uppermost Triassic (Kobayashi, 1973). Moreover, the plant fragments are also found in beds 1-1 and 1-11 but cannot be identified to any part of plants due to poor preservation and extremely weathered condition. Gypsums are found mostly along the beds 3, 4, and 5 especially beds 3-8 are illustrated 1.5-2.0 cm in thickness. As the results, the palaeoenvironment of this section controlled the sediments that fill up basin under the effect of the mostly semi-arid condition with slightly humid condition at the first stage. The underlying sandstone is yellowish

brown and the uppermost sandstone is purple in colour. The underlying sandstone (yellowish brown sandstone) has no the conglomerate preservation which is a prime characteristics of the Huai Hin Lat Formation (Norian age). But the reddish purple one is located at the western hill that forms the mesa-shaped mountains. It has characteristics of true red shale, siltstone, and sandstone with many importantly interbedded conglomerates. These conglomerates are the prime characteristics that belong to the Nam Phong Formation of the Lowest Khorat Group.

Apart from this exposure, the float rocks of polymictic conglomerate are found which may have fallen from the upper hill. The clasts range from few millimeters to cobble in size, consisting of red sandstone, quartz, quartzite, and limestone. Conglomerate shows the matrix-supported texture. The clasts have low sphericity and angular that indicates less transportation. Moreover, the hill in the eastern part of the studied section (47Q 737426 N and 1896547 E) also reveals the polymictic conglomerates. The pebbles and cobbles are composed mainly of red sandstone, mudstone, conglomerate, meta-sandstone, quartzite, and shale interbedded with limestone. Their sizes range from a few millimeters to cobble of the matrix-supported texture. The clasts have low sphericity but more rounded than the overlying rock exposures. However, they can be identified as poorly sorted which indicate less transportation as well. Therefore, these polymictic conglomerates also have prime characteristics of the Nam Phong Formation and the clasts are of older rocks which may have been derived from the Huai Hin Lat Formation and Permian strata.



Figure 4.14 Field investigation of the Dat Syo section (47Q 736501 N and 1895756 E) which (a) to (f) show the lower to upper sections and the uppermost section shows a contact between the Huai Hin Lat Formation and the overlying Nam Phong Formation in the NW direction.

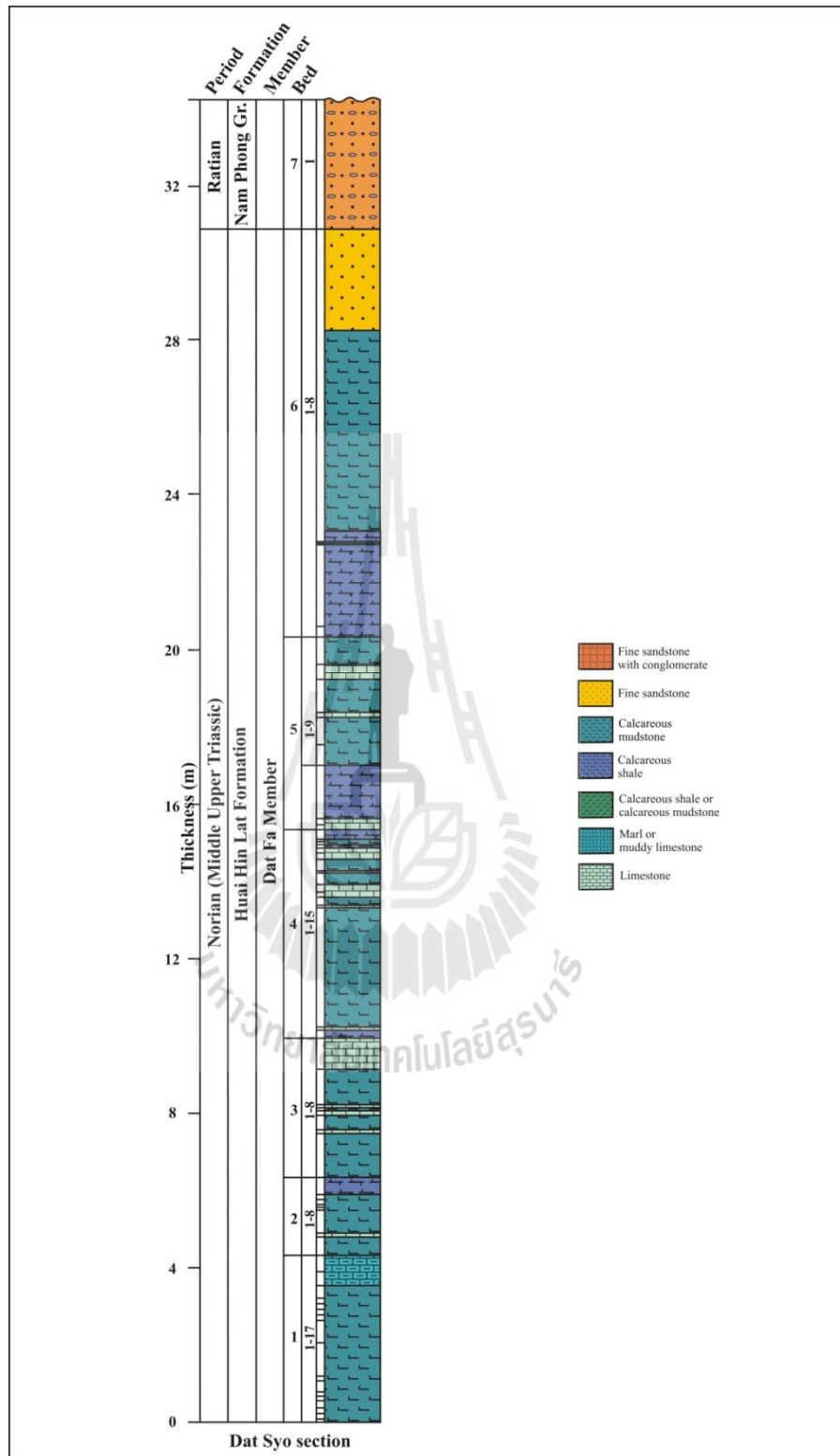


Figure 4.15 Stratigraphic column of the Dat Syo section of the Huai Hin Lat Formation in the Na Pho Song Basin.

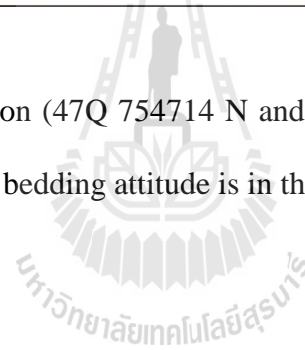
4.1.2.3 Dat Kloi Nuea section

This measured stratigraphic section is in the area of Ban Dat Kloi Nuea, Sila sub-district, Lom Kao district, and Petchabun province at Km 77+050 which along the rural road No. 2216. It is located at 47Q 754714 N and 1880033 E on the Royal Thai Survey Department, topographic map sheet WGS 84, series L7018, 5242 I, Ban Tha Chang, map scale 1:50,000. The studied location is plotted in Figure 4.11.

The Dat Kloi Nuea section (Figures 4.16 and 4.17) is 50 m thick and composed mainly of volcanic rocks and pyroclastic rocks that are interbedded with fine-grained sedimentary rocks. Basalts are discovered and conformed to the fine-grained sedimentary bed through the section. The pyroclastic rocks are in the upper part of the section and are mainly of light grey, greenish grey, and purplish grey in colours. The upper part of light grey contains more quartz and feldspar pebbles having high sphericity and roundness. However, greenish grey and purplish grey parts are lack of these clasts. According to pyroclastics, they have vesicular texture due to the clasts are lost from the extreme weathering which are not original deposition. The fine-grained sedimentary rocks mainly comprise the calcareous sandstones and mudstones which have moderate reactions with acid. Their beds range from a few centimeters to 2 m in thickness. Although these rocks are affected by the volcanic, however, these rocks may not or rarely present the evidences of extreme deformation. As the results, sandstones are rarely deformed as meta-sandstone, harder, and cross-bedding structure is also appeared. The bedding attitude is approximately 268/43.



Figure 4.16 Field investigation of the Dat Kloï Nuea section (47Q 754714 N and 1880033 E) showing the rock exposure of volcanic, pyroclastic, and fine-grained rocks which their bedding attitude is in the E direction.



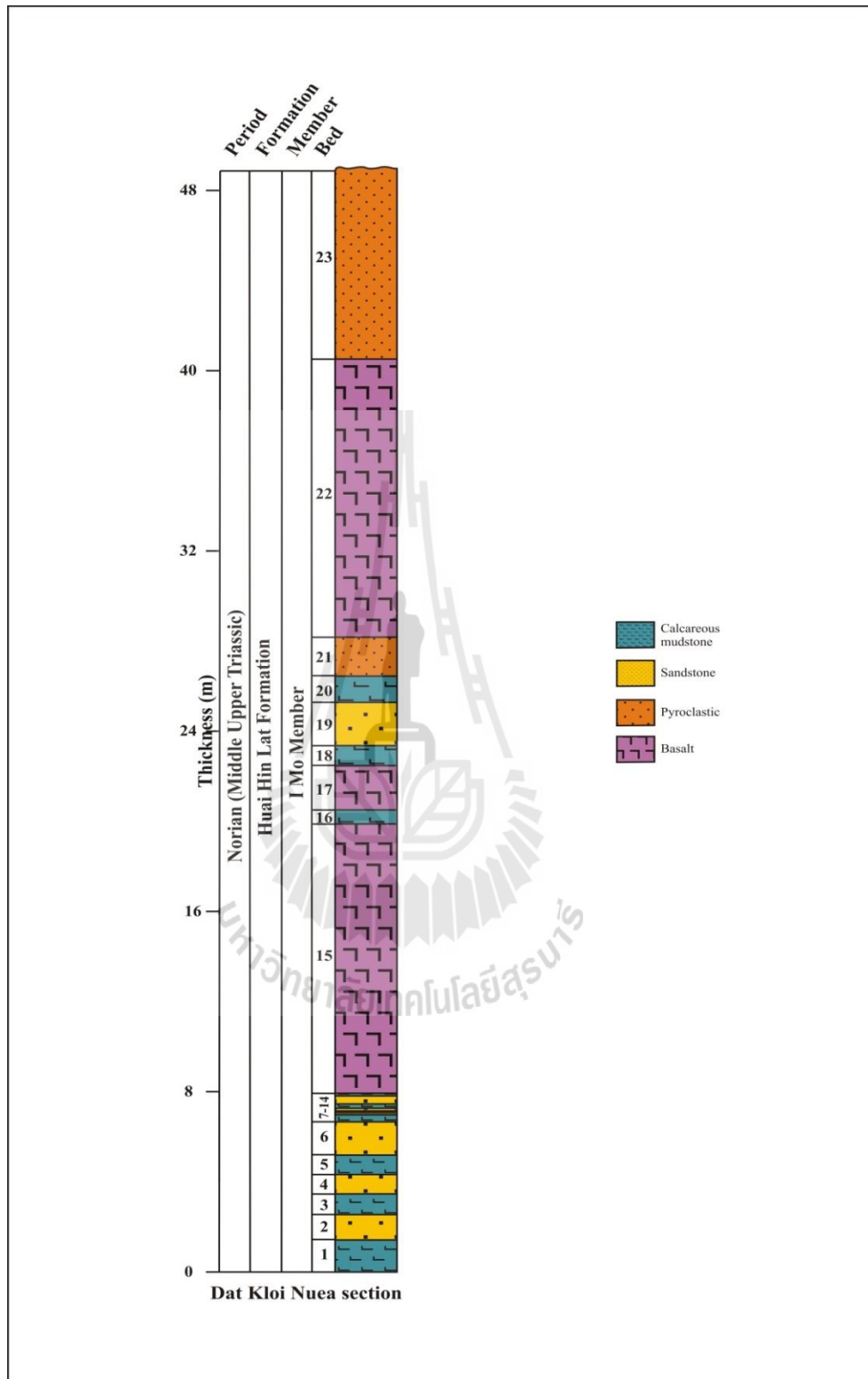


Figure 4.17 Stratigraphic column of the Dat Kloi Nuea section of the Huai Hin Lat Formation in the Na Pho Song Basin.

4.1.2.4 Lak Dan section

This measured stratigraphic section is in the area of Ban Lak Dan, Lak Dan sub-district, Nam Nao district, Petchabun province at Km 67+200 along the rural road No. 2216 or at the location of 47Q 760707 N and 1880500 E on the Royal Thai Survey Department, topographic map sheet WGS 84, series L7018, 5242 I, Ban Tha Chang, scale 1:50,000. The studied location is plotted in Figure 4.11.

The Lak Dan section, 39 m thick, has high angle in the eastern part and declines to lower angle in the western part. This section (Figures 4.18 and 4.19) is composed mainly of fine sandstones, calcareous shale, and mudstones. The calcareous shale and mudstones are generally greyish black to dark black in colour. The calcareous shale clearly shows fissility through beds and has no plant fragments and common fossils. Sandstones in the upper part are fine-grained with grey, greyish black, and chiefly dark black in colour. In the upper part, the sediments are graded from the fine-grained to coarse-grained from the bottom to top. Bed 82 comprises sandstones with feldspar, mica, and small chert. Their bedding attitudes are approximately 270/27, 243/43, and 270/46.



Figure 4.18 Field investigation of the Lak Dan section (47Q 760707 N and 1880500 E) showing mainly calcareous shale and overlying calcareous sandstone which (a) and (b) are in left and right of the outcrop respectively.

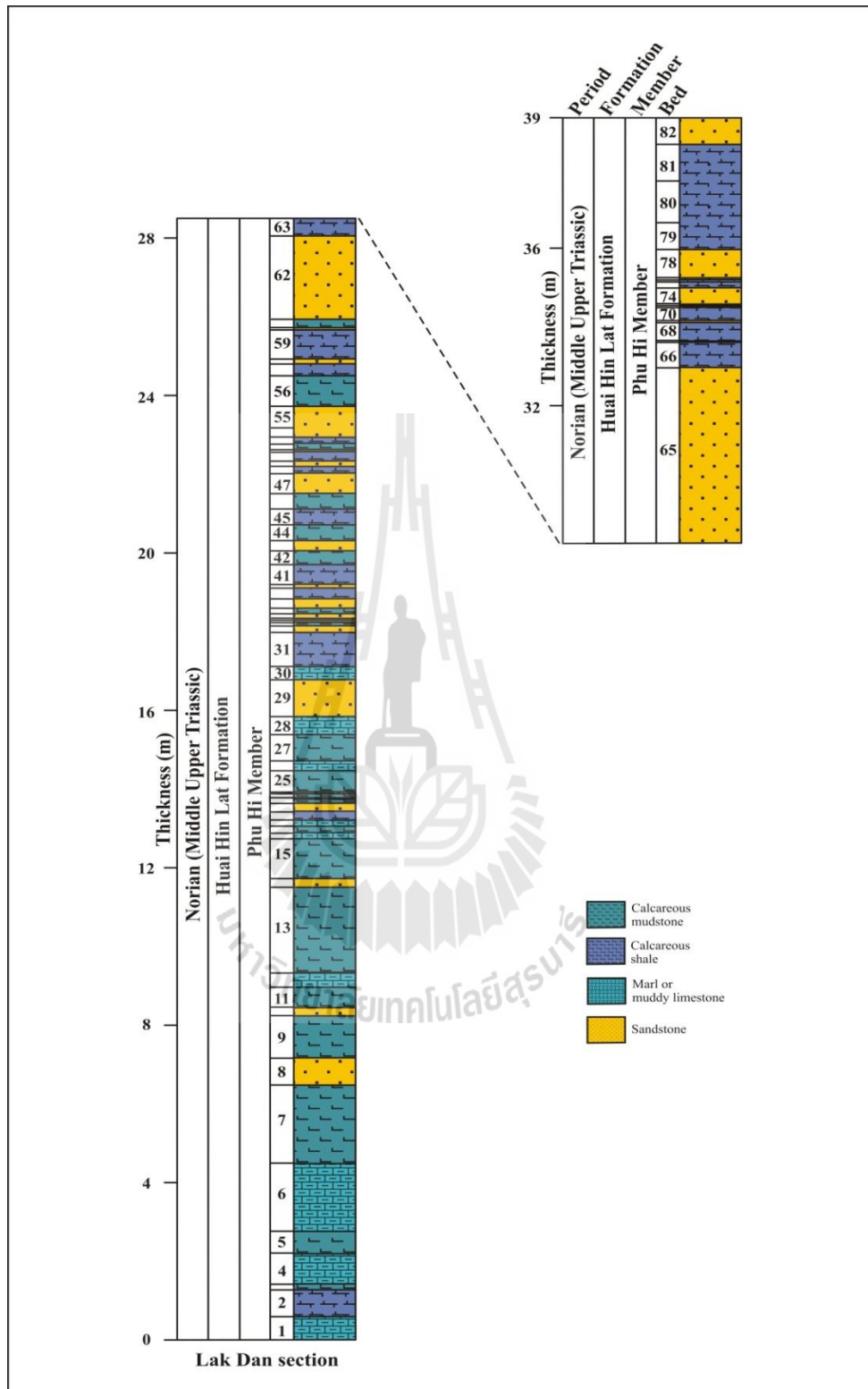


Figure 4.19 Stratigraphic column of the Lak Dan section of the Huai Hin Lat Formation in the Na Pho Song Basin.

4.1.2.5 Sarn Chaopoh Hin Tang section

This measured stratigraphic section is situated in the area of Ban Huai Sanam Sai, Huai Sanam Sai sub-district, Nam Nao district, Petchabun province at Km 2+150 along the rural road No. 2216. It is located at 47Q 792362 N and 1845710 E on the Royal Thai Survey Department, topographic map sheet WGS 84, series L7018, 5342 III, Khuean Chulabhorn, 1:50,000 in scale. The studied location is in Figure 4.11.

The Sarn Chaopoh Hin Tang section (Figures 4.20 and 4.21), more than 32 m thick, chiefly consists of calcareous shale, calcareous mudstones, and is overlain by thick coal-bearing strata. The calcareous shale clearly shows fissility throughout the beds. The calcareous mudstones are more massive than the calcareous shale in which both rocks are greyish black to dark black in colour. Plant fragments and common fossils (*Estheria*) are not found in this section. However, the outcrop opposite to the studied area contains abundant and well preserved ostracods especially in limestones. The coal-bearing unit is mostly dull black in colour with more brittle, light reflectance, and lightweight. It can be classified into four units (Unit I-IV) and details of each unit are described as follows. Unit I is the lowest grade coal and lack of significant structure. Its beds are parallel and conformed to the underlying rocks. The overlying unit (unit II) is higher grade of coal. The bed of Unit II is corresponded to the underlying unit I. Unit I is 1.0 m thick while unit II is 0.85 m in thickness. Unit III is a high grade coal with 2.30 m thick and rests on high angle beds of unit I and unit II. The high angle of unit I and unit II may tilt before the accumulation of unit III forming as a wedge. Slumped structures (Figure 4.22) are discovered through unit III. They form on an unstable slope during dewatering of the slump after it came

to rest. They are associated with penecontemporaneous faulting with moderate angle zones of slide planes. Recrystallized beds of calcite are formed along the slide planes and coal matrix in several directions which have been found only in unit III. They commonly show clear evidences of extensive lateral movement of delta fronts in active subsidence (Selley, 2000). Lastly, unit IV is high grade coal interbedded with mudstone with gently dipping beds that are more than 10 m in thickness. The coal is impure (high clay content) and interbedded with layered mudstones. It is also highly weathered, therefore, showing the unclear bedding. In addition, the mud crack structures are also found in the upper hill of the unit IV. This indicates shallow basin that is gradually getting shallower from unit I to unit IV.

In fresh-water coal deposition, it accumulates in the back swamps and marshes of flood plains and flood basins between/or adjacent to rivers. These environments are located in inland areas, usually in water-filled depressions corresponding to tectonic (graben structures, such as rift valleys) or climatic conditions. They are permitting the development of a lake with shores occupied by forest or herbaceous vegetation mires (Suárez-Ruiz et al., 2012). These lands are mainly occurred in shallow basins which are poorly drained as illustrated in Figure 4.23. According to the main facies models of moor types of coal lithotypes and the petrographic composition (Teichmuller et al., 1982; Suárez-Ruiz et al., 2012), it can be indicated to open water moortype. It has less plant fragments of megascopic features but is dark in colour. However, it is high in clay minerals of microscopic features of detrital sediments. The coal-bearing unit appears in several meters from the underlying fine-grained calcareous mudstones and grades upwardly to the overlying calcareous sandstones at Km 1+975 with bedding attitude of approximately

237/27. These features also confirm that this measured stratigraphic section was deposited in swamp associated with dominant fluvial facies of nearly fully filled basin stage.





Figure 4.20 Field investigation of the Sarn Chaopoh Hin Tang section (47Q 792362 N and 1845710 E) showing thick beds of coal similar to the nearby Ban Huai Sanam Sai, Nam Nao district, Petchabun province which (a) and (b) are in left and right of the outcrop respectively.

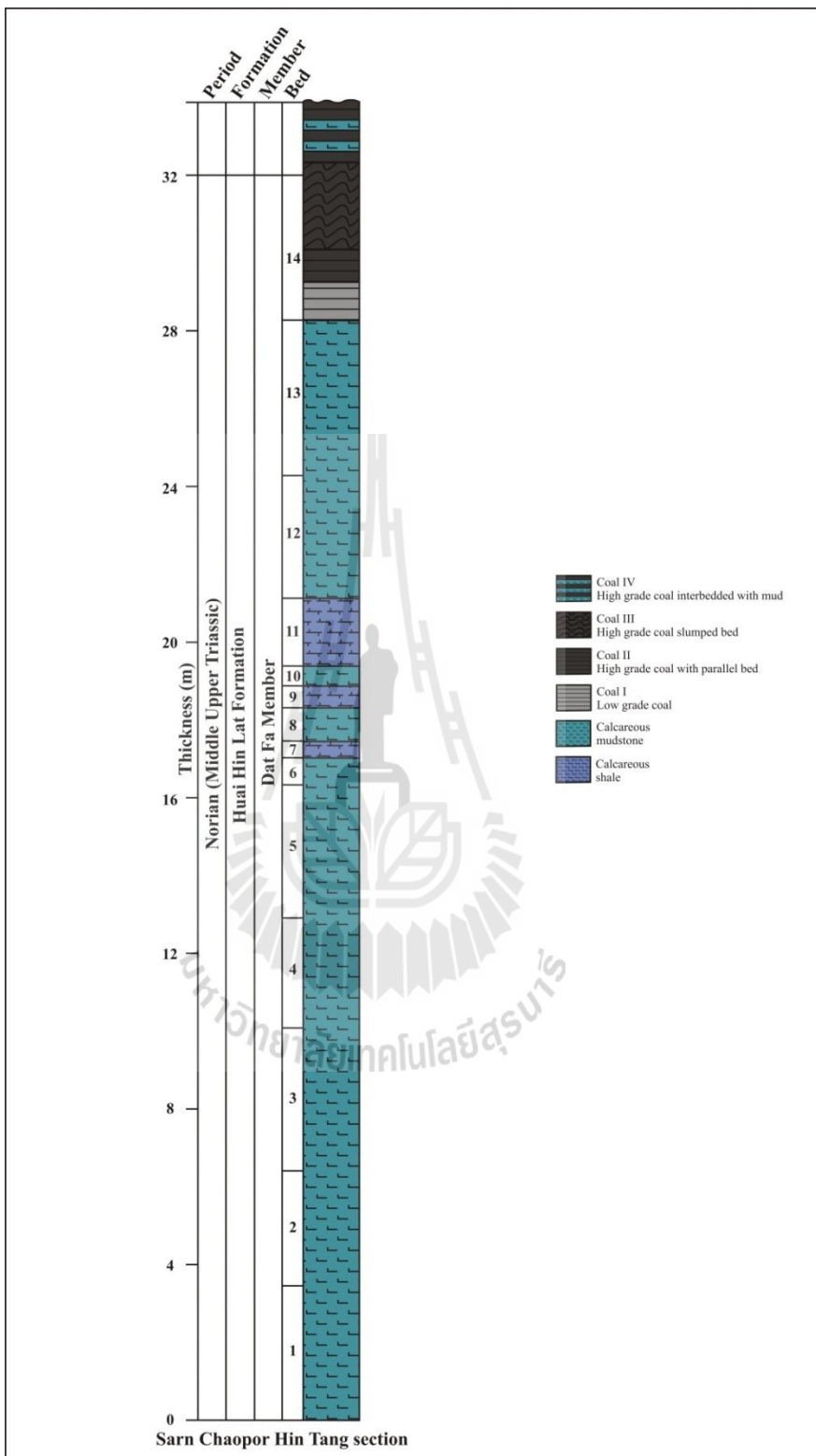


Figure 4.21 Stratigraphic column of the Sarn Chaopoh Hin Tang section of the Huai Hin Lat Formation in the Na Pho Song Basin area.

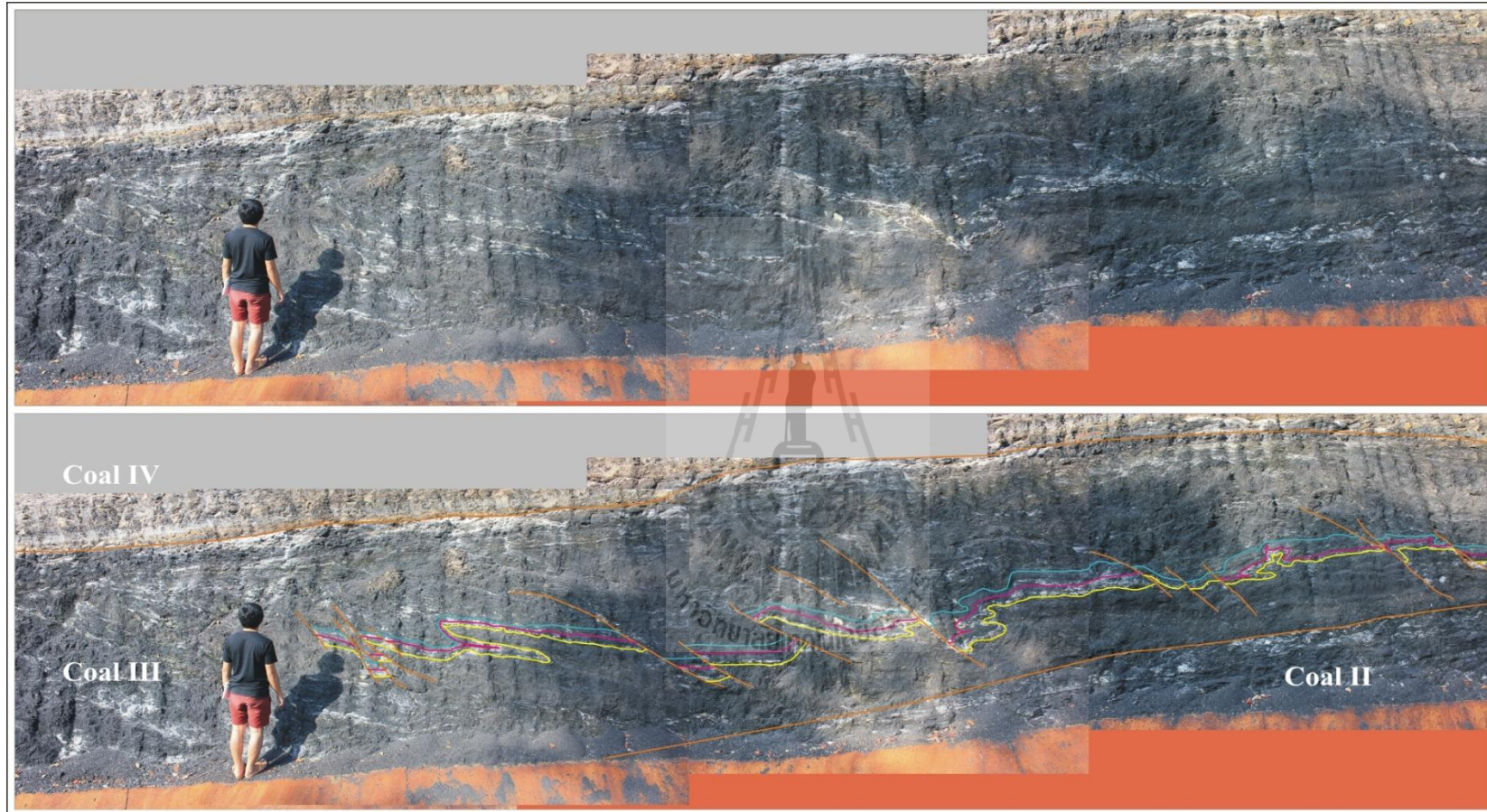


Figure 4.22 Slumped structures which associated with penecontemporaneous faulting and low angle of slide planes.

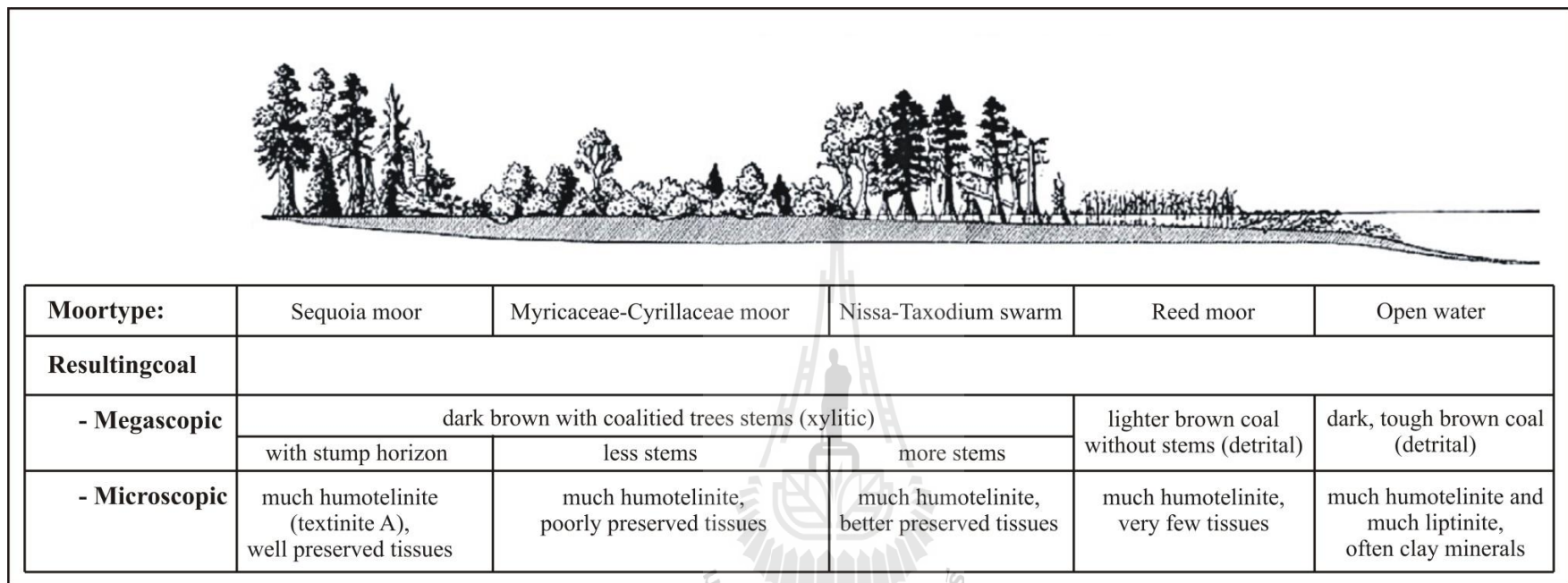


Figure 4.23 Moor types and resulting brown coal lithotypes and petrographic composition of the Miocene Rhenish coals (Teichmüller et al., 1982) as indicated to swamp sub-facies of the Na Pho Song Basin.

4.1.2.6 Dat Yai section

This measured stratigraphic section is located in Ban Dong Maphai, Koke Mon sub-district, Nam Nao district, and Petchabun province. It is along the rural road No. 2216, approximately at Km 8+500, and turn to a Dat Yai waterfall. It is located at 47Q 796604 N and 1850718 E on the Royal Thai Survey Department, topographic map sheet WGS 84, series L7018, 5342 II, Amphoe Khon San, scale 1:50,000. The studied location is plotted in Figure 4.11.

Figure 4.24 of the Dat Yai section is illustrated along the flow directions of Dat Yai waterfall with 42 m thick. Figure 4.25 of the Dat Yai section is formed as the lowest facies of the Huai Hin Lat Basin due to these rocks were deposited in deep lake basin with high preservation of organic matters and sediment supply. This section is composed chiefly of calcareous shale, calcareous mudstone, and argillaceous limestone. They have light black to dark black with mostly dull texture. The argillaceous limestone is very resistant with massive bed. In addition, the rock matrix is appeared to be calcite crystals dispersed through their beds and the calcite bed about 0.5-1 cm is formed. The calcareous shale forms a thin bed of unclear fissility with 2-5 cm thick but the calcareous mudstones are thicker. They are associated with small dispersed calcite crystals and formed as layers in some parts of fine-grained rock matrix. These layered calcite crystals are a few millimeters to 1 cm thick. The lower part has more abundant bedding planes than the upper part and the dissolved calcite traces along their beds are observed. In addition, pyrites are found as unshaped bulbs and weathered pyrite minerals are illustrated as yellowish brown in colour similar to clay nodules. These pyrites have more dispersing and abundance through their beds especially in upper part. The plant fragments are more abundant in

the upper part of beds 9 and 31 but cannot be identified to maceral group due to poor preservation. Moreover, the common fossils of *Estheria* sp. are abundant in beds 4, 8, and 9. They are identified to the Norian age following the reasons and suggestions of Kobayashi (1973). These plant fragments and *Estheria* sp. are accumulated as organic matters and generate the hydrocarbons for petroleum system. The forces have affected to this section as shown by bedding of joints with their bedding attitude is approximately 208/82 and 343/88 on bed 10, 335/68, 014/89, and 114/66 on bed 19, and 251/85 and 333/88 on bed 16. DMR (2012) studied thin sections of black earth minerals in Dat Yai waterfall and found interesting structures. They suggested that the diagenetic processes have affected this measured stratigraphic section. The diagenetic processes generate the stylolitic structure which is formed as saw teeth style. It is discovered along the dissolved bed due to influence of pressure solution (DMR, 2012).

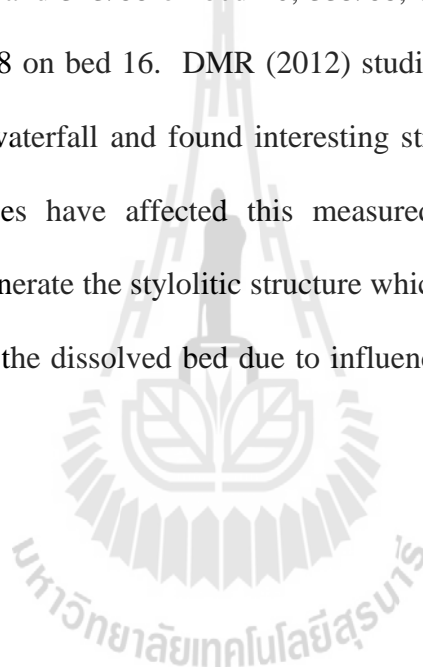




Figure 4.24 Field investigation of the Dat Yai section (47Q 796604 N and 1850718 E)

showing a natural outcrop exposed along the flow directions of the Dat

Yai water fall and (a) to (f) show lower to upper sections respectively.

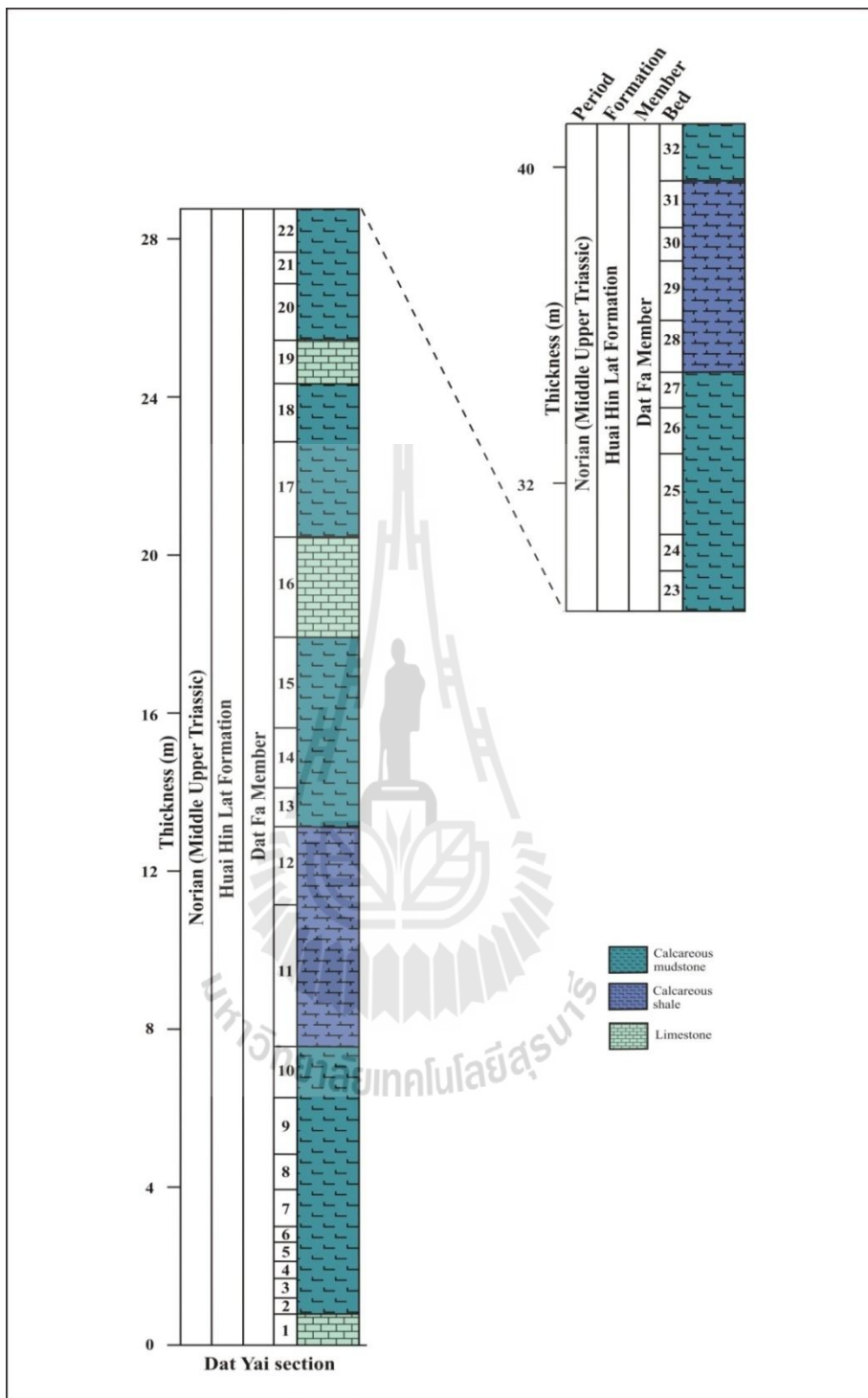


Figure 4.25 Stratigraphic column of the Dat Yai section of the Huai Hin Lat Formation in the Na Pho Song Basin.

4.1.2.7 Ban Huai Sai Thong section

This measured stratigraphic section is situated in the area of Ban Huai Sai Thong, Thung Phra sub-district, Khon San district, and Chaiyaphum province at Km 431 which is along the Highway No. 12. It is located at 47Q 793057 N and 1843768 E on the Royal Thai Survey Department, topographic map sheet WGS 84, series L7018, 5342 III, Khuean Chulabhorn, scale 1:50,000. The studied location is plotted in Figure 4.11.

The Ban Huai Sai Thong section (Figures 4.26 and 4.27) is located along Chern River with 196 m in length. The rocks are composed mainly of limestone, conglomerate, and sandstone. The underlying limestone is black, greyish black, and grey in colour and original components are not bounded together during deposition. It is a mud-supported texture with less than 10 % fusulinid grains and can be classified to mudstone or micrite following the methods of Dunham (1962) and Embry and Klovan (1971). The conglomerate is light grey in colour and its texture is a clast-supported as formed an orthoconglomerate. It may be divided into a type of lithic or polymictic conglomerate which is composed mainly of limestone and chert fragments associated with diagenesis chert nodules. It is of moderate sorting varying in size from granule (2-4 mm) up to cobble (64-256 mm). It is sub-rounded to well-rounded of low sphericity varying in shape as sphere, disk, roller, and blade. These limestone pebbles contain well preserved fusulinid and crinoid faunas indicative of the Permian age as well as the containing chert fragments. The lower contact (between limestone and conglomerate) and upper contact (between conglomerate and sandstone) are located at 47Q 793212 N and 1843663 E and 47Q 792988 N and 1843728 E respectively. As the results, they are 187 m in thickness of conglomerate.

The overlying sandstone has the colour varying from greenish grey to black through the section and reddish pink for weathered colour. It is not associated with the conglomerate and not reacted with acid. The coarse-grained sandstones are shown at the contact and graded upwardly to finer grains. Bedding attitudes are approximately around 282/44 and 266/51.



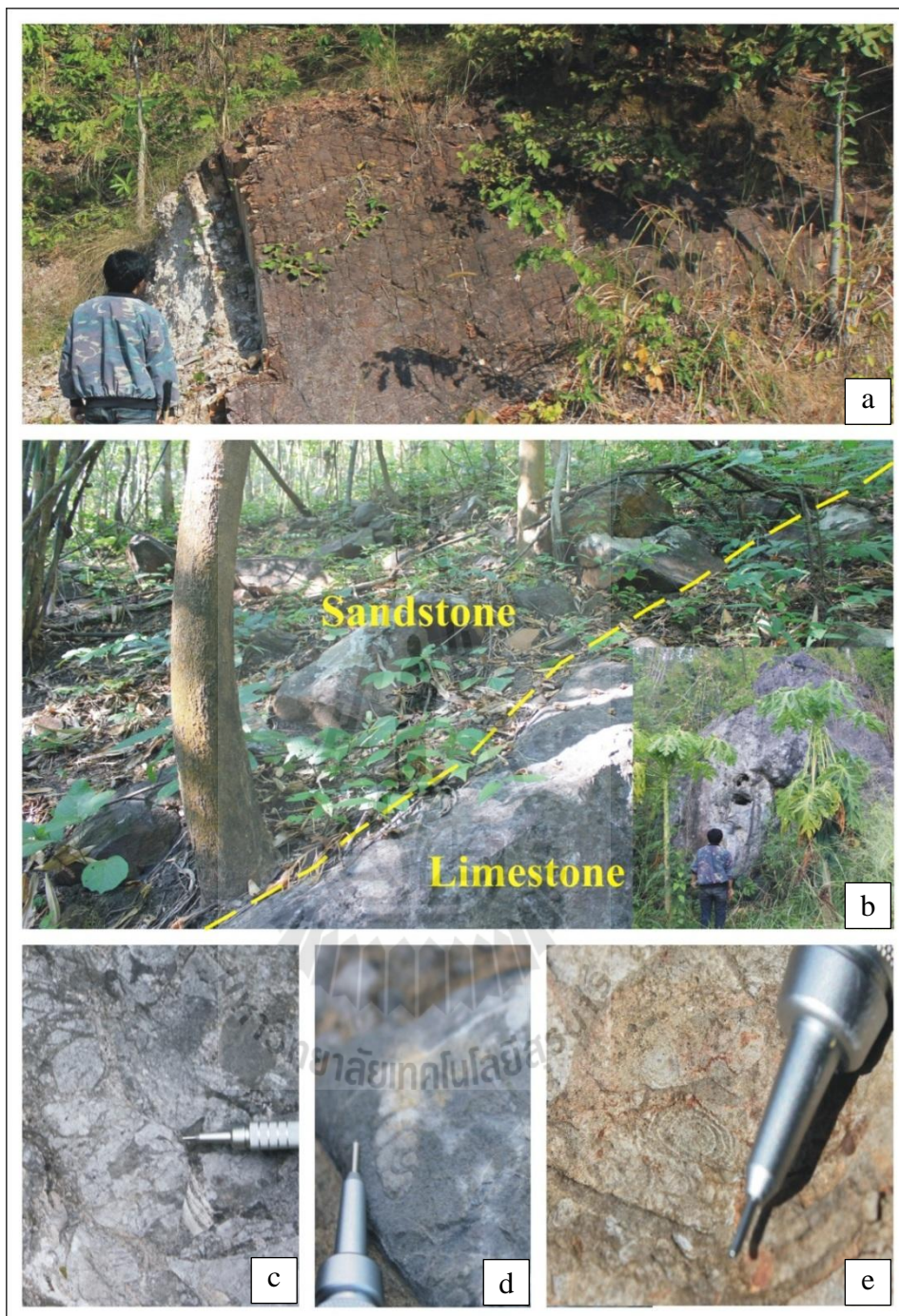


Figure 4.26 Field investigation of the Ban Huai Sai Thong section (47Q 793057 N and 1843768 E) showing a contact (b) between overlying sandstone (a) and basal conglomerate (c-d) containing crinoid and fusulinid faunas.

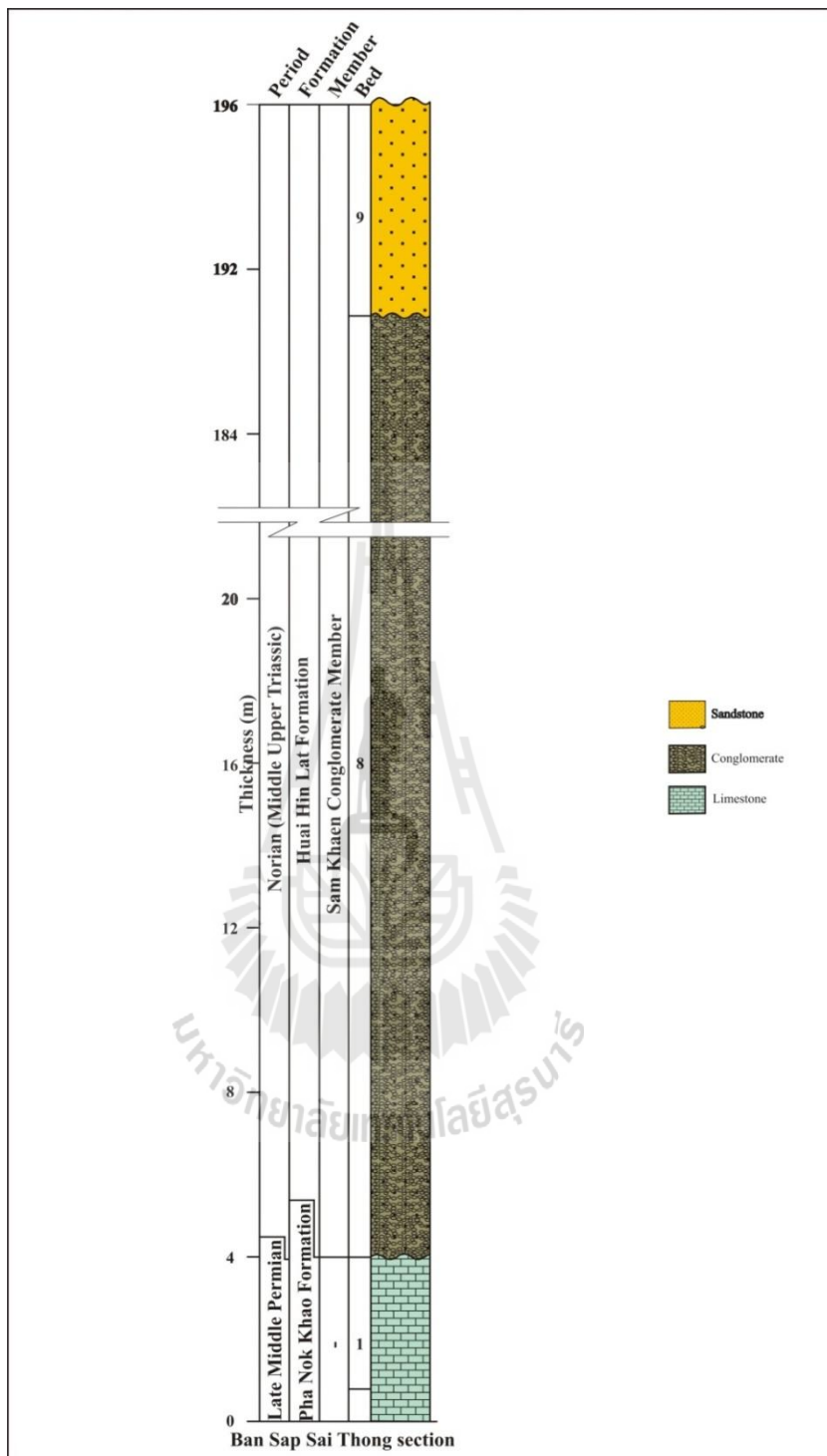


Figure 4.27 Stratigraphic column of the Ban Huai Sai Thong section of the Huai Hin Lat Formation in the Na Pho Song Basin.

4.2 Establish sequence for source rock evaluation

The hydrocarbon source sequence was carried out by the study in detail for more understanding. This study will be correlated and formed a dominant factor that controlled sedimentary supply for establishing of high potential on petroleum source and reservoir rocks.

4.2.1 Stratigraphic correlation

The characteristics of the sections can be correlated to a stratigraphy of the Ban Dat Fa section and established to members of the Huai Hin Lat Formation. These sections have been studied bed by bed with their lithologic characteristics. The type section was designated by Iwai and others (1966) which locates in Chum Phae district of Khon Kaen province. The type section is along a small creek of Huai Hin Lat crossing the Khon Kaen-Loei Highway at Km 109.5. It is located in the Royal Thai Survey Department topographic map sheets Ban Na Nong Thum (47Q/Fa20) and Ban Nong Chan (48Q/AA17), 1:50,000 in scale, grid reference 195504 to 805501 (Chonglakmani and Sattayarak, 1978).

The studied sections in this thesis were selected in the new areas that are not proposed or studied by other authors. They may probably indicate both structures and characteristics to resolve the tectonic events. Moreover, based on the study of petroleum geology in more detail and more precise to get the hope for new petroleum fields.

The Huai Hin Lat stratigraphy is compared with the Ban Dat Fa section. Chonglakmani and Sattayarak, (1978) suggested that the Ban Dat Fa section of the Huai Hin Lat Formation is in Petchabun province northwest of the Khorat Plateau, on the Thai Royal Survey Department map sheet 47Q/FA20, Ban Na Nong

Tum, scale 1:50,000, grid reference 008498 to 976510 and the Thai Royal Survey Department map sheet 47Q/FA19, Ban Na Pho Song, scale 1:50,000, grid reference 883515 to 906541. Details are established by Chonglakmani and Sattayarak (1978) that are a prime document to identify them to each member. The classification and facies relation of the various members of the Huai Hin Lat Formation (Figure 4.28) will be described as follows:

1) Pho Hai Member

It is mainly volcanic rocks, consisting of tuff, agglomerates, rhyolite, and andesite with some intercalations of sandstones, mudstones, and conglomerates. In most places, these rock types of the Pho Hai Member are underlain by the Permian rocks and formed as the lowest member of its formation.

2) Sam Khaen Conglomerate Member

It is chiefly of conglomerate with some intercalations of finer sediments. The conglomerates are polymictic, red in colour, and usually found intercalated with red sandstones and shale. It is mainly a lateral equivalent of the Pho Hai Member but locally overlies it.

3) Dat Fa Member

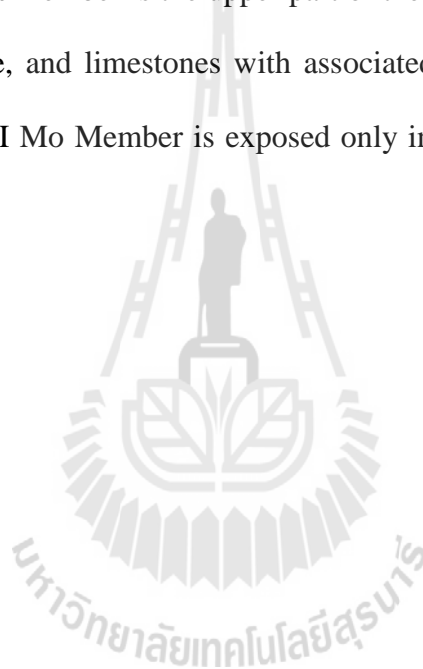
It is mainly of grey to black carbonaceous, calcareous, well bedded shale, and argillaceous limestone. It contains both flora (plant fragments) and fauna (*Estheria*) indicating a Late Triassic (Norian age).

4) Phu Hi Member

It is composed of grey sandstones, shale, and argillaceous limestone with some intercalations of conglomerate beds. It conformably overlies the Dat Fa Member having the upper contact with the overlying Nam Phong Formation consisting of red siltstones, sandstones, and conglomerate bed at the base.

5) I Mo Member

This member is the upper part of the upper sequence. It consists of grey sandstones, shale, and limestones with associated intermediate volcanic rocks. This rock type of the I Mo Member is exposed only in the area of Lom Kao district and adjacent regions.



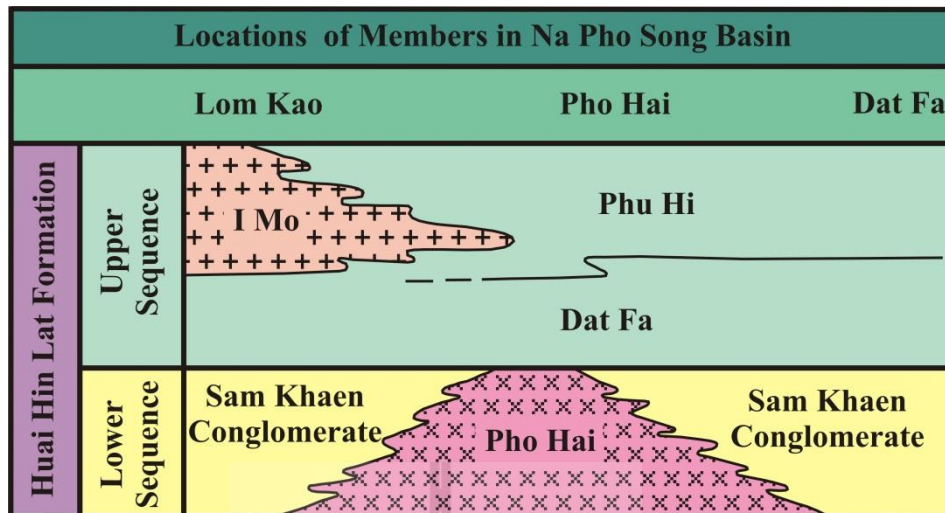


Figure 4.28 Succession of the Huai Hin Lat Formation showing classification and facies relation of the various members from Ban Dat Fa to Lom Kao district (Chonglakmani and Sattayarak, 1978).

4.2.1.1 Correlation of the Sap Phlu Basin

The entire sections of the Sap Phlu Basin are described and correlated to the type section of the Ban Dat Fa as shown in Figure 4.29. The Wat Tham Nong Sai section and the Khao E-Dang section are recognized as the Sam Khaen Conglomerate Member. They contain mainly of massive limestone (Wat Tham Nong Sai section) and silicified fine-grained rocks (Khao E-Dang section) in the lower part. As the massive fusulinid-bearing limestones is probably of established *Verbeekina* sp. of Permian Period. The upper part of both sections is composed of conglomerate with limestone containing fusulinids. These fusulinids are similar to the *Verbeekina* sp. of the lower part which indicates that the conglomerates were accumulated in age of the Triassic. Therefore, the upper section of conglomerates is formed as an unconformity and is called basal conglomerate. The Ban Nong Sai

section is younger than the Wat Tham Nong Sai and Khao E-Dang sections. It conforms to the definition of the Dat Fa Member which chiefly consists of the fine-grained of calcareous mudstone, calcareous shale, marl, and limestone. The Southern Sap Phlu section and the Northern Sap Phlu section have more coarse-grained sediments overlying the Ban Nong Sai section. The Northern Sap Phlu section is the uppermost part of the formation which still belongs to the Dat Fa Member. The other members are not discovered in the section because of poor preservation through the Sap Phlu Basin.



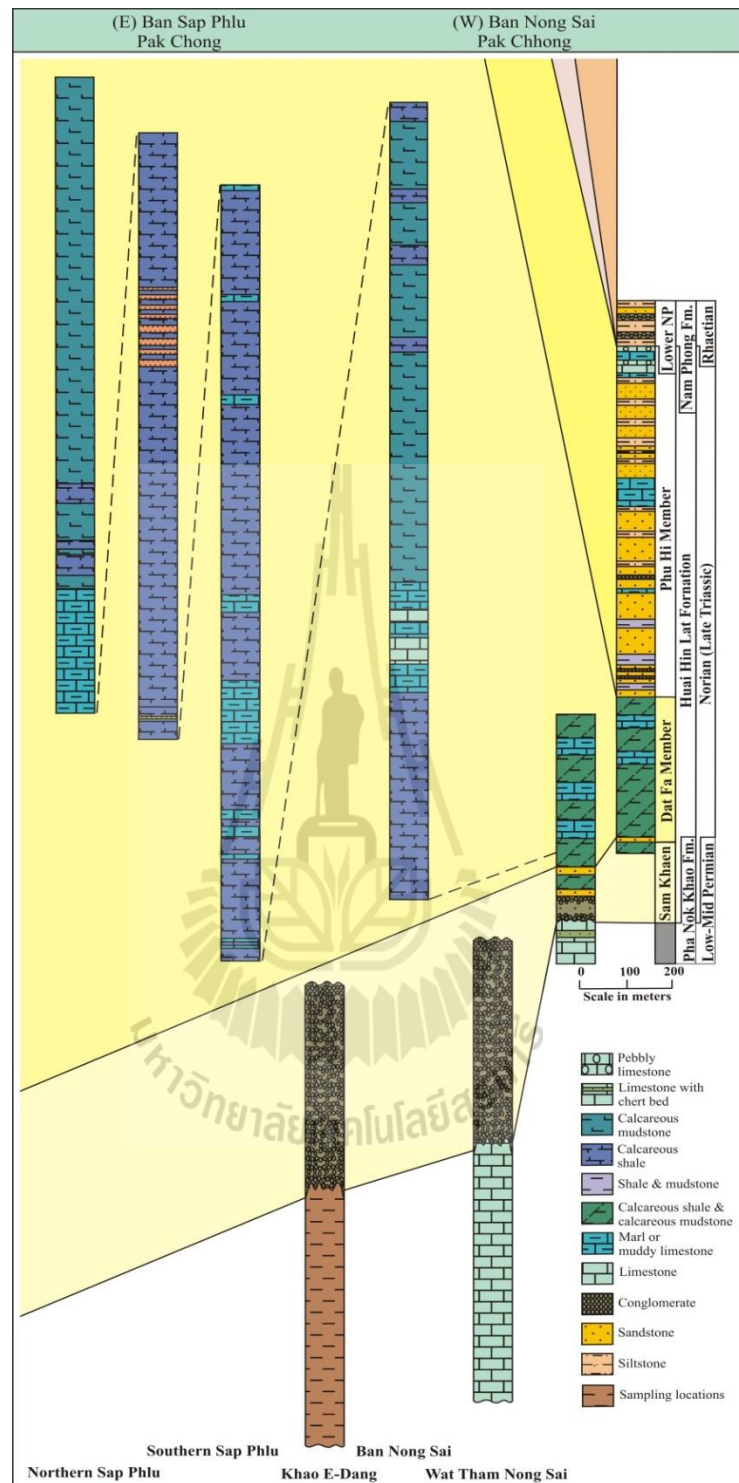


Figure 4.29 Measured stratigraphic sections showing classification and members of the Huai Hin Lat Formation along rural road No. 2048 from Ban Sap Phlu to Ban Nong Sai, Pak Chong district, Nakhon Ratchasima province.

4.2.1.2 Correlation of the Na Pho Song Basin

The definitions of all studied sections are recognized, described, and correlated to the Ban Dat Fa section as shown in Figure 4.30. The Sarn Chaopoh Hin Tang section and the Dat Yai section are recognized to the Dat Fa Member. They are mainly composed of the fine-grained rocks of calcareous mudstone, calcareous shale, and limestone. The environment of the Sarn Chaopoh Hin Tang section is shallower than the Dat Yai environment as indicated by overlying coal-bearing accumulation. The Dat Yai section is designated to the deeper basin among the other studied sections which affect preservation. The Lak Dan, the Dat Syo, and the Sila sections are corresponding to the definition of the Phu Hi Member which chiefly consists of sandstones and thin-bedded of siltstones, shale, and limestone through the section. The Dat Syo section is probably indicated to the lowest part of the Phu Hi Member due to it has more association with the fine-grained shale and mudstones. Then it is grading to fine sandstone of the uppermost Phu Hi Member and continuing upward to coarser sandstone with conglomerate. The latter is a typical characteristic of the overlying Nam Pong Formation. The Lak Dan section probably belongs to the middle Phu Hi Member due to it still has the association of fine-grained rocks. The Sila section probably belongs to the upper Phu Hi Member because it mostly consists of sandstones and grading to coarser grains. The Dat Kloi Nuea section is composed mainly of volcanic rocks (basalt) and pyroclastic rocks interbedded with thin-bedded of sandstones, siltstones, shale, and mudstones. It can be recognized to the I Mo Member. The intermediate volcanic rocks are not revealed in this studied section, however, the basalt is served as an indicator. The Ban Huai Sai Thong section contains the conglomerate as a typical characteristic of the initial

stage of the basin evolution. Therefore, it is named as basal conglomerate and indicated to the Sam Khaen Conglomerate Member. All sections are not associated with volcanic rocks of tuff, rhyolite, andesite, and polymictic conglomerate and hence are not corresponded to the Pho Hai Member.



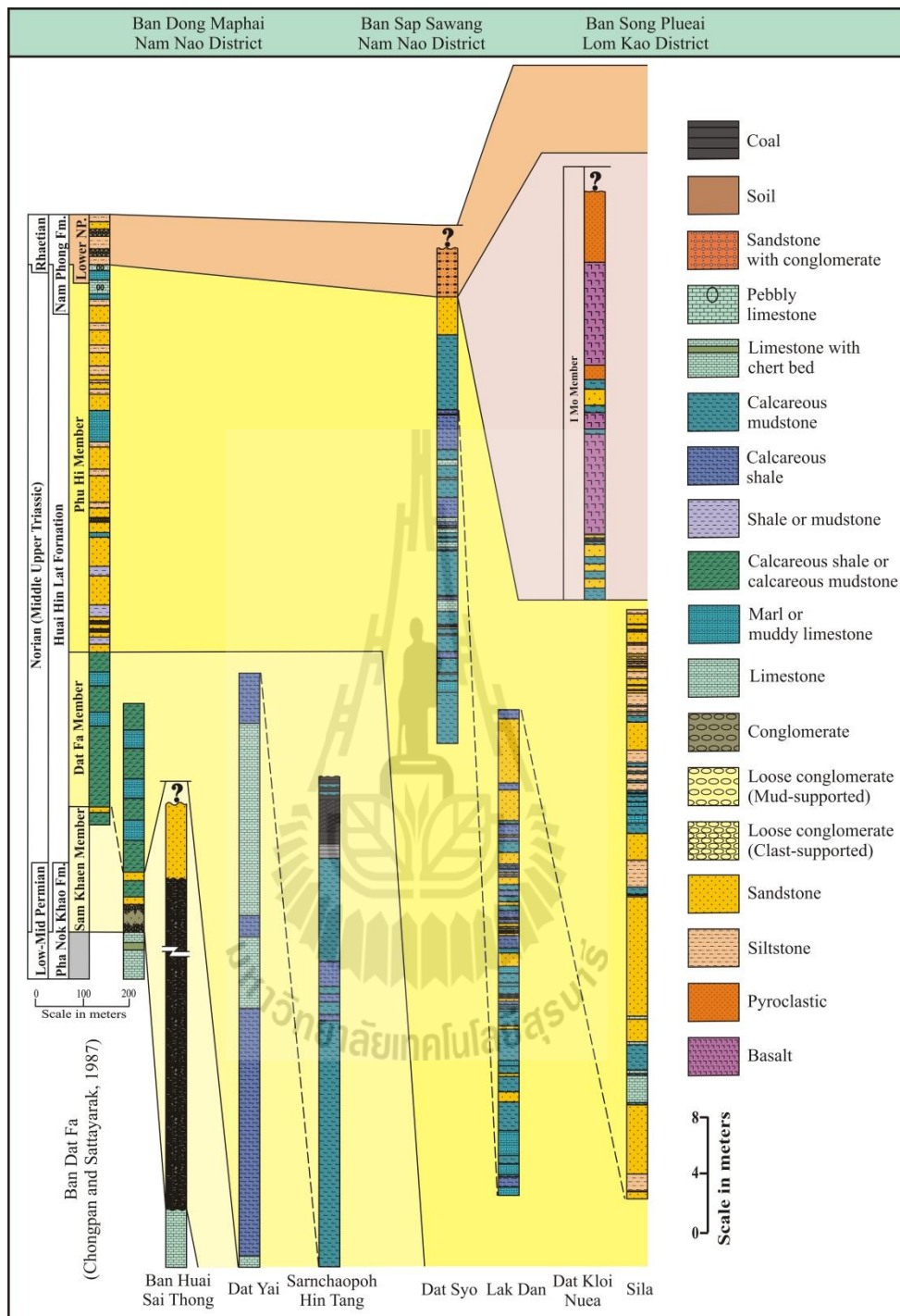


Figure 4.30 Measured stratigraphic sections showing classification and members of the Huai Hin Lat Formation along the rural road No. 2216 from Ban Dong Maphai, Nam Nao district to Ban Songplueai, Lom Kao district, Petchabun province and Dan Sai district, Loei province.

4.2.2 Selected sections for source rock evaluation

Based on the study of petroleum system, the most sections of both studied areas are mainly composed of sandstone and siltstone forming as the reservoir formation. The other measured stratigraphic sections are chiefly composed of the fine-grained sediments which has potential to be source rocks. Sattayarak (1987) proposed source rocks in the Khorat Plateau based on the geological survey along highway No. 12 as dark limestones and shale of the Permian Saraburi Group and shale and grey to dark limestones of the Huai Hin Lat Formation in Ban Huai Sanam Sai of Nam Nao district. The Ban Nong Sai, Southern Sap Phlu, and Northern Sap Phlu sections of the Sap Phlu Basin and the Sarn Chaopoh Hin Tang and Dat Yai sections of the Na Pho Song Basin are mainly of fine-grained sediments that conform to Sattayarak's suggestions. They probably have the source rock potential for the hydrocarbon generation. On the basis of unconventional gas shale study, they can be both source rocks and in-situ reservoir rocks which kept generated hydrocarbons. But the Southern Sap Phlu and the Northern Sap Phlu sections of the Sap Phlu Basin are extremely weathered. They are hard to collect samples as well as the Sarn Chaopoh Hin Tang section of the Na Pho Song Basin. In contrast, the budget is limited and the Ban Nong Sai section (Sap Phlu Basin) and the Dat Yai section (Na Pho Song Basin) are thicker, more well preserved, and more well abundance of organic matters. They have more potential and, therefore, are selected for further evaluation on the unconventional shale gas potential.

CHAPTER V

PETROGRAPHIC AND GEOCHEMICAL RESULTS

Integrations of the obtained fieldworks, fossil extraction, geochemical and physical properties, and visual petrographic analysis lead to understanding the more precise characterizations of the palaeoenvironmental condition and hydrocarbon potentials of the Sap Phlu Basin and the Na Pho Song Basin of the Huai Hin Lat Formation. They could be related to the productivity and development of the reducing event of the basins in the past with hydrocarbon recently.

5.1 Palaeoproductivity and palaeoredox analysis

For more understanding the accumulation and preservation of organic matters which are kept in the formation. The palaeoproductivity and palaeoredox are the key control conditions as carried out by petrographic and geochemical analysis.

5.1.1 Palaeoproductivity and palaeoredox proxies

5.1.1.1 Palaeoproductivity proxies

The potential of palaeoproductivity can also be evaluated based on palynofacies, TOC, excess SiO₂, and normalized Ba/Al and P/Al ratios.

1) Palynological assemblage

Palynological assemblage of the studied samples comprises abundant AOM and phytoclasts. The productivity is indicated by the abundance of these palynological components. AOM is structureless products

derived from phytoplankton or bacteria, higher plant resins, and reworked microbiological matters. They are no form varying in colour. It often comprises palynomorphs, pyrite inclusions, and may exhibit fluorescence (Suarez-Ruiz et al., 2012). Acritarchs are small organic structures of varying origins. The common type is the resting cysts of dinoflagellata or chlorophyta (Shen et al., 2012). Phytoclasts are microscopic plant fragments. The recovered small amount of spores and pollen are true representative of the parent vegetation from the adjacent landmass (Shen et al., 2012) and were transported to accumulate in the lake.

2) Total organic content (TOC)

TOC is Organic detritus passing from the photic zone through the water column to the sea floor controls nutrient regeneration, fuels benthic life, and affects burial of organic matters in the sediments (Suess, 1980, Veto et al., 1997). It records only a fraction of the total biological productivity in the surface waters of ocean (Tribovillard et al., 2006) and the lacustrine as well. The concentration of sedimentary organic matter (Gupta and Kawahata, 2006) and organic carbon content can also be used as a palaeoproductivity indicator (Meyers, 1997; Martin-Puertas et al., 2011). Higher productivity is marked by elevated organic matters and organic carbon content (Martin-Puertas et al., 2011).

3) Excess SiO₂

According to Yamamoto (1987) and Rona (1988), the silica in sediments is derived from hydrothermal, terrigenous, or biogenic sources. The source of silica of the studied samples is not associated with the hydrothermal sources as shown in Figure 5.1 and they are partly affected by biogenic SiO₂ as represented by the excess silica value.

$$\text{Excess SiO}_2 (\%) = \text{SiO}_2 (\text{measure}) - (\text{Al} (\text{measure}) \times (\text{SiO}_2/\text{Al})_{\text{PAAS}}) \quad (5.1)$$

Where $\text{SiO}_2 (\text{measure})$ and $\text{Al} (\text{measure})$ are percentage by weight of samples and $(\text{SiO}_2/\text{Al})_{\text{PAAS}}$ is ratio of SiO_2/Al of the Post-Archean Australian Shales (Taylor and McLennan, 1985). The high excess of silica concentrations is common in sediments of high productivity regions of the modern ocean (Murray and Leinen, 1993; Shen et al., 2012) as well as in lacustrine environment. Therefore, the excess silica present in this section is a good geochemical indicator for use as a palaeoproductivity proxy (Cohen, 2003; Bertrand et al., 2008; Martin-Puertas et al., 2011). The concentration of accumulation is proportional to diatom productivity and is a reflection of total primary productivity in the lake (Cohen, 2003 and Martin-Puertas et al., 2011). Diatoms are related to algae that can photosynthesize by themselves and can survive in both of marine and fresh water lacustrine environment. Their hard parts are made of hydrated silicon dioxide or frustule and probably preserved in benthic floor of lacustrine as high concentration may indicate to high productivity.

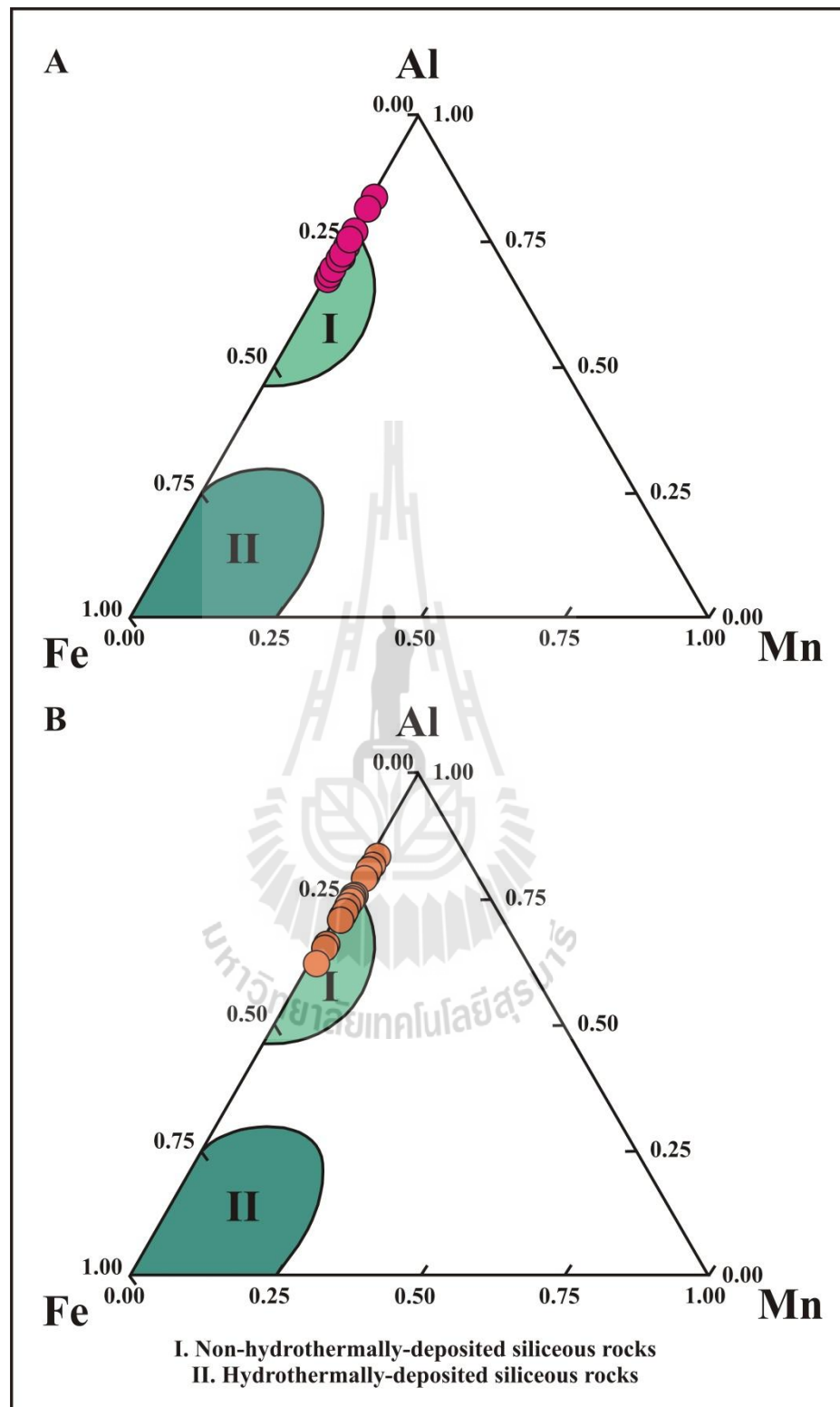


Figure 5.1 Al-Fe-Mn ternary diagrams of fine-grained rocks of the Ban Nong Sai section (A) and the Dat Yai section (B) (after Adachi et al., 1986).

4) Normalized trace element concentrations (Ba/Al, P/Al)

To compare trace element proportions in the samples, it is usually normalized trace element concentrations to aluminum content (Calvert and Pedersen, 1993; Reolid et al., 2012). Van der Weijden (2002) suggested that aluminum normalization of elemental concentrations is useful procedure for examining the degree of enrichment of an element in sediments. Aluminum can be considered as an indicator of the aluminosilicate fraction of the sediments with very little ability to move during diagenesis in most sedimentary deposits (including lake sediments) (Brumsack, 1989; Calvert and Pederson, 1993; Morford and Emerson, 1999; Piper and Perkins, 2004; Tribovillard et al., 2006).

The normalized Ba/Al is extensively used as a proxy for palaeoproductivity (Reolid et al., 2012). Ba is present in the form of barite (BaSO_4) and is mainly composed of detrital plagioclase crystals (Bishop, 1988; Rutch et al., 1995; Tribovillaed et al., 2006). Many studies have examined the link between surface productivity, export of organic matters from the photic zone, and biogenic Ba abundance in the water column (Dymond et al., 1992; Gingele and Dahmke, 1994; Monnin et al., 1999; Jeandel et al., 2000) as well as in the surface sediments (Paytan et al., 1996, 2003; Paytan and Kastner, 1996; Prakash Babu et al., 2002; Tribovillaed et al., 2006). Thus, a set of proxies constituted by Ba/Al (Reolid et al., 2012) was applied for the palaeoproductivity assessment.

Mackenzie et al. (1993) and Trappe (1998) suggested that the content of phosphorus in most marine sediments and sedimentary rocks is higher than the average crustal abundance which is about 0.01% phosphorus. The main source of phosphorus contributed to sediments is the phytoplankton necromass which

reaches the sediment water interface (including fish scales and bones). Van Cappellen and Ingall (1994) confirmed that anoxic bottom water of marine and lacustrine settings enhances the regeneration efficiency of phosphorus from sediments. Phosphorus is a structural element in DNA and RNA, as well as in many enzymes, phospholipids, and biomolecules (Tribovillard et al., 2006). Thus the distributions of phosphorus in sediments or sedimentary rocks are linked to the supply of organic matter possibly resulting from high productivity.

5.1.1.2 Palaeoredox proxies

The palaeoredox condition of the water and sediment interface can be evaluated based on the elemental composition of the sediment. The widely used geochemical palaeoredox proxies, i.e., U/Th, V/Cr, Ni/Co, (Cu+Mo)/Zn, V/(V+Ni), Ni/V, and Ce anomalies are considered in this study.

1) U/Th relationship

Uranium and thorium are present in detrital fraction associated with heavy minerals or clays (Jones and Manning, 1994). The authigenic uranium enrichment in sediment is controlled by the oxygen penetration depth and the sedimentation rate. The slow sedimentation rate allows more time for diffusion of uranyl ions from the water column into the sediment (Crusius and Thomson, 2000; Tribovillard et al., 2006). As the intensity of sulfate reduction activity is linked to the abundance of reactive organic matters, the uranium abundance usually shows a good correlation with the organic carbon content (McManus et al., 2005; Tribovillard et al., 2006). Th is relatively immobile in the low-temperature surface environment and is concentrated during weathering in resistant minerals. Therefore, the U/Th trend may indicate

high organic matter accumulation in the water as U also tend become enriched in marine sediments under reducing condition (Algeo and Maynard, 2004; Tribovillard et al., 2006).

2) V/Cr relationship

Vanadium is present in a quasi-conservative form of vanadate oxyanions and adsorbs on both Mn- and Fe-oxyhydroxide (Calvert and Piper, 1984; Wehrly and Stumm, 1989) and possibly kaolinite (Breit and Wanty, 1991 and Tribovillard et al., 2006). Chromium is usually incorporated within the detrital clastic fraction of sediment and it may substitute Al in clays. It can be adsorbed or occurred as chromite (Bjorlykke, 1974; Patterson et al., 1986, Jones and Manning, 1994). The ratio V/Cr has been employed as an index of palaeo-oxygenation in a number of studies (Ernst, 1970; Bjorlykke, 1974; Krecji-Graf, 1975; Dill, 1986; Dill et al., 1988; Jones and Manning, 1994). Ernst (1970) and Krecji-Graf (1975) suggested that the V/Cr values of above 2 represent an anoxic depositional condition with H₂S present in the water column overlying the sediment. Values below 2 are indicative of less reducing condition and values around 1 suggest the O₂-H₂S interface within the sediments (Jones and Manning, 1994).

3) Ni/Co relationship

Nickel is probably incorporated as an insoluble NiS into pyrite, even if the kinematics of the process is slow (Huerta-Diaz and Morse, 1990, 1992; Morse and Luther, 1999; Tribovillard et al., 2006). Lewen and Maynard (1982) and Grosjean et al. (2004) suggested that under reducing of anoxic/euxinic condition, the nickel may be preserved in sediments by the organic matters. Cobalt in anoxic water forms the insoluble sulfide CoS which can be taken up in solid solution by authigenic Fe-sulfides (Huerta-Diaz and Morse, 1992). Ni/Co ratio indicates the

relation with pyrite diagenesis of the higher value (>1) of Ni/Co (Jones and Manning, 1994). If the values are lower than, they probably indicate the higher oxidizing conditions. Therefore, it is used as a reliable redox proxy because of its more abundance in clastic material.

4) (Cu+Mo)/Zn relationship

Copper behaves partly as a micronutrient (Calvert and Pederson, 1993). It may be released to pore waters and incorporated in solid solution of pyrite (Huerta-Diaz and Morse, 1990, 1992; Morse and Luther, 1999; Tribovillard et al., 2006). Zinc may be released from organometallic complexes to pore waters and also incorporated as solid solution phase in pyrite (Huerta-Diaz and Morse, 1992; Daskaladis and Helz, 1993; Morse and Luther, 1999; Tribovillard et al., 2006). Molybdenum concentrations have been widely used as a proxy for the benthic redox (Meyers et al., 2005) due to their enrichment associated with increasing redox potential. The (Cu+Mo)/Zn ratios are expected to increase under reducing conditions and decrease while the environment is more oxidizing effect. Hallberg (1976, 1982) proposed the (Cu+Mo)/Zn relationship as an indicator of the oxygenation of bottom waters. Thus the ratios have also been used to interpret the depositional environment and the higher degree of reducing environment is detected by higher Cu than Zn contents.

5) V/(V+Ni) and Ni/V relationship

Ni and V are associated with reducing environment. Lewan and Maynard (1982) and Lewan (1984) suggested that the abundances of Ni and V are controlled by the factors that supply them through diffusion from the overlying water column. The V/(V+Ni) denoted a reductive environment with values

exceed 0.46 (Yarincik et al., 2000, Li et al., 2013). In contrast, the ratio Ni/V in bitumens and oils will be decreased in a reducing environment due to the availability of V and removal of nickel as sulphide (Jones and Manning, 1994).

6) Ce/Ce* relationship

Ce anomalies are a useful paleoredox proxy (German and Elderfield, 1990; Kakuwa and Matsumoto, 2006; Shen et al., 2012). The higher concentration indicates a more reducing environment and an anoxic condition are achieved if the value exceeds 0.8 which is the cutoff between the oxic-dysoxic and anoxic environments (Shen et al., 2012).

5.1.2 Palaeoproductivity and palaeoredox analysis

The productivity of the Huai Hin Lat Formation in the Sap Phlu and Na Pho Song Basins are evaluated based on the relevance and the abundance of palynofacies which was preserved in rock samples. Moreover, the association of TOC, excess SiO₂, and normalized trace element concentrations (Ba/Al and P/Al) are incorporated in the assessment of the palaeoproductivity in this study.

For understanding the palaeoenvironment of the Huai Hin Lat Formation, the relevant geochemical indices for palaeoredox condition, e.g., the changing relationship of U and Th and the ratios of various trace metals (V/Cr, Ni/Co, (Cu+Mo)/Zn, V/(V+Ni), Ni/V) and REEs (Ce/Ce*) have been employed.

5.1.2.1 Evaluation of the Ban Nong Sai section (Sap Phlu Basin)

5.1.2.1.1 Petrographic analysis

The depositional setting of the Ban Nong Sai section of the Huai Hin Lat Formation is reflected in the particulate organic matter (POM) or palynofacies present in the rock which comprised the mixture of lacustrine

palynomorphs and a significant amount of terrestrial organic particles. The studied samples contain a significant amount of amorphous organic matter (AOM), palynomorphs, phytoclasts, and a few spores and pollen but they lack of diversity (Figure 5.2). The organic matters were in extremely poor preservation and almost impossible to identify. Nevertheless, a distinctive palynological assemblage was identified. The point-count result and their fraction in a cumulative percentage are given in Table 5.1 and Figure 5.2 and 5.3A.

AOM concentration (Figure 5.2M and 5.3B) of the lower part is moderate with an average value of 5,478 particles/g rock. It shows two high peaks of 8,869 and 12,606 particles/g rock in Beds 1 and 7 respectively. The middle part is low with an average value 3,404 particles/g rock but exhibits one peak of 10,060 particles/g rock in Bed 10. The upper part shows the high value with an average of 8,350 particles/g rock. It shows an increasing trend with two peaks of 11,844 and 13,347 particles/g rock in Beds 14 and 19 respectively.

Acritarch shows occasional blooms of a few acritarch species (Figure 5.2A-D) and its concentration is low in the lower part with the upward decreasing trend and is approximately 1,700 particles/g rock in average (Figure 5.3C). However, it shows the high peak of 4,896 particles/g rock in the basal part (Bed 1). The middle part is high ranging from 395 to 7997 with an average of 3,107 particles/g rock. It shows two peaks of 7997 and 3,178 particles/g rock in Beds 9 and 11 respectively. The upper part is high, ranging from 2,211 to 6,520 with an average of 5,100 particles/g rock. It shows three peaks of 6,520, 6,048, and 4,975 particles/g rock in Beds 13, 15-16, and 19 respectively.

Phytoclast concentration (Figure 3H-M and 5D) is generally lower than the other two. The trend is closely conformed to those of acritarchs. The trend is higher in the lowest and the top of the lower part with an average value of 1,418 particles/g rock. The trend shows the peak in Bed 9 of the middle part as those of acritarchs. The concentration of the upper part is moderate except the two high peaks at the middle of Bed 13 and Beds 15-17 similar to the acritarchs trend.

Spores and pollen concentration (Figure 5.2E-G) is generally low throughout the section. The spore colouration index (SCI) is 7.5-8.5. The dark brown colour and almost opaque palynomorphs indicate a value of 6-7 on the thermal alteration scale (TAS) which corresponds to the temperature exposure between 170-200 °C in the late catagenesis stage (Schneebeli-Hermann et al., 2012; Batten, 1996).

The organic matters of the studied samples consist mainly of AOM and acritarchs which suggest that they belong to type I and type II kerogen respectively. They also contain some mixtures of type III kerogen by the presence of phytoclasts in the assemblage (Suarez-Ruiz et al., 2012). The organic matters of the Huai Hin Lat Formation, based on the kerogen type and the thermal history, have already generated oil and some gas.

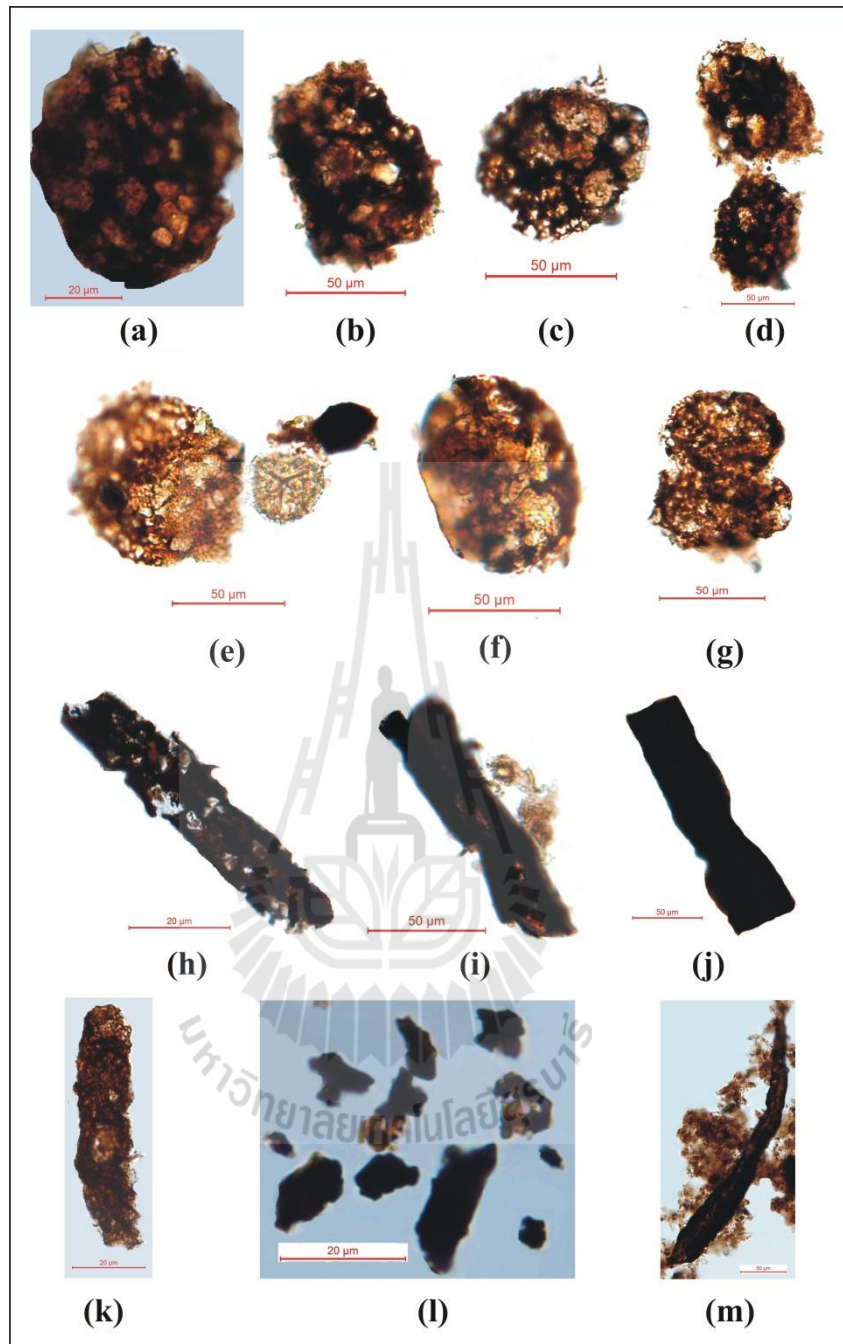


Figure 5.2 Photomicrographs of palynological assemblage of the Ban Nong Sai section consisting of palynomorphs (A-G), opaque biostructured phytoclasts (H-I), non-opaque biostructured phytoclast as stripe (J) and cuticle (K), non-opaque biostructured phytoclast (L), and non-opaque biostructured phytoclasts as striped elongate shape with AOM (M).

Table 5.1 Palynofacies point count (particles/g rock) and fraction in a cumulative percentage of AOM, acritarchs, and phytoclasts as compared with TOC data of the Ban Nong Sai section, the Sap Phlu Basin.

Bed	Palynofacies point count (Particles/g rock)			Palynofacies fraction (Cumulative percentage)			TOC (%)
	AOM	Acritarchs	Phytoclasts	AOM	Acritarchs	Phytoclasts	
20	10,537	4,790	1,382	63.1	28.7	8.2	5.33
19	13,347	4,975	2,764	63.3	23.6	13.1	1.90
18	10,820	2,211	1,273	75.6	15.5	8.9	5.39
17	7,900	4,013	5,159	46.3	23.5	30.2	5.07
16	7,047	6,048	5,592	37.7	32.4	29.9	4.07
15	2,874	5,988	5,343	20.2	42.2	37.6	4.95
14	11,844	3,790	1,658	68.5	22.0	9.5	3.67
13	2,916	6,520	4,252	21.3	47.6	31.1	2.34
12	62	1,184	948	2.8	54.0	43.2	3.48
11	289	3,178	3,178	4.4	47.8	47.8	3.61
10	10,060	395	5,212	64.2	2.5	33.3	4.51
9	2,112	7,998	6,702	12.6	47.6	39.8	4.53
8	1,187	603	264	57.8	29.4	12.8	5.33
7	12,606	1,437	4,146	69.3	7.9	22.8	5.56
6	1,132	479	553	52.3	22.1	25.6	4.98
5	4,235	1,800	1,543	55.9	23.8	20.3	5.27
4	3,979	676	614	75.5	12.8	11.7	5.31
3D	5,428	2,556	1,451	57.5	27.1	15.4	5.81
3C	4,436	369	958	77.0	6.4	16.6	6.01
3B	6,735	762	381	85.5	9.7	4.8	7.06
3A	2,317	553	276	73.7	17.5	8.8	6.93
2	2,257	1,726	539	49.9	38.2	11.9	6.15
1	8,869	4,896	2,132	55.8	30.8	13.4	5.37

5.1.2.1.2 Geochemical analysis

1) Total organic content (TOC)

The TOC proxy of the studied section is showing the values are range from 1.9 % to 7.1 % with an average of 4.9 % indicates a high productivity especially in the lower section. It shows the peak in Bed 3 which is not corresponded with the relatively low values of AOM, acritarchs, and phytoclasts. The trend shows consistently declining from base of the middle part to middle of Bed 13 of the upper part (Figure 5.3E). This lowest TOC is not corresponded with the high peaks of acritarchs and phytoclasts. The trend then increases upward to a high value of about 4.34 % on the average.

2) Excess SiO₂

The excess silica of the studied samples was mainly derived from hard parts of diatom. The values range from 1-13.4 % with an average of 5.5% as shown in Figure 5.3F. The values are slightly declining upward in the lower part (averaging 5.86 %). They show two high peaks of 7.8 and 8.4 % in Beds 1 and 6 respectively. The middle part shows high value averaging 6.89 % with the two high peaks in the carbonate rocks of Beds 10 and 12 respectively. The lower peak is corresponded with the high peaks of phytoclasts, acritarchs, and AOM. The values of the upper part are relatively low with an average value of 5.6 %.

3) Normalized Ba/Al

The ratio of Ba/Al in rocks of the measured section varies between 11.9 (10^{-4}) to 49.6 (10^{-4}) with an average of 25.1 (10^{-4}) (Figure 5.3G). The lower part is highly fluctuated with the high peaks in Beds 1 and 6 which are corresponded with the high peaks of excess SiO₂, phytoclasts, and AOM. The

middle part shows an average value of 28.1 (10^{-4}) and the high peak of 33.1 (10^{-4}) in Beds 9-10. The pattern is corresponded with the high peaks of AOM, acritarchs, phytoclasts, and excess silica. The upper part is in general declining with the low average value of 18.1 (10^{-4}).

4) Normalized P/Al

The normalized P/Al trend is similar to the trend of excess SiO_2 and normalized Ba/Al throughout the section. The values are ranging from 0.01 (10^{-4}) to 0.02 (10^{-4}) with an average of 0.014 (10^{-4}) as shown in Figure 5.3H. The lower part shows two high peaks which are corresponded with Ba/Al, excess SiO_2 , phytoclasts, and AOM. The trend is declining through the carbonate of the middle part to the upper part with an average of 0.016 (10^{-4}) and 0.011 (10^{-4}) respectively.

The TOC concentration is moderate to high which suggests a relatively high productivity of the surface water. A covariation between acritarch concentration and TOC shows the coefficient $R = 0.266$ (Figure 5.4B) which indicates moderate relation. However, the positive covariation of coefficient $R = 0.523$ between acritarch and phytoclast concentration exhibits close relation (Figure 5.4C). The Ba/Al and P/Al show similar trends which are depleted in the middle beds of lower part and most of the upper part. The positive covariation between the normalized Ba/Al and P/Al exhibits the coefficient $R = 0.522$ (Figure 5.4A) which suggests the close association between them.

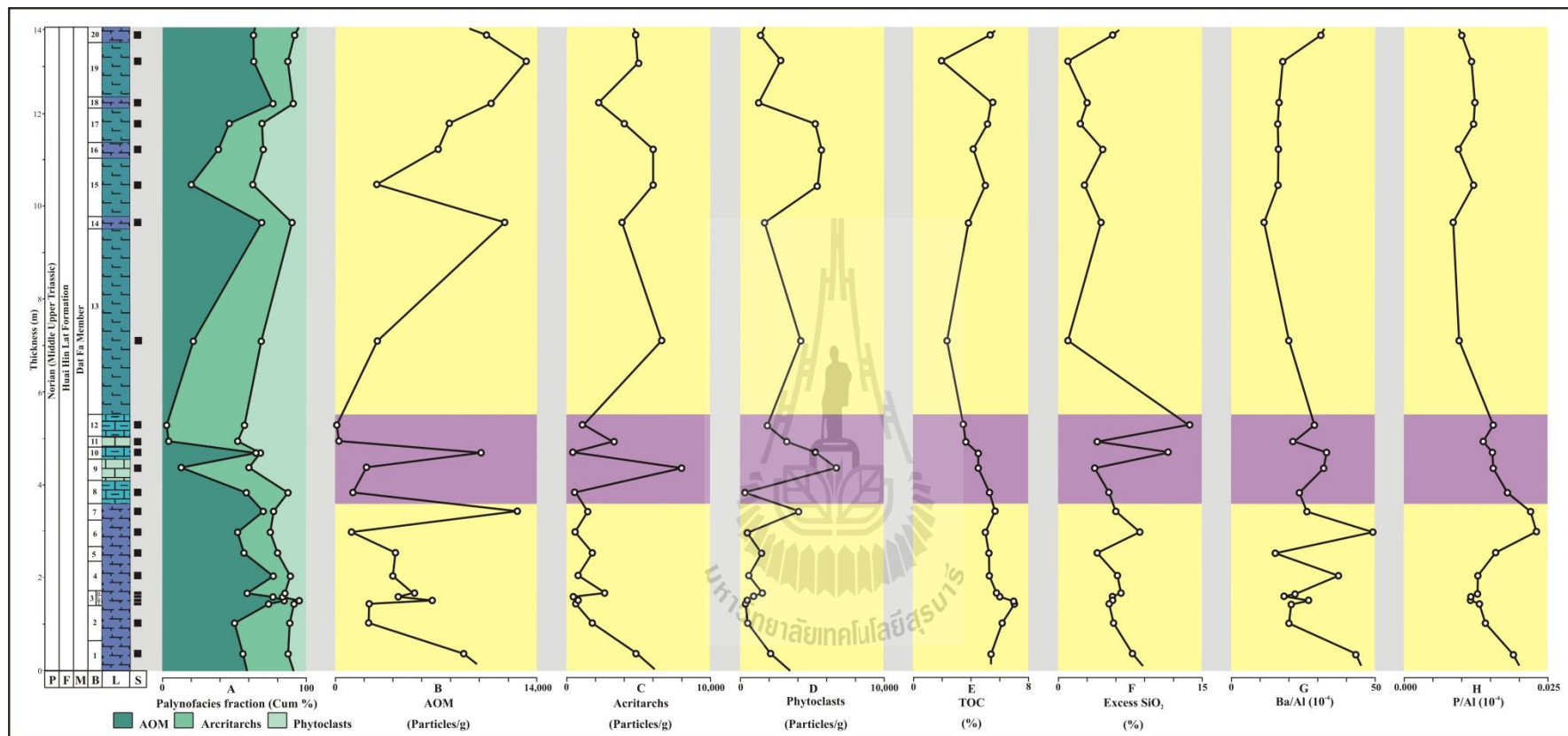


Figure 5.3 Bio- and chemostratigraphic data: (A) Palynofacies (AOM, acritarchs, and phytoclast fraction); (B) AOM; (C) Acritarch concentration; (D) Phytoclast particle concentration; (E) Total organic carbon (TOC); (F) Excess SiO₂; (G) The normalized Ba/Al trend; and (H) The normalized P/Al trend.

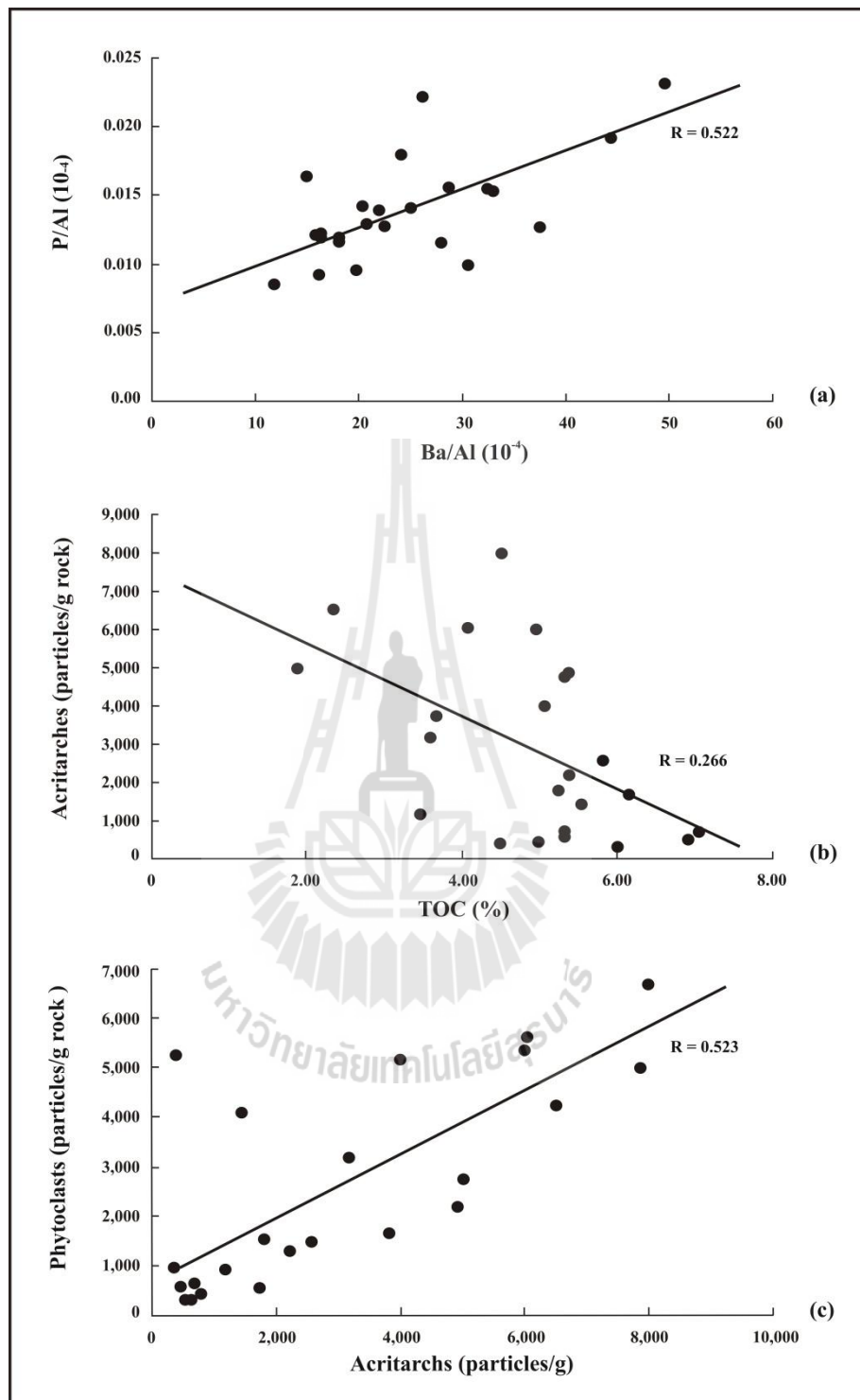


Figure 5.4 Crossplots of palaeoproductivity proxies; (A) Normalized P/Al (10^{-4}) and Ba/Al (10^{-4}), (B) Acritarchs (particles/g rock) and TOC (%), (C) Phytoclasts (particles/g rock) and Acritarchs (particles/g rock).

5) U/Th relationship

The U/Th ratio trend illustrated in Figure 5.5A shows relatively high fluctuation throughout the section. The ratios maintain a high value averaging 0.17 and are ranging around 0.12-0.20. The lower part shows a high value of > 0.15 with two peaks in Beds 3 and 6 with the value of about 0.18. The middle part is declining to approximately 0.12-0.16 in marlstone and argillaceous limestone. The upper part is constantly increasing and shows a relatively high value (0.19) with a low interval in Bed 19.

6) V/Cr relationship

The V/Cr ratio ranges from 1.5-3.3 and is 2.6 on the average as illustrated in Figure 5.5B. The lower part shows substantial variation of high values (1.9-3.3, averaging 2.8) with a high peak as those of U/Th in Bed 3 with the value of 3.3. The values are abruptly declined (averaging 2.1) in the middle part of carbonate rocks. They show two peaks in Beds 9 and 11 with about the same value of 2.1. The upper part is increasing (averaging 2.6) and shows three high peaks in middle of Bed 13, Bed 15 and Bed 17 with the value of 2.9, 3.0, and 3.3 respectively.

7) Ni/Co relationship

The ratios of Ni/Co vary between 0.4-1.3 and are 0.65 on the average. The lower and the middle parts are rarely fluctuated. They maintain a normal level ranging around 0.5-0.8 and stabilize at an average value of 0.6 with a slight high peak in Bed 3 (Figure 5.5C). In the upper section, the trend has risen but is highly fluctuated. It shows high peaks in Beds 13, 15, and 19 with an average value of 0.75.

8) (Cu+Mo)/Zn relationship

The (Cu+Mo)/Zn relationship is ranging from 0.52-1.04 with an average of 0.73 (Figure 5.5D). The lower part shows moderate value with substantial variation, ranging from 0.61-0.81 with an average of 0.71. It exhibits three high peaks in Bed 3, Bed 4-5, and Bed 7. The peak in Bed 3 is well corresponded with the peaks shown in U/Th, V/Cr, and Ni/Co. The trend declines to around 0.69-0.52 with an average of 0.59 in the middle part of carbonate rocks. Then the trend is rising in the upper part, ranging from 0.65-1.03 with an average of 0.86. It shows three high peaks in Beds 14, 15, and 19.

9) Ni/V relationship

The Ni/V ratios are ranging from 0.10-0.16 with an average of 0.13 at the lower part. The low peak in Bed 3 is corresponded with the high peaks of U/Th, V/Cr, Ni/Co, and (Cu+Mo)/Zn. The values rise in the middle part and maintain a level ranging around 0.16-0.20. They stabilize at an average value of 0.19. The values of the upper part are relatively moderate and frequently fluctuated. They are ranging from 0.09 to 0.19 with an average of 0.14 as shown in Figure 5.5E. They show high peaks in middle Beds 13 and 15 which are corresponded with the low peaks of (Cu+Mo)/Zn.

10) Ce/Ce* relationship

The section contains high ratio of Ce anomalies with the value ranging from 0.84-1.19 and an average of 0.97 (Figure 5.5F). The lower part increases from 0.84 to 1.01 with an average of 0.92. It exhibits two high peaks in Beds 3 and 6 which are corresponded with the high peaks of U/Th. The values rise to 0.88-1.19, averaging 1.03 in the middle part. The upper part is

about 1.00 on the average and shows a slight declining trend with a sudden increasing shift interval in Bed 19.



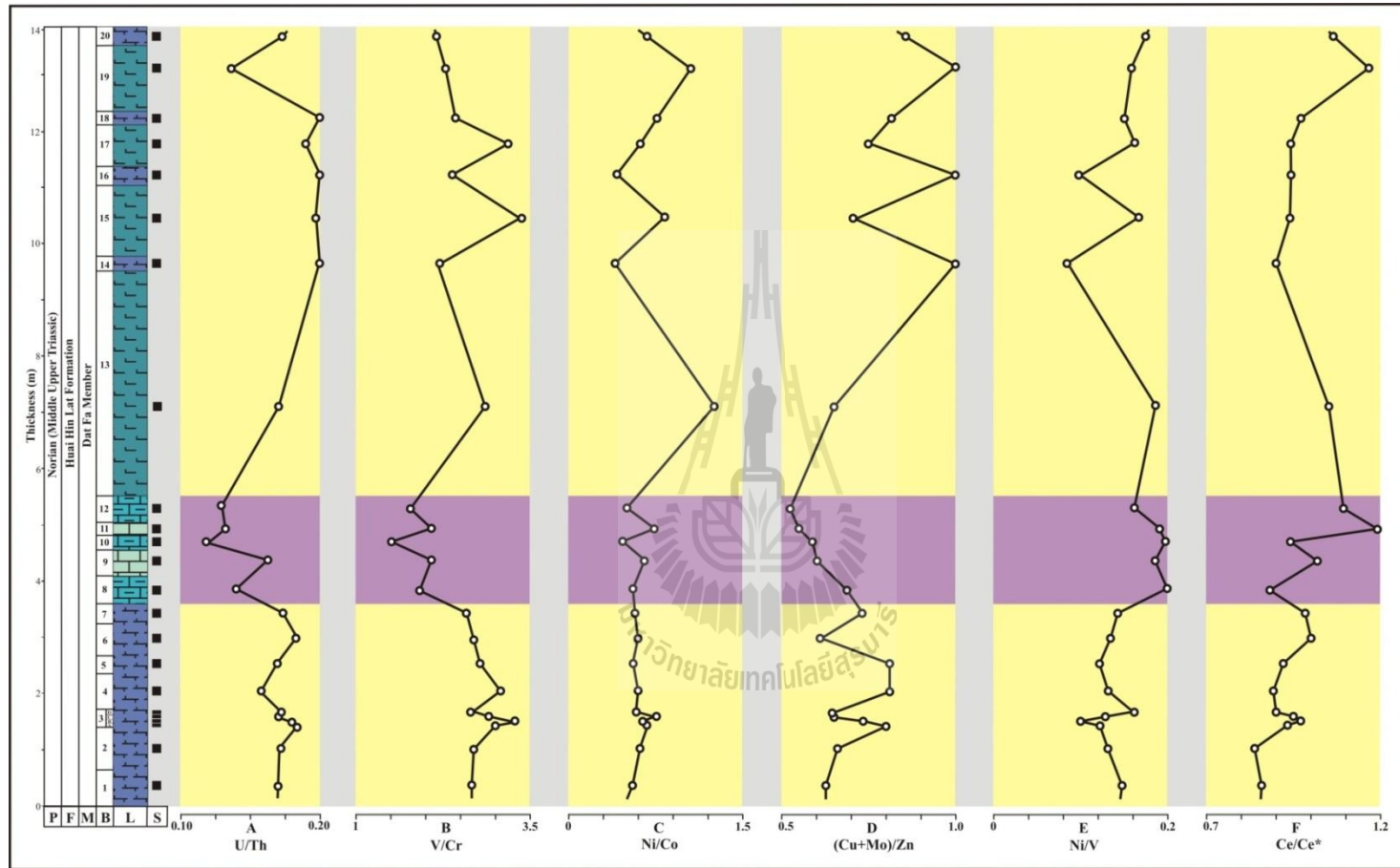


Figure 5.5 Chemostratigraphic data: (A) U/Th relationship; (B) V/Cr relationship; (C) Ni/Co relationship; (D) (Cu+Mo)/Zn relationship; (E) Ni/V relationship; (F) Ce/Ce* relationship.

5.1.2.2 Evaluation of the Dat Yai section (Na Pho Song Basin)

5.1.2.2.1 Petrographic analysis

The depositional setting and palaeoproductivity of the Dat Yai section is also reflected in palynofacies present in the rock similar to the Ban Nong Sai section. The studied samples contain a significant amount of amorphous organic matter (AOM) and phytoclasts. The acritarchs and spores and pollen are not discovered in the studied rocks (Figure 5.6). The organic matters were in extremely poor preservation and almost impossible to identify. Nevertheless, some palynological assemblages were identified in the studied samples. The point-count results and their fraction in a cumulative percentage (Figure 5.7A) are given in Table 5.2.

AOM concentrations (Figure 5.6C) show relatively high fluctuates through the section (Figure 5.7B). It shows occasional blooms of the cluster of AOM. They show the values ranging from 8,794 to 967,019 particles/g rock and stabilize at an average value of 378,182 particles/g rock. They are generally higher than the other one of palynofacies. The trend is low in the lowest and increasing upward to the top of the lower part with an average value of 374,302 particles/g rock. The trend shows five peaks in the lower part in Beds 5, 8, 11, 12, and 14 with the value of 687,747, 603,592, 553,477, 576,646, and 967,019 particles/g rock. The concentrations of the upper part are high as increasing upward to Bed 22 and decreasing upward to the uppermost. The trend shows four high peaks in Beds 18, 22, 27, and 30 with the value of 513,274, 815,070, 559,152, and 472,777 particles/g rock as corresponded with the AOM trend.

Phytoclasts are identified and shown into two type of opaque and non-opaque biostructured. The opaque biostructured are pitted and elongated in shape of fragments (Figures 5.6A) and non-opaque biostructured are pitted and elongated in shape of fragments (Figures 5.6B). Their concentration show relative fluctuations through the section (Figure 5.7C). They show the values ranging from 799 to 2,214,967 particles/g rock and stabilize at an average value of 312,275 particles/g rock. Their concentrations of the lower part are low with an average value of 52,061 particles/g rock. They show four high peaks in Beds 5, 8, 11, and 14 with the value of 114,624, 71,011, 113,534, and 153,191 particles/g rock respectively. The upper part shows the higher values with the values ranging from 45,538 to 2,214,967 and the average of 563,772 particles/g rock. It shows an increasing trend with five peaks in Beds 16, 22, 25, 27, and 32 with the value of 866,420, 140,876, 2,214,967, 1,118,304, and 1,525,532 particles/g rock respectively.

Acitarchs and spores and pollen concentrations are not discovered throughout the section due to the position of lake, where they the deposits did not support the palynomorphs to settle down.

The organic matters of the studied samples consist mainly of AOM which suggest that they belong to the type I kerogen. They also comprise some mixtures of type III kerogen by the presence of phytoclasts in the palynological assemblage (Suarez-Ruiz et al., 2012). The organic matters of the Huai Hin Lat Formation is, therefore, generate mainly oil and some gas, when they are mature.

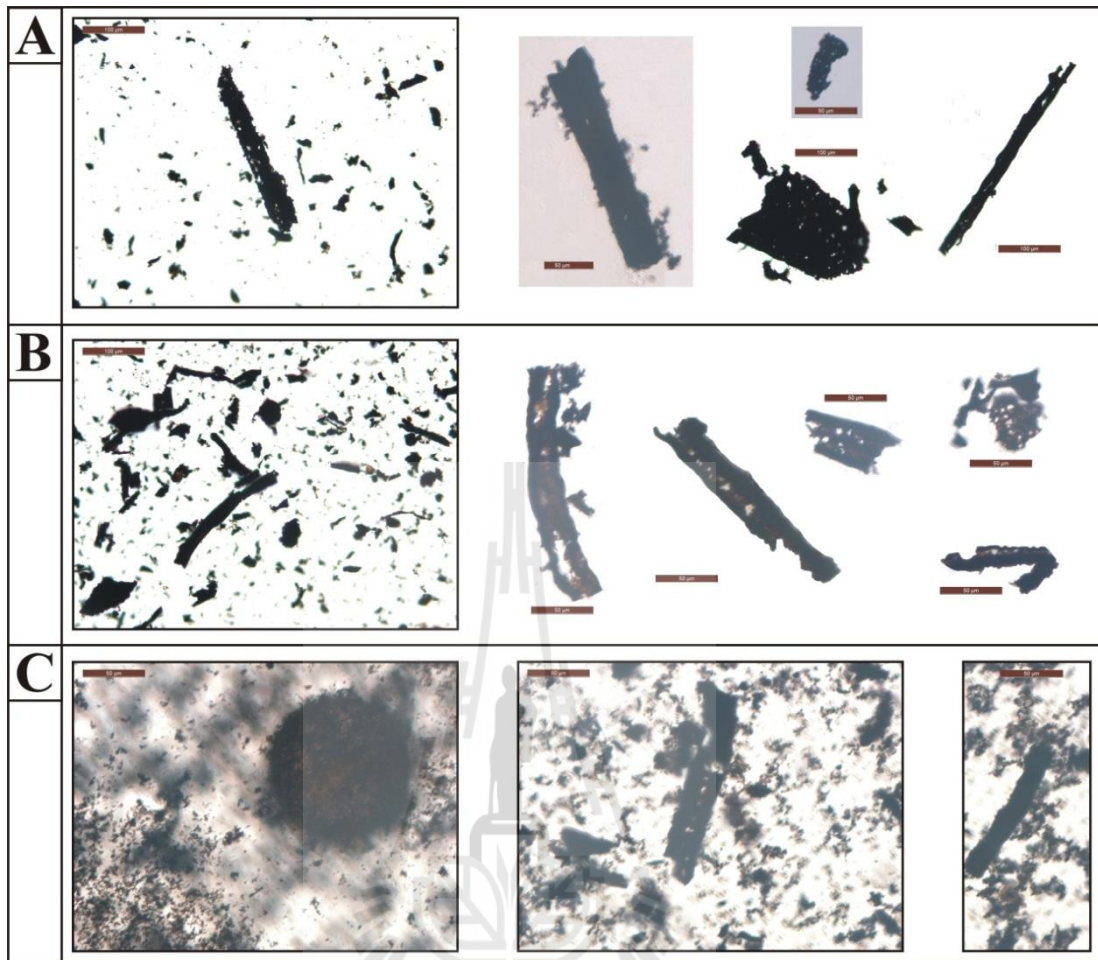


Figure 5.6 Photomicrographs of particulate organic components of selected samples under transmitted light; (A) Phytoclasts performed mainly of opaque biostructured as pitted and elongated in shape of fragments; (B) Phytoclasts are mainly of non-opaque biostructured as pitted and elongated in shape of fragments; (C) Phytoclasts and structureless palynology are amorphous organic matter (AOM) as illustrated in cluster in the uppermost Dat Yai section.

Table 5.2 Palynofacies point count (particles/g rock) and fraction in a cumulative percentage of phytoclasts, AOM, and palynomorphs as compared with TOC data of the Dat Yai section, the Na Pho Song Basin.

Bed	Palynofacies point count (Particles/g rock)			Palynofacies fraction (Cumulative percentage)			TOC (%)
	Phytoclasts	AOM	Palynom.	Phytoclasts	AOM	Palynom.	
32	194,749	1,525,532	0.00	11.32	88.68	0.00	7.79
31	413,450	856,431	0.00	32.56	67.44	0.00	7.78
30	472,777	118,194	0.00	80.00	20.00	0.00	8.09
29	252,971	233,511	0.00	52.00	48.00	0.00	8.10
28	489,797	827,990	0.00	37.17	62.83	0.00	5.76
27	559,152	1,118,304	0.00	33.33	66.67	0.00	5.77
26	319,760	75,238	0.00	80.95	19.05	0.00	6.78
25	113,589	2,214,967	0.00	4.88	95.12	0.00	6.93
24	393,709	64,018	0.00	86.01	13.99	0.00	6.13
23	462,975	89,608	0.00	83.78	16.22	0.00	6.19
22	815,070	140,876	0.00	85.26	14.74	0.00	6.13
21	416,351	45,538	0.00	90.14	9.86	0.00	4.67
20	308,540	71,201	0.00	81.25	18.75	0.00	5.59
19	340,267	61,867	0.00	84.62	15.38	0.00	6.00
18	513,274	85,546	0.00	85.71	14.29	0.00	7.46
17	282,727	55,924	0.00	83.49	16.51	0.00	6.52
16	157,531	866,420	0.00	15.38	84.62	0.00	8.08
15	315,860	38,520	0.00	89.13	10.87	0.00	7.23
14	967,019	153,191	0.00	86.32	13.68	0.00	7.37
13	620,727	64,659	0.00	90.57	9.43	0.00	5.99
12	576,646	48,054	0.00	92.31	7.69	0.00	7.42
11_2	121,879	52,234	0.00	70.00	30.00	0.00	7.53
11_1	553,477	113,534	0.00	82.98	17.02	0.00	7.70
10	221,950	31,707	0.00	87.50	12.50	0.00	6.74
9	477,457	44,937	0.00	91.40	8.60	0.00	10.09
8	603,592	71,011	0.00	89.47	10.53	0.00	8.17
7	65,971	9,425	0.00	87.50	12.50	0.00	8.17
6	387,913	31,283	0.00	92.54	7.46	0.00	-
5	687,747	114,625	0.00	85.71	14.29	0.00	6.74
4	304,698	39,743	0.00	88.46	11.54	0.00	-
3	203,316	23,460	0.00	89.66	10.34	0.00	6.30
2	203,760	29,885	0.00	87.21	12.79	0.00	-
1_3	135,854	13,863	0.00	90.74	9.26	0.00	6.84
1_2	53,558	6,301	0.00	89.47	10.53	0.00	-
1_1	8,794	799	0.00	91.67	8.33	0.00	-

5.1.2.2.2 Geochemical analysis

1) Total organic content (TOC)

The TOC proxy of the studied section shows the values ranging from 4.67 % to 10.09 % with an average of 7.03 % (Table 5.2) indicating high productivity especially in the lower section (Figure 5.7D). The trend is high (6.84 %) at the basal part with the average value of 7.49 %. It is increasing upward to the Bed 9 and constantly declining upward to the upper of its part. It shows the peak in Beds 1, 9, 11, 12, and 14 with the value of 6.84, 7.70, 5.99, and 7.37 %. It is moderately corresponded with the peaks of AOM and phytoclasts. Then it shows slightly declining to the Bed 20 and increasing upward to the uppermost with 6.66 % of averaging value. It shows four high peaks in the Beds 16, 18, 25, and 30 with the value of 8.08, 7.46, 6.93, and 8.09. It is not corresponded with the peaks of acritarchs and phytoclasts.

2) Excess SiO₂

The excess silica of the studied samples was mainly derived from hard parts of diatom. The values range from a very low value up to 11.99 % with an average of 4.89 % as shown in Figure 5.7E. The values are the highest in the basal part and generally declining upward in the lower part (averaging 5.62 %). They show three peaks in the Beds 3, 9, and 12 with the value of 11.99, 9.00, and 7.04 % respectively. The upper part shows the values are ranging up to 10.40 % and are relatively low with average value of 4.46 %. The six high peaks are shown in the Beds 17, 20, 22, 24, 27, and 30 with the value of 7.48, 10.40, 8.03, 4.45, 4.89, and 6.13 %.

3) Normalized Ba/Al

The ratio of Ba/Al in rocks of the measured section varies between 19.90 (10^{-4}) to 67.39 (10^{-4}) with an average of 33.41 (10^{-4}) (Figure 5.7F). The lower part is shown the highest peak at the Bed 3 and averaging value of 37.20 (10^{-4}). The other high peaks are still appeared in the Beds 8, 12, and 14 with the value of 44.75 (10^{-4}), 40.40 (10^{-4}), and 35.37 (10^{-4}) respectively. They are corresponded with the peaks of excess SiO_2 , phytoclasts, and AOM. The upper part shows the high peak in Beds 17, 22, 27, and 30 with the value of 47.67 (10^{-4}), 38.93 (10^{-4}), 31.88 (10^{-4}), and 35.81 (10^{-4}) respectively. The pattern is still corresponded with the peaks of AOM, phytoclasts, and excess silica. The upper part is constantly slight declining with the slightly low average value of 30.62 (10^{-4}).

4) Normalized P/Al

The normalized P/Al trend shows the values are ranging from 0.0061 (10^{-4}) to 0.0217 (10^{-4}) with an average of 0.0091 (10^{-4}) as shown in Figure 5.7G. The lower part shows three peaks of 0.0131 (10^{-4}) of averaging which are corresponded with the others except the peak at the basal part is accorded with only TOC. The Bed 1 is the highest peak and the value of both Beds 12 and 14 are 0.0094 (10^{-4}) and 0.0099 (10^{-4}). Then the trend is increasing upward to Bed 27 of 0.0084 (10^{-4}) and slightly decline to the uppermost with an average of 0.0071 (10^{-4}).

5) Ni/Co relationship

The trend is fluctuated (Figure 5.8A) as shown the ratios of Ni/Co vary between 0.62-1.17 with the average value of 0.65. The lower part, it maintains a normal level ranging around 0.62-1.07 and stabilizes at an average

value of 0.91. It shows three high peaks in Beds 5, 10-11, and 12 with the value of 1.02, 1.07, and 1.07 respectively. In the upper part, the trend has slightly risen with the value ranging approximately 0.71-1.17 and 0.97 of averaging. It show six peaks in Beds 16, 20, 24, 27, 30 and 32 with the value of 1.15, 1.15, 1.09, 1.17, 0.90, and 1.16.

6) U/Th relationship

The U/Th ratio trend illustrated in Figure 5.8B shows relatively high fluctuation throughout the section. The ratios maintain a high value averaging 0.51 and are ranging around 0.74 with occasional declination to around 0.36. The lower part shows the average value of 0.49 as high at the basal part and occasional declination. It shows four peaks in Beds 5, 8, 10, and 13 with the value of 0.74, 0.57, 0.48, and 0.45 respectively. The upper part is constantly increasing to approximately 0.38-0.68 and 0.54 in average. It shows a relatively high value of 0.58, 0.53, 0.57, and 0.67 in Beds 19, 23, 25, and 27 respectively.

7) V/Cr relationship

The V/Cr ratio is fluctuated and ranging from 1.84-2.46 with averaging of 2.07 as illustrated in Figure 5.8C. The lower part shows a high value at the lowermost and slightly declining upward. The substantial variations range from 1.87-2.46 with 2.8 of averaging. They show four high peak in Beds 5, 8, 11, and 13 with the value of 2.44, 2.20, 2.02, and 2.15 respectively. These peaks are relatively corresponded with Ni/Co and U/Th trends. In the upper part, the trend is slightly increasing upward in which the values range from 1.84-2.22 with the average value of 2.01. It shows three peaks in Beds 17, 22, 25, and 29 with the value of 2.12,

2.07, 2.10, and 2.22 respectively. They are less corresponded with the high peaks of Ni/Co and U/Th trends however; some parts still exhibit the same pattern.

8) V/(V+Ni) relationship

The section contains high ratio of V/(V+Ni) with the value ranging from 0.67-0.85 and an average of 0.79 (Figure 5.8D). The lower part increases from 0.75-0.85 with an average of 0.81. It exhibits five high peaks in Beds 5, 8, 11, and 14 with the value of 0.85, 0.85, 0.83, and 0.75. These peaks are corresponded with the high peak of Ni/Co and U/Th. Then the values decline to 0.67-0.83, averaging 0.78 in the upper part and sudden declination in the uppermost part. They show four peaks in Beds 17, 22, 25, and 29 as corresponded with the high peaks of V/Cr trend.

9) Ni/V relationship

The Ni/V ratios of the measured section are ranging from 0.17-0.48 with an average of 0.27 at the lower part (Figure 5.8E). The lower part is low at the base and increasing upward with the value ranging from 0.17-0.34 to 0.24 of averaging. It exhibits four peaks in Beds 3, 7, 9-10, and 14 with the value of 0.23, 0.25, 0.27, and 0.34. In the upper part, the values are still rising in the upper part to the uppermost part and maintain a level ranging around 0.21-0.48 with stabilize at an averaging value of 0.29. They show high peaks in Beds 19 and 23 with the value of 0.27 and 0.32 which Bed 32 is the highest value. All peaks are exhibited its pattern which is significant contrast with the pattern of V/Cr and V/(V+Ni).

10) (Cu+Mo)/Zn relationship

The (Cu+Mo)/Zn relationship of the studied section is ranging from 0.44-0.84 with an average of 0.63 (Figure 5.8F). They are

fluctuated through the section which the lower part is high values at the base, declining upward to Bed 9, and increasing again to Beds 13-14. The substantial variation is ranging from 0.44-0.84 with an average of 0.68. It exhibits three high peaks in Beds 3, 8, and 13 with the value of 0.83, 0.84, and 0.81 respectively. The trend generally declines to the uppermost with the values around 0.44-0.80 and an average value of 0.59. It shows four peaks in Beds 17, 20, 25, and 30 with the values of 0.77, 0.80, 0.65, and 0.66. It exhibits few peaks are corresponded with the high peaks of the other proxies.



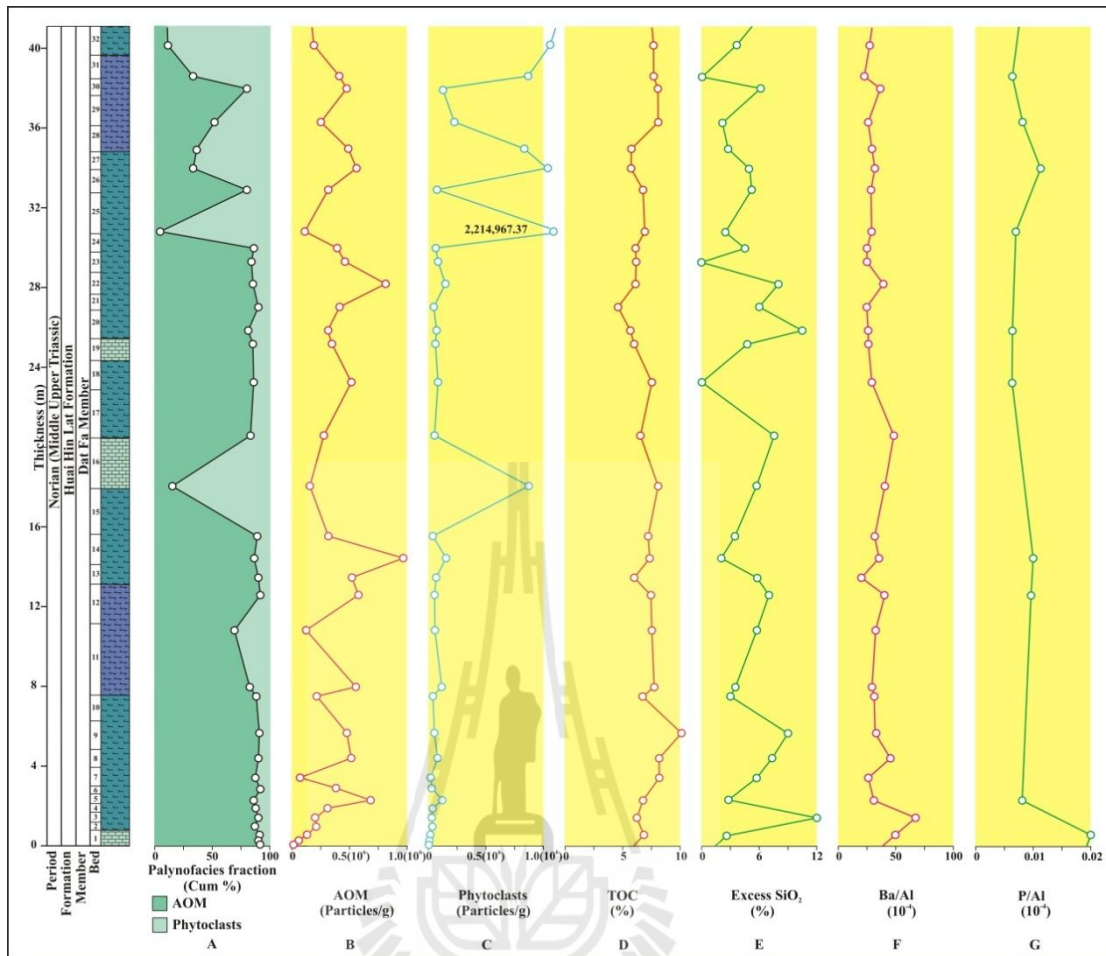


Figure 5.7 Bio- and chemostratigraphic data: (A) Palynofacies (AOM, and phytoclast) fraction; (B) AOM; (C) Phytoclast abundance; (D) Total organic carbon (TOC); (E) The normalize Ba/Al trend; and (F) The normalize P/Al trend.

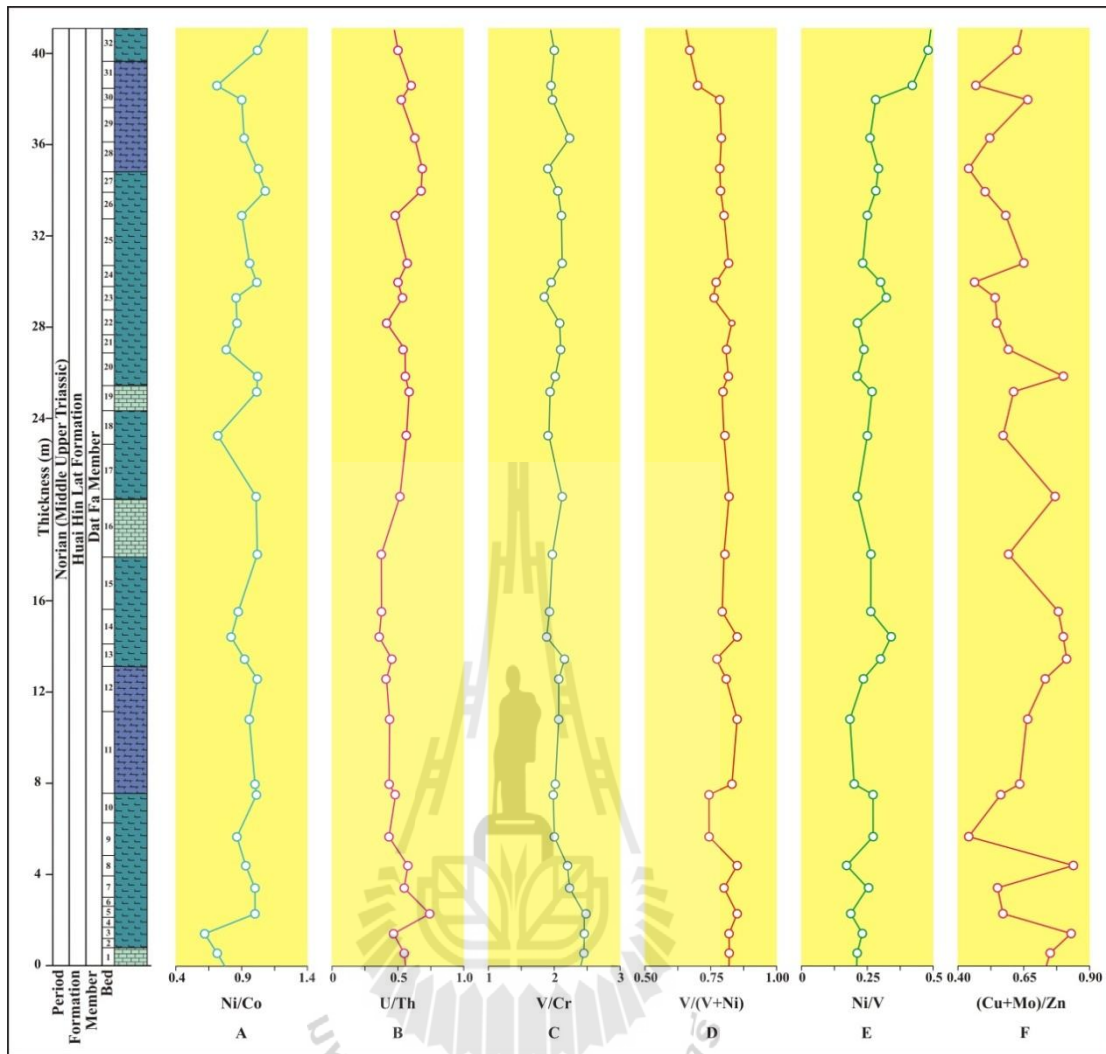


Figure 5.8 Chemostratigraphic data: (A) U/Th relationship; (B) U/Th relationship; (C) V/Cr relationship; (D) V/(V+Ni) relationship; (E) Ni/V relationship; (F) (Cu+Mo)/Zn relationship.

5.1.3 Palynofacies analysis

Based on the study of palynofacies analysis suggested by Suarez-Ruiz et al., (2012) combined with organic petrography studies provides more accurate information for the inference of organic facies and depositional paleoenvironments. Palynofacies studies depend on characterization of the organic matter origin (botanical precursors) and the organic matter assemblage using a combination of morphology and optical properties such as size and preservation. Many classifications for different types of organic matter have been recognized into three main morphological groups of kerogen concentrates are;

1) Amorphous organic matter (AOM) is the group of structureless amorphous products derived from phytoplankton or bacteria and higher plant resins.

2) Palynomorphs are the group of organic-walled constituents that remain after acid maceration: sporomorph, phytoplankton, and zoomorph. Each morphological group has been further divided in subgroups of sporomorph, freshwater and marine microplankton, zoomorph, and the others.

3) Phytoclasts are the group of fragments of tissues derived from higher plants or fungi which identified to opaque and non-opaque (translucent).

Measurement of abundance is percentage frequency of any component related to the total population of particles present and relative frequency. The numeric frequency of any component(s) related to any other component(s). The data is commonly plotted in percentage logs showing vertical variation of individual components or ternary diagrams which can spatially separate samples into associations or assemblages (Suarez-Ruiz et al., 2012). According to ternary plot of the normalized concentrations of AOM-phytoclast-palynomorph (APP) are the most

commonly used to characterize the palynofacies assemblage (Mendonca Filho et al., 2011c; Tyson, 1993, 1995; Suarez-Ruiz et al., 2012). These characterize of kerogen assemblages in order are shown differences in relative proximity to terrestrial organic matter sources and redox status of the depositional subenvironment which controls AOM preservation (Suarez-Ruiz et al., 2012).

The AAP ternary diagram is plotted by Ban Nong Sai extracted data in percentage of individual kerogen group. Twenty three samples disperse in five fields of palynofacies and environments as shown in pink solid circles of Figure 5.9. One sample of Bed 11 is plotted in field III of proximal shelf as nearby the cluster of Beds 9, 12, 13, and 15 in field V of mud-dominated oxic shelf. Seven samples of Beds 1, 2, 3D, 5, 6, 8, 16, and 17 is shown in field VII of distal dysoxic-anoxic shelf. The samples of Beds 3A, 3B, 4, 14, 18, 19, and 20 disperse in distal dysoxic-oxic shelf (field VIII). Lastly, four samples of Beds 3B, 3C, 7, and 10 appear in the field IX of distal suboxic-anoxic shelf, restricted marine or lagoon. Then twenty eight data of Dat Yai rock extracted data are also plotted in the APP diagram as shown in yellow solid circles (Figure 5.9). They are chiefly filled in field IX of distal suboxic-anoxic shelf carbonatic shelf, restricted marine or lagoon. One sample of Bed 25 is plotted in field I of highly proximal shelf or basin. Four samples of Beds 16, 27, 31, and 32 indicate field II of marginal dysoxic-anoxic basin and two samples of Beds 28 and 29 reflect the field VI of proximal suboxic-anoxic shelf. The palaeodepositional model of both sections will be explained later in next chapter.

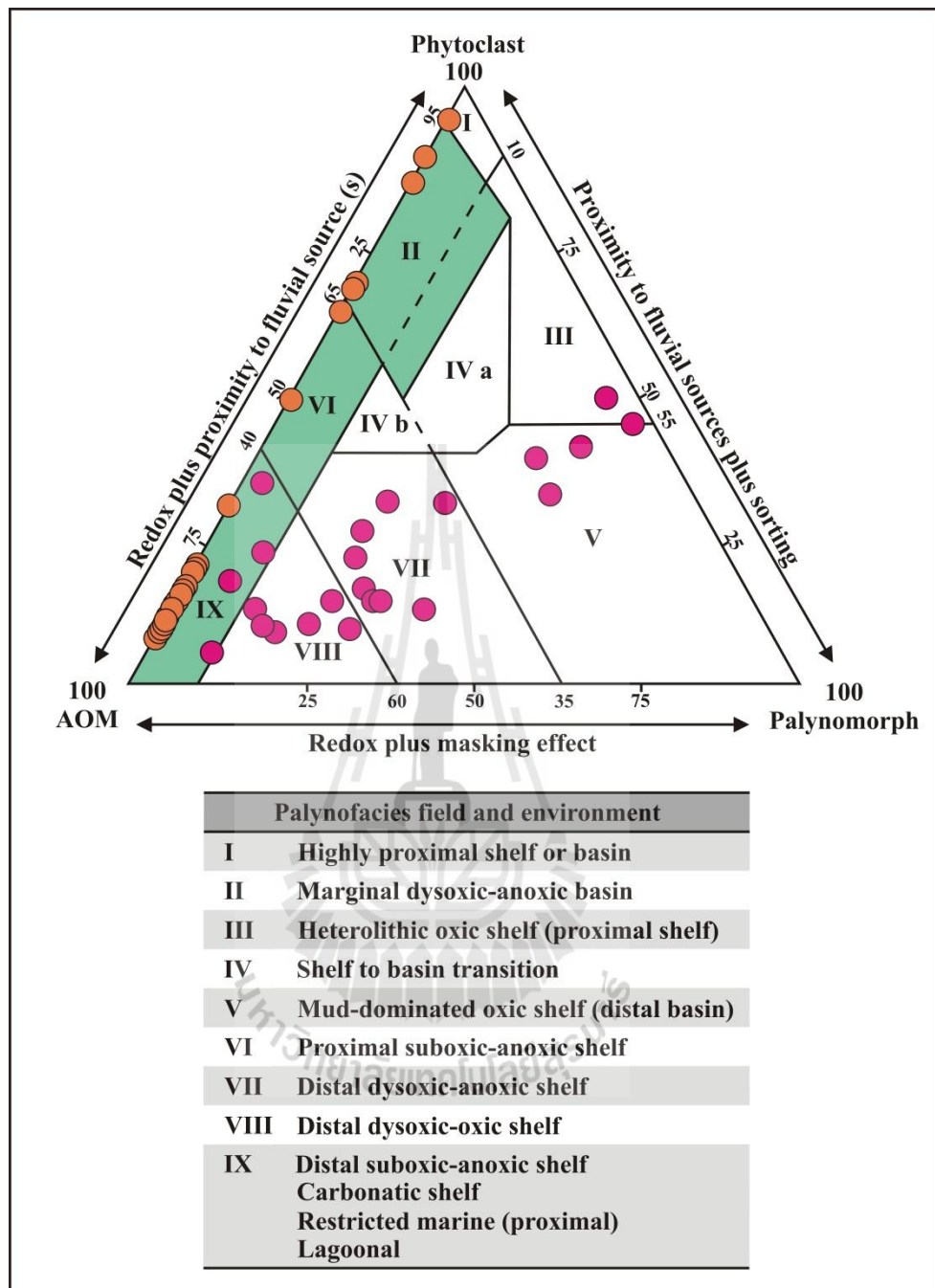


Figure 5.9 Kerogen plot AOM-Phytoclast-Palynomorph (APP) of the Ban Nong Sai section (pink) and the Dat Yai section (orange). In the APP diagram it is possible to define nine fields using the percentages of the 3 main kerogen groups. These fields represent different environmental conditions (Tyson, 1995; Suarez-Ruiz et al., 2012).

5.2 Hydrocarbon analysis

Hydrocarbon accumulation is a secondary storage which generated hydrocarbons were supplied from the organic rich shale. Hydrocarbon rich-region and proper engineering of industrial airflow is the key to the exploration and development. The possession of the key control conditions are divided into two conditions as below.

5.2.1 Source rock analysis

The organic rich shale that can produce the hydrocarbons may be analyzed by both petrographic and geochemical methods. Both methods are used to interpret the petroleum source rock assessment as below.

5.2.1.1 Visual petrographic analysis

Walters (2006) suggested that most of the organic carbon is bounded in a condensed, insoluble macromolecular material, and termed kerogen which has comparatively few functional groups. Kerogen has been called a geopolymer but this misnomer as a term implies that there is a repetition of distinct monomers and some structural orders. In contrast, the kerogen has no unique molecular structure and can only be defined in terms of bulk elemental composition and average molecular distribution. The kerogen formation is begun at the point when living cells die and their biochemical are exposed to the geologic environment. The processes and thermal regime under mild thermal conditions ($< 80\text{ }^{\circ}\text{C}$) as diagenesis terms occur the kerogen forms.

The samples carried out and performed the maceral types in percentage of each subgroup are, therefore, indicated to the kerogen types. The procedure is strictly normalized and codified by the International Committee for Coal

Petrography (ICCP) (Stach et al., 1982; Durand, 1993). The ICCP distinguish maceral families into 3 types are liptinite, vitrinite, and inertinite. This study distinguishes them into 2 types of sapropelic and humic. The sapropelic maceral is unconsolidated aquatic sediment rich in lipid organic matter and usually found under anoxic conditions that comparable to peat. It is recognized into sapropelic amorphous body, sapropelic vitrodetrinite, and alginite subgroups for more precise interpretation. The alginite is composed of algae, green algae, and acritarchs which may define to liptinite as other suggestions. But this study, it is grouped to sapropelic as rich in hydrogen rich-maceral as conformed to other members in this type. The humic group is identified into liptinite or exinite, vitrinite, and inertinite as accorded with suggestion of the ICCP. The liptinite or exinite is made of weak reflectance, strong fluorescence of organic particles, and often includes particles whose biological origin is clearly recognizable (Durand, 1993). It formed from substances rich in volatiles and hydrogen of algae, higher plants, and bacteria that relatively resistant to bacterial and fungal degradation and oxidation. Its families contain submacerals of resinite (fossil resin), sporinite (spores and pollen), suberinite (cork), cutinite (cuticle), chitin body, and bituminite (amorphous fluorescent matter). The vitrinite is referred to particles as exceed 0.03 mm dimension. It is made of amorphous particles having a medium reflectance which are weakly or not at all fluorescent (Durand, 1993). It is a major component of most coal seams which derived from plant tissues of stem, root, bark, and leaf as appeared grey reflected light. Its families comprise submacerals of texto-ulminite (well preserved cell wall), densinite (tissue fragmented clast), gelovitrinite (granular vitrinite gel). Lastly, the inertinite is made of particles having strong reflectance and no fluorescence (Durand, 1993). It is formed from woody

tissues which have been oxidized or undergone incomplete combustion of forest fires or erosion of already deeply matured sediments during transportation and sedimentation (Durand, 1993). It contains the distinctive fusinite (cell structure) and sclerotinite (fungal remain) of teloinertinite submaceral.

According to the Ban Nong Sai and Dat Yai sections, the percentages of maceral identification are shown in the summarizing tables of maceral types. Both sections are mainly composed of sapropelic, vitrinite, and inertinite as descending which no relation with liptinite. The Ban Nong Sai section is mainly of the sapropelic (80.7-90.3 %) as extremely relevant to sapropelic amorphinite and the sapropelic vitrodetrinite except alginite (Table 5.3). The sapropelic amorphinite values are ranging from 57.7-73.0 % with an average of 65.6 %. The sapropelic vitrodetrinite values vary between 16.0-24.0 % with an average of 20.2 %. The vitrinite is lesser composition of 9.7-19 %. It is defined to the values are ranging from 5.0-8.7 %, 4.3-11.0 %, and 0.3 % of densinite, gelovitrinite, and texto-ulminite respectively. The inertinite is the lowest of 0.3 % fusinite and shows no sclerotinite. The Dat Yai section, both sapropelic amorphinite and sapropelic vitrodetrinite are identified and performed (Figure 5.4) in range of 55.7-69.7 % (63.7 % averaging) and 17.3-26.3 % (21.6 % averaging) respectively. For totally of sapropelic maceral is approximate 85.9 % that more precise in kerogen type interpretation. The vitrinite is identified into four distinctive submacerals as shown texto-ulminite is too less of 0.3 % in the lowermost section. Densinite and gelovitrinite are ranging from 4.3-9.0 % (6.4 % averaging) and 6.0-10.7 % (8.2 % averaging) respectively. For the totally proportional identification of this group is approximate 14.6 % as no fluctuated characteristics in the section. The proportional results of inertinite show the values

and an average of 0.3 %. They are dispersing in the lower section particularly but sclerotinite shows no relation. All types of macerals classification are generated the hydrocarbon as oil and gas are, therefore, determined and discussed in kerogen typing.

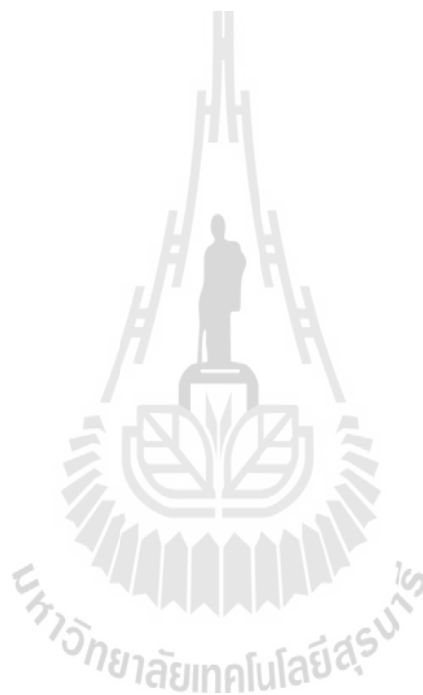


Table 5.3 Maceral types determined by visual petrographic analysis of the Ban Nong Sai section of the Huai Hin Lat Formation.

Sample	Bed	Sapropelic							Humic															
		SA	SV	Alginite				Total	Liptinie / Exinite							Total	Vitrinite			Total	IN		Total	
				AL	GA	AC	Other		RE	SP	SE	CT	CRP	BI	Other		TE	DE	GE		FU	SC		
A5G	20	199	48	-	-	-	-	247	-	-	-	-	-	-	-	-	0	1	18	33	52	1	-	1
		66.3	16.0	-	-	-	-	82.3	-	-	-	-	-	-	-	-	-	0.0	0.3	6.0	11.0	17.3	0.3	-
A4G	18	179	72	-	-	-	-	251	-	-	-	-	-	-	-	-	0	1	23	25	49	-	-	-
		59.7	24.0	-	-	-	-	86.7	-	-	-	-	-	-	-	-	-	0.0	0.3	7.7	8.3	16.3	-	-
A3G	16	188	64	-	-	-	-	252	-	-	-	-	-	-	-	-	0	1	26	21	48	-	-	-
		62.7	21.3	-	-	-	-	84.0	-	-	-	-	-	-	-	-	-	0.0	0.3	8.7	7.0	16.0	-	-
A2G	14	202	56	-	-	-	-	258	-	-	-	-	-	-	-	-	0	1	18	23	42	-	-	-
		67.3	18.7	-	-	-	-	86.0	-	-	-	-	-	-	-	-	-	0.0	0.3	6.0	7.7	14.0	-	-
16G	10	173	69	-	-	-	-	242	-	-	-	-	-	-	-	-	0	1	24	32	57	1	-	1
		57.7	23.0	-	-	-	-	80.7	-	-	-	-	-	-	-	-	-	0.0	0.3	8.0	10.7	19.0	0.3	-
13G	7	194	65	-	-	-	-	259	-	-	-	-	-	-	-	-	0	1	18	21	40	1	-	1
		64.7	21.7	-	-	-	-	86.3	-	-	-	-	-	-	-	-	-	0.0	0.3	6.0	7.0	13.3	0.3	-
11G	5	204	63	-	-	-	-	267	-	-	-	-	-	-	-	-	0	-	15	18	33	-	-	-
		68.0	21.0	-	-	-	-	89.0	-	-	-	-	-	-	-	-	-	0.0	-	5.0	6.0	11.0	-	-
6G	3A	212	57	-	-	-	-	269	-	-	-	-	-	-	-	-	0	-	17	14	31	-	-	-
		70.7	19.0	-	-	-	-	89.7	-	-	-	-	-	-	-	-	-	0.0	-	5.7	4.7	10.3	-	-
5G	2	219	52	-	-	-	-	271	-	-	-	-	-	-	-	-	0	-	16	13	29	-	-	-
		73.0	17.3	-	-	-	-	90.3	-	-	-	-	-	-	-	-	-	0.0	-	5.3	4.3	9.7	-	-

SA: Sapropelic amorphinite; SV: Sapropelic vitrodetrinite; AL: Algae; GA: Green algae; AC: Acritarch; RE: Resinite; SP: Sporinite; SE: Suberinite; CT: Cutinite;

CRP: Chitin remained particle; BI: Bituminite; TE: Texto-ulminite; DE: Densinite; GE: Gelovitrinite; IN: Inertodetrinite; FU: Fusinite; SC: Sclerotinite

Table 5.4 Maceral types determined by visual petrographic analysis of the Dat Yai section of the Huai Hin Lat Formation.

Sample	Bed	Sapropelic							Humic															
		SA	SV	Alginite				Total	Liptinie / Exinite						Total	Vitrinite			Total	IN		Total		
				AL	GA	AC	Other		RE	SP	SE	CT	CRP	BI		Other	TE	DE		GE	FU		SC	
T34-1	31	186	70	-	-	-	-	256	-	-	-	-	-	-	-	-	0	-	16	28	44	0	-	0
		62.0	23.3	-	-	-	-	85.3	-	-	-	-	-	-	-	-	0.0	-	5.3	9.3	14.7	0.0	-	0.0
T32-1	29	192	67	-	-	-	-	259	-	-	-	-	-	-	-	0	-	16	25	41	0	-	0	
		64.0	22.3	-	-	-	-	86.3	-	-	-	-	-	-	-	0.0	-	5.3	8.3	13.7	0.0	-	0.0	
T28-1	25	207	56	-	-	-	-	263	-	-	-	-	-	-	-	0	-	14	23	37	0	-	0	
		69.0	18.7	-	-	-	-	87.7	-	-	-	-	-	-	-	0.0	-	4.7	7.7	12.3	0.0	-	0.0	
T26-2	23	198	68	-	-	-	-	266	-	-	-	-	-	-	-	0	-	13	21	34	0	-	0	
		66.0	22.7	-	-	-	-	88.7	-	-	-	-	-	-	-	0.0	-	4.3	7.0	11.3	0.0	-	0.0	
T24-2	21	188	63	-	-	-	-	251	-	-	-	-	-	-	-	0	-	20	28	48	1	-	1	
		62.7	21.0	-	-	-	-	86.7	-	-	-	-	-	-	-	0.0	-	6.7	9.3	16.0	0.3	-	0.3	
T20-1	17	209	52	-	-	-	-	261	-	-	-	-	-	-	-	0	-	18	21	39	0	-	0	
		69.7	17.3	-	-	-	-	87.0	-	-	-	-	-	-	-	0.0	-	6.0	7.0	13.0	0.0	-	0.0	
T18-1	15	203	55	-	-	-	-	258	-	-	-	-	-	-	-	0	-	23	18	41	1	-	1	
		67.7	18.3	-	-	-	-	86.0	-	-	-	-	-	-	-	0.0	-	7.7	6.0	13.7	0.3	-	0.3	
T14-2	11	167	79	-	-	-	-	246	-	-	-	-	-	-	-	0	-	21	32	53	1	-	1	
		55.7	26.3	-	-	-	-	82.0	-	-	-	-	-	-	-	0.0	-	7.0	10.7	17.7	0.3	-	0.3	
T10-1	7	172	75	-	-	-	-	247	-	-	-	-	-	-	-	0	-	24	28	52	1	-	1	
		57.3	25.0	-	-	-	-	82.3	-	-	-	-	-	-	-	0.0	-	8.0	9.3	17.3	0.3	-	0.3	
T7-1	5	188	63	-	-	-	-	251	-	-	-	-	-	-	-	0	1.0	27	21	49	0	-	0	
		62.7	21.0	-	-	-	-	86.7	-	-	-	-	-	-	-	0.0	0.3	9.0	7.0	16.3	0.0	-	0.0	

SA: Sapropelic amorphinite; SV: Sapropelic vitrodetrinite; AL: Algae; GA: Green algae; AC: Acritarch; RE: Resinite; SP: Sporinite; SE: Suberinite; CT: Cutinite;

CRP: Chitin remained particle; BI: Bituminite; TE: Texto-ulminite; DE: Densinite; GE: Gelovitrinite; IN: Inertodetrinite; FU: Fusinite; SC: Sclerotinite

5.2.1.2 Hydrocarbon geochemical analysis

The hydrocarbon geochemical analysis is necessarily used for more precise determination on their hydrocarbon source potential. This mainly analysis may divide into TOC, vitrinite reflectance, and Rock-Eval pyrolysis as follows:

5.2.1.2.1 Total organic carbon (TOC)

The organic carbon is organically rich sediments (Bordenave, 1993). It is primary importance for understand how organic has been incorporated into sediments. The climatic, oceanographical, and geological settings corresponding to source rock habitat (Bordenave, 1993) are the first screening parameter for determining the potential of petroleum generation (Khositchaisri, 2012). For the lake of land deposition, most of the organic matter is oxidized. However, in warm and humid climates, large rivers carried large amounts of terrestrial organic matters (Bordenave, 1993) into the basin where accumulation. The organic matter quantity may reduce by oxidation during outcrop weathering (Leythaeuser, 1973; Clayton and Swetland, 1978; Peters, 1986; Stanley, 1987; Stanley et al., 1992). However, the quantity of organic matters in the samples is also indicated in terms of total organic carbon (Stanley et al., 1992) and organic matter quality will be described in next parts.

According to both studied sections, the samples were analyzed as referred to the great amount of organic matters. The TOC values of the Ban Nong Sai section are high as performed in Table 5.1. They are ranging from 1.90-7.06 % and an average of 4.86 %. They are highest in the lower part especially Bed 3 and constantly decline to the middle and the upper parts. The lower values are

shown in Beds 13 and 19 of 2.34 % and 1.90 % respectively. The Dat Yai section is less fluctuation of TOC values throughout the section. The TOC value is highest in Bed 9 and the lowest in Bed 21 are therefore, very high as shown in Table 5.2. Their values vary from 4.67 to 10.09 % and 7.03 % averaging as contained more organic matters.

5.2.1.2.2 Vitrinite reflectance (R_o)

During the processes of pre- and post-deposition, the sediments with organic matters are accumulated in the basin. The main chemical and physical properties are changed especially in organic matters. The organic matters condensation, carbon content increase, moisture and volatile matter content decrease, porosity increase, low density, and hardness etc. These characteristics are affected from the thermal maturation. The term maturation has long been used to describe the diagenetic evolution of the dispersed organic matters with increasing burial depth and temperature as leading to the formation of oil and gas (Tissot and Welt, 1984; Taylor et al., 1998; Suarez-Ruiz et al., 2012). The thermal maturity of the formation may be carried out by the method of coal rank, fluorescence properties of organic constituent, colour changes of organic matter in microfossils (thermal alteration index (TAI), conodont colour alteration index (CAI), spore colouration index (SCI), transmittance colour index (TCI) etc.), geochemical testing (CPI, Tmax, productivity index (PI), wt% elements (C, H, H/C etc.), and optical method. The optical method is divided into reflectance of vitrinite, solid bitumen, and zooclasts (graptolite). The reflectance of vitrinite is more comfortable to analyze and determine their thermal maturation. Moreover, vitrinite reflectance can be extrapolated from

reflectance measurements of some macerals of telocollinite (exinite) (Alperm, 1970; Peter and Cassa, 1994).

Analysis of vitrinite reflectance is a widely accepted method by the oil and gas industry (Fowler et al., 2005; Peter et al., 2005; Fraser et al., 2012) as the amount of light reflected by vitrinite macerals is a key test for their thermal maturity (McCarthy et al., 2011) and level of a sedimentary rocks comprising dispersed organic matter (ICCP, 1971; Stach et al., 1982; Taylor et al., 1998; Suarez-Ruiz et al., 2012). The intensity of incident white light reflected with the sample is measured at hundreds of points along a microscopic sampling area. Then a statistical analysis was used to determine the amount of vitrinite in the sample (McCarthy et al., 2011) under oil immersion (Stach et al., 1982; Peter and Cassa, 1994). As the result, oil immersion in analyzing is referred to subscript o in R_o parameter (Peter and Cassa, 1994). In case of low R_o can be affected from poor polishing whereas high values are typical of oxidized vitrinite as the atomic O/C and H/C ratios decrease (Suarez-Ruiz et al., 2012). The optical anisotropy is linked to the overburden pressure and generally rises with increasing rank (Davis, 1984; Suarez-Ruiz et al., 2012) and tectonic stress in directions other than vertical may also produce reflectance maxima with different orientations (Hower and Davis, 1981; Levine and Davis, 1989, 1990; Suarez-Ruiz et al., 2012).

The selecting samples of both Ban Nong Sai and Dat Yai sections have no any fluctuation appeared. The Ban Nong Sai section, eleven samples were sent for testing. Most of the samples are not found the measuring points and appropriated for detecting except Beds 14, 15, and 17 (Table 5.3) as the vitrinite reflectance values of Beds 14 and 17 are 0.82 % and 0.86 %. The higher value of

1.04 % is shown in Bed 15 which is more affected from influencing temperature. Ten samples were collected from the Dat Yai section for analyzing. Only three samples of Beds 15, 25, and 29 cannot analyze and appear in list as the same reason as Ban Nong Sai samples. All values are very high and ranging from 1.67-1.86 % with an average of 1.74 %. The highest value of 1.86 % is shown in the lower section and gradually decline up to the uppermost section where the lowest value is. These values are rarely different as shown in Table 5.4. They are not precise to promote to other maturity stages as overlapping.

Table 5.5 Vitrinite reflectance (R_o) testing by using optical method of the Ban Nong Sai section of the Huai Hin Lat Formation.

Sample	Beds	Vitrinite reflectance (R_o) %			Spot number	Standard deviation	Remark
		Minimum	Maximum	Mean			
A5G	20	-	-	-	5	-	No spots
A4-5G	19	-	-	-	-	-	No spots
A3-4G	17	-	-	0.86	2	0.0071	-
A3G	16	-	-	-	-	-	No spots
A2-3G	15	-	-	1.04	2	0.0283	-
A2G	14	-	-	0.82	14	0.0649	-
A1-2G	13	-	-	-	-	-	No spots
12G	6	-	-	-	-	-	No spots
10G	4	-	-	-	-	-	No spots
5G	2	-	-	-	-	-	No spots
1-4G	1	-	-	-	-	-	No spots

Table 5.6 Vitrinite reflectance (R_o) testing by using optical method of the Dat Yai section of the Huai Hin Lat Formation.

Sample	Beds	Vitrinite reflectance (R_o) %			Spot number	Standard deviation	Remark
		Minimum	Maximum	Mean			
T34-1	31	1.63	1.70	1.67	5	0.0268	-
T32-1	29	-	-	-	-	-	No spots
T28-1	25	-	-	-	-	-	No spots
T26-2	23	1.63	1.83	1.72	14	0.0591	-
T24-2	21	1.60	1.84	1.74	13	0.0804	-
T20-1	17	1.63	1.85	1.73	12	0.0732	-
T18-1	15	-	-	-	-	-	No spots
T14-2	11	1.62	1.79	1.73	12	0.0491	-
T10-1	7	1.71	2.00	1.86	10	0.0760	-
T7-1	5	1.60	1.79	1.70	12	0.0713	-

5.2.1.2.3 Rock-Eval pyrolysis

Pyrolysis was developed in the mid-sixties as an exploration tool for estimating the potential of rock sample by measuring the difference between its current total carbon (C_T or TOC) and residual carbon (C_R) after pyrolysis (Giraud, 1970; Gransch and Eisma, 1970; Bordenave et al., 1970, 1993). Rock-Eval pyrolysis is the method used widely especially by the petroleum industry (Bordenave et al., 1993) as rapidly evaluating the quality, thermal maturity (Espitalie et al., 1977, 1984; Clementz et al., 1979; Tissot and welte, 1984; Peter, 1986; Stanley et al., 1992), and type of organic matter (McCarthy et al., 2011) of prospective petroleum source rocks. For the analyzing, the sample was pulverized and let them to the instrument. Then Rock-Eval pyrolysis was starting in processes of the automatically programmed pyrolysis as described in detail in methodology chapter. This technique is involved pyrolysis of a small amount of sample under precisely controlled temperature gradual increase. The organic matter of sediments is usually

divided into bitumen of soluble of organic solvent and insoluble residue or kerogen. The difference of solubility/insolubility is directly related to the size of organic molecules (Bordenave et al., 1993). Generally, the complex molecule structures of organic matter are spent high thermal heating to break down their chemical bonds to simple one. The results may represent the simple molecules are transformed and expelled the generatively gaseous products due to range of input temperature. Therefore, the programmed pyrolysis results will be performed the various values of S_1 , S_2 , S_3 , and T_{max} in Table 5.5 and their quantity below.

S_1 represents the products are evolved with temperature up to 300 °C that the area under peak corresponds to thermal distillation of free or absorbed hydrocarbon from bitumen as ranging from C_1 to C_{40} . The ten samples of the Ban Nong Sai section were analyzed and performed the S_1 values are ranging from 0.03-0.18 mg/g rocks and an average of 0.09 mg/g rock. The most values are close to zero but Beds 3, 4, 10, and 14 of 0.12, 0.13, 0.16, and 0.18 mg/g rocks respectively are higher. The Dat Yai samples show the values are extremely low as compared with Ban Nong Sai samples. The most values are not exceeding 0.01 mg/g rock except Beds 11 and 15 which are rarely higher (0.02 and 0.03 mg/g rock). The low values indicate that free gases are slightly kept.

S_2 represents the products are totally evolved with temperature range of 300-500 °C. The area under peak represents the amount of HC-like products cracked from the kerogen (NSO compositions, Bordenave et al., 1993) and indicates the major proportion of the convertible carbon. The Ban Nong Sai samples were analyzed and shown the S_2 values ranging from 0.26 to 23.91 mg/g rocks and 7.93 mg/g rock of averaging. The Beds 3 and 4 of 23.91 and 14.34 mg/g

rocks are also higher than others. The values of 0.33 and 0.26 mg/g rocks in Beds 7 and 10 are the lowest. The samples of the Dat Yai section are very low varying between 0.11 to 0.18 mg/g rocks and an average of 0.14 mg/g rock. The values are slightly higher (0.15 to 0.18 mg/g rocks) than the lower part, however, they are still too low. They indicate that the kerogen is cracked and lack of potential kerogen.

S_3 represents the products are corresponded to CO_2 generating in the processes. Due to oxygen-containing compounds are quickly decomposed into hydrocarbons, water, and especially CO and CO_2 mixture during pyrolysis (Bordenave et al., 1993). The samples of the Ban Nong Sai section were analyzed and performed S_3 values varying between 0.21 to 0.90 mg/g rocks with 0.51 mg/g rock averaging. The Dat Yai section, the values are also high as ranging from 0.21 to 0.36 mg/g rocks and an average of 0.28 mg/g rock.

T_{max} represents the temperature of maximum rate of release of hydrocarbon (over S_2 peak) from the kerogen cracking processes. According to the Ban Nong Sai section, the T_{max} values are ranging from 443 to 451 °C. The values can produce the hydrocarbon but not precise to promote to other maturity stages as overlapping. The Dat Yai samples show the T_{max} values varying between 598 to 605 °C and an average of 602.6 °C which are slightly different as comparing to the others. They are extremely high because of probably less potential carbons are remaining.

Table 5.7 T_{\max} , S_1 , S_2 , and S_3 testing by Rock-Eval pyrolysis of the Ban Nong Sai section (Sap Phlu Basin) and the Dat Yai section (Na Pho Song Basin) of the Huai Hin Lat Formation.

Ban Nong Sai section						Dat Yai section					
Sample	Bed	T_{\max} (°C)	Pyrolysis (mg/g rock)			Sample	Bed	T_{\max} (°C)	Pyrolysis (mg/g rock)		
			S_1	S_2	S_3				S_1	S_2	S_3
A5G	20	444	0.03	3.51	0.77	T34-1	31	604	0.01	0.14	0.28
A4G	18	443	0.04	7.12	0.53	T32-1	29	604	0.01	0.13	0.24
A3G	16	443	0.04	2.65	0.57	T28-1	25	602	0.01	0.14	0.28
A2G	14	447	0.18	7.94	0.30	T26-2	23	605	0.01	0.12	0.36
16G	10	445	0.16	0.26	0.21	T24-2	21	602	0.01	0.11	0.21
13G	7	444	0.03	0.33	0.44	T20-1	17	601	0.01	0.12	0.26
11G	5	447	0.05	7.26	0.36	T18-1	15	603	0.02	0.15	0.34
10G	4	451	0.13	14.34	0.23	T14-2	11	605	0.03	0.17	0.26
6G	3A	448	0.12	23.91	0.74	T10-1	7	604	0.01	0.18	0.36
5G	2	445	0.03	3.63	0.90	T7-1	5	598	0.01	0.16	0.22

5.2.2 Reservoir property analysis

The reservoir rocks that storage and retaining the generated hydrocarbon are analyzed based on the physical properties of the reservoir formation. The development of gas storage conditions as affected on both their primary deposition and preservation. The lithology, mineral compositions, and produced micropores and porosity are acted as a key for successful reservoir interpretation.

5.2.2.1 Mineralogical analysis based on XRD method

The studied sections are begun with the rocks as available outcrops. They contain calcareous fine-grained mudstones and shales, and argillaceous limestones. The mineralogical analyses were conducted by standard X-ray diffraction (XRD) and both quantitative and qualitative minerals are decomposed on the same samples utilized for the TOC determination. They are considered to

evaluate only inherent minerals of detrital (quartz, feldspar, calcite, dolomite, zeolite, and hematite) and authigenic (clay minerals; smectite, chlorite, illite, and montmorillonite) minerals.

The Ban Nong Sai section, clay and calcite are the dominant minerals presented in the formation in which quantitative mineralogies are shown in Table 5.6. The clay and calcite contents are ranging from 20-65 % with 42.61 % of averaging and 13-43 % with an average of 27.91 % respectively. The general increase in weight percent of clay with maturity is accompanied by a general decrease in weight percent of K-feldspar (Fishman et al., (2012). In 100 % clay, the chlorite and illite are the most fraction as shown by the average of 83.91 % and 12.39 % respectively. The other mineral compositions e.g., feldspar, quartz, dolomite, and zeolite are lesser as descending. The other minerals of feldspar and quartz are ranging from 6-27 % and 3-18 % with the average of 13.13 % and 8.96 % respectively. Then the dolomite is lesser of 5.52 % averaging and zeolite is the lowest. Table 5.7 shows the results of the Dat Yai section having an extremely complex mineral composition as dominated feldspar, dolomite, and clay. The feldspar mineral is ranging from 16-33 % and average content of 24.31 %. The dolomite mineral is ranging from 16-34 % with an average of 28.47 % and clay mineral varies between 16-34 % with an average of 23.59 %. Then the other mineral compositions are quartz, calcite, and hematite are lesser as descending. The quartz mineral is ranging from 5-24 % with an average of 12.94 % and lesser calcite mineral is ranging from 4-28 % with an average of 9.25 %. The quartz and calcite are high in the lower section of Beds 1-17 with the average contents of 19.9 % and 12.2 % respectively but the upper section is still quite low. The minor composition of hematite ranges up to 2 % and an average content of 1.81

%. Moreover, clay minerals were also favorable for the formation and development of shale gas reservoir (Chen et al., 2011). Their results show no contents of montmorillonite and chlorite but illite is extremely high through the section as it is suggested all samples are composed mainly of illite.

Table 5.8 Mineralogic and clay fraction XRD data of the Ban Nong Sai section.

Bed	Total minerals						Total amount of clays		
	Zeolite	Quartz	Feld	Cal	Dol	Clay	Smect	Chlorite	Illite
Weight percent									
20	3	6	10	31	4	46	0	90	10
19	3	9	12	23	0	53	75	10	15
18	0	6	10	30	5	49	0	90	10
17	2	6	8	29	2	53	0	90	10
16	3	10	21	34	5	27	0	90	10
15	2	3	8	20	2	65	0	90	10
14	3	7	20	21	5	44	0	80	20
13	2	10	19	43	2	24	0	90	10
12	0	18	10	13	4	56	0	90	10
11	2	12	9	29	3	44	0	80	20
10	2	12	8	31	5	42	0	90	10
9	2	9	8	31	6	44	0	80	20
8	0	11	11	35	12	31	0	90	10
7	2	6	6	27	3	56	0	90	10
6	3	15	10	32	4	36	0	90	10
5	2	11	12	33	6	36	0	90	10
4	2	13	24	33	8	20	0	90	10
3D	2	7	8	28	4	51	0	90	10
3C	2	10	17	35	12	24	0	90	10
3B	2	8	15	21	7	47	10	80	10
3A	2	5	11	20	10	52	0	80	20
2	2	6	18	25	8	41	0	90	10
1	0	6	27	18	10	39	0	80	20

Remark; Feld = feldspar, Cal = calcite, Dol = dolomite, Smect = smectite

Table 5.9 Mineralogic and clay fraction XRD data of the Dat Yai section.

Bed	Total minerals						Total amount of clays		
	Quartz	Feld	Cal	Dol	Hem	Clay	Mont	Chlorite	Illite
Weight percent									
32	5	24	6	33	2	30	0	0	100
31	5	28	4	32	2	29	0	0	100
30	5	26	7	32	2	28	0	0	100
29	7	28	5	34	2	24	0	0	100
28	5	28	5	29	2	31	0	0	100
27	15	28	4	32	2	19	0	0	100
26	5	32	5	30	2	26	0	0	100
25	5	26	5	28	2	34	0	0	100
24	5	32	5	28	2	28	0	0	100
23	5	32	4	30	2	27	0	0	100
22	5	32	6	29	2	26	0	0	100
21	5	33	8	28	2	24	0	0	100
20	5	30	8	32	2	23	0	0	100
19	5	32	5	32	2	24	0	0	100
18	5	32	4	32	2	25	0	0	100
17	16	23	10	24	2	25	0	0	100
16	16	22	10	28	2	22	0	0	100
15	16	23	7	30	2	22	0	0	100
14	18	18	13	26	2	23	0	0	100
13	20	17	9	24	2	28	0	0	100
12	22	22	9	23	2	22	0	0	100
11-2	19	18	10	32	2	19	0	0	100
11-1	18	20	10	28	2	22	0	0	100
10	20	19	16	27	2	16	0	0	100
9	21	18	12	32	0	17	0	0	100
8	22	16	14	26	2	20	0	0	100
7	22	18	8	34	0	18	0	0	100
5	24	18	11	26	2	19	0	0	100
3	22	18	16	24	2	18	0	0	100
1	22	16	28	16	2	16	0	0	100

Remark; Feld = feldspar, Hem = hematite, Cal = calcite, Dol = dolomite, Mont =
montmorillonite

5.2.2.2 Micro-CT

The micro-CT is a useful tool for the determination of petrophysical parameters (Lima et al., nd) by preparing core plug. The large differences between the efficient attenuation of X-ray by solids are relative to that of pore space (Blissett et al., 2007) which the spatial variations are recorded. It records of tridimensional structure (Lima et al., nd) which may be corresponding to pore distribution (Blissett et al., 2007) and ultimately permits the imaging and quantification of interparticle, intraparticle, and fracture of porosity (Mees et al., 2003; Blissett et al., 2007). The records may still resolve and calculate the total volume of entire porosity of each sample. Then integration of total porosity data (free gas potential) with sorbed gas capacities provide a measure of the maximum potential gas capacity which is used to determine the economic feasibility of the shale gas reservoir (Ross and Bustin 2007; Chen et al., 2011).

According to the sections, four samples of 7G and A2G of the Ban Nong Sai section and T8-1 and T35-2 of the Dat Yai section are collected on locality where the lower and upper section for more precise in evaluation. The samples are scanned in each layer for the region of interest (ROI). The ROIs are probably used to interpret the porous media in the samples and the entire of four data sets are illustrated in Table 5.5 as follows. The scanned samples of 7G and A2G of the Ban Nong Sai section are shown the values of 8,030,055 μm^3 and 8,166,899 μm^3 of total volumes of interest and 7,494,882 μm^3 and 7,599,901 μm^3 of object volumes which are calculated to 93.33 % and 93.06 % respectively. The analyzing of porosity is recognized into closed and opened porosity by their number and volume. The closed pores of 7G are measured in number of 31,565 pores, pore volume of 432,449

μm^3 , and porosity of 5.46 %. The opened pores are measured in number of 102,723 μm^3 and 1.28 % of porosity. The samples of A2G, the closed pores are measured in number of 29,899 pores, pore volume of 429,830 μm^3 , and 5.35 % of porosity. The opened pores are measured in number of 137,167 μm^3 and porosity of 1.68 %. The closed and opened porosity of samples 7G and A2G are calculated to the total porosity of 6.66 % and 6.94 % (Figure 5.10) respectively. The samples of T8-1 and T35-2 of the Dat Yai section perform the total volumes of interest of 8,057,276 μm^3 and 8,111,995 μm^3 , object volumes of 7,361,435 μm^3 and 6,923,414 μm^3 as estimated to 91.36 % and 85.35 % respectively. The micro-CT is distinguished the pores into closed and opened porosity. The sample of T8-1 is identified to closed pore quantitation in number of 32,780 pores, pore volume of 531,504 μm^3 , and 6.73 % of closed porosity. The volume of opened pore is 164,317 μm^3 , and 2.04 % of porosity. The sample of T35-2 is identified to closed pore quantitation in number of 16,948 pores, pore volume of 164,429.78 μm^3 , and 2.32 % porosity. The opened pore quantitation is 1,024,151.29 μm^3 as shown 12.63 % of porosity. As the result, the porosity is summarized including of closed and opened pores of 8.64 % and 14.65 % for T8-1 and T35-2 (Figure 5.11) respectively. Therefore, the mean identical porosity as formed a proxy of the Ban Nong Sai and Dat Yai sections are 6.8 % and 11.64 % with the connectivity of 2550.5 and 6111.5 respectively.

Table 5.10 Description of collected samples of the Ban Nong Sai and Dat Yai sections of the Huai Hin Lat Formation which were scanned by Micro-CT instrument. They show the concentrations of object volume, porosity both closed and opened pores, and connectivity.

Description	Ban Nong Sai section		Dat Yai section		Unit
	7G	A2G	T8-1	T35-2	
Total VOI volume	8,030,055	8,166,899	8,057,276	8,111,995	um ³
Object volume	7,494,882	7,599,901	7,361,453	6,923,414	um ³
Object volume	93.33	93.06	91.36	85.35	%
Total VOI surface	240,125	242,848	240,668	241,757	um ²
Object surface	1,462,854	1,525,782	1,778,589	2,444,307	um ²
Number of closed pores	31,565	29,899	32,780	16,948	
Volume of closed pores	432,449	429,830	531,504	164,429	um ³
Surface of closed pores	1,037,469	1,029,892	1,233,950	411,793	um ²
Closed porosity	5.46	5.35	6.73	2.32	%
Volume of open pore space	102,723	137,167	164,317	1,024,151	um ³
Open porosity	1.28	1.68	2.04	12.63	%
Total volume of pore space	535,173	566,997	695,822	1,188,581	um ³
Total porosity	6.66	6.94	8.64	14.65	%
Connectivity	2,326	2,775	3,537	11,866	
Connectivity density	0.00029	0.00034	0.00044	0.00146	um ⁻³

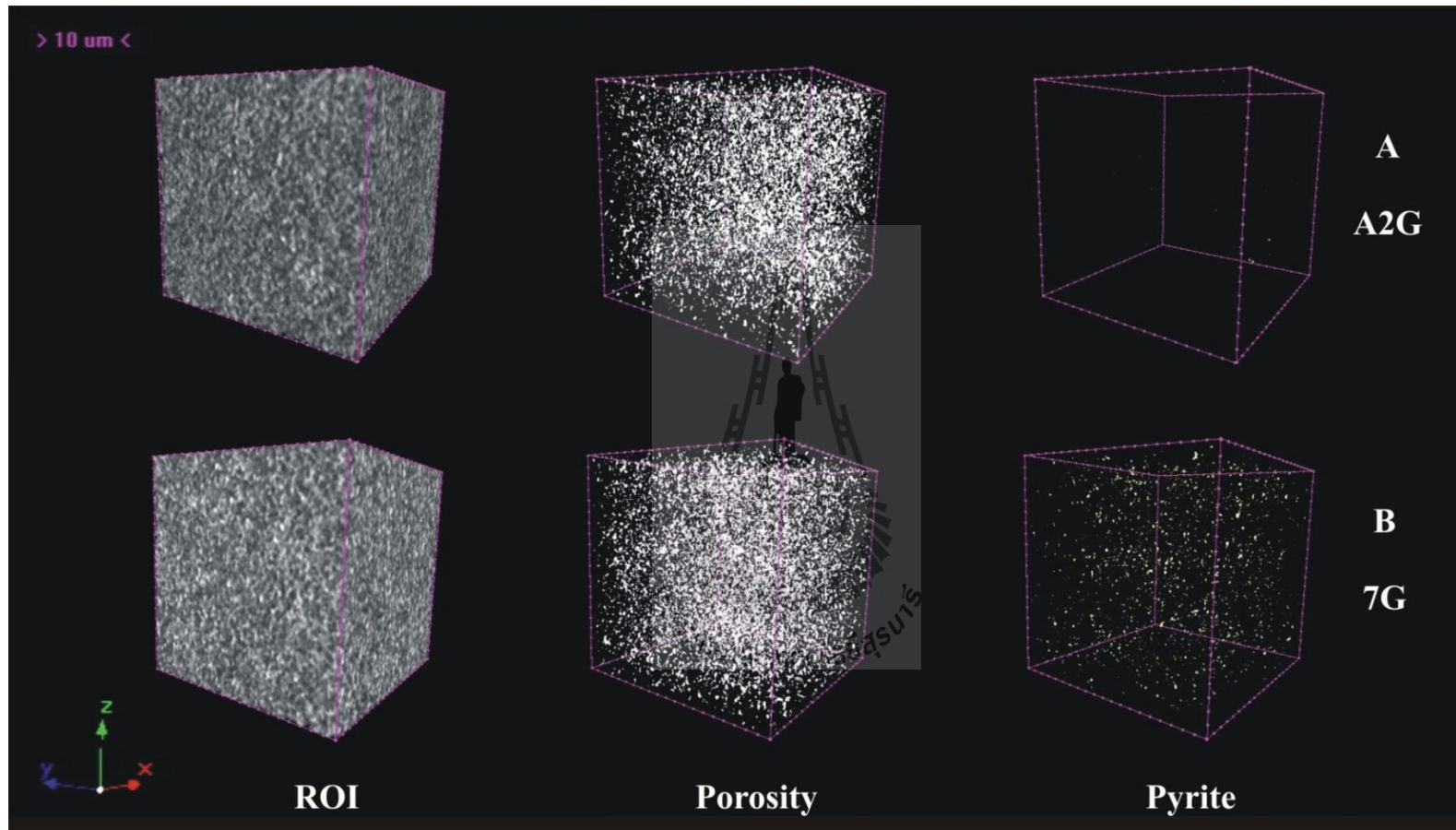


Figure 5.10 Region of interest (ROI) is used to interpret the characteristics and distributions both porous media and pyrite which observed in the Ban Nong Sai section of the Huai Hin Lat Formation, the Sap Phlu Basin.

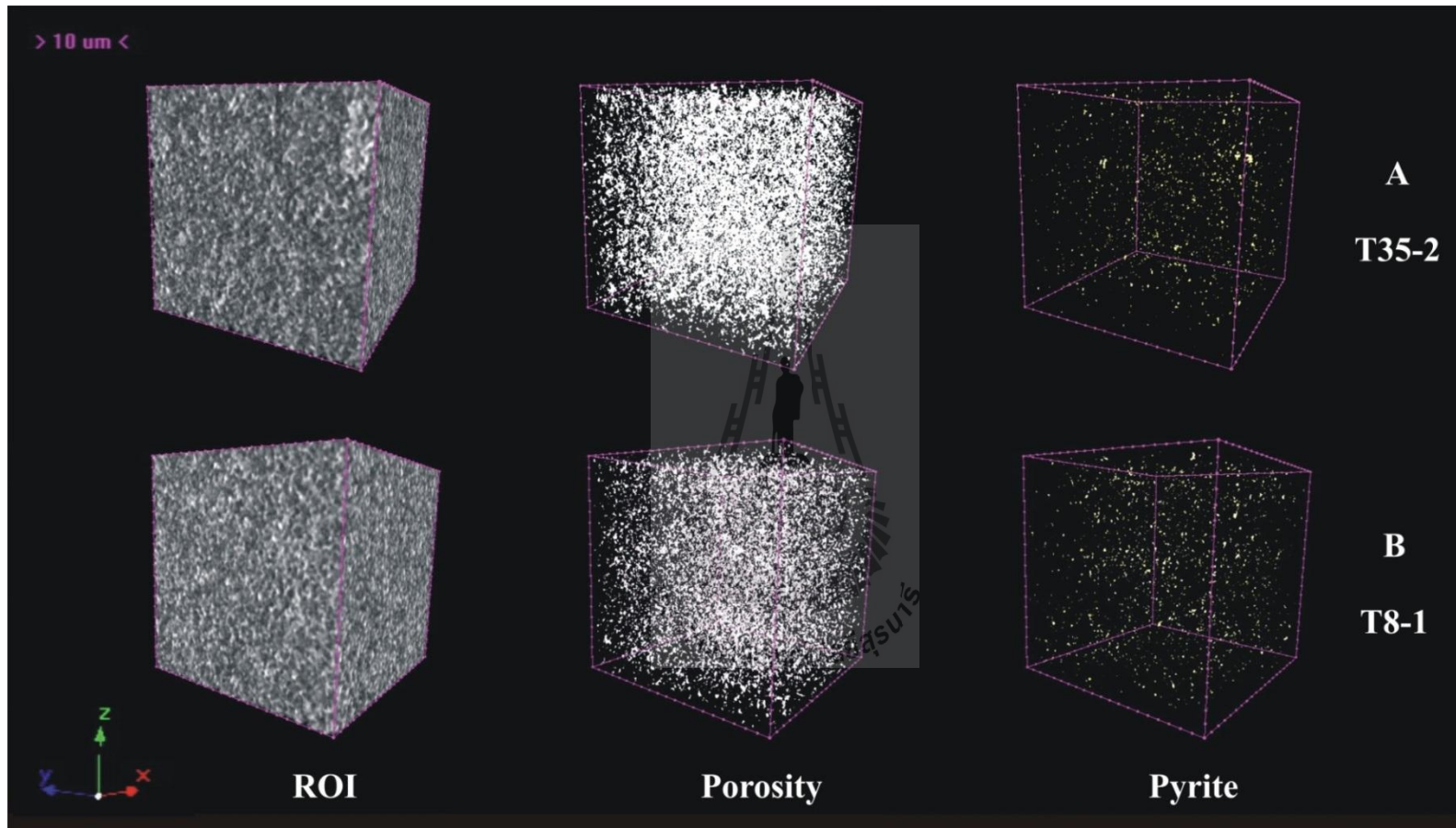


Figure 5.11 Region of interest (ROI) is used to interpret the characteristics and distributions both porous media and pyrite which observed in the Dat Yai section of the Huai Hin Lat Formation, the Na Pho Song Basin.

5.2.2.3 Scanning electron microscopy (SEM)

Tian et al. (2011) described the pore sizes grow greater during thermal maturation. The pores are abundant, bigger, morphology changed (striped, elliptical and connection) and perform in FESEM images cause kerogen is converted to hydrocarbons (Loucks et al., 2009). Total organic carbon (TOC) of the Ban Nong Sai section is high with an average of 4.86 % and the Dat Yai section is very high with yielding of 7.026 %. R_o of the Ban Nong Sai and Dat Yai sections show yielding concentrations of 0.91 and 1.74 % are exactly mature and higher mature respectively (more details of TOC and R_o are described clearly above). Therefore, both TOC and R_o are shown a definite stratigraphic trend within the section, clearly relationships of paleoenvironment, deposited organic matters, and deeply burial to generate pores. The pores are measured a few microns as referred to micropores which including the pores are lesser than 1 μm across in nanometer-scaled (nanopores).

The FESEM technique is viewing pores that are occurred in the formation but cannot quantify porosity as lacked any direct porosity measurements. Nevertheless, it is considered a necessary step in understanding overall porosity in the formation by identifies pore types and their variability as a function of thermal maturity. The pore types are criteria used to distinguish which are naturally occurred pores. They are likely to be present in the rocks. The abilities to produce, store, and transmit hydrocarbons is fundamental properties of economically producing self-sourced reservoirs like gas shale.

5.2.2.3.1 Common microscopic analysis (pore types)

The microscopic analysis is used to recognize the discovered pores into several types. The pores in samples of the Ban Nong Sai and Dat Yai sections are classified into eleven and nine types respectively. The details of all pore types will be shown in Figure 5.12 and described as follows:

1) Organic matter pores

They occurred in parts of the organic matter as dispersed in samples. They are natural and different from the characteristics of artificial pores as presume typical features. The artificial pores have sharp boundaries and typically occur along the common edge between difference of organic and inorganic constituents.

2) Interparticle pores

They occurred between grains and vary in type as depended on their origins. Their geometries are differed significantly as a function of both primary pore preservation and diagenetic alteration. The pores are abundant in young or shallow buried sediments and commonly well connection. They form an effective pore networks (permeable) and more advantages for shale gas systems. The terminology and description above are used to characterize them into four types of flocculation, intergranular, interrigid-grained rim, and intercrystalline pores.

2.1) Flocculation pores

They associated to fluid migrations and probably linkd to depositional processes as affected to mud microfabrics (Schieber et al., 2007). If a mud accumulated from current transported floccules, one might expect a network of larger pores, poorer sealing capacity, and easier release of liquid and

gaseous hydrocarbons. Flocculation phenomenon in which a number of these parameters such as settling velocity, floccule size, grain-size distribution, ion exchange behavior, and organic content are brought to come together. A joining of smaller particles is formed larger aggregates as floccules. The floccules enhance the deposition rate of fine-grained sediments and its understanding is critical for model the behavior of mud in sedimentary environment. They are clumps of electrostatically charged clay flakes that sink toward as they can form a cardhouse structure of individual edge-face- or edge-edge oriented flakes and/or domains of face-face- oriented flakes (O'Brien, 1971, 1972; Bennett et al., 1991; Slatt and O'Brien, 2011). If the pores or collapsed flocs are preserve presence, they will illustrate the interparticle pores.

2.2) Intergranular pores

They are a part of the matrix-related pore types or interparticle pores between each of rock-forming compositions as controlled the shapes, features, and size of the pores. The rock-forming compositions are more divers are also probably generated more pores.

2.3) Interrigid-grained rim pores

They are associated with characteristics of crystal-forming minerals. They occur in spaces between crystal of minerals and surrounding rock matrix. Moreover, the edges or rim of rigid grains of minerals were formed by partial secondary origin or shrinkage of grained crystals in rock matrix. The gaps between the rigid-grained rim or edge and surrounding matrix are formed the pores as well.

2.4) Intercrystalline pores

The descriptions of this pore type are associated with the characteristics of crystal-forming minerals. They occur in spaces between the overlapping crystals of minerals when they are growing. The similar or different crystals are probably overlapping and also produce the pores.

3) Intraparticle pores

They occurred within detrital grains or crystals as some of these pores are primary in origin and although the most are probably diagenetic. They appeared as varied in age as in young muds and mudrocks can be very abundant. Common types are recognized by their origins such as intraparticles of pyrite framboids, clay particles, fossil fragments, and grain or crystal dissolutions etc. Consequently, the term of descriptive pore types may recognize them into four types of intracrystalline, intraplatelet, intrafossil fragment, and intracovering pyrite crystal/grain pores.

3.1) Intracrystalline pores

They occurred within the crystalline minerals. These grains may have internal pores between these microcrystals or each of minerals of secondary origins (Slatt and O'Brien, 2011). They usually dispersed within the shale matrix especially pyrite framboids and quartz crystals.

3.2) Intraplatelet pores

They occurred within clay aggregates/particles. These pores are occluded with organic matters or authigenic clay platelets and pores may be flocculates are generally linear and parallel to one another (Loucks et al., 2012).

3.3) Intrafossil fragment pores

They occurred within fossil fragments and body-cavity. The pores may generate after soft tissues were degraded and include primary pore chambers within faunal and floral fossil grains (Loucks et al., 2012). Moreover, they may produce after secondary origins of diagenesis alteration.

3.4) Intracovering pyrite crystal pores

They mean to the pores are occurred within crystals or grains of pyrite as are likely formed by primary origin of individual pyrite crystals. These individual pyrite were formed an inner and outer coverings of cubical crystals when they occurred in this formation.

4) Microfractures and microchannels-related pores

They are chiefly porous media channels as occurred within rock matrix. They are affected from natural forces of tectonics in regional and adjacent areas. The natural forces have generated fractures and cracks which cut across the rock matrix as weakness. These features are shown by microfractures and sets of joints which are not artifacts produced by fracturing the sample, handling, and preparation as should be appeared sharp curve features. They are likely formed the original fractures that preserve in the undisturbed rock matrixes. Moreover, smaller microchannels are appeared which formed subparallel to bedding plane in rock matrix as well.

4.1) Microfracture-related pores

They are very important in shale gas systems where they exist and are not completely cemented (Loucks et al., 2012). The natural fractures have been proposed as storage, transport mechanism for hydrocarbon

(Dewhurst et al., 1999), and have a significant effect on hydrocarbon production (Eichhubl and Boles, 1998; Pitman et al., 2001; Clarke, 2007; Gale and Holder, 2010; Loucks et al., 2012). The narrow fractures are the best ways for migration and can be bypassed to the others or contributed to reservoir storages as enhance permeability. Incomplete microfractures are opened; both regular and irregular forms are generated by crosscut through the rock matrix along the weak zones.

4.2) Microchannel-related pores

The features of microchannels-related pores are along the rock matrix that difficult to determine. They are a few pore throat produced by processes of natural mechanism along the weak zones of bedding planes. These microchannels are connected and linked to the others which affect to probably increase the permeability.



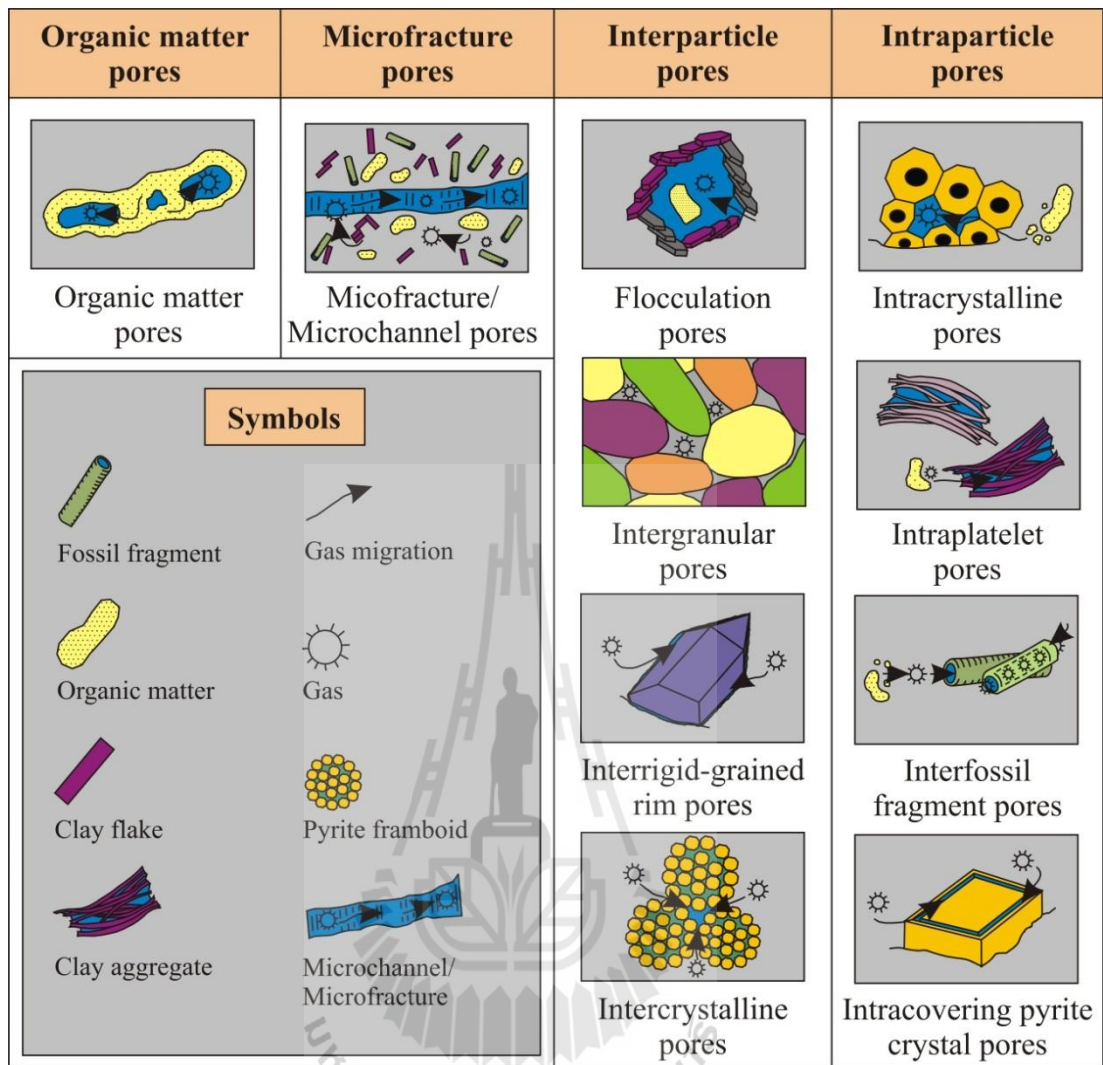


Figure 5.12 Pore type classifications of the Ban Nong Sai (Sap Phlu Basin) and the Dat Yai sections (Na Pho Song Basin) including pores of organic matter, interparticle, intraparticle, and microfractures and microchannels (after slat and O'Brien, 2011; Loucks et al., 2012).

5.2.2.3.2 Microscopic analysis of the Ban Nong Sai section

The Huai Hin Lat Formation of the Sap Phlu Basin consists mainly of fine-grained rocks of calcareous shales, calcareous mudstones, marlstones, and argillaceous limestone. The pores are discovered the

various in both types and sizes and performed in Figure 5.12. The pore characteristics in various types of rocks in the section are compared as shown in Table 5.9 and will be described as below.

1) Organic matter pores

They are in the organic matter as commonly isolated, rounded to oval, rectangular, elongate, and irregular in shapes and sizes (Figure 5.13A-B). They are ranging from oval to elongate in shapes that mainly typical on a few microns across of less than 1 μm (appropriately referred to as nanopores). The connect-elongated pores are also across approximately 1.5-2.5 μm in length. They are commonly subparallel to parallel to their directed alignment. The nanopores are presumed as the smallest pores in a few microns but the total organic carbon are illustrated the volume of organic contents as very high. Consequently, the high of total organic carbon is presumed much more of the organic matter contents and indicated the largest volume of organic matter pores.

2) Interparticle pores

2.1) Flocculation pores

They are commonly open and the gap pores of clay oriented flakes form the cardhouse structureless. The pores range in size approximately 50-90 nm across and up to 2 μm in length (Figure 5.13C). Most of pores show the imperfect or unclear cardhouse structures of oriented clay flakes. Each of particle pores is formed close to parallel alignment.

2.2) Intergranular pores

They are produced from the dissolution or diagenetic processes as performed in FESEM micrograph viewings. The FESEM viewings show that the pores are rounded to oval, elongate, cubic minerals, and irregular. They range from 10-160 nm across (Figures 5.13D and 5.14F) and few features are in range of 0.25 to 1.0 μm both width and length.

2.3) Interrigid-grained rim pores

Most of pores range approximately 570 nm in width and length as depended on the dimension of the cubic-forming pyrites (Figure 5.13E). The features of this pore types are probably appeared between the rim of rock matrix and rigid quartz minerals (Figure 5.13F).

2.4) Intercrystalline pores

They show pore shapes varying as depended on types and sizes of minerals. They are smallest round to polygonal, elongate, and irregular (Figure 5.14A). They range from 20-250 nm and up to 1.5 μm in width and length that is commonly similar.

3) Intraparticle pores

3.1) Intracrystalline pores

They occurred within framboidal pyrite. These porous grains may have internal pores between microcrystals of secondary origin and usually dispersed within the shale matrix (Slatt and O'Brien, 2011). The two characteristics of framboidal pyrite (Figure 5.14B) are observed as micro-pellet pyrite and pyrite framboids. The micro-pellet pyrite performs the internal pores range in size around 20-100 nm across and pyrite framboids are a few microns and up to 1.4

μm . Consequently, these pore sizes are varying up to $1.4 \mu\text{m}$ in both regular and irregular shape forms and mainly connected as are expected a network of larger pores.

3.2) Intraplatelet pores

They are produced as common forms of slot-like or interspersed between curve clay mineral plates. They are ranging in size up to $2.2 \mu\text{m}$ across and up to $10 \mu\text{m}$ in length of the striped curve between these flakes (Figure 5.14C-D). Moreover, clay minerals are flaky, irregular lath, silk thread-like aggregates in which the apertures are generally up to $1 \mu\text{m}$ in length. The mineralogical XRD data show the high percentage of clay fraction of 20-65 % (average 42.61 %) in which chlorite and illite has controlled the pore patterns.

3.3) Intrafossil fragment pores

They have been performed between outer covering part of fossils approximately $1.5 \mu\text{m}$ across (Figure 5.14E). Interior chamber is probably opened, filled (Slatt and O'Brien, 2011), and illustrated a few microns of pore sizes as multiple long strip in length.

3.4) Intracovering pyrite crystal/grain pores

The internal voids between these coverings are generated (original pores), ranging approximately 300-400 nm in width, and 2-2.5 μm in length (Figure 5.13E).

4) Microfracture and microchannel-related pores

4.1) Microfracture-related pores

They are found with a variety of scale approximately 220 nm in width and the length is long strip as results of magnification of external forces (Figure 5.15A-B). They are found that the calcite growth inside due to compose of calcareous fine-grained clastics and carbonate rocks. However, they are a key issue how hydrocarbon can be migrated and moved to other potential storages in reservoir.

4.2) Microchannel-related pores

The pores are performed narrow and commonly less than 200 nm in width between different compositions of rock matrix when its deposition. The other features occurred between the different compositions in rock matrix are also developed to microchannels (Figure 5.15C-D). In addition, the microchannels along joints (Figure 5.15B) are also observed and performed which commonly narrow not more than 50 nm. The stratigraphic column of the Ban Nong Sai section has reported 3 directions of joint sets and performed in Beds 15 and 17 of calcareous mudstone beds but they do not extend entirely in the studied samples. The mineralogical XRD data has shown a high percentage of carbonate minerals of 13-43 % (average 27.91 %). It is overgrown in both microchannels/fractures as provided a permeability but they are not more significance.

Table 5.11 Comparison of pore characteristics among the various types of rocks in the Dat Yai section of the Sap Phlu Basin.

Pore types		Type of rocks			
		Argillaceous limestone	Marlstone	Calcareous mudstone	Calcareous shale
Interparticle	OM pores	The pores are small that ranged approximately 40 nm across and typically random distribution in organic matter boundaries.	The various pore sizes and complete micronized stone in part of the organic matter are ranged from 0.02-2.0 μm . They are round to oval rectangular and irregular in shapes.	The pores are small and close to circle that are less than 130 nm in organic matters. The alignments or imperfect elongated pores in organic matter are ranged from 0.5-1.5 μm in length.	The pore is less than 650 nm in width and various shapes are round, irregular, and rectangular.
	Flocculation	Not found	Not found	The electrostatic charges of the clay-like structure of the network-shaped and gap pores are nearly parallel alignments following the individual edge-face and edge-edge oriented flakes. They are probably communicated of 60-90 nm pore sizes.	The edge-face oriented flakes of clay particles produced gap pores. They formed the incomplete parallel alignments that are less than 50 nm.
	Intergranular	The pores are varied with shapes that round to oval, elongate, and rectangular. Their sizes are range from 80-700 nm across and 1 μm in length as randomly disperse in rock matrix.	The shapes are commonly smallest as round to oval. The size is less than 100 nm across.	The pores are small, less than 170 nm, across oval and round in shapes, and poor alignment.	The pores are revealed in many shapes as smallest round to oval, elongate, irregular, and rectangular forming like pyrite cubic. They disperse generally around 2 μm across (commonly 200-500 nm).
	Interrigid-grained rim	Not found	The pores occur between rim of flexible rock matrix and rigid quartz crystals. The opening pore sizes are less than 530 nm and appear along rim of two weak compositions like microchannels.	The opening pore sizes are around 300 nm in width and 4 μm in length. Shapes are formed likely microcrack as along outer covering of cubical pyrite.	The grain-rim of interparticle pores are revealed between rock matrix and cluster of pyrite framboids which are less than 570 nm pore sizes (FESEM viewings).
	Intercrystalline	The pores are small between the individual micropellet pyrite that less than 140 nm. Several forms are referred to both of regular and irregular that depended on their overlapping in tight micropellet pyrite.	The pores are very small and show less than 100 nm that difficult to identify due to overgrow of dense microcrystal pyrite.	The sticks and commonly cubical forms of overlapping minerals are generated pores. They are ranged commonly 20-250 nm and up to 6.5 μm .	These pores are ranged from 0.2-2 μm approximately which several pore shapes are produced between many clumping of pyrite overgrowth.

Table 5.12 Comparison of pore characteristics among the various types of rocks in the Dat Yai section of the Sap Phlu Basin (Continued).

Type of pores		Type of rocks			
		Argillaceous limestone	Marlstone	Calcareous mudstone	Calcareous shale
Intraparticle	Intracrystalline	The micropellet pyrite is more common within bureau by several small pyrite-crystals. It generated the internal pores between these microcrystals are 20-100 nm as measured of pore sizes.	The porous grains between microcrystals of pyrite minerals due to compaction of crystals when its origin as shown approximately 20-60 nm pore sizes.	The micropellets and framboidal pyrite are generated intraparticle pores within overlapping crystals that are less than 1.4 μm approximately.	The internal pore sizes are less than 85 nm of secondary origin and commonly dispersed within the shale matrix.
	Intraplatelet	The clay aggregate pores are less than 80 nm of general lineation. Moreover, they are parallel to others within clay.	The common pores between clay flaks are flaky, elongate, linear, and parallel to others which illustrated 300 nm pore sizes.	The pores are commonly formed silk thread-like, sticky, and slot-like forms between curve clay mineral plates which ranging from a few microns to 2.2 μm in width and lengths. They are opening along plates.	The common of quartz and illite and kaolinite of clay minerals were generated pores as formed flaky, sticky, cleavage-sheet, and irregular laths. Apertures are opened along clay sheet cleavage that less than 90 nm in width and length.
	Intrafossil fragment pore	The porous fossil particles were generated within the interior chamber. They probably open and formed to pores which ranged from 1.4 μm to 55 μm of multi-long strip length.	The porous interior chambers of fossils are ranged from 250-500 nm across and connected to long strip length.	The porous fossil particles have been appeared between outer coverings of fossils as ranging 1.5 μm across. The interior chamber was probably opened and illustrated a few microns and long strip length of pore sizes.	The internal fossils were probably opened and filled.
	Intracovering pyrite crystal	The pores are poor separation which illustrated less than 60 nm in shape sizes.	Not found	The porous media between the outer and inner covering cubic of pyrite are high potential on shale gas storages which ranging 300-400 nm in width and 2-2.5 μm in length. They are depended on magnifications of cubical pyrite.	The incomplete coverings of cubical pyrite are appeared the poorly porous. It is less than 75 nm in size shapes.
Microfractures/microchannels	The microfractures are incomplete as ranged from 50-110 nm in width. They are crosscutted along rock matrix but not connected to others.	The one direction of fracture has been effected to this locality of 220 nm in width and lengthily narrows. In addition, large numbers of natural microjoint systems are crosscutted rock matrix and preservation.	The presence of natural fracture systems are width as ranging 250 nm with regular and irregular forms of microfractures.	The natural fractures were opened approximately 530 nm, both regular and irregular forms are along the weak zones of rock matrix as shown 12 μm at least in length.	

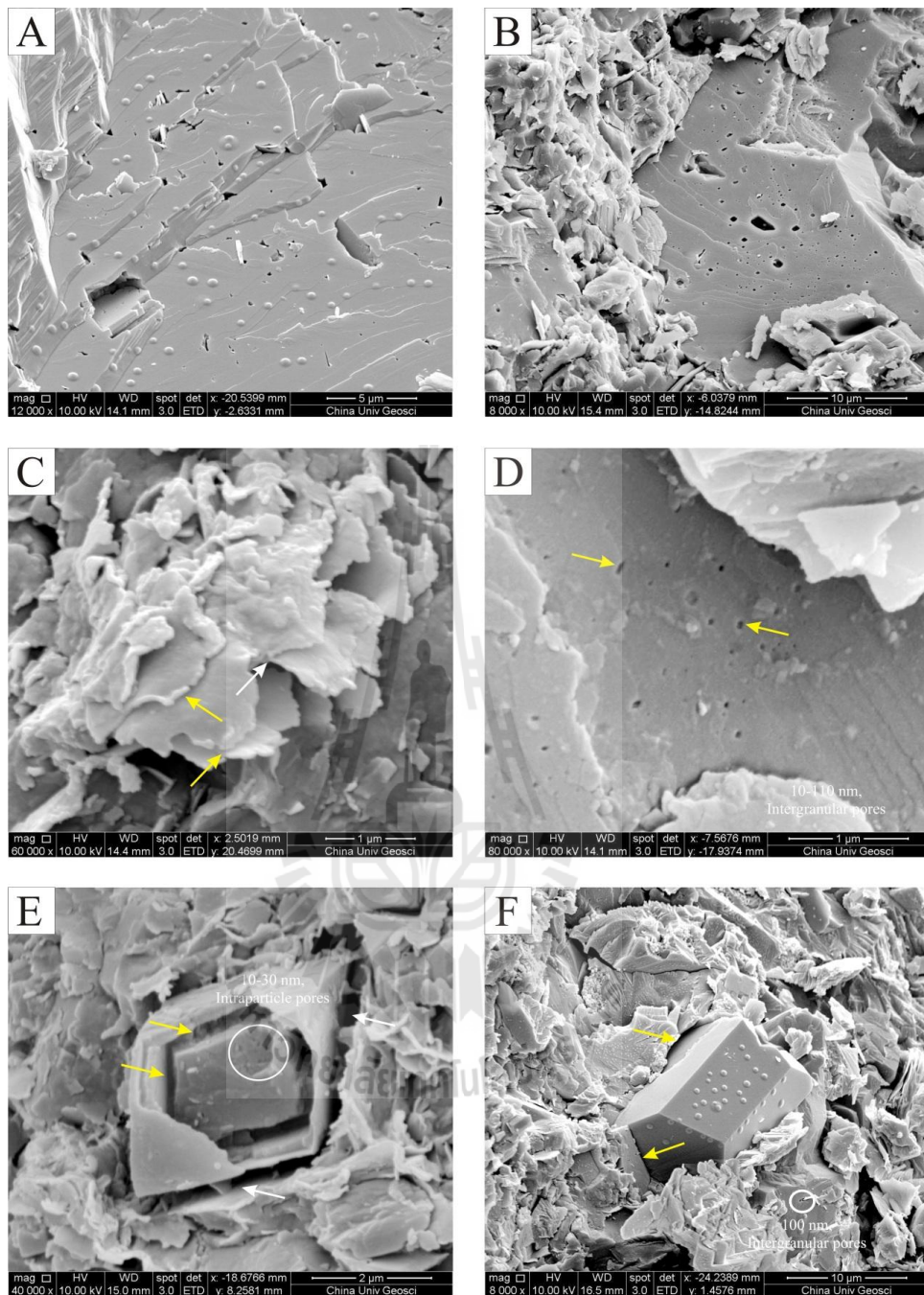


Figure 5.13 (A, B) Different forms of organic matter pores, (C) typical flocculated clay microfabric, random edge-face (yellow arrows) and edge-edge (white arrows) clay flake orientations, (D) intergranular pores, (E) rigid individual pyrite crystal pores (white arrows) and covering pyrite crystal pores (yellow arrows), (F) pores along rim of rigid solitary quartz.

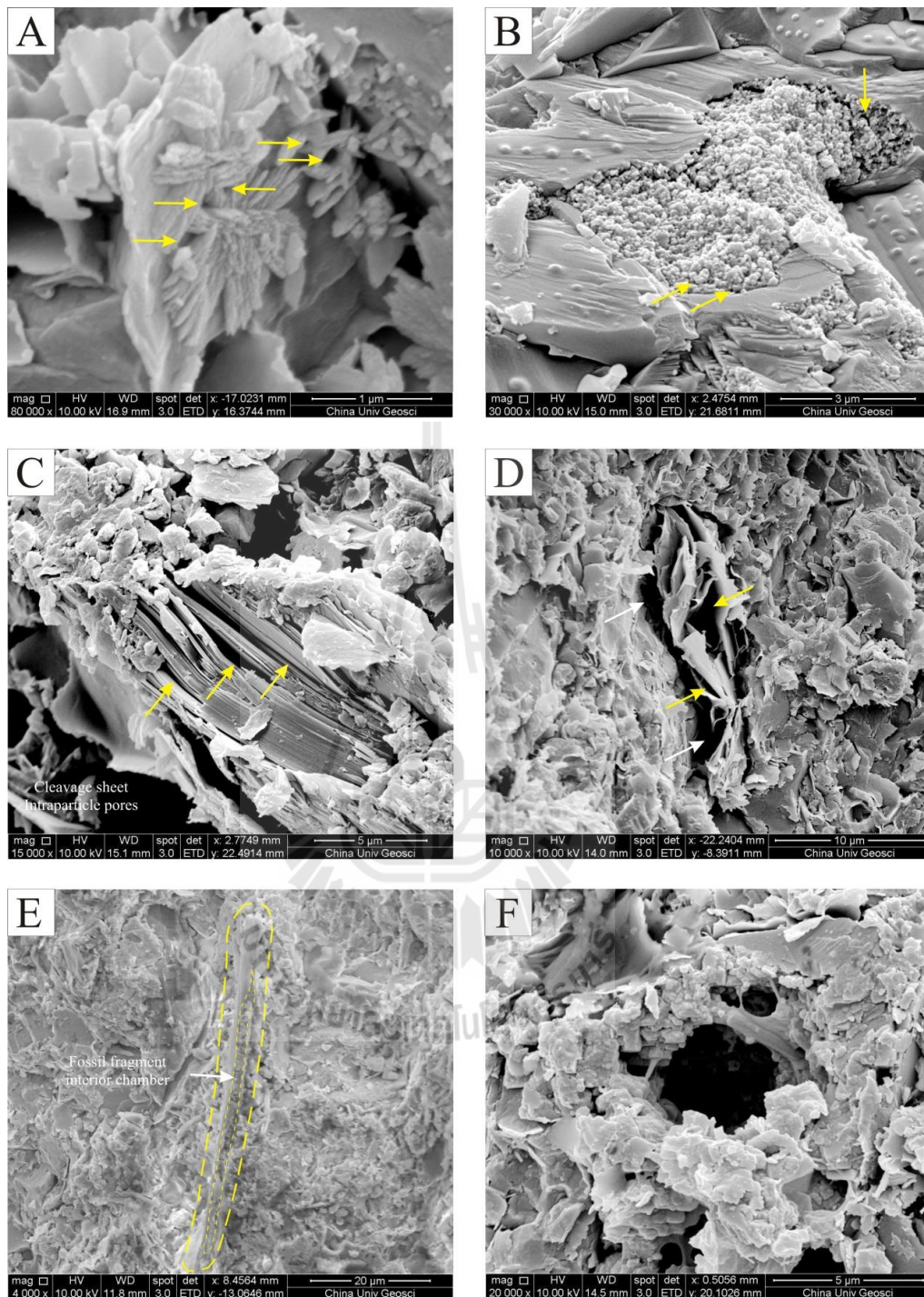


Figure 5.14 (A) Interparticle pores between crystals of minerals, (B) intercrystalline pores, (C, D) different forms of intraplatelet pores cause clay types, (E) internal chamber of fossil fragment pores, (F) complex interparticle pores.

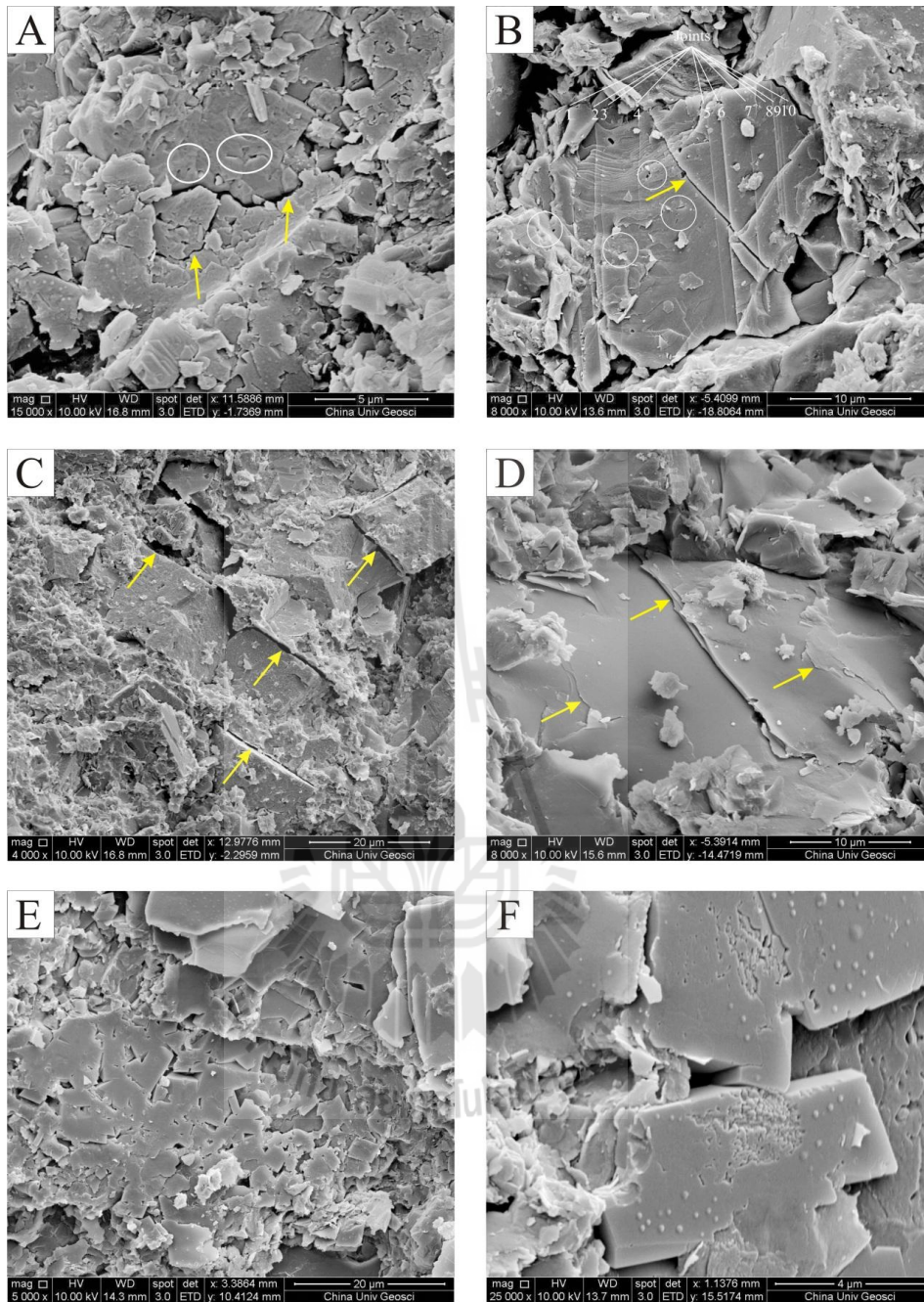


Figure 5.15 (A) Irregular microfractures (yellow arrows) and neighboring micropores, (B) microfracture related-pores (yellow arrows) and microjoints, (C) artificial fractures along changed compositions, (D) interparticle platelets of rock matrix are forming the microchannel related-pores, (E) carbonate minerals, (F) phosphate minerals.

5.2.2.3.3 Microscopic analysis of the Dat Yai section

The micropores of the Dat Yai section of the Na Pho Song Basin (mainly of fine-grained rocks of calcareous shales, calcareous mudstones, and argillaceous limestone) show the various types and sizes including any related to natural fractures. The pore characteristics (Figure 5.12) will be described as below.

1) Organic matter pores

The various size pores reveal and complete micronized stone in part of the organic matter in the organic matter. The pores are generated by dissolve of organic matter when buried in deeper as indicated by maturity values of burial history (Figure 5.16A). The pore types are not connected and aligned through the matrix with shape both of regular (round to oval and rectangular) and irregular, approximately 70-950 nm.

2) Interparticle pores

2.1) Flocculation pores

The pores are generated by overlay of electrostatic charges of the clay-like structure of the network-shaped. The individual edge-face, edge-edge, and face-face oriented flakes of clay particle are generated interparticle gap pores to form nearly parallel alignments (Figure 5.16B-C). All of interparticle gap pores are about 1 μm in width and 5 μm in length.

2.2) Intergranular pores

The pores are revealed in rock matrix that occurred between each of granular of rock-forming compositions. The processes of dissolution and rock-forming minerals etc. are produced and preserved them in.

These pores vary in shapes of smallest round to oval, elongate, irregular, and rectangular forming like euhedral pyrite in the tight rock matrix (Figure 5.16D-F). All of pores are generally dispersed and are approximately 0.4-5.0 μm .

2.3) Interrigid-grained rim pores

The pores are produced between the differences of rock-forming minerals as opened along the weak layers of outer of cubical minerals. These opening pores are generated between the rim of flexible rock matrix and rigid mineral crystals as shown in SEM micrograph viewings (Figure 5.17A-B). These pores are likely microcracks/microchannels along the boundaries and the sizes are about 600 nm in width and 8 μm in length or depend on mineral sizes.

3) Intraparticle pores

3.1) Intracrystalline pores

These pores are porous grain pores that produce within the particles of microcrystals or between each of minerals. The siliceous and limestone-forming pyrites are more common within bureau by several small crystals. Moreover, several characteristics are also generated these pore types within the overlapping crystals and commonly dispersed within the shale matrix (Figure 5.17C-D). These internal pore types are approximately 625 nm in width and 1.563 μm in length.

3.2) Intraplatelet pores

This pore is pore that produce within clay particle aggregates (16-34 % clay fraction) such as illite, and kaolinite with specific features of flaky, sticky, cleavage-sheet, irregular lath, elongate, slot-like

form, and linear, and parallel to another. All pores are opened by effect of subsidence of the formation as detected by high maturation. The pores are preserved and show the pore sizes approximate 150 nm in width and 11.5 μm in length or depend on the length of clay particles (Figure 5.17E-F).

3.3) Intrafossil fragment pores

These pores are porous fossil particles which have been appeared in the interior chambers. The interior chambers probably open, filled with detrital or autigenic minerals, and appear at least 500 nm of pore sizes, the length is approximated about 70 μm of multi-long strip length and they are connected (Figure 5.18A-C).

4) Microfracture and microchannel-related pores

4.1) Microfracture-related pores

The microfractures are the presences of natural fracture which have been affected to this locality of the study area. Incompletely microfractures are opened; both regular and irregular forms are generated by crosscut rock matrix along the weak zone (Figure 5.18D-E). The microfractures are appeared as shown in several directions forming to migration pathways but less connected. According to pore sizes, the width is ranging 230 nm and length is long strip length as depended on each one.

4.2) Microchannel-related pores

The microchannel is a few pore throat that produced by processes of natural mechanism along the weak zone of bedding planes (Figure 5.18F). These channels have been connected and linked with the other pores effect to probably increase the permeability of the interested formation.

Although the microchannels are few pore throats, however, they are also appeared in nanometer and larger scale along the plane bed.



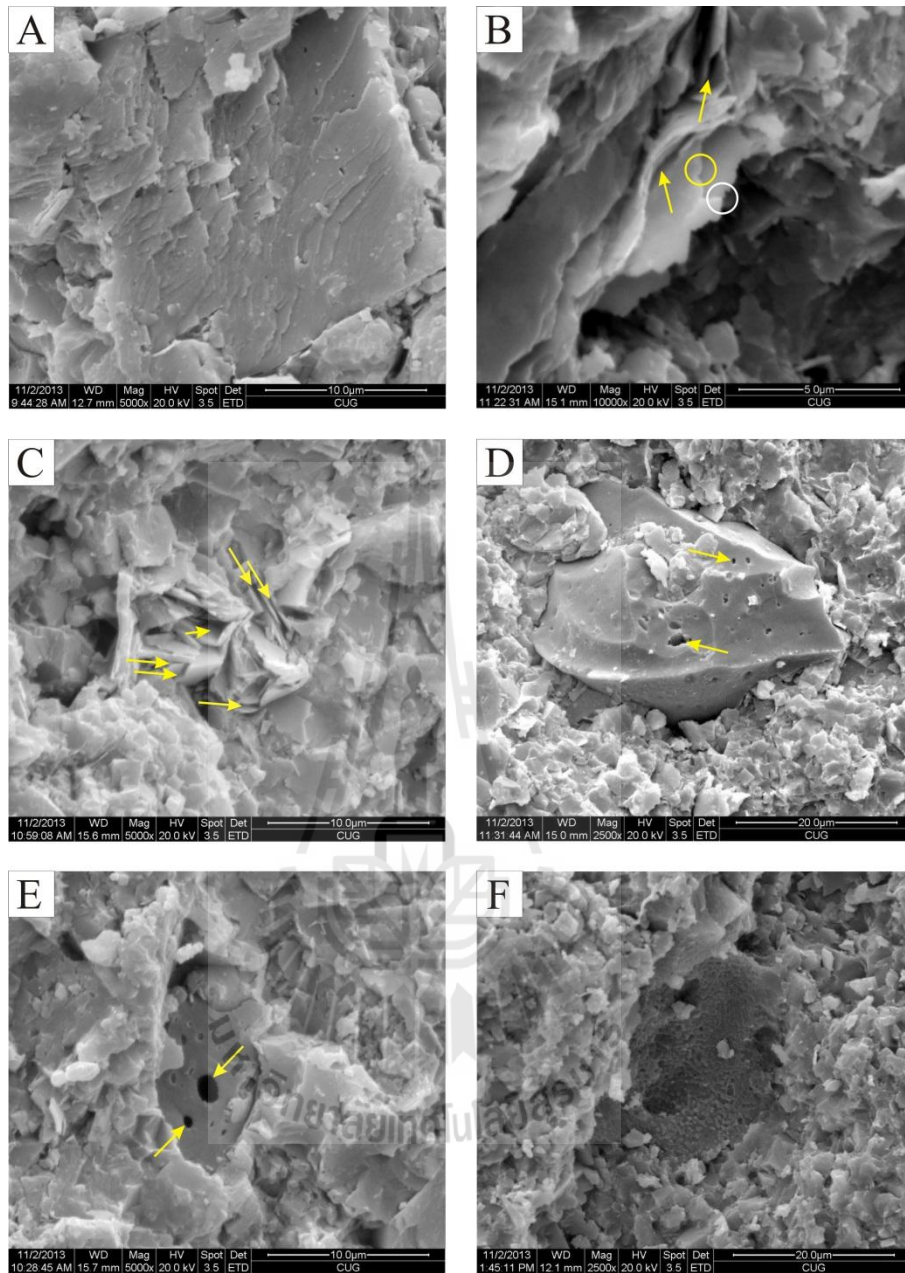


Figure 5.16 (A) Organic matter is dispersed with small organic matter pores, (B) typical flocculated clay microfibrils, random edge-face (yellow circle) and edge-edge (white circle) clay flake orientations, (C) other forms of clay aggregates as produced elongate pores, (D, E) intergranular pores in rigid grain, (F) the soluble composition is dissolved as produced intergranular pores.

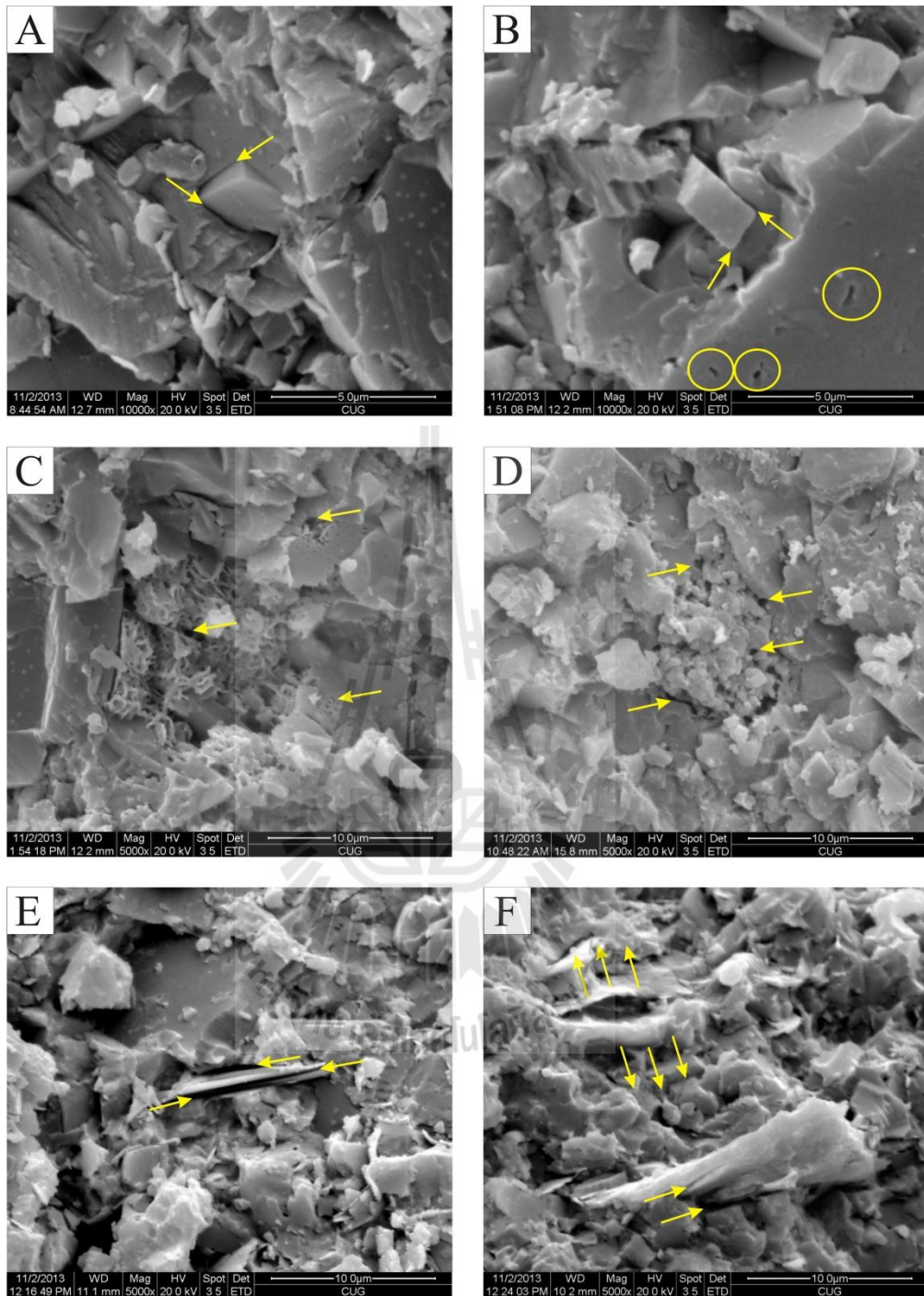


Figure 5.17 (A, B) Intergranular pores along rim of rigid solitary grain crystal, (C, D) intercrystalline pores are produced by growth of micro-pellet pyrite and irregular-shaped mineral, (E, F) different forms of intraplatelet pores as elongate and irregular lath shape cause other clay types.

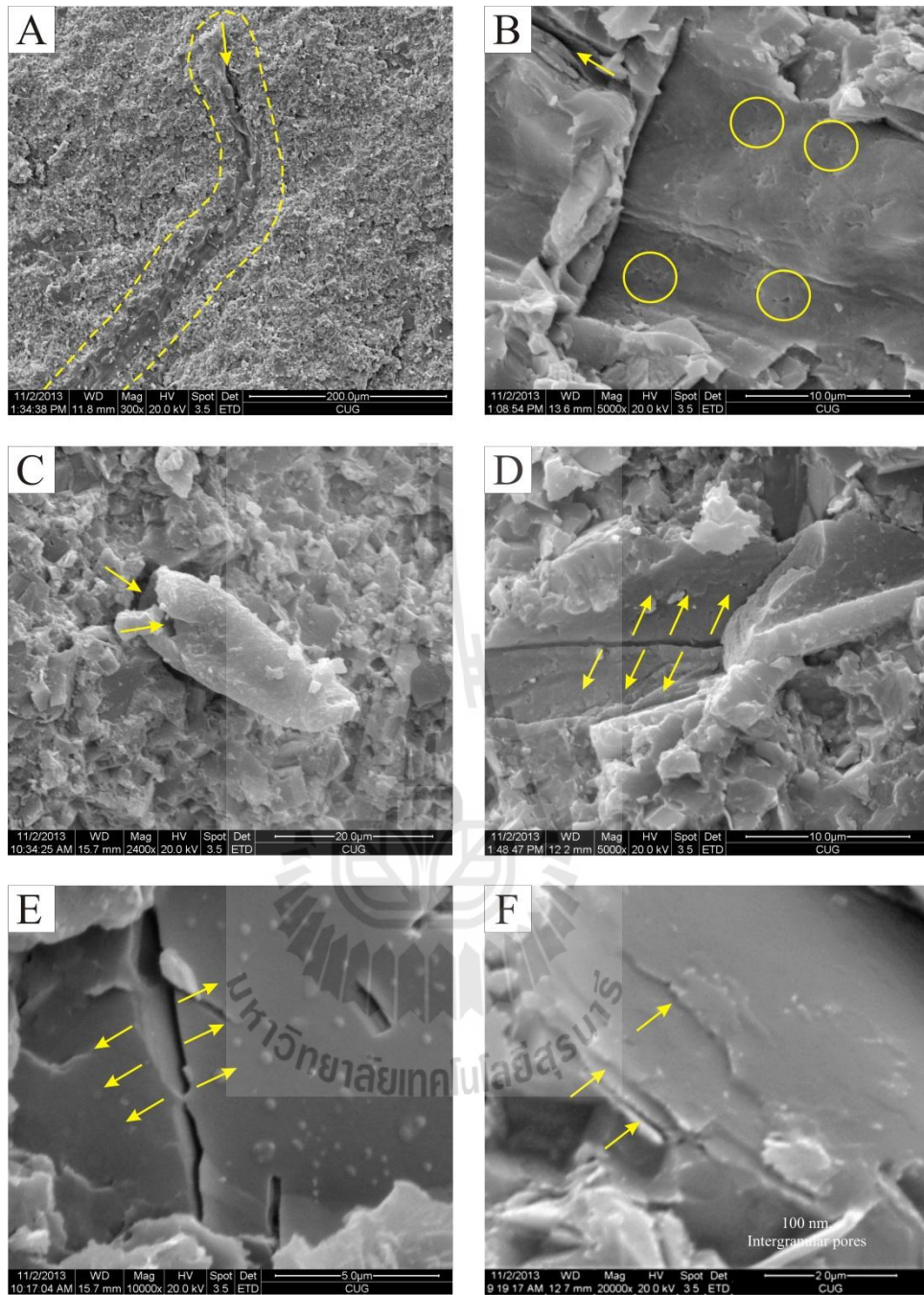


Figure 5.18 (A, C) Micropores of internal chamber of fossil fragment as multi-long strip length, (B) round pores are dispersed in fossil texture, (D, E) microfracture related-pores are produced from the external forces, (F) micropores among the bedding planes in rock matrix are forming the microchannel related-pores.

CHAPTER VI

DISCUSSIONS

For assessment of unconventional and conventional natural gas reservoirs, gas in generation phase is similar basis. But the structural conditions and reservoir characteristics are still different. Therefore, the analysis i.e., palaeodepositional environment, organic matter, thermal maturity, generated hydrocarbon volume, reservoir-forming minerals, and hydrocarbon storages etc., are the basis of a favorable development.

6.1 Source rock evaluation

Based on conventional hydrocarbon evaluation, the entire data are concluded as research idea of hydrocarbon source evaluation. It is performed on a potential of generated hydrocarbon in source rocks as described below.

6.1.1 Palaeoproductivity and palaeoredox condition

Integrations of the obtained geochemical and petrographical results lead to a more precise characterization of the palaeoenvironmental conditions of the Huai Hin Lat Formation. They could be related to the palaeoproductivity and development of the reducing events of the basin.

6.1.1.1 Palaeoproductivity

The petrographical and geochemical palaeoredox indices, i.e., AOM, acritarchs, phytoclasts, TOC, excess SiO₂, Ba/Al, and P/Al have been calculated from the analyzed result of fine-grained sediments of the studied section.

The analyzed results indicate the presence of a photic zone of surface water and a reducing environment of deposition in the study section.

The studied section may identify the location, where the high organic matter accumulation as depended on its palaeoenvironment. The high palaeoproductivity can be distinguished by the high peaks or high values of the palaeoproductivity proxies.

1) Ban Nong Sai section

The lower part shows two prominent high peaks of AOM, acritarchs, phytoclasts, excess SiO₂, Ba/Al, and P/Al in the lower and upper beds (Beds 1 and 7). These beds indicate a high palaeoproductivity which is supported by the high TOC. Although the middle bed (Bed 3) shows relatively lower productivity based on the palaeoproductivity proxies but the TOC exhibits the highest peak which can be explained by the high rate of preservation of organic matters.

The middle part shows a high peak in Beds 9 and 10 which are exhibited in high AOM, acritarchs, phytoclasts, excess SiO₂, and Ba/Al. Although the high peak in P/Al is not shown however, the values are relatively high. It indicates the relatively high productivity in the beds of the middle part which is supported by the high TOC.

The upper part shows three high peaks in Beds 13, 15-16, and 19. The lower peak is shown only in acritarchs and phytoclasts but the concentrations of AOM, excess SiO₂, Ba/Al, P/Al, and TOC are relatively low. It indicates lower productivity comparing to the other two. The middle peak is similar to the lower one but the concentration of SiO₂ and TOC are higher, so it indicates a higher productivity than the lower peak. The upper peak shows high concentration of

AOM, acritarchs, and phytoclasts but TOC is in the low peak. It suggests that the productivity is high but the rate of preservation is low.

The high peaks of palynological and the geochemical proxies of the studied section reflect a variation of high productivity. Two relatively lower productivity intervals are present in the middle portion of the lower part (Bed 3) and the lower Bed 13 of the upper part. The Bed 3 of the lower part shows the highest peak TOC, which can be explained by the excellent preservation condition. The lower Bed 13 shows relatively lower TOC which indicates a poorer preservation condition than the Bed 3.

2) Dat Yai section

The lower part shows the four high peaks as appeared in Beds 3, 9, 12, and 14. The sharp peak of Bed 3 supports to correspond with excess SiO₂, Ba/Al, and P/Al (still high). The sharp peak of Bed 9 supports to correspond with AOM and excess SiO₂. Moreover, the sharp peaks of Beds 12 and 14 supports to correspond with phytoclasts, AOM, excess SiO₂, Ba/Al, and P/Al. They may have been used to indicate the high productivity, where they show. These high peaks may have been used to indicate the lowest productivity.

The upper part shows the six high peaks as appeared in Beds 16, 17, 22, 27, 30, and 32 distributed through its part. The high peaks of Beds 16 and 17 supports to correspond with AOM, phytoclasts, excess SiO₂, and Ba/Al. The Bed 16 shows the unclear peak in excess SiO₂ and Ba/Al, however, they still exhibit the high values. The high peak of the Beds 22 and 27 supports to correspond with AOM, phytoclasts, excess SiO₂, Ba/Al, and P/Al. The high peak of Bed 30 supports to correspond with AOM, excess SiO₂, and Ba/Al. The high peak of Bed 32

supports to correspond with phytoclasts, excess SiO_2 , and Ba/Al. They are high as similar as the lower part except some peaks are slightly low which indicate the similar high productivity.

The palynological and the geochemical proxy peaks in the lower and upper parts reflect the high productivity. One relatively high productivity interval is present in the Beds 3 and 27. Both beds show the lower peak TOC which can be explained by the poorer preservation condition. The lower productivity of Bed 18 of the upper part shows the high peak TOC which indicates a good preservation condition also.

6.1.1.2 Palaeoredox conditions

The geochemical palaeoredox indices, i.e., Ni/Co, U/Th, V/Cr, V/(V+Ni), Ni/V, (Cu+Mo)/Zn, and Ce anomaly have been calculated from the analysis result of fine-grained sediments of the studied section. Benthic redox condition of both sections may identify the location, where the high reducing is dominant. The degree of the palaeoredox condition may be evaluated based on the values and high peaks of the relevant indices.

1) Ban Nong Sai section

The lower part shows two prominent high peaks of U/Th, V/Cr, Ni/Co, (Cu+Mo)/Zn, and Ce/Ce* in Beds 3 and 6. They indicate the relatively high reducing condition. The Bed 3 is substantiated by the high peaks of V/Cr, Ni/Co, and Ce/Ce* and the low peak of Ni/V.

The trends of U/Th, V/Cr, and (Cu+Mo)/Zn are fluctuated and declining upward in the middle part suggests a less reducing condition. The upward increasing trend of Ni/V also supports this interpretation.

The upper part shows three high peaks in Beds 13, 15, and 17. The lower peak of Bed 13 is shown in V/Cr and Ni/Co and is corresponded with a high value of U/Th. The Beds 15 and 17 exhibit high peaks or high values of V/Cr and Ni/Co which are supported by the high values of U/Th and Ce/Ce*. All the high peaks of the upper part are therefore, indicating the high reducing condition.

The study section shows many high peaks or high values of palaeoredox proxies except the middle part and the lower bed (lower Bed 13) of the upper part. It indicates that the section was mainly under reducing condition which is supported by Ce/Ce* and V/Cr values. The studied samples yield the Ce/Ce* ranging 0.84-1.19 which is above the cutoff value of 0.8 for the anoxic condition. The V/Cr values are 2.6 on the average which is also above the cutoff value of 2.0 for the anoxic condition. The middle of lower part (Bed 3) shows the lower productivity but it contains the highest peak TOC which is conformed to the excellent preservation in the reducing condition. The middle part which shows high productivity exhibits a less reducing condition. So it comprises relatively lower TOC comparing to the more reducing intervals. The lower Bed 13 of the upper part shows less reducing condition and low TOC which is conformed to the lower productivity.

2) Dat Yai section

The lower part shows high values except the uppermost part with high peaks in Beds 5, 8, and 13. The peaks of Beds 5 and 8 support to correspond with Ni/Co, U/Th, V/Cr, V/(V+Ni), and (Cu+Mo)/Zn. The peak of Bed 13 supports to correspond with U/Th, V/Cr, and (Cu+Mo)/Zn. All sharp peaks are similar in value and pattern which indicate high degree of reducing condition. They are supported by the low peaks of Ni/V as indicated by a more reducing condition.

The trends of the upper part are fluctuated and show three high peaks in Beds 17, 20, and 25. The peaks in Beds 17 and 20 are shown in the lower of its part. They support by correspond with Ni/Co, V/Cr, V/(V+Ni), and (Cu+Mo)/Zn. The peaks of Beds 25 support by correspond with Ni/Co, U/Th, V/Cr, and V/(V+Ni). They are high which may have been used to indicate the high reducing condition. They are supported by the low peaks of Ni/V in the same bed as indicated a more reducing condition also. The other peaks are higher values which indicate the more oxygenation effect to the benthic floor.

The many high peaks or high values of palaeoredox proxies are shown in the studied section. The high peaks, V/(V+Ni), and V/Cr values indicate that the section was mainly under reducing condition. The studied samples yield the V/(V+Ni) are range from 0.67 to 0.85 which exceed the cutoff value of 0.46 of reducing environment. The V/Cr values are 2.07 on the average which is also exceeds the 2.0 of anoxic condition. The lower part (Bed 3) and the upper part (Bed 27) show the higher productivity and lower TOC which are conformed to lower reducing condition. The Bed 9 of the lower part contains highest peak TOC but not high degree of preservation in the reducing condition. This highest TOC is the result from the dominant palaeoproductivity. The Bed 21 of the lower upper part shows the lower productivity and exhibit a poor reducing effect. It contains the lowest peak TOC which is comparable to the other peaks. As the result, most of organic matters were supplied and kept in the benthic floor is therefore, fitted the associated sediments of the black shale. The light grey in colour of sediments is not appeared in strata due to the organic matter in benthic floor is not affected by the extremely oxidizing condition.

6.1.2 Palaeodepositional model

The APP ternary diagram shows the associations of phytoclasts-palynomorph, palynomorph-AOM, and AOM-phytoclasts. It indicates the proximity to fluvial sources plus sorting, redox condition plus masking effect, and redox condition plus proximity to fluvial sources respectively.

1) Ban Nong Sai section

The ternary diagram of the Ban Nong Sai section shows that it was deposited in the subenvironments of proximal shelf, distal basin, and distal oxic-anoxic shelf. These fields of marine subenvironments are accorded to the restricted basin of lacustrine. The internal sources and even lack detrital inputs were filled initially (Beds 1 and 2) in the deeper basin of distal shelf where dysoxic-anoxic dominance. Bed 3A is plotted in distal dysoxic-oxic shelf and continued to the distal shelf where suboxic-anoxic (Beds 3B and 3C) and dysoxic-anoxic (Bed 3D) respectively. Then the conditions are fluctuated in distal shelf where dysoxic-oxic (Bed 4), dysoxic-anoxic (Beds 5 and 6), and suboxic-anoxic (Bed 7). The middle part is fluctuated which shows upward decrease of reducing conditions from the distal suboxic-anoxic shelf to the proximal shelf and the distal basin of more oxic effects. The lower upper part (Beds 13 and 15) is still more effect of oxic condition as the same as the middle. But Bed 14 is more reducing effect of dysoxic in distal shelf. Moreover, the supplied sediments of Beds 16 and 17 and Beds 18 to 20 are setting in distal shelf of high and higher reducing conditions. As the results, the sequence and depositional model are high reducing condition but the middle section is slightly lower as accorded to the interpretation based on the palaeoredox method.

2) Dat Yai section

The palynofacies are mainly plotted in the ternary diagram as indicated that they were deposited in the subenvironments of distal shelf, carbonatic shelf, restricted marine or lagoon. These marine subenvironments are also conformed to the lacustrine basin. The lacustrine model indicates that these palynofacies may deposit in the deeper distal shelf associated with the deepest basin. This deeper subenvironment is supported by lesser or even lack of detrital inputs. It was filled from the internal basin sources and the clastic input sites at the lake margins which finally to the products. The supplied sediments were filled continuously from the basal to Bed 15 which became shallower in Bed 16 of the marginal basin. Beds 17-24 became again to the deeper as similar to the lower part. This basin may subside from tectonic events. Bed 25 turned into highly proximal shelf and became the deeper as tectonic effects in Bed 26 of the distal shelf. Then it was constantly filled up in Beds 28-29 and Beds 31-32 of proximal shelf and the marginal basin respectively. But Bed 30 is deeper than the other two of the overlying and underlying beds. These subenvironments were associated with the palaeoredox conditions of anoxic as conformed to the palaeoredox interpretation in subtopic above.

In comparison, both sections are deposited in the deep basin but the Ban Nong Sai section is shallower and closer to land sources. The sequence and depositional model of both sections are high reducing condition but the Ban Nong Sai section is slightly lower. Therefore, they are appropriated to evaluate on shale gas potential.

6.1.3 Organic matter quality of kerogen types

The various types of kerogens initially are associated with specific geological settings (Tissot and Welte, 1984). Suarez-Ruiz et al. (2012) described the distinctive characteristics of type I kerogen occurred in lacustrine environments where selective accumulation of algal material or serve biodegradation of the organic matter took place. Type II kerogen is related to open marine and fresh water lacustrine environment where autochthonous organic matter is derived from a mixture of phyto- and zooplankton. Type III kerogen is essentially derived from the terrestrial plants (Durand, 1993) that can be associated with terrestrial inputs into lacustrine or marine settings. And type IV kerogen is composed of aromatic carbonized organic matter with no potential for hydrocarbon generation.

The kerogen structure can determine its petroleum generation products. The different bonds require different thermal energy to break to the gas molecular precursors from the kerogen. Basic differences in the chemical structure of sapropelic (Type I and Type II) and humic (Type III and IV) kerogen are illustrated in Figure 6.1. Sapropelic kerogen is enriched in aliphatic structures and isolated ring structures (Behar and Vandenbroucke, 1987). Humic gas-generating kerogen contains only a few short chains with some single methyl groups and a large number of condensed rings with oxygenated functional groups (Behar and Vandenbroucke, 1987) with abundance of aromatic rings and heteroatoms (Ko, 2010).

The rock-Eval pyrolysis technique is a famous method for petroleum source rock evaluation. It is used to assesses the kerogen types (organic matter types) by comparing hydrogen index (mg HC/g TOC) and oxygen index (mg HC/g TOC) data. Both values are shown in Table 6.1 and Table 6.2 and plotted on a modified van

krevelen diagram. The result of Ban Nong Sai samples (purple solid circles) is shown in Figure 6.2 that dispersed in Type II (5 samples), Type III (3 samples). Two samples are plotted near the lower left portion of diagram but cannot indicate to any kerogen type. Then Figure 6.3 is plotted between the hydrogen index and T_{\max} ($^{\circ}\text{C}$) values as illustrated that the HI were affected on temperature. It shows 5 samples located in mixing of Type II-III but the others are out of identification. The plotting is varied and some are lost in evaluation due to the effect of temperature. The result of Dat Yai samples (orange solid circles) cannot identify to any type because all data is also plotted near the lower left portion of diagram (Figure 6.2). This result is accorded to the result of comparing hydrogen index and T_{\max} ($^{\circ}\text{C}$) values. The values also show the values in Table 6.1, Table 6.2, and Figure 6.3. They are plotted near the lower right portion of diagram which all lines of kerogen type are merged together. They cannot indicate the true type of organic matter. As the results, the HI and OI plotting is properly used in immature source rocks as well as HI and T_{\max} plotting. These inexplicit cases are probably found in the identification during catagenesis and metagenesis stages of thermal maturation.

The HI/OI technique is used to determine source rock quality (kerogen type) of immature rocks and the HI and OI change compositions of mature source rocks (Tissot and Welte, 1984). The hydrocarbon products cause the kerogen become depleted in hydrogen and relatively enriched in carbon in composition (Peter and Cassa, 1994). The average HI values of both Ban Nong Sai (130.28 mg HC/g TOC) and Dat Yai samples (2.04 mg HC/g TOC) in mature stages are lower than 150 mg HC/g TOC which indicated source material present to be mainly gas-prone (Core Laboratories, 1993). They are corresponded to the HI/OI ratios which converge

toward the origin leading one to a more gas-prone type III (Tissot and Welte, 1984) or type IV interpretation. Therefore, HI and OI are not indicative of the original kerogen quality in mature source rocks (Tissot and Welte, 1984).

The visual petrographic analysis is studied based on both maceral and submaceral types. The procedure consists of making a maceral analysis of classifying organic particles into categories having similar optical properties by analogy with minerals. The proportions are established of these categories by reflectance and fluorescence properties (Durand, 1993). The Ban Nong Sai section, the maceral is composed mainly of sapropelic amorphinite (57.7-73.0 %) and sapropelic vitrodetrinite (16.0-24.0 %) of sapropelic group. The gelovitrinite (4.3-11.0 %), densinite (5.0-8.7 %), and texto-ulminite (0.3 %) of vitrinite group and fusinite of inertinite are lower and lowest respectively. The Dat Yai section, the organic particles or palynofacies are composed mainly of sapropelic amorphinite (55.7-69.7 %) and sapropelic vitrodetrinite (17.3-26.3 %) of sapropelic group. They are lesser of densinite (4.3-9.0 %) and gelovitrinite (6.0-10.7 %) of vitrinite group and lack of inertinite group. The sapropelic amorphous particles are expressed as a strongly amorphous groundmass of both sections. Their numerous types are derived from biological degradation including resinite, suberinite, bituminite, and exsudatinitite (Pashin, 2008). In contrast, the study section is not discovered of these materials but other materials of microbes, plants, and other animals may derive. The sapropelic group generates mainly of liquid hydrocarbon because it can supply many hydrogen atoms. As the results, they indicate to the mainly type I kerogen that presented in the source rock of both sections.

For better classification, Taiming and Shanfan (1990) described them by using the primary variables for identify the primary composition of kerogen type. The validity of each should be tested statically. The result of mathematical analyzing by equation is produced the numerical kerogen type index. The equation is applied the atomic H/C and O/C data and vitrinite reflectance which obtained as follows:

$$TI = 119.42 \left(\frac{H}{C} \right) + 27.93 \left(\frac{H}{C} \right) (R_o) - 35.67 \left(\frac{H}{C} \right)^2 - 95.08 \left(\frac{O}{C} \right) (R_o) + 55.27 \left(\frac{O}{C} \right) (R_o)^2 - 43.29 \quad (6.1)$$

The constants are calculated type index value (Table 6.3) as ranged from zero to 100. Their values relate to kerogen type from Type II through Type I. The types are sapropelic type (Type I), humic-sapropelic type (Type II₁), and sapropelic-humic type (Type II₂) (Chen et al., 2011). The values are lower than zero indicating to humic type (Type III) (Chen et al., 2011) and the other cases are Type IV. According to the Ban Nong Sai and Dat Yai sections, samples of 5G, 6G, 11G, and T26-2 show the value exceeds 80.0 of type index (Table 6.4) which identifies to Type I of sapropelic organic matter. It refers to the type is rich in lipids that have a hydrogen-carbon atomic ratio of about 1.10 or higher and an oxygen-carbon atomic ratio of 0.15 or less. It reflects the presence of abundant aliphatic and alicyclic structures. This type of kerogen can be brightly fluorescent and has a distinctive green to yellow colour under the blue-light optical microscopy (Pashin, 2008). Moreover, the other samples are ranging from 66.2-75.5 of the Ban Nong Sai section and 68.4-78.5 of the Dat Yai section. They can be indicated to Type II₁ of humic-sapropelic organic matter. They refer to the type is also rich in lipids that has a hydrogen-carbon ratio between 0.75 and 1.75 and an oxygen-carbon ratio between

0.05 and 0.20. They reflect that contain a mixture of aliphatic and aromatic structures as well as ketone and carboxylic acid group. This type of kerogen can be fluorescent and has a range from bright yellow through orange, red, and dull brown under the blue-light optical microscopy as depended on both original composition and thermal maturity (Pashin, 2008). The subscript 1 of Type II₁ refers to consist dominantly of organic matter that produced richer lipids (mainly sapropelic) than the same type of Type II₂. These organic matter compositions are higher hydrogen atoms than the organic matter compositions of Type II₂. They are behaved similar to Type I because their type index values are quite close to 80.0 of upgrading. Although, the organic matters are composed mainly of Type I and Type II₁. However, both types are belonging to sapropelic amorphous particles and sapropelic vitrinite may identify to exact Type I which the most Type II are not preserved as determined by visual petrographic analysis.

As the results of the modified van Krevelen diagram is identified to unclear of Type II, III, and IV for peak mature stage of the Ban Nong Sai samples and cannot identified to any type for higher peak mature stage of the Dat Yai samples. A few hydrogen atoms are preserved in both sections recently as demonstrated by less S₂ of rock-Eval pyrolysis. They are suggested by Core Laboratories (1993) that original Type I can be shown the HI values exceed 400 mg HC/g TOC for oil prone sources. Both HI and OI values are high in immature stage and continuously depleted in mature sources rocks. Especially, they are more depleted in higher mature stages. Therefore, Type I are mostly abundant and important constituents through both sections.

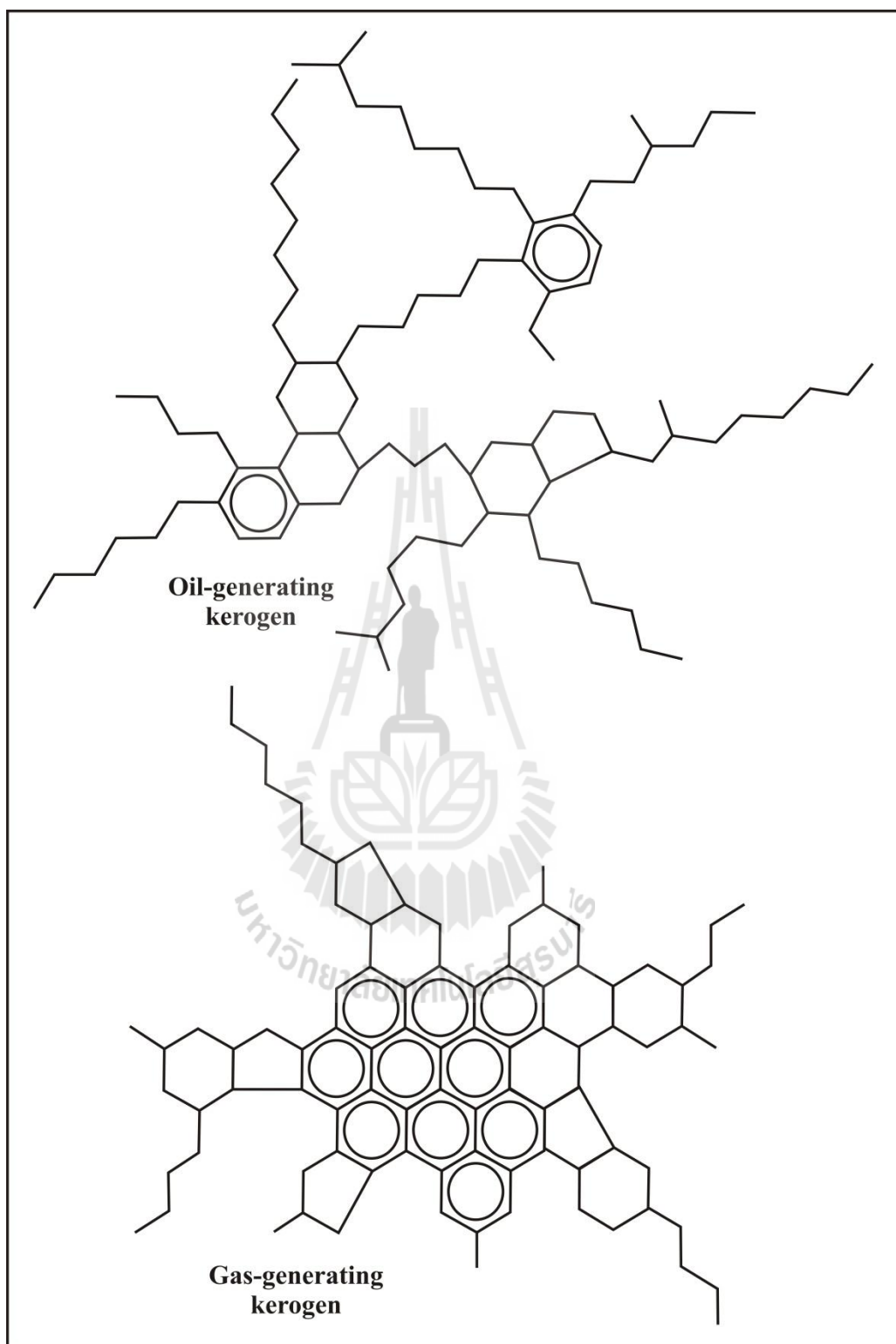


Figure 6.1 Schematic chemical structures of oil-generating sapropelic kerogen and gas generating humic kerogens (Hunt, 1996).

Table 6.1 Average TOC, rock-Eval, and vitrinite reflectance values and computations of the Ban Nong Sai section, the Sap Phlu Basin.

Sample	TOC (%)	Pyrolysis (mg/g rock)			HI	OI	PI S ₁ /(S ₁ +S ₂)	T _{max} (°C)	Calculated R _o (from T _{max})	Measured R _o (%)	Gas in rock from S ₁ (mcf/ac-ft)	Generation potential from S ₂ (mcf/ac-ft)
		S ₁	S ₂	S ₃								
A5G	5.326	0.03	3.51	0.77	65.90	14.46	0.0085	444	0.83	-	3.94	461.00
A4G	5.391	0.04	7.12	0.53	132.07	9.83	0.0056	443	0.81	-	5.25	935.14
A3-4G	5.073	-	-	-	-	-	-	-	-	0.86	-	-
A3G	4.069	0.04	2.65	0.57	65.13	14.01	0.0149	443	0.81	-	5.25	348.05
A2-3G	4.953	-	-	-	-	-	-	-	-	1.04	-	-
A2G	3.673	0.18	7.94	0.30	216.17	8.17	0.0222	447	0.89	0.82	23.64	1,042.84
16G	4.507	0.16	0.26	0.21	5.77	4.66	0.3810	445	0.85	-	21.01	34.15
13G	5.562	0.03	0.33	0.44	5.93	7.91	0.0833	444	0.83	-	3.94	43.34
11G	5.265	0.05	7.26	0.36	137.89	6.84	0.0068	447	0.89	-	6.57	953.53
10G	5.310	0.13	14.34	0.23	270.06	4.33	0.0050	451	0.96	-	17.07	1,883.42
6G	6.933	0.12	23.91	0.74	344.87	10.67	0.0050	448	0.90	-	15.76	3,140.34
5G	6.149	0.03	3.63	0.90	59.03	14.64	0.0082	445	0.85	-	3.94	476.76
Avg	5.184	0.08	7.10	0.51	130.28	9.55	0.0595	445.7	0.86	0.91	10.64	931.86

Remark; HI = (S₂/TOC)×100 (mg HC/g TOC), OI = (S₃/TOC)×100 (mg HC/g TOC), Oil in rock from S₁ (mcf/ac-ft) = S₁×131.34,

Generation potential from S₂ (mcf/ac-ft)=S₂×131.34, and calculated R_o (from T_{max}) = (0.018×T_{max}) - 7.16

Table 6.2 Average TOC, rock-Eval, and vitrinite reflectance values and computations of the Dat Yai section, the Na Pho Song Basin.

Sample	TOC (%)	Pyrolysis (mg/g rock)			HI	OI	PI S ₁ /(S ₁ +S ₂)	T _{max} (°C)	Calculated R _o (from T _{max})	Measured R _o (%)	Gas in rock from S ₁ (mcf/ac-ft)	Generation potential from S ₂ (mcf/ac-ft)
		S ₁	S ₂	S ₃								
T34-1	7.78	0.01	0.14	0.28	1.80	3.60	0.0667	604	3.71	1.67	1.31	18.39
T32-1	8.10	0.01	0.13	0.24	1.60	2.96	0.0714	604	3.71	-	1.31	17.07
T28-1	6.93	0.01	0.14	0.28	2.02	4.04	0.0667	602	3.68	-	1.31	18.39
T26-2	6.19	0.01	0.12	0.36	1.94	5.82	0.0769	605	3.73	1.72	1.31	15.76
T24-2	4.67	0.01	0.11	0.21	2.36	4.50	0.0833	602	3.68	1.74	1.31	14.45
T20-1	6.52	0.01	0.12	0.26	1.84	3.99	0.0769	601	3.66	1.73	1.31	15.76
T18-1	7.23	0.02	0.15	0.34	2.07	4.70	0.1176	603	3.69	-	2.63	19.70
T14-2	7.70	0.03	0.17	0.26	2.21	3.38	0.1500	605	3.73	1.73	3.94	22.33
T10-1	8.17	0.01	0.18	0.36	2.20	4.41	0.0526	604	3.71	1.86	1.31	23.64
T7-1	6.74	0.01	0.16	0.22	2.37	3.26	0.0588	598	3.60	1.70	1.31	21.01
Avg	7.00	0.01	0.14	0.28	2.04	4.07	0.0821	602.8	3.69	1.74	1.71	18.65

Remark; HI = (S₂/TOC)×100 (mg HC/g TOC), OI = (S₃/TOC)×100 (mg HC/g TOC), Oil in rock from S₁ (mcf/ac-ft) = S₁×131.34,

Generation potential from S₂ (mcf/ac-ft) = S₂×131.34, and calculated R_o (from T_{max}) = (0.018×T_{max}) - 7.16

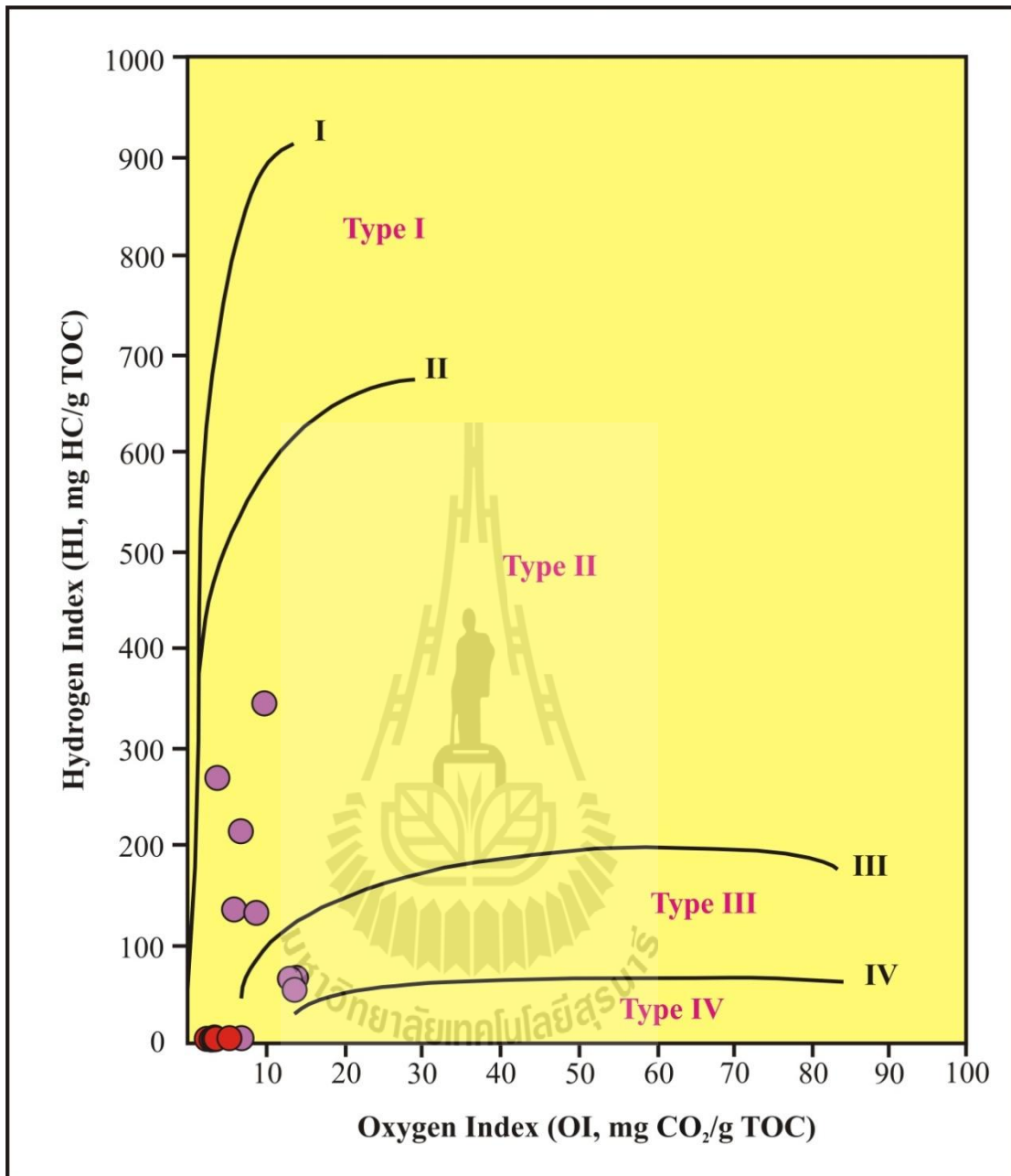


Figure 6.2 Modified van Krevelen diagram for identifying the kerogen types of the Ban Nong Sai samples (purple solid circles) and the Dat Yai samples (orange solid circles) of the Huai Hin Lat Formation.

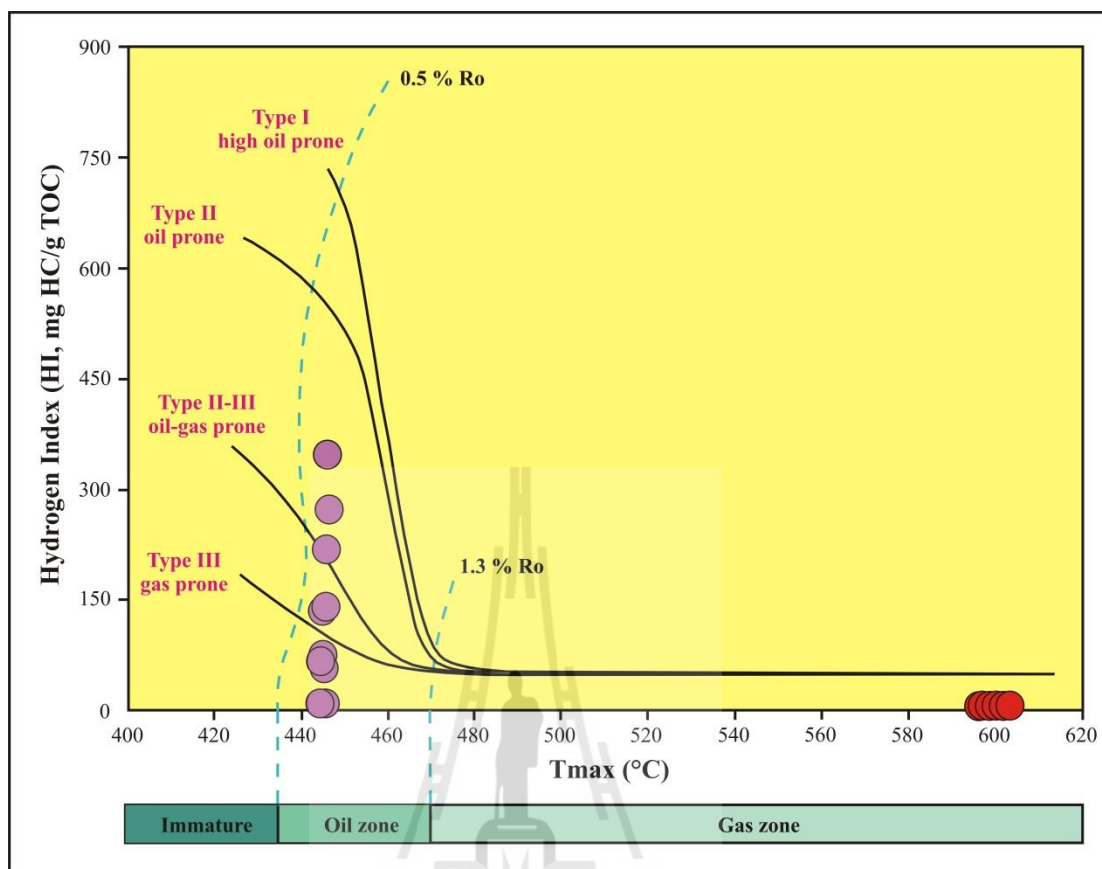


Figure 6.3 Hydrogen index versus T_{\max} temperature for kerogen type of the Ban Nong Sai samples (purple solid circles) and the Dat Yai samples (orange solid circles) of the Huai Hin Lat Formation.

Table 6.3 Organic matter type is classified by maceral of kerogen (Dai et al., 2008, Chen et al., 2011).

Organic matter type	Maceral of kerogen (TI value)
Sapropelic type (I)	>80
Humic-sapropelic type (II ₁)	40-80
Sapropelic-humic type (II ₂)	0-40
Humic type (III)	<0

Table 6.4 Type index (TI) and kerogen type classifications of the Ban Nong Sai section and Dat Yai section.

Type index classification					
Ban Nong Sai section			Dat Yai section		
Sample	Bed	Type index (TI)	Sample	Bed	Type index (TI)
		Type			Type
A5G	20	69.0	T34-1	31	74.3
		II ₁			II ₁
A4G	18	74.5	T32-1	29	76.0
		II ₁			II ₁
A3G	16	72.0	T28-1	25	78.5
		II ₁			II ₁
A2G	14	75.5	T26-2	23	80.2
		II ₁			I
16G	10	66.2	T24-2	21	74.4
		II ₁			II ₁
13G	7	76.0	T20-1	17	77.3
		II ₁			II ₁
11G	5	80.8	T18-1	15	75.4
		I			II ₁
6G	3A	82.0	T14-2	11	68.4
		I			II ₁
5G	2	83.0	T10-1	7	69.0
		I			II ₁
			T7-1	5	74.5
					II ₁

6.1.4 Organic matter quantity and quality

The quantitation of organic matter can be presented in quantitative means of present-day total organic carbon (TOC_{pd} or TOC) and original total organic carbon (TOC_o). The TOC is used to evaluate the source rock potential and it is reduced from the expulsion of hydrocarbon.

6.1.4.1 Present-day total organic carbon

The term source rock is applied to a rock unit that comprises sufficient organic matter of suitable chemical composition to generate the expelled hydrocarbons via biogenic or thermal processes (Miles, 1994). This can be applied to irrespective of whether its organic matter is mature or immature (Tissot and Welte, 1984; Potter et al., 1993; Belaid et al., 2010; Suarez-Ruiz et al., 2012). However, the quantitation of organic matter is also necessary evaluation. It is one factor that controlled the volume of expelled hydrocarbon from the source rocks.

The higher amount of organic matter represents the greater potential to be a good source rocks. Peter and Cassa (1994) classified TOC content for shale into 5 potential levels. Gehman (1962) suggested that organic content of shale is four times of that organic content of limestone as given the same hydrocarbon content (Table 6.5). The whole sections of the Ban Nong Sai and the Dat Yai show the total organic carbon content (TOC) is in the range of 1.90-7.06 % and 4.67-10.09 % respectively. The results of the Ban Nong Sai samples are consistent with the TOC values which are mainly excellent except the Bed 19 is good and the Beds 13 and 14 are very good (Figure 6.4). The Dat Yai samples are quite excellent source rocks (Figure 6.5). Therefore, they indicate that the potential of both sections are excellent source rocks.

Jarvie et al. (2007) suggested that there are three basic components are composed of total organic carbon in the source rocks. The three basic components are organic carbon in retained hydrocarbon (C_{hc}), organic carbon that can be converted to hydrocarbon (C_c), and dead carbon or residual organic carbon (C_r). They also explained the immature source rocks have high TOC values as well as the

average generation potential (S_2). The present-day TOC with high thermal maturity is reduced. Removal of residual organic carbon in retained hydrocarbon (C_{hc}) and organic carbon that can be converted to hydrocarbon (C_c) in rock-Eval S_1 and S_2 yields as a present dead carbon or residual organic carbon (C_{rpd}). The present-day TOC is still high (dead carbon) but lack the generation potential except the Ban Nong Sai samples (Table 6.1 and 6.2).

6.1.4.2 Original total organic carbon

The original total organic carbon (TOC_o) is complicated to determine due to thermal maturation. However, the consideration of the components of TOC assists in understanding how to restore highly mature TOC to TOC_o . The TOC_o of source rocks provides a quantitation to estimate the total volume of hydrocarbons that can be generated (Jarvie et al., 2007). The determining TOC_o consists of first determining HI_o that can be computed from the visual kerogen assessments for four types. The equation is used by Jarvie et al. (2007) and obtained as follows:

$$HI_o = \left(\frac{\% \text{ type I}}{100} \times 750 \right) + \left(\frac{\% \text{ type II}}{100} \times 450 \right) + \left(\frac{\% \text{ type III}}{100} \times 125 \right) + \left(\frac{\% \text{ type IV}}{100} \times 50 \right) \quad (6.2)$$

This equation requires input of maceral percentages of the source rocks as showing in Table 5.3 and 5.4. For example, using the sample of 5G that is 90.3 % Type I, 0.0 % Type II, 9.7 % Type III, and 0.1 % Type IV. The sample of T7-1 comprises 86.7 % Type I, 0.0 % Type II, 16.3 % Type III, and 0.0 % Type IV. The calculated HI_o values are 689.38 and 670.63 mg HC/g TOC respectively. The samples of the Ban Nong Sai and Dat Yai sections are in range of 629.15-689.38

mg HC/g TOC (Table 6.6) and 637.28-679.38 mg HC/g TOC (Table 6.7). At 100 % Type I, the HI_o would be 750 mg HC/g TOC. These values can be comparable to those measured on high thermal maturity.

Then Claypool's equation (Peters et al., 2005; Jarvie et al., 2007; Kuchinsskiy et al., 2012) is used. The transformation or fractional ratio (TR) is derived from the change in original HI to present-day HI values (Espitalie et al., 1984; Pelet, 1985; Peters et al., 2006; Jarvie et al., 2007). The equation is obtained as follows:

$$TR = 1 - \left[\frac{HI_{pd} (1200 - HI_o (1 - PI_o))}{HI_o (1200 - HI_{pd} (1 - PI_{pd}))} \right] \quad (6.3)$$

This equation is incorporated with formula of Pelet (1985) for calculating the kerogen transformation. 1200 is the maximum amount of hydrocarbons that can be formed 83.33 % of average carbon content in hydrocarbons. PI is the production index as $PI_o = 0.02$ to PI_{pd} (Peters et al., 2006). The transformation ratios of the Sap Phlu and Na Pho Song Basins are range from 69.00 to 99.59 % (Table 6.6) and 99.83 to 99.89 % (Table 6.7) respectively. They are extremely high and can be evaluated to thermal maturation as will be explained next.

Lastly, the calculation of TOC_o from the low-maturity samples, HI_o , and TR_{HI} can be succeeded by following equation (Peters et al., 2005; Jarvie et al., 2007; Kuchinsskiy et al., 2012).

$$TOC_o = \frac{(HI_{pd}) \left(\frac{TOC_{pd}}{1+k} \right) (83.33)}{\left[(HI_o)(1 - TR_{HI}) \left(83.33 - \left(\frac{TOC_{pd}}{1+k} \right) \right) \right] - \left[HI_{pd} \left(\frac{TOC_{pd}}{1+k} \right) \right]} \quad (6.4)$$

k is $TR_{HI} \times C_R$. It is a correction factor based on residual organic carbon being enriched in carbon over original values at high maturity (Burnham, 1989; Jarvie et al., 2007). C_R is an increase in residual carbon that depend on Kerogen type as Type I, Type II, and Type III are 50 %, 15 %, and 0 % respectively.

The calculated TOC_o values range from 5.13-10.74 % (Table 6.6) and 7.81-14.86 % (Table 6.7) for the Ban Nong Sai and Dat Yai sections. These TOC_o values are increasing approximately 57.21 % which comparable to the TOC_{pd} for the Ban Nong Sai samples and up to 76.92 % for the Dat Yai samples. The TOC_o is changed to the present-day due to the carbons incorporated with hydrogen and expelled from the source rocks. The extremely change in carbon content is caused by the effect of high thermal maturity. For comparison, the Dat Yai section got the higher effects than the Ban Nong Sai section however, the effects are still high.

Table 6.5 Classification of potential source rock in shale and limestone based on TOC values (Gehman, 1962; Peter and Cassa, 1994).

TOC (%)		Potential
Shale	Limestone	
< 0.5	< 0.12	Poor
0.5 - 1.0	0.12 - 0.25	Fair
1.0 - 2.0	0.25 - 0.50	Good
2.0 - 4.0	0.50 - 1.0	Very good
> 4.0	> 1.0	Excellent



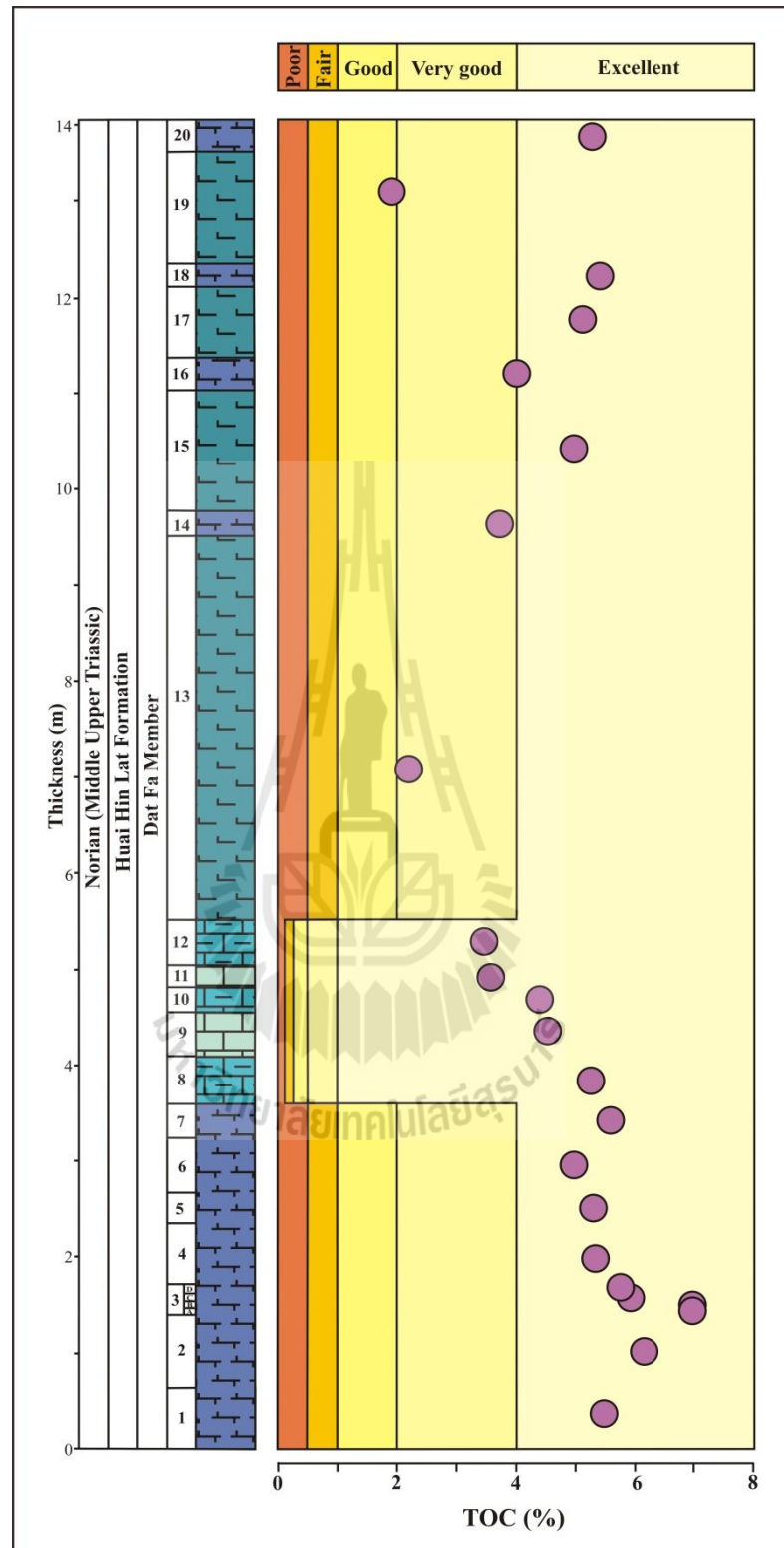


Figure 6.4 Classification of potential source rocks of the Ban Nong Sai section based on total organic carbon content (TOC).

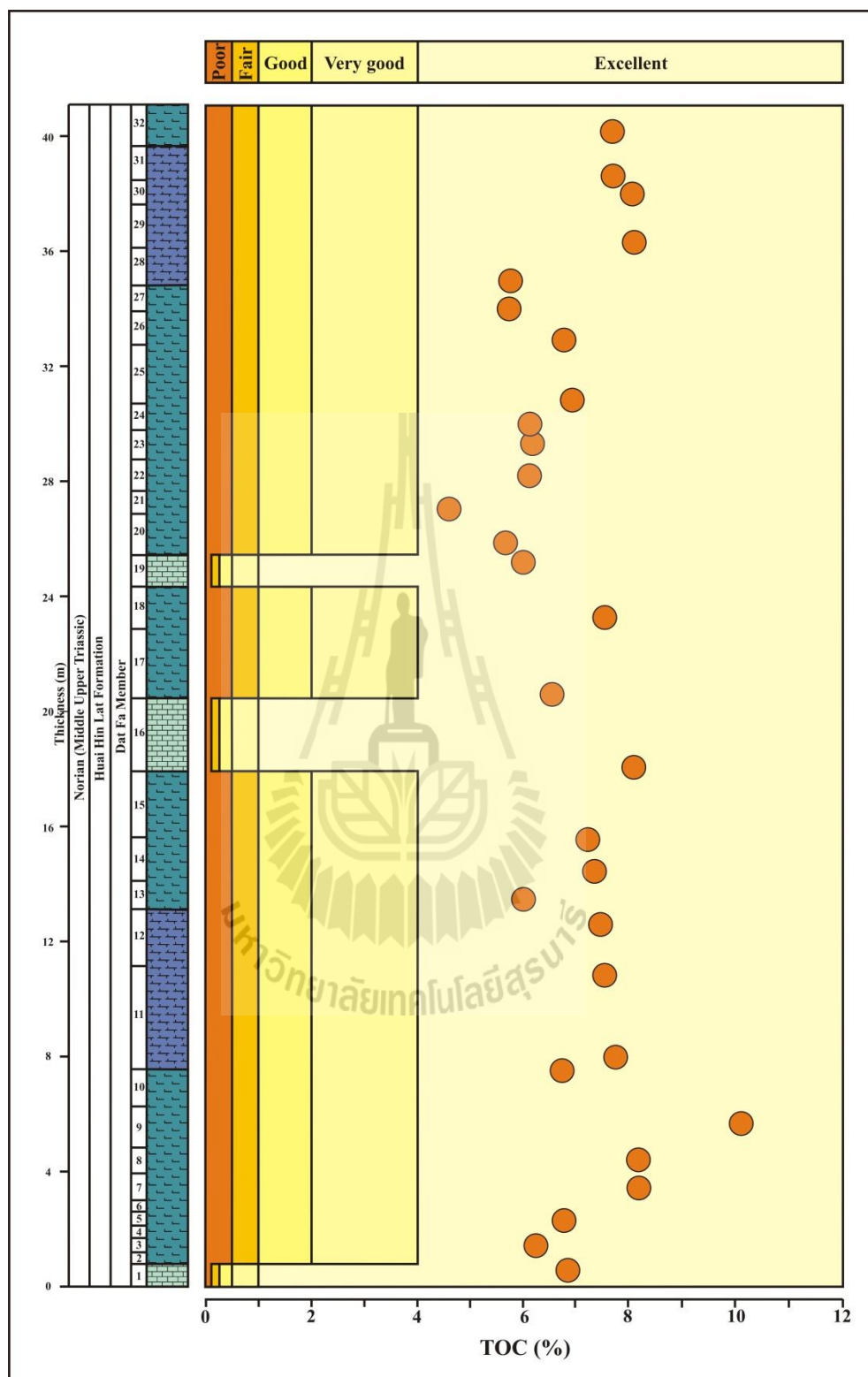


Figure 6.5 Classification of potential source rocks of the Dat Yai section based on total organic carbon content (TOC).

Table 6.6 Original hydrogen index (HI_o), transformation or conversion ratio (TR_{HI}), and original total organic carbon (TOC_o) of the Ban Nong Sai section, the Sap Phlu Basin.

No	Sample	Visual kerogen assessment				HI_o	HI_{pd}	PI_o	PI_{pd}	TR	TOC_{pd} (%)	k ($TR_{HI} \times C_R$)	TOC_o (%)
		Type I	Type II	Type III	Type IV								
1	A5G	82.3	0.0	17.3	0.3	639.03	65.90	0.02	0.0085	0.9479	5.326	0.4739	8.21
2	A4G	86.7	0.0	16.3	0.0	670.63	132.07	0.02	0.0056	0.9000	5.391	0.4500	8.44
3	A3-4G	-	-	-	-	-	-	-	-	-	5.073	-	-
4	A3G	84.0	0.0	16.0	0.0	650.00	65.13	0.02	0.0149	0.9503	4.069	0.4752	6.18
5	A2-3G	-	-	-	-	-	-	-	-	-	4.953	-	-
6	A2G	86.0	0.0	14.0	0.0	662.50	216.17	0.02	0.0222	0.8182	3.673	0.4091	5.13
7	16G	80.7	0.0	19.0	0.3	629.15	5.77	0.02	0.3810	0.9955	4.507	0.4978	6.93
8	13G	86.3	0.0	13.3	0.3	664.03	5.93	0.02	0.0833	0.9959	5.562	0.4979	9.41
9	11G	89.0	0.0	11.0	0.0	681.25	137.89	0.02	0.0068	0.8986	5.265	0.4493	8.34
10	10G	-	-	-	-	-	-	-	-	-	5.310	-	-
11	6G	89.7	0.0	10.3	0.0	685.63	344.87	0.02	0.0050	0.6900	6.933	0.3450	9.98
12	5G	90.3	0.0	9.7	0.0	689.38	59.03	0.02	0.0082	0.9607	6.149	0.4803	10.74
Avg		86.1	0.0	14.1	0.1	663.51	114.75	0.02	0.0595	0.9063	5.184	0.4532	8.15

Remark; $_o$ = original, $_{pd}$ = present day, $PI_o = 0.02$, k = the correction factor, C_R = an increase in residual carbon that depend on Type I, Type II, and Type III of 50 %, 15 %, and 0 % respectively

Table 6.7 Original hydrogen index (HI_o), transformation or conversion ratio (TR_{HI}), and original total organic carbon (TOC_o) of the Dat Yai section, the Na Pho Song Basin.

No	Sample	Visual kerogen assessment				HI_o	HI_{pd}	PI_o	PI_{pd}	TR	TOC_{pd} (%)	k ($TR_{HI} \times C_R$)	TOC_o (%)
		Type I	Type II	Type III	Type IV								
1	T34-1	85.3	0.0	14.7	0.0	658.13	1.80	0.02	0.0667	0.9987	7.78	0.4994	13.95
2	T32-1	86.3	0.0	13.7	0.0	664.38	1.60	0.02	0.0714	0.9989	8.10	0.4994	14.86
3	T28-1	87.7	0.0	12.3	0.0	673.13	2.02	0.02	0.0667	0.9986	6.93	0.4993	12.48
4	T26-2	88.7	0.0	11.3	0.0	679.38	1.94	0.02	0.0769	0.9987	6.19	0.4994	11.03
5	T24-2	86.7	0.0	16.0	0.3	670.40	2.36	0.02	0.0833	0.9984	4.67	0.4992	7.81
6	T20-1	87.0	0.0	13.0	0.0	668.75	1.84	0.02	0.0769	0.9987	6.52	0.4994	11.49
7	T18-1	86.0	0.0	13.7	0.3	662.28	2.07	0.02	0.1176	0.9986	7.23	0.4993	12.85
8	T14-2	82.0	0.0	17.7	0.3	637.28	2.21	0.02	0.1500	0.9983	7.70	0.4992	13.20
9	T10-1	82.3	0.0	17.3	0.3	639.03	2.20	0.02	0.0526	0.9983	8.17	0.4992	14.26
10	T7-1	86.7	0.0	16.3	0.0	670.63	2.37	0.02	0.0588	0.9984	6.74	0.4992	12.00
	Avg	85.9	0.0	14.6	0.12	662.34	2.04	0.02	0.0821	0.9986	7.003	0.4993	12.39

Remark; $_o$ = original, $_{pd}$ = present day, $PI_o = 0.02$, k = the correction factor, C_R = the increase in residual carbon that depend on Type I, Type II, and Type III of 50 %, 15 %, and 0 % respectively

6.1.5 Thermal maturity

Recently, the operating gas fields are published the high gas content is caused by the volumes of generated hydrocarbons and thermal maturity. Then liquid hydrocarbons are cracking to gas (Jarvie et al., 2007). Vandenbroucke et al. (1999) described that cracking referred to kerogen is progressively transformed during burial of sediments into smaller molecules and low molecular weight. The successive steps of this kinematic transformation are diagenesis through metagenesis.

Diagenesis of first few meters of the sediments is loss of nitrogen which escapes mainly NH_3 . The burial zone is corresponded to temperature lower than 70-80 °C that loss of oxygen in form of water, carbon mono and dioxide, and limited amounts of other oxygenated compounds.

Catagenesis, the almost hydrogen is loss by additional heating of 90-140 °C. C-C bonds were broke within polar compounds and residual kerogen (Walters, 2006). As the results, hydrocarbon-rich fluid is expelled as formed heavy oil through lighter, and condensate or wet gas.

Metagenesis, the temperature is higher than 150 °C is referred to deep where only methane is produced. It is formed a methyl-groups that are cleavage from highly condensed aromatic structure (Walters, 2006). The low maturity is produced gaseous hydrocarbon which low flow rate. But the contrasting gas flow rates are the result of high maturity.

The maturation parameters are indicative of the maximum palaeotemperature that a source rock has reached and formed a key geochemical parameter to assess the likelihood of high flow rate shale gas (Jarvie, 2004; Jarvie et al., 2007). For this study, it also made a combination of the applying parameters of

visual and chemical results. The vitrinite reflectance, T_{\max} , production index (PI), and kerogen transformation ratio are selected for substantiate their temperature affected to both sections.

6.1.5.1 Vitrinite reflectance (R_o)

Vitrinite reflectance is now used to help geochemists evaluate kerogen maturation over temperatures. It is a range spanning the sequence of petroleum generation, preservation, and destruction in rocks (Senftle and Landis, 1991; McCarthy et al., 2011). It is conventionally described using a distribution of activation energies (Waples and Marzi, 1998) that include the calculation increase in vitrinite reflectance (Sweeney and Burnham, 1990; Waples and Marzi, 1998) and hydrocarbon generation from kerogen (Burnham, 1989; Tissot et al., 1987; Waples and Marzi, 1998). During early maturation vitrinite reflectance will begin to change before any significant hydrocarbon generation has occurred (Waples and Marzi, 1998). Moreover, T_{\max} is associated with thermal maturation that referred to have more association to vitrinite reflectance. Then Jarvie et al. (2001) published the correlation between T_{\max} and vitrinite reflectance as following equation.

$$R_o(eq) = 0.0180 (T_{\max}) - 7.16 \quad (6.5)$$

Following the equation, T_{\max} of the Ban Nong Sai and Dat Yai sections are in range of 443-451 °C and 598-605 °C respectively. They show the results of calculated R_o that are range from 0.81-0.96 % (Table 6.1) for the Ban Nong Sai section and 3.60-3.73 % (Table 6.2) for the Dat Yai section. For comparison, the calculated R_o of the Ban Nong Sai samples is rarely differed from the values of

measured R_o which demonstrated by the sample of A2G. That value shows 0.89 % of calculated R_o and 0.82 % of measured R_o . But the average R_o of calculation and measurement of the Dat Yai section are shown 3.69 % and 1.74 % respectively. The calculated R_o is higher due to higher contain of dead carbons. As the results, the higher temperature should be supplied and produced the generated hydrocarbons. According to the post mature samples, the results of calculated and measured R_o are different in values by using T_{max} and petrographic analysis. Although the calculated and measured R_o of the Dat Yai samples are quite different, however, both measured and calculated R_o of both sections are still using for evaluation of the thermal maturity stages.

The thermal maturity stages are classified by the values of R_o as shown in Table 6.8. Less than 0.60 % R_o is interpreted to immature stage. 0.60-0.65 % R_o , 0.65-0.90 % R_o , and 0.90-1.35 % R_o are classified to the stages of early, peak, and late mature respectively. The higher stage of post mature is evaluated by the R_o value of 1.35. According to the Ban Nong Sai section, the most samples are classified to peak maturity stage except two samples of A2-3G (measured R_o) and 10G (calculated R_o) are in late maturity stage (Figure 6.6A). They may generate both liquid and some gaseous hydrocarbons. The Dat Yai samples are classified to post mature both measured and calculated R_o (Figure 6.8A) is therefore, produced the gaseous hydrocarbon. The Dat Yai section shows the R_o is higher than the R_o of the Ban Nong Sai section. As the results, the Dat Yai section of the Na Pho Song Basin is more effects of tectonic and subsidence than other one. It was quite effect due to quite difference in R_o values of both sections. It indicates the late mature (measured

R_o) and post mature (calculated R_o) however, both stages can be generated the gaseous hydrocarbons.

6.1.5.2 Maximum temperature (T_{max})

Maximum temperature that is recorded for the maximum of the generation potential peak varies. It is a function of the thermal of the thermal maturity of the organic matter (Tissot and Espitalie, 1975). Bordenave (1993) suggested the mature organic matter is more condensed, more difficult to pyrolyze, and requires a higher activation energy (higher temperature). Chemical bonds that survived in most highly mature kerogens are those requiring the highest energy be broken. T_{max} is linked to the kinetics of the cracking of organic matter. Type I and Type II kerogens are known to have relatively simpler molecular structures than Type III. It implies a narrower distribution of cracking activation energies and a lesser temperature range (Tissot and Espitalie, 1975).

The thermal maturity stages are classified by the values of T_{max} as shown in Table 6.8. T_{max} is less than 435 °C indicating thermal immaturity. 435-445 °C, 445-450 °C, and 450-470 °C indicates the stages of early, peak, and late mature of the main phase of oil window. While measuring the values are greater than 470 °C are considered to be within the gas window. The T_{max} values of the Ban Nong Sai section are in range of 443-451 °C (Table 6.1) and plotted as shown in Figure 6.6B. The four samples indicate the early mature and the other six indicate the peak mature. The T_{max} of early mature samples range from 443-445 °C as will be upgraded to peak mature. Therefore, the Ban Nong Sai section can be evaluated to the stage of peak mature which the mixing of oil and gas are produced. The Dat Yai section ranges from 598-605 °C (Table 6.2). It is evaluated to a post mature due to all

samples are plotted in this portion (Figure 6.8B). It shows the high T_{\max} value is higher than the Ban Nong Sai section that is more production of dry gas. The higher production of gas is referred to lack of hydrogen and high remaining carbon. As the results, the higher energy as shown in term of extremely high T_{\max} is used to generate yielding S_2 . However, it still shows a few amounts due to less remaining potential of source rock.

6.1.5.3 Production index (PI)

The production index ($PI = S_1/(S_1 + S_2)$) is mainly increase due to the cracking of the kerogen. At a lesser extent to both thermal-vaporization and cracking of asphaltenes which cause the S_2 peak to be progressively transformed into S_1 (Bordenave, 1993).

The classification of thermal maturity stages by using the values of production index (PI) are shown in Table 6.8. Less than 0.10 in value is indicated to immature stage. 0.10-0.25 and 0.25-0.40 are interpreted to early and peak mature and while measurement is higher 0.40 that considering to stage of late mature. According to the Ban Nong Sai and Dat Yai sections, they are range from 0.0050-0.3810 and 0.0526-0.1500 respectively (Table 6.1 and 6.2). The most data of both sections is considered to be within the immature stage (Figure 6.7A and 6.9A). The immature stage is not conformed to other proxies due to producing hydrocarbon (S_1) is less detection. The S_1 is less due to it has been expelled and migrated from the primary places which are less preserved in pores of rock samples.

6.1.5.4 Kerogen transformation ratio (TR)

Jarvie et al. (2007) suggested the kerogen transformation ratio (TR) is feasible to evaluate conversion directly by measuring changes in organic

matter yields. The conversion of organic matter can be assessed by the change in TR values from the low to high maturity. The TR is calculated by the claypool's equation follows the method of TOC_o calculation as explained clearly in the original total organic carbon of overlying subtopic.

The classification of thermal maturity stages by using the TR proxy are followed the suggestion of Jarvie et al. (2007) as shown in the Table 6.8. The TR is range from 0.0-50.0 % that indicates primary oil and 50-80 % TR indicates mixed oil and gas. 80-90 %TR evaluates to the earliest gas window. The dry gas window requires the increasing values are higher than 90 %TR. The TR values of the Ban Nong Sai and the Dat Yai sections are converted to percentage as range from 69.00 % to 99.59 % (Table 6.6) and 99.83 % to 99.89 % (Table 6.7) respectively. The most TR values of the Ban Nong Sai section are indicated to be within mixing of wet and dry gases (Figure 6.7B). And all TR of the Dat Yai section are indicated to be within the dry gas window (Figure 6.9B). Both stages are conformed to the classification of other proxies.

In conclusion, the vitrinite reflectance, T_{max} , PI, and TR are formed the better keys for reveal the palaeotemperature however, they cannot be described the clearly thermal maturity stages. The PI is not used to interpret due to both sections are considered to be within immature exactly. The Ban Nong Sai section indicates the peak mature that is accorded to the R_o and T_{max} . As the results, the TR diagram shows the primary gas to dry gas phases that is produced from its samples. According to the Dat Yai section, although the measured R_o indicates the late mature but the calculated R_o indicates the higher stage. However, both stages also produced the gasses. This post mature stage is conformed to the T_{max} and the TR

diagram which shows the dry gas phase is produced through the section due to high temperature.

Table 6.8 Classification of thermal maturity stages by T_{\max} , vitrinite reflectance (R_o), production index (PI) (Peters and Cassa, 1994; Espitalié and Bordenave, 1993; Bacon et al., 2000), and transformation ratio (TR) (Jarvie et al., 2005, 2007).

Thermal maturity stage	T_{\max}	R_o (%)	Production index (PI)	Transformation ratio (TR)	
Immature	< 435	< 0.60	< 0.10	-	
Mature	Early	435 - 445	0.10 - 0.25	Oil	0 - 50 %
	Peak	445 - 450	0.25 - 0.40	Oil and gas	50 - 80 %
	Late	450 - 470	> 0.40	Wet gas	80 - 90 %
Post mature	> 470	> 1.35	-	Dry gas	> 90 %



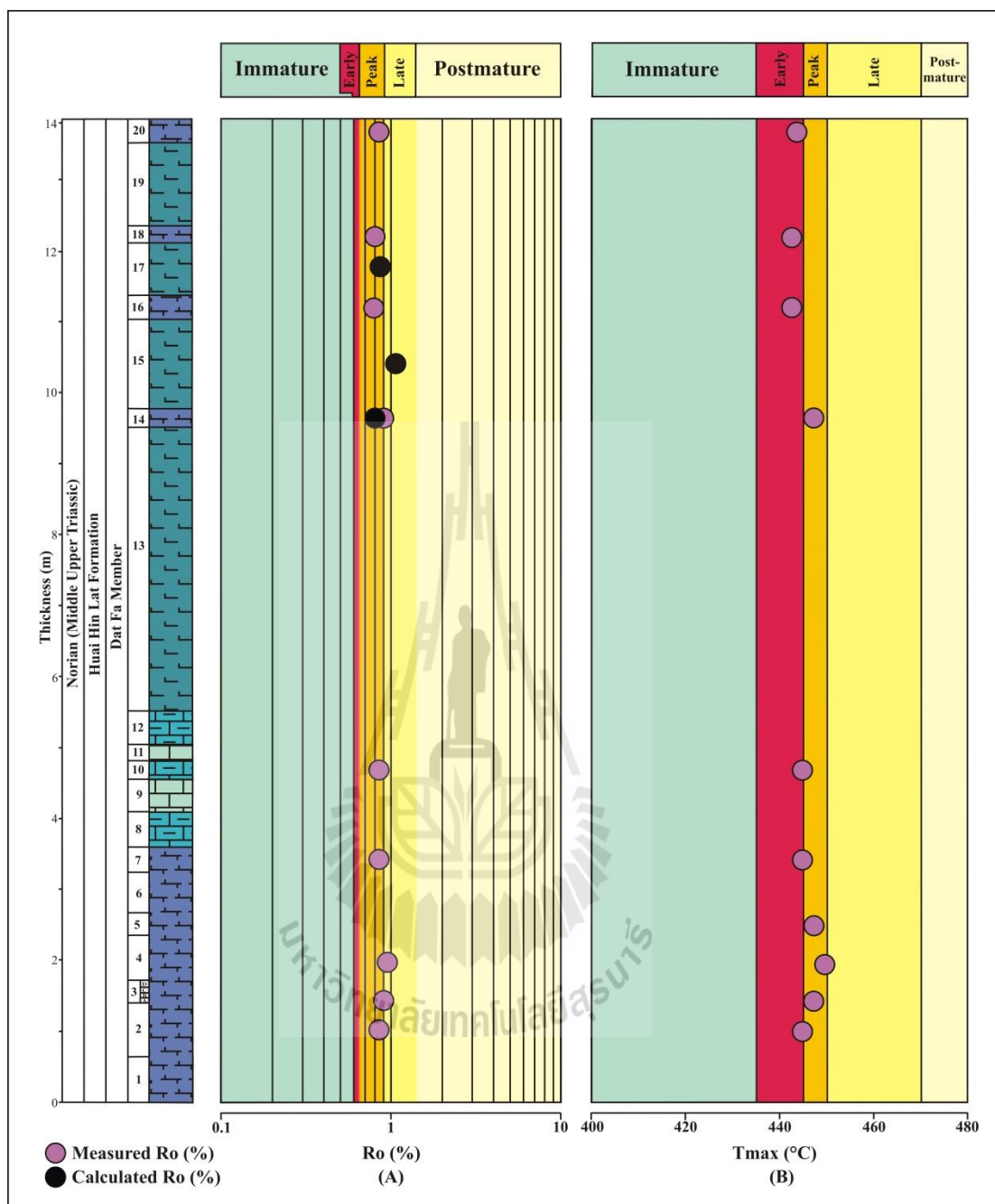


Figure 6.6 Thermal maturity stages of source rocks of the Ban Nong Sai section, the Sap Phlu Basin that evaluated by (A) vitrinite reflectance (R_o) of visual analysis (purple) and calculation from T_{max} (black) and (B) T_{max} ($^{\circ}$ C).

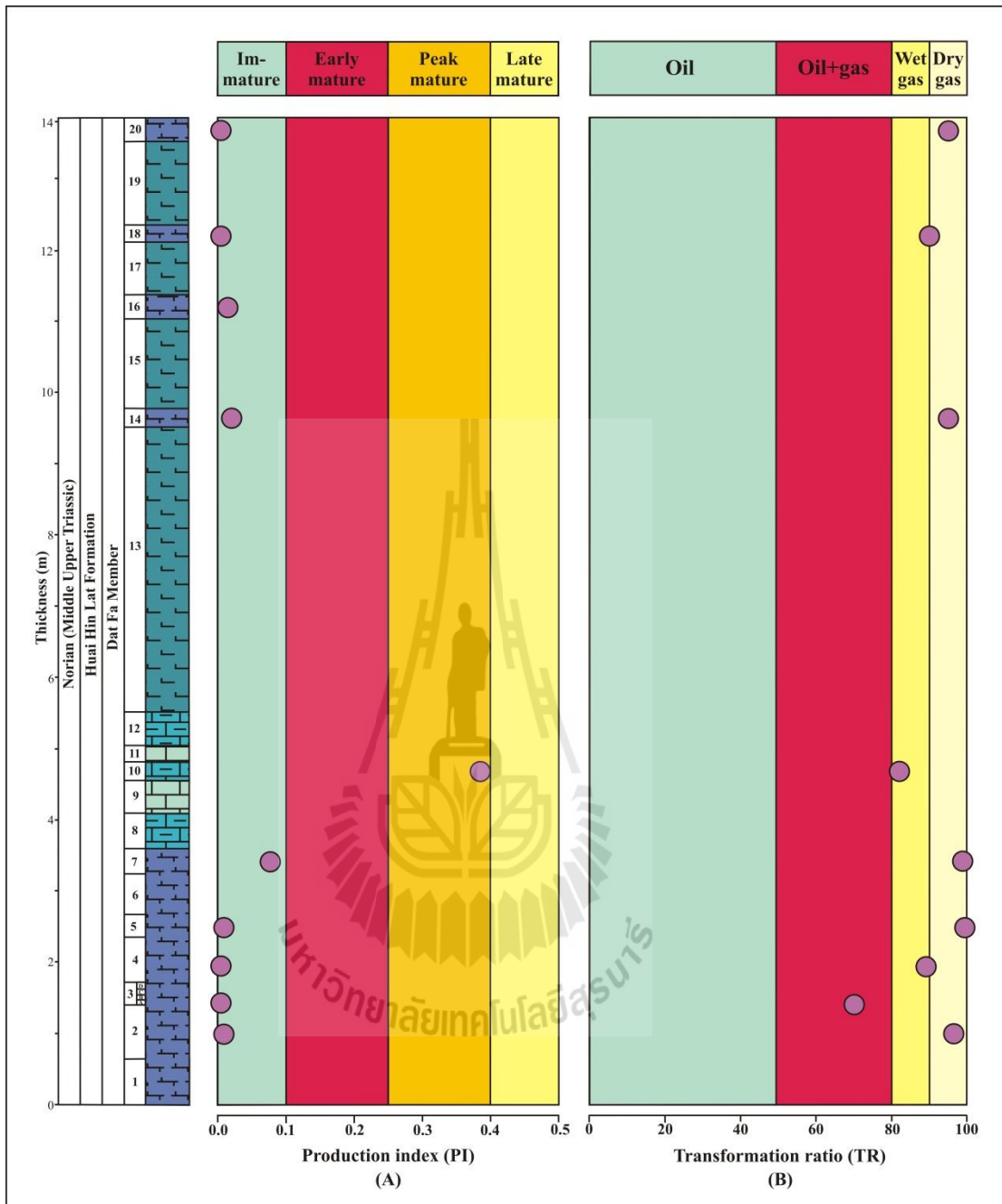


Figure 6.7 Thermal maturity stages of source rocks of the Ban Nong Sai section, the Sap Phlu Basin that evaluated by (A) production index (PI) and (B) transformation ratio (TR).

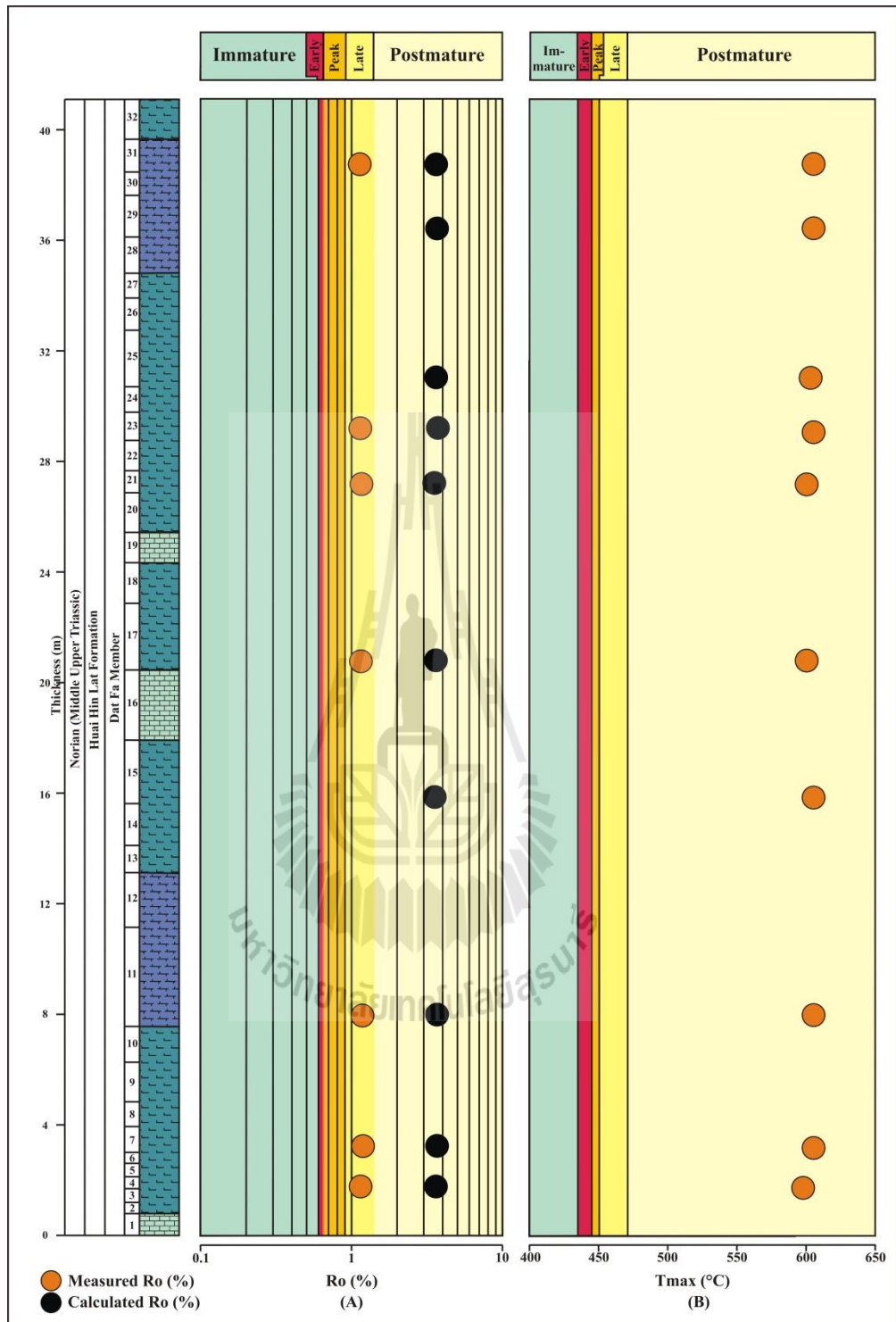


Figure 6.8 Thermal maturity stages of source rocks of the Dat Yai section, the Na Pho Song Basin that evaluated by (A) vitrinite reflectance (R_o) of visual analysis (orange) and calculation from T_{max} (black) and (B) T_{max} (°C).

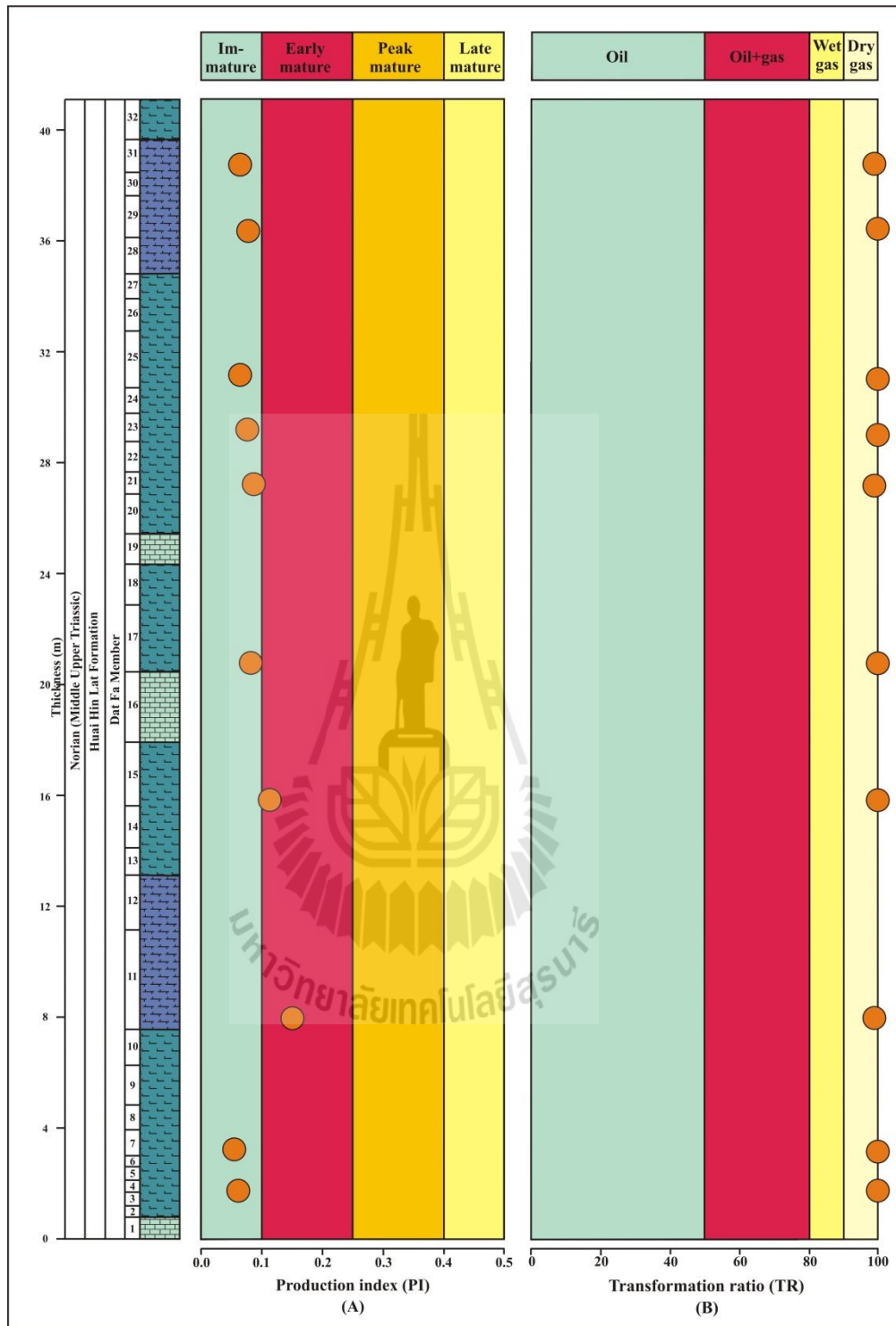


Figure 6.9 Thermal maturity stages of source rocks of the Dat Yai section, the Na Pho Song Basin that evaluated by (A) production index (PI) and (B) transformation ratio (TR).

6.1.6 Volume of generated hydrocarbon in source rocks

Jarvie et al. (2007) suggested three distinct process result of thermogenic gas within shale are the decomposition of kerogen to gas and bitumen. The decomposition of bitumen to oil and gas is decomposition of oil to gas and pyrobitumen. The first step, the generated hydrocarbon (S_2) is used to describe the remaining- or the present-day generation potential. The pyrolysis amounts can be converted to 931.86 mcf/ac-ft (Table 6.1) and 18.65 mcf/ac-ft (Table 6.2) of the Ban Nong Sai and Dat Yai sections. Although the Ban Nong Sai section is higher remaining potential than another however, it is still not too high. This result is conformed to the low gas in rocks from S_1 of 10.64 mcf/ac-ft and 1.71 mcf/ac-ft as shown in Table 6.1 and 6.2. Therefore, the second consideration is calculated for understanding how large volume of the most generated gasses.

The shales of both sections can be generated the hydrocarbons and can be knew hydrocarbon volumes by using the equation of Schmoker (1994). This equation is associated with the present-day (remaining) S_2 and the calculated original potential (S_{2o}). The present-day S_2 can be detected from the pyrolysis (Table 6.1 and 6.2) but original S_{2o} should be backwardly calculated following the incorporation with formula of TOC_o (Peters et al., 2005; Jarvie, 2007) and HI_o . The equation is provided for backward calculation of original S_{2o} is obtained as follows:

$$S_{2o} = \left(\frac{HI_o \times TOC_o}{100} \right) \quad (6.6)$$

Following the equation, the TOC_o and HI_o of the Ban Nong Sai section (5.13-10.74 °C and 629.15-689.38 mgHC/gTOC) and the Dat Yai section (7.81-14.86 °C

and 637.28-679.38 mgHC/gTOC) are shown in Table 6.6 and 6.7 respectively. As the results, the original S_{20} is in range of 33.99-74.04 mg/g rock (Table 6.9) and 52.36-98.73 mg/g rock (Table 6.10) for the Ban Nong Sai section and the Dat Yai section respectively.

Lastly, the generated hydrocarbon volume can be determined by using the equation is derived from the change in calculated original potential (S_{20}) to present-day or remaining potential (S_2) values. The provided equation for the generated hydrocarbon is obtained as follows:

$$\text{Generated hydrocarbon} = \text{Original potential } (S_{20}) - \text{Remaining potential } (S_2) \quad (6.7)$$

Following the S_{20} and S_2 of both sections, the generated hydrocarbons are shown in Table 6.9 and 6.10 which are ranged from 26.05-70.41 mg/g rock and 52.25-98.60 mg/g rock for the Ban Nong Sai section and the Dat Yai section respectively. The generated hydrocarbon can be converted to the hydrocarbon yields by using the converting factor of 131.34 (mcf/ac-ft). As the results, the average hydrocarbon yields of the Ban Nong Sai and the Dat Yai sections are shown in values of 6,309.51 mcf/ac-ft (Table 6.9) and 10,604.90 mcf/ac-ft (Table 6.10) respectively. For comparison, the Dat Yai section is higher hydrocarbon yield than another which is excellently expelled from its formation.

Table 6.9 Calculated original potential (S_{20}), generated hydrocarbons, and average hydrocarbon yield of the Ban Nong Sai section, the Sap Phlu Basin.

No	Sample	HI _o	TOC _o	S ₂₀	S ₂	Generated hydrocarbons	Hydrocarbon yields
		(mgHC/gTOC)	(%)	(mg/g rock)			
1	A5G	639.03	8.21	52.46	3.51	48.95	6,429.67
2	A4G	670.63	8.44	56.60	7.12	49.48	6,498.86
3	A3-4G	-	-	-	-	-	-
4	A3G	650	6.18	40.17	2.65	37.52	4,927.88
5	A2-3G	-	-	-	-	-	-
6	A2G	662.5	5.13	33.99	7.94	26.05	3,420.91
7	16G	629.15	6.93	43.60	0.26	43.34	5,692.29
8	13G	664.03	9.41	62.49	0.33	62.16	8,163.47
9	11G	681.25	8.34	56.82	7.26	49.56	6,508.72
10	10G	-	-	-	14.34	-	-
11	6G	685.63	9.98	68.43	23.91	44.52	5,846.71
12	5G	689.38	10.74	74.04	3.63	70.41	9,247.57
Average		663.51	8.15	54.08	6.29	47.79	6,309.51

Remark; Hydrocarbon yields (mcf/ac-ft) = $(S_{20}-S_2) \times 131.34$

Table 6.10 Calculated original potential (S_{20}), generated hydrocarbons, and average hydrocarbon yield of the Dat Yai section, the Na Pho Song Basin.

No	Sample	HI _o	TOC _o	S ₂₀	S ₂	Generated hydrocarbons	Hydrocarbon yields
		(mgHC/gTOC)	(%)	(mg/g rock)			
1	T34-1	658.13	13.95	91.81	0.14	91.67	12,039.82
2	T32-1	664.38	14.86	98.73	0.13	98.60	12,949.71
3	T28-1	673.13	12.48	84.01	0.14	83.87	11,015.04
4	T26-2	679.38	11.03	74.94	0.12	74.82	9,826.28
5	T24-2	670.40	7.81	52.36	0.11	52.25	6,862.28
6	T20-1	668.75	11.49	76.84	0.12	76.72	10,076.32
7	T18-1	662.28	12.85	85.10	0.15	84.95	11,157.72
8	T14-2	637.28	13.20	84.12	0.17	83.95	11,026.12
9	T10-1	639.03	14.26	91.13	0.18	90.95	11,944.81
10	T7-1	670.63	12.00	80.48	0.16	80.32	10,548.65
Average		662.34	12.39	81.95	0.14	81.81	10,604.90

Remark; Hydrocarbon yields (mcf/ac-ft) = $(S_{20}-S_2) \times 131.34$

6.1.7 Evaluation of conventional gas potential

The hydrocarbon resource plays are high in the Ban Nong Sai section and extremely high in the Dat Yai section as followed the overlying subtopic of volume of generated hydrocarbon in source rocks.

Both the Ban Nong Sai and Dat Yai sections are an organic-rich, type I and II₁, and oil prone that originally averaged about 4.86 %TOC and 7.03 %TOC respectively. The thermal maturity is evaluated to peak mature and post mature that oil was mostly converted to gas. Calculation of the original generation potentials based on S_{2o} and S₂ yields are about 6,309.51 mcf/ac-ft and 10,604.90 mcf/ac-ft for the Ban Nong Sai section and the Dat Yai section respectively. The Ban Nong Sai section and the Dat Yai section show the average HI_{pd} (114.75 and 2.04 mg HC/g TOC) and average PI (0.0595 and 0.0821) are too low due to S₂ are quite low. Low in S₂ was the result from high thermal maturation that can be indicated to low in present potential. That the originally existing potential of the source rocks was cracked and expelled as are exactly high in S₁. In contrast, S₁ (free hydrocarbon) was detected in low of volume is therefore, the other free hydrocarbons had been migrated to the adjacent reservoirs.

Both sections have a high potential on gas source rocks. The hydrocarbons are mostly migrated from the most calculated original potential. We can trace the ways they gone and where are they accumulated. They are not accumulated in overlying sandstones due to Booth (1998) suggested that lack of any shows in the sandstone in the upper part of the Kuchinarai Group (Huai Hin Lat Formation) in Dong Mun-1 well. Booth (1998) also suggested that the shales of the lower portion of this formation provide a good top seal. The shales are not allowed

the gas passing through to the overlying sandstones but may allow to the formation where is more available. The adjacent Pha Nok Khao Formation where there are more spaces or associated with dolomitization processes may have been more available accumulation. It is conformed to both Nam Phong and Sin Phu Horm gas fields which the Pha Nok Khao Formation is the main producing zones as well as the Dong Mun gas field. Therefore, this thesis can be proved some gases that produce from the three gas fields were supplied from the source rocks of the Huai Hin Lat Formation.

6.2 Shale gas evaluation

Shale gases are blooming especially shale gas source which is a future long-term energy source among others (Slatt and O'Brien, 2011). Khorat Plateau is also expected high potential of shale gases especially the Huai Hin Lat Formation. The potential of unconventional shale gas is evaluated for development eventually more highly increasing reserve.

The free hydrocarbon is shown in S_1 may not migrated to adjacently secondary reservoirs. They are probably trapped in the source rocks as formed the in-situ reservoir. They can be supply the high volume of gases like other shale gas fields. The shale gas field can be developed that it is commercial production and completed evaluation on gas source rock and reservoir condition. Based on evaluated shale gas, the entire data are concluded as a research idea of gas source rock and reservoir condition evaluation. It will be performed on risk evaluation (source rock and reservoir condition data) as described below.

6.2.1 Risk evaluation of source rock data

A risk plot of source rock evaluation is modified from Jarvie et al. (2005). It is a simple means to compare various parameters and their application to initial economic assessment.

The shale gas assessment based on maximum temperature (T_{max}), vitrinite reflectance (R_o), production index (PI), transformation ratio (TR), TOC, shale thickness, and organic matter type. The good risks refer to condition that can be generated the gaseous hydrocarbons as shown in Table 6.9. The poor risk data will be plotted and shown in the yellow hatched area (Figure 6.10A). In cases of the parameters that are plotted in this area, referring to the nonproductive shale gas formation. The productive shale gas has to plot in large enclosed area (light yellow). The Ban Nong Sai and the Dat Yai sections are good for shale gas resource is caused by both larger enclosed areas (Figure 6.10B and 6.10C). The Dat Yai section is higher shale gas production than the Ban Nong Sai section. However, the PI is lower than the good risk criteria indicating less free hydrocarbons were stored in the formations. The lower PI refers to lower S_1 which comparable to S_2 although the S_2 is already too low. Normally, the peak mature to the post mature affected a lower S_2 and higher in S_1 . The S_2 of both sections is low as similar to normal case but the S_1 is contrasted. As the results, the S_1 is mostly generated and then some of them migrated through the porous formation to the available places. The extreme mature of the Dat Yai section is effect to changing in chemical properties of the hydrocarbons is therefore, they are high expulsion. Therefore, low of S_1 indicates less remaining of free hydrocarbons were stored in the formations based on shale gas evaluations.

Table 6.11 The criteria of source rock evaluation show the seven excellent parameters of T_{\max} , vitrinite reflectance (R_o), production index (PI) (Peters and Cassa, 1994; Espitalié and Bordenave, 1993; Bacon et al., 2000), transformation ratio (TR), TOC, thickness (Jarvie et al., 2005; Jarvie et al., 2007), and organic matter type.

Parameters	T_{\max} (°C)	R_o (%)	PI (%)	TR (%)	TOC (%)	Thickness (ft)	Organic matter type
Good risk criteria of gas	450	0.90	0.40	80	2.0	50	Type III



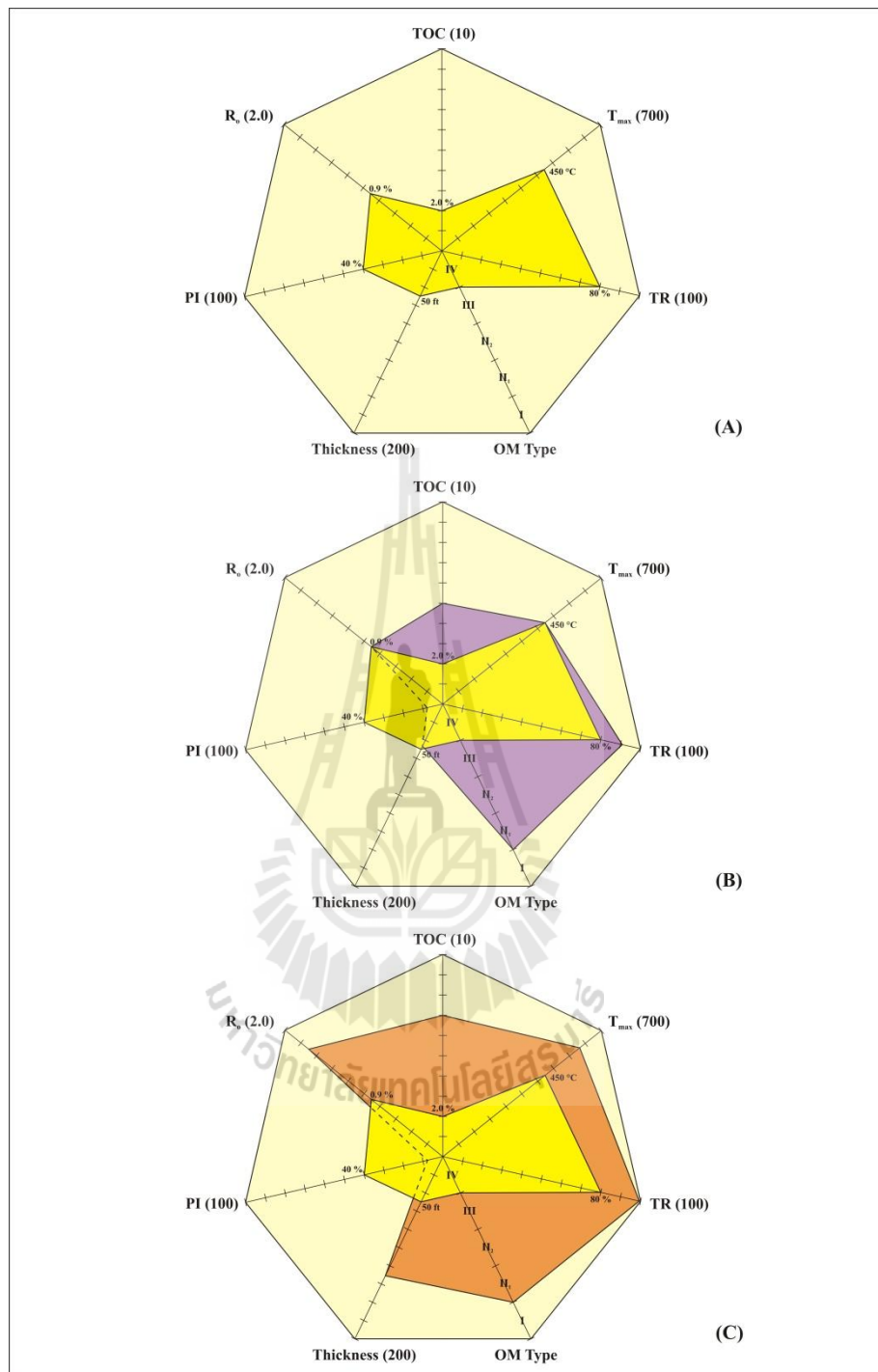


Figure 6.10 Polar shale-gas risk plot with various visual and chemical assessments; (A) Good conditions for comprehensive evaluation (yellow), (B) Polar shale-gas risk plot of the Ban Nong Sai section, (C) Polar shale-gas risk plot of the Dat Yai section.

6.2.2 Reservoir-forming minerals

The studied sections refer to effective reservoir condition of the Huai Hin Lat Formation. The Ban Nong Sai section contains clay and calcite. The Dat Yai section consists mainly of feldspar, dolomite, and clay which the lower section shows the quartz and the calcite is higher than the upper part. The quartz and calcite are high where the quantity of the feldspar, dolomite, and clay are decline. The changes in mineralogical characteristics indicate the change in the sedimentary environment, accommodation space, and tectonic activity within the study area. They are the depositional conditions shifted from carbonate (calcite and dolomite) deposition to clastic deposition (Chalmers et al., 2012). A greater influx of clastic rocks in the lower part is either due to increasing tectonic activity or to reduction in accommodation space as a base-level regression. The carbonate and clay sedimentations are not occurring simultaneously as indicated by strong negative correlation between clay and carbonate (Figure 6.11). Therefore, the mineral appears to be a key factor that characterizing the best condition (Bowker, 2003a, Jarvie et al., 2007).

X-ray diffraction (XRD) is a common method that using to determine the mineral composition of shale. It is important in determining a formation's brittleness or fracability (mechanically-induced fracture development) (Fraser et al., 2011). The brittleness of the shale is more likely to respond to type of stimulation by creating complex fracture network (Clarkson et al., 2012) that providing linkage between the well-bore and the microporosity (Jarvie et al., 2007). The brittle efficiency of the studied sections is performed by total quartz and carbonate (brittle mineral) and total clay percentages. These mineral percentages are recalculated out of

100% and plotted in the ternary diagrams (Figure 6.12). The diagram of the Ban Nong Sai section and Table 5.6 are shown the average effective brittle and clay minerals are 45.87 % and 42.61 % respectively. The diagrams of the Dat Yai section and Table 5.7 are performed the average quantity of average effective brittle and clay minerals are 50.66 % and 23.59 % respectively. Although the quantity of brittle minerals is low however, the summation is higher than clay and/or more than 50 %. As current producing shale gas reservoirs, clay should be less than 50 % and brittle mineral tend to have more than 50 %. They are more brittle and respond well to current stimulation practices (Passey et al., 2010). The information is conformed to Fraser et al. (2011) that published the further information about the quartz component would enhance the study. It has been suggested the detrital quartz is lesser effective (Thyberg et al., 2009) but the biogenic opaline silica is the most effective quartz component for reservoir stimulation (Javie et al., 2007). These biologically deposited siliceous rocks are shown in Figure 5.1. Moreover, the sections are more brittleness and capable of fracturing due to less porous phosphatic bed (Slatt et al., nd) and has very good to excellent total organic content. Therefore, these analyzing strata herein have the potential to host unconventional hydrocarbons under proper burial condition based on mineral-forming reservoir evaluation.

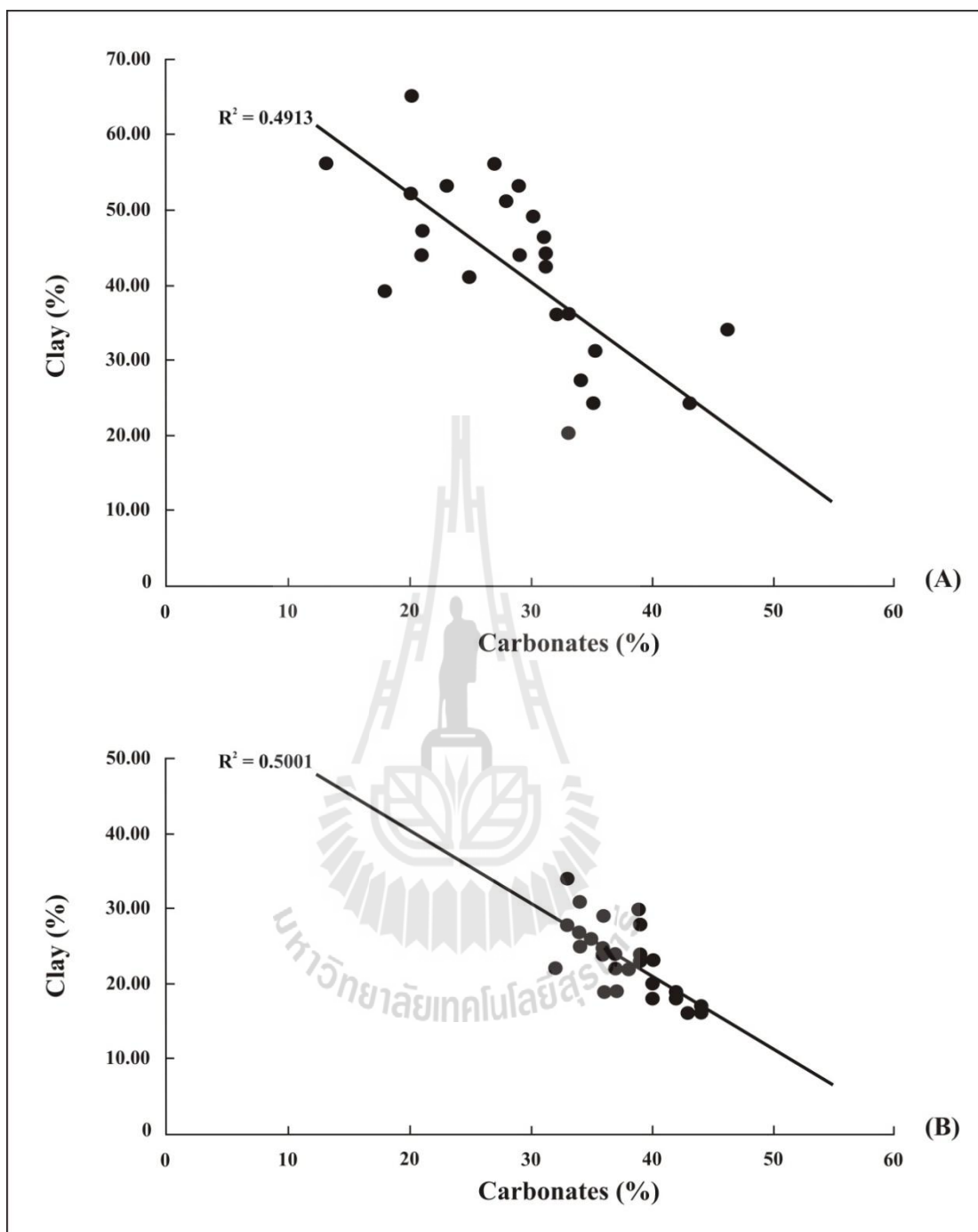


Figure 6.11 The correlation between clay and carbonate minerals as shown a strong relationship of the Ban Nong Sai section (A) and the Dat Yai section (B).

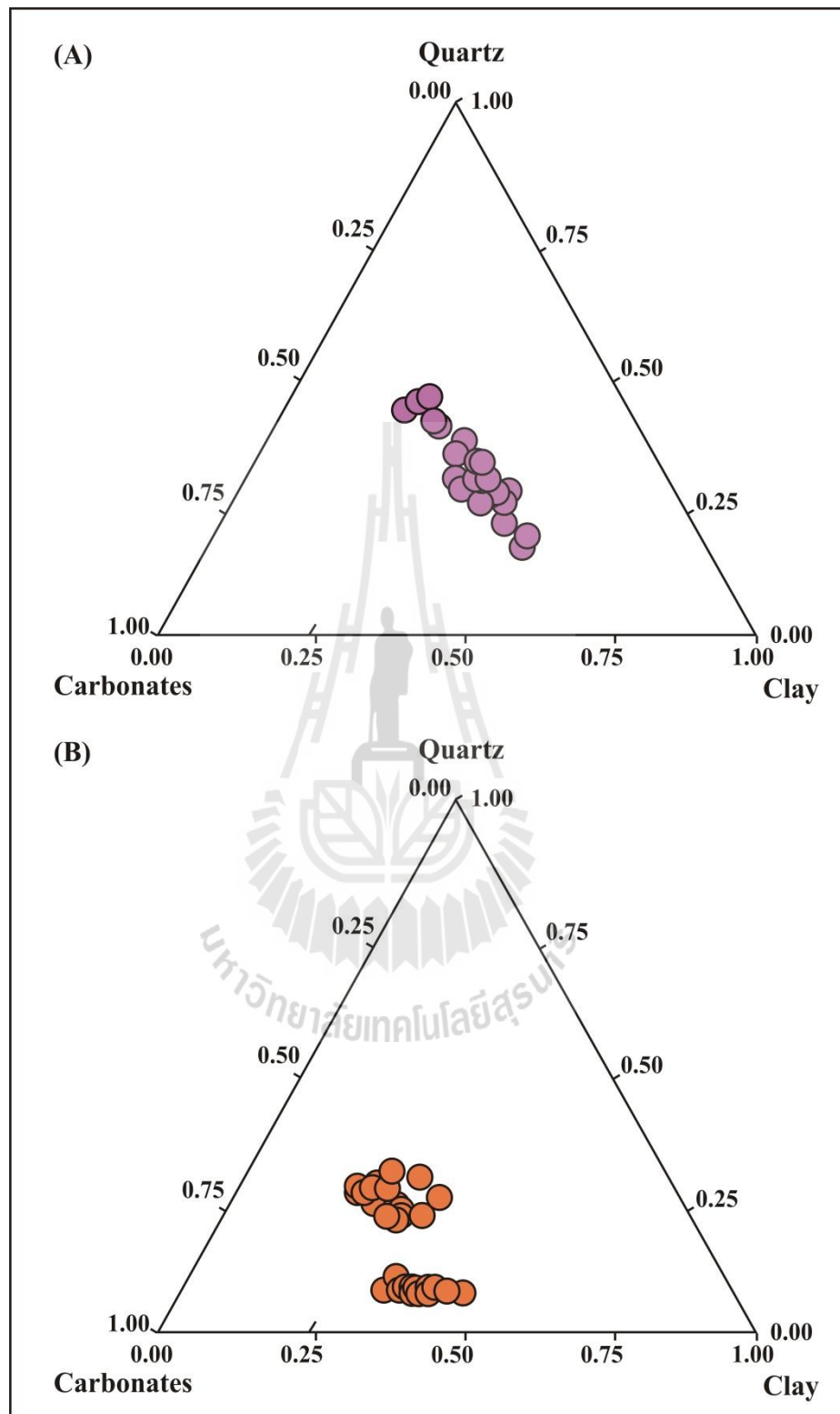


Figure 6.12 Ternary diagrams of quartz, carbonate, and clay minerals of the Ban Nong Sai section (A) and the Dat Yai section (B).

6.2.3 Hydrocarbon storages

6.2.3.1 Micropores

The effects of burial diagenesis through the period of pre- and post-depositions are revealed by the key parameters of R_o , T_{max} , and kerogen transformation ratio. As the results, the mineral-composed matrix is changed and produced micropores in several types. For the micropores, they are an important step toward understanding where gas is stored. It described how it might migrate from the fine-grained sediments into induced fractures which enable production (Loucks et al., 2009). The micropore types can be classified into several types which are related to gas storage capacities and permeability pathways based on their functions. The maximum gaseous hydrocarbon might store in the micropores of in-situ reservoir and the permeability pathways are a function related to gas storages and mobility in its reservoir of microfracture and microchannel-related pores.

1) Gas storage capacity

Gas storage capacity is the maximum gaseous hydrocarbon might content in the keeping storages of in-situ reservoir. These storage pores are formed during sediment depositions but decrease and perform smaller by the effect of cementation. However, the deep subsidence or burial history of the formation may have been altered with process of diagenetic alteration or thermal maturation as the micropores are produced. Which they might be divided into 2 key types of relevant gas storage capacities in both organic and inorganic matter pores as follows:

Organic matter pores incorporate with detritus that is expected for mats are growth on the seafloor (Schieber, 1998; 1999). The research

over several decades has shown that the amounts of organic carbon buried into the geologic record. It was depended on the primary productivity (Aplin and Macquaker, 2011) and redox process. Loucks et al. (2009) suggested during the thermal maturation are affected to the decomposition of organic matter leads to the formation as hydrocarbons. Simultaneously, the pores in in-situ organic matters are produced. The pores were conformably as the explosion in organic matters that cause by the generation of CO₂ or other gasses (methane) under a high voltage electron beam (Slatt et al., nd). Therefore, the storages may have been developed large permeability of migration pathways as the result of high TOC contents and higher thermal maturity.

Inorganic matter pores are affected of the generations and occurrences during syn- and post depositional processes. The minerals of mechanical and chemical stability parameters were generated the micropores in the formation as well. The pores are divided into 2 subtypes as depended on their rock matrix-composed minerals. Phyllosilicate or clay minerals are associated with feldspar and the effect of chemically altered process. As the results, the feldspar is weathered and transformed themselves to clay minerals that supplied to the depositional basin. Normally, clays are easily ductile and compact as during post-deposition of high temperature by deeply burial. The ordinary clays are rearranged and transformed their parallel to other subparallel types. Therefore, intraplatelet pores within clay aggregates are provided more potential storage capacity in this section. Other silica and pyrite minerals are growth during syn- and post-depositional bacterial decomposition of the mats that probably resulted in the formation of anaerobic conditions. Their forms were generated and formed themselves to micropores as might be captured of expelled gas in in-situ reservoir. Although these pores are

probably composed of gas hydrocarbon that are not contributed the more permeability. However, in case of fossil fragment pore types, it is probably connected and aligned forming adequate beds as also may have been provided more permeability.

2) Permeability pathways

Permeability pathways are the term of key elements of the study next to the porosity and their occurrence. The gas behavior in subsurface reservoirs (original places or gas capture storages) can move directly into induced pathways to anywhere which enables production. In fact, the pore characteristics cannot form themselves to permeability pathways except only the microfractures and microchannels related-pores are interconnected.

The SEM micrograph viewings show the aligned and tensional microfractures of mineral crystal structures as depended on matrix-composed minerals. They might be helped initiate microfracture (Slatt et al., nd) that too lengthily narrow and more sufficiency to allow gas from any storage sites migrate through. The gas moved through their fractures to other production zones which a significant effect on hydrocarbon production (Eichhubl and Boles, 1998; Pitman et al., 2001; Clarke, 2007; Gale and Holder, 2010). Moreover, well documents for greater interconnected samples produced a large permeable of natural fractures as probably presented in open microfractures forms. Therefore, they improve and provide more permeability or migration pathways in reservoirs.

6.2.3.2 Porosity network and distribution

Micro (X-ray) computed tomography is the equipment that using to obtain the information of the internal homogeneity. The samples are scanned

with a low resolution in order to obtain an overview of the internal structures. The scanning image analysis is performed on the selected pixels. A number of black pixels are surrounded by white pixels that may identify to pores.

The unconventional shale gas evaluation, the reservoir sections have become more interesting for research. Among these sections is less publication which may focus on the importance of fracture in the tighter reservoir. For better understanding of the pore networks, pore connectivity, and fracture structures are a new approaches of traps and adsorbed storages of the Huai Hin Lat Formation. The meaningful parameters are giving you information about the shale gas reservoirs. The analyzed software was used to serve this purpose to a large extend that is often evaluated the number of pores and pore volume. The software can be distinguished between closed and open pores. The closed pores are fully surrounded on all side by white voxel. The open pores are connecting channels that located inside an object and may connect to the space outside the volume. Total pores can be evaluated to porosity and porosity networks which were threshold and cropped into a bar and cube shape. The pore networks of both sections are illustrated in Figure 5.10 and 5.11 which the pore bodies and pore throats are represented to white spots.

The total porosity and open porosity of the Ban Nong Sai section are range from 6.66 % to 6.94 % and 1.28 % to 1.68 % respectively from the lower to upper section. The Dat Yai section shows the total porosity and open porosity from the lower to upper part are in range of 8.64 % to 14.65 % and 2.04 % to 12.63 %. As the results, the total porosity of both sections is upwardly increasing respectively. These networks are even easier in order to simulate flows through the pore throats or permeability pathways. They refer to the upper part of both sections

are less in healing effects on its carbonate composition. But the lower porosities are more effects that the carbonate may heal the fractures and other pore throats as tighter. Moreover, the lower part is more effects from the deeper that the underlying strata are compressed. As the results, the porosities including open porosities of the lower part are lower than the upper part. These results are conformed to the connectivity density that upwardly increasing both sections.

Pyrite minerals are detected which dispersed in both sections as illustrated in Figure 5.10 and 5.11 of lightly yellow spots. The upper part shows the pyrite is more disperse than the lower part. Although the pyrite is not appeared in table of mineralogic and clay fraction due to its quantitation is lower than the minimum efficiency of XRD equipment. However, its pyrite may respond to the internal and external forces and is easier cracking which increasing the permeable in the reservoir rocks. Its behavior also respond to the effects of hydraulic fracturing while well is developing. The closed pores in both sections are high and may have connection after the hydraulic fracturing processes of well stimulation. The gaseous hydrocarbon can be passed through from individually closed storages to existing, stimulated the open porosities, and accumulation. Therefore, both sections may have high efficiency to store and simulated flow the hydrocarbon through the pores or permeability pathways.

6.2.4 Risk evaluation of reservoir condition data

A risk plot of reservoir rock evaluation shows the physical and chemical properties. It is the simple mean of the various properties that support the hydrocarbon storage conditions to initial economic assessment.

The good reservoir condition depends on gaseous storage capacity, shale (reservoir) thickness, and brittle and clay minerals. The brittle minerals are including the quantity of quartz, calcite, and dolomite minerals as easily responded to fracturing. And the fractures can be detected to a part of porosity. The good risks refer to condition that can be stored the gaseous hydrocarbons as shown criteria values in Table 6.10. The poor risk data will be plotted and shown in the yellow hatched area (Figure 6.13A). The larger and largest enclosed areas indicate the higher and highest shale gas storages. They are substantiating by the polar plots which shown in Figure 6.13B and 6.13C of the Ban Nong Sai section and the Dat Yai section respectively. The Ban Nong Sai section is lesser potential which is comparable to the conditions of the Dat Yai section. Shales of the Ban Nong Sai section contain slightly low brittle minerals but they are relatively good because of their lower clay minerals. The porosities are higher than the criteria value is therefore, still have the storage potential of existing hydrocarbons. The Dat Yai section shows the excellent storage conditions. The brittle minerals are not too high but they are mostly higher than 50 % of the criteria values. The clay minerals are low and others are quite high as quite higher than their criteria values also. Moreover, the lower Dat Yai section of Beds 1-17 (Figure 6.14B) is higher potential than the upper part (Figure 6.14A). However, the porosity of the upper section is showing the high value as indicated the high potential also. For stimulation, the physical properties of reservoir rocks are low compressive strength and density assist the operations are completely. Moreover, the higher brittle minerals of rock-forming minerals are easily produced the fractures following the impacted forces is therefore, occurred in both sections.

Table 6.12 The criteria of reservoir rock evaluation as shown the four excellent parameters of porosity, brittle minerals, clay minerals (Passey et al., 2010), and thickness (Jarvie et al., 2005; Jarvie et al., 2007).

Parameters	Porosity (%)	Brittle minerals (%)	Clay minerals (%)	Thickness (ft)
Good risk criteria of gas	> 4.0	> 50.0	< 50.0	> 50



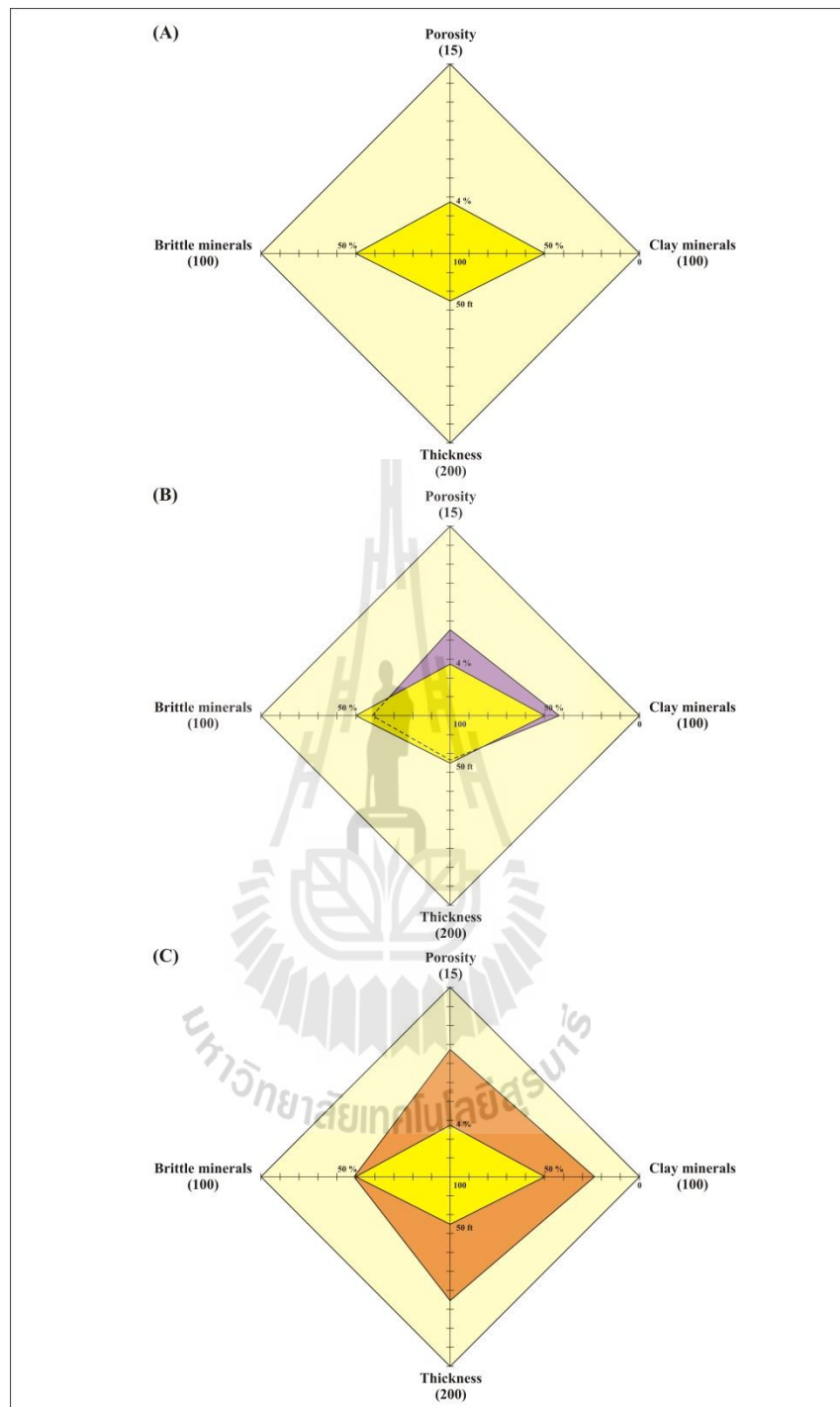


Figure 6.13 Polar shale-gas risk plot with various physical and chemical assessments; (A) Good conditions for comprehensive evaluation (yellow), (B) Polar shale-gas risk plot of the Ban Nong Sai section, (C) Polar shale-gas risk plot of the Dat Yai section.

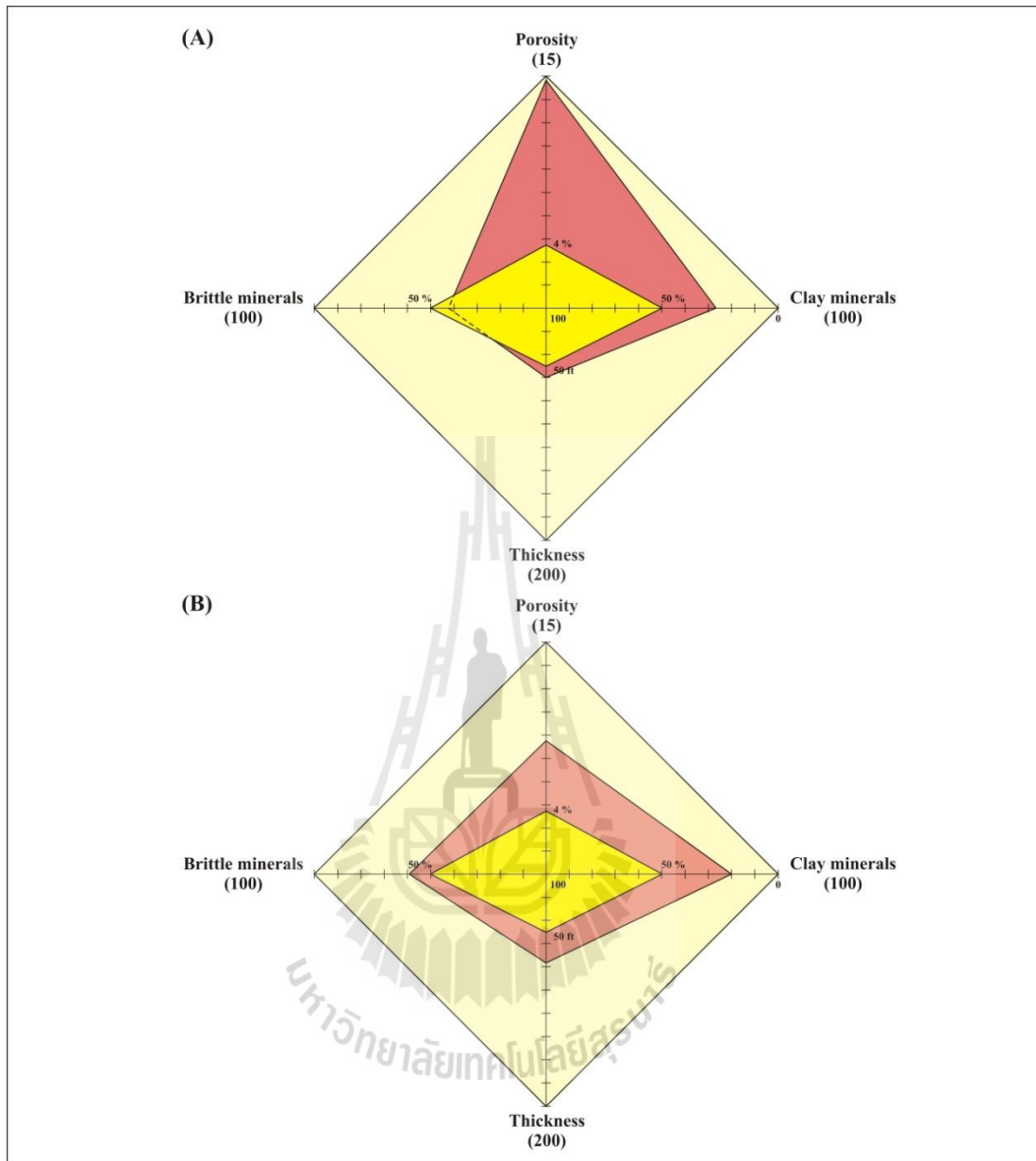


Figure 6.14 Polar shale-gas risk plot of the upper Dat Yai section (A) and the lower Dat Yai section (B).

6.2.5 Zone of shale gas accumulation

The zone of shale gas accumulation is an integration of multiple subsurface data. The multiple subsurface data, e.g., seismic profiles, hydrological condition, and subsurface well data have been integrated to understanding the shale gas intervals where are rich.

The seismic profiles of the studied area are using to interpret their structural geology. The structures controlled the preservation that tectonic movements in the area of shale gas reservoirs probably assisted to increasing of the shale gas accumulation. Fractures formed the important structures of anticline and syncline as complex. The compression and rock extrusion activated the steep fracture and other associated structures also let us understanding its in-situ reservoir information. The hydrological conditions can be referred to the circulation of groundwater that is poor. They are in a closed to semi-closed state which will assist to preserve the shale gas. Lastly, the subsurface well data is obtained the roof and floor conditions that combined with the seismic profiles. Although this study cannot get the entire subsurface data however, the field investigation of the studied areas also gained the precise information.

The roof and floor conditions are closed effect that also conductive to the preservation of shale gas in the reservoir. They are impermeable rocks that can be seal the gas as stored in the in-situ reservoir. According to the Sap Phlu Basin, it is very weathering and not too clearly exposure. The outcrops were studied that are not composed of the clear impermeable rocks. Except limestone of the middle part of the Ban Nong Sai section (Beds 9 and 11) is proper characteristics. It forms the roof and floor conditions for the lower and upper parts of the Ban Nong Sai section

respectively. That the thick sequence of basal conglomerate (Khao E-Dang and Wat Tham Nong Sai sections) may form as the floor condition but the overlying strata are not suitable functions. According to the Na Pho Song Basin, it is excellent preservation that the gypsum beds are shown in the Dat Syo section. The gypsum beds are the suitably impermeable rocks that can be exactly preserved the gas. Their beds are very thin (1.5-2.0 cm) and discontinuous is therefore less potential to preserve the gas. However, the sections are represented the Dat Fa Member is still have more potential especially, the Dat Yai section. It shows the calcareous shale and calcareous mudstone are interbedded intermittently with limestone like a sandwich-like structure. That interval limestone is behaved to the roof and floor conditions as depended on the meaning that will be referred to. The gases of both studied sections are preserved by the roof and floor conditions. But the associated faults in the regional areas can be assisted the formation is fractured and cracked. The fractures can be connected and let the ready gases in migration. Therefore, the roof and floor conditions can be preserved some gases in in-situ reservoir.

6.2.6 Evaluation of unconventional shale gas potential

A variety of unconventional shale gas resource plays and gas types associated with these play exist. High fractured with variable bulk mineralogical composition is controlled the brittle and the ductile nature of the shale (Jarvie et al., 2007). As the results, the shale gas resource plays are high potential in the Ban Nong Sai section and extremely high in the Dat Yai section. They can be composed of the mostly indigenous gas and migrated gas.

According to all parameters of TOC, T_{max} , TR, organic matter type, thickness, PI, R_o , porosity, and percentage of clay and brittle minerals are used to

evaluate the shale gas resource. They exceed the criteria values which conform to the five main features of the U.S. gas shale (Table 6.11) except PI. The PI is too low due to S_2 is too low as well as S_1 . The S_1 should be high in value and accumulated in formation if S_2 is low on high degree of thermal maturation. But S_1 of both sections are still low as probably indicated to free hydrocarbon is less in preservation. Less in preservation is the effects of regional tectonic and not good of roof and floor conditions. That both effects let the available free hydrocarbons were migrated to the secondary reservoirs.

Therefore, shales of both studied sections have a good reservoir conditions but they have a low potential for unconventional gas resources due to low volume of trapped remaining free hydrocarbons.

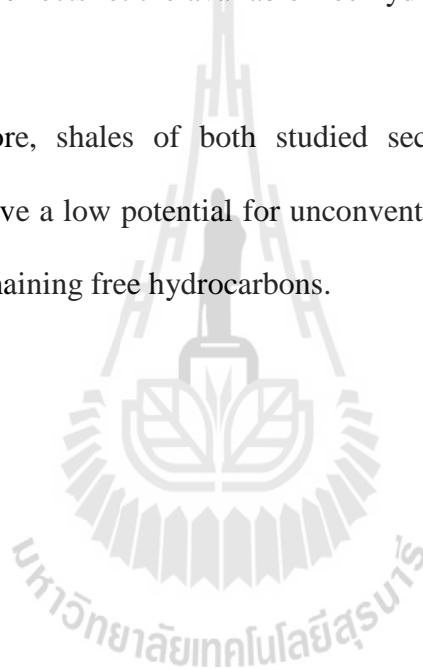


Table 6.13 The main features of the U.S. gas shale (Curtis, 2002).

Basin	Appalachian	Michigan	Illinois	Rich Wentworth	San Juan
Shale name	Ohio	Antrim	New Albany	Barnett	Lewis
Basin type	Piedmont depression	Clarithromycin-pass	Sag basin	Foreland basin	Sag basin
Layer	Devonian	Devonian	Devonian	Carboniferous	Cretaceous
Burial depth(m)	610-1,524	183-730	183-1,494	1,981-2,591	914-1,829
TOC (%)	0.5-4.7	1.0-20.0	1.0-25.0	2.0-7.0	0.45-2.5
Gross thickness (m)	91-305	49	31-122	61-90	152-579
Net thickness (m)	9-31	21-37	15-30	15-61	61-91
R _o (%)	0.4-1.3	0.4-0.6	0.4-1.0	1.1-2.2	1.6-1.88
Total porosity (%)	4.7	9.0	10.0-14.0	4.0-5.0	3.0-5.5
Adsorbed gas content (%)	50	70	40-60	20	60-85

CHAPTER VII

CONCLUSIONS AND RECOMMENDATIONS

7.1 Conclusions

In this study, the potential of petroleum resource is evaluated based on conventional hydrocarbon and unconventional shale gas interpretation. The methods that support the interpretation are composed of field works and laboratory works.

1) The Ban Nong Sai section and the Dat Yai section are selected for detailed study. They are composed mainly of shale and mudstone which were systematically collected for microfossils extraction, geochemical analysis, and physical analysis. Petroleum assessment was performed based on the laboratory results of source rock and reservoir rock properties.

2) The palaeoproductivity and palaeoredox condition of studied sections.

2.1) The Ban Nong Sai section

The studied section shows high peaks in Beds 1, 7, 9, 10, 13, 15-16, and 19 which indicate a high palaeoproductivity. Two relatively lower productivity intervals are present in the middle of the lower part (Bed 3) and the lower Bed 13 of the upper part but they show relatively high TOC. They indicate a high preservation condition which is supported by high values of the palaeoredox proxies. Moreover, Ce/Ce^* and V/Cr are exceed 0.8 and 2.0 respectively which indicate that the section was mainly under anoxic or reducing condition.

2.2) The Dat Yai section

The high palaeoproductivity is present as shown in the high peaks of Beds 3, 9, 12, 14, 20, 16, 17, 22, 27, 30, and 32. The relatively lower palaeoproductivity is shown in Bed 18 of the upper part but it is high in TOC. It indicates a high preservation condition which is corresponded to high values of the palaeoredox proxies. The higher values than 2.07 and 2.0 of $V/(V+Ni)$ and V/Cr respectively also indicate an anoxic condition. Moreover, two relatively higher palaeoproductivity layers but lower TOC are shown in Beds 3 and 27 of the lower and the upper parts respectively which indicate a lower reducing condition.

3) The organic matters of both sections are composed mainly of sapropelic amorphous particles and sapropelic vitrinite which belong to Type I oil prone kerogen. The Ban Nong Sai section and the Dat Yai section show the present-day total organic carbon content (TOC_{pd}) in the range of 1.9-7.1 % and 4.7-10.1 % respectively. The original total organic carbon content (TOC_o) values are ranged from 5.1-10.7 % and 7.8-14.9 % for the Ban Nong Sai and the Dat Yai sections respectively. The thermal maturity of the Ban Nong Sai section and the Dat Yai section are in peak mature and postmature stages respectively based on the R_o , T_{max} , and TR. The generated hydrocarbon quantity can be calculated as 6,309.5 mcf/ac-ft and 10,604.9 mcf/ac-ft for the Ban Nong Sai and the Dat Yai sections respectively based on the quantity of TOC_o , S_{2o} and S_2 .

4) The shale gas assessment based on maximum temperature (T_{max}), vitrinite reflectance (R_o), production index (PI), transformation ratio (TR), TOC, shale thickness, and organic matter type indicates that both the Ban Nong Sai section and the Dat Yai section are good for source potential. The porosity of the shale samples

from the Ban Nong Sai and Dat Yai sections is high ranging from 6.7-6.9 % and 8.6-14.7 % based on the study of micropore types. The good reservoir condition is enhanced by abundant brittle minerals (more than 50 % of the criteria values) and lower clay (less than 50 % of the criteria values). Although shales of both studied sections have good source and reservoir potentials but they have a low potential for unconventional gas resources due to low volume of trapped remaining free hydrocarbons.

7.2 Recommendations

The study of source rock and unconventional shale gas potential of this study is based on a limited available data. More data of geochemical and physical analyses should be obtained for more accurate assessment of source rock and reservoir potentials. Moreover, seismic profiles and well data should be obtained for evaluation of the petroleum potential in the future. The methods used in this study can be applied to evaluate the petroleum potential in other petroliferous formation.

REFERENCES

- Adachi, M., Yamamoto, K., and Sugisaki, R. (1986). Hydrothermal chert and associated siliceous rocks from the northern Pacific: their geological significance and indication of ocean ridge activity. **Sedimentary Geology**. 47: 125-148.
- Agbogun, H.M.D. (2011). Three-Dimensional Measurement of Porosity and Solute-Concentration Distributions during Diffusion in Porous Geologic Media Using X-ray Micro-Computed Tomography. **Doctoral Thesis**, Academic Unit of Earth Sciences, University of New Brunswick, England.
- Algeo, T.J., and Maynard, J.B. (2004). Trace-element behavior and redox facies in core shales of Upper Pennsylvanian Kansas-type cyclothems. **Chem. Geol.** 206: 289-318.
- Alpern, B. (1970). **Classification pétrographique des constituants organiques fossiles des roches sédimentaires**. Revue Institut Français du Pétrole et Annual Combustion Liquid, Paris. 25: 1233-1266.
- Altumi, M.M., Elicki, O., Linnemann, U., Hofmann, M., Sagawe, A., and Gärtner, A. (2013). U–Pb LA-ICP-MS detrital zircon ages from the Cambrian of Al Qarqaf Arch, central-western Libya: Provenance of the West Gondwanan sand sea at the dawn of the early Palaeozoic. **Journal of African Earth Sciences**, 79: 74-97.
- American Clean Skies Foundation, (2008). **U.S. Fuel Goals**. <http://www.cleanskies.org>.

- Aplin, A.C., and Macquaker, H.S. (2011). Mudstone diversity: origin and implications for source, seal, and reservoir properties in petroleum systems. **AAPG Bulletin**. 95(12): 2031-2059.
- Bacon, C.A., Calver, C.R., Boreham, C.J., Leaman, D.E., Morrison, K.C., Revill, A.T. and Volkman, J.K. (2000). The petroleum potential of onshore Tasmania: a review. **Bulletin Geological Survey Tasmania**. 71: 93.
- Barr, S.M., and Charusiri, P. (2011). Volcanic rocks. In: Ridd, M.F., Barber, A.J., Crow, M.J., (eds.). **The Geology of Thailand**. Geological Society of London. pp. 415-439.
- Barr, S.M., and Macdonald, A.S. (1991). Toward a late Paleozoic-early Mesozoic model for Thailand. **Journal of Thai Geosciences**. 1: 11-22.
- Batten, D.J. (1996). Palynofacies and petroleum potential. In: Jansonius J, McGregor D.C., (eds.). **Palynology: Principles and Applications**. American Association of Stratigraphic Palynologists Foundation, Dallas: TX. pp 1065-1084.
- Behar, F., and Vandenbroucke, M. (1987). Chemical modeling of kerogen. **Organic Geochem**. 11: 15-24.
- Behar, F., Beaumont, V., and Penteadó, H.L. (2001). **Rock-Eval 6 Technology: Performances and Developments**. Oil and Gas Science and Technology- Revue de l'Institut Francais du Petrole. 56: 111-134.
- Belaid, A., Krooss, B.M., and Littke, R. (2010). Thermal history and source rock characterization of a Paleozoic section in the Awbari Trough, Murzuq Basin, SW Libya. **Marine and Petroleum Geology**. 27: 612-632.

- Bennett, R.H., O'Brien, N.R., and Hulbert, M.H. (1991). Determinants of clay and shale microfabric signatures: Processes and mechanisms. In: Bennett, R.H., Bryant, W.R., and Hulbert, M.H., (eds.). **Microstructure of fine-grained sediments: From mud to shale**. New York, Springer-Verlag. (nd): 5-32.
- Berger, M.J., Hubbell, J.H., Seltzer, S.M., Chang, J., Coursey, J.S., Sukumar, R., Zucker, D.S., and Olsen, K. (2010). **XCOM: Photon Cross Section Database (version 1.5)**. National Institute of Standards and Technology, Gaithersburg, MD
- Bertrand, S., Charlet, F., Charlier, B., Renson, V. and Fage, N. (2008). Climate variability of southern Chile since the Last Glacial maximum: A continuous sedimentological record from Lago Puyehue (40_S). **Journal of Paleolimnology**. 39: 179-195.
- Bish, D.L., and Reynolds, R.C. (1989). Sample preparation for x-ray diffraction. In: Bish, D.L., and Post, J.E., (eds.). **Modern powder diffraction**. Mineralogical Society of America, Washington, DC. pp. 73-100.
- Bishop, J.K.B. (1988). The barite-opal-organic carbon association in oceanic particulate matter. **Nature**. 332: 341-343.
- Bjørlykke, K. (1974). Depositional history and geochemical composition of epicontinental sediments from the Oslo region. **Nor. Geol. Unders. Arsmelding**, 305: 87-95.
- Blissett, D., Keighley, D., Al, T., and Butlerand, K. (2007). Micro CT Analysis of Porosity and Mineral Phases in Carbonate Reservoirs of Eastern Canada. **Let it Flow, 2007 CSPG CSEG Convention** (pp. 494-495). November, 2007.

- Booth, J.E. (1998). The Khorat plateau of NE Thailand-Exploration history and hydrocarbon potential. **Proceedings of the 1998 SEAPEX Exploration Conference** (pp. 169-203), December 2-3, 1998, Singapore.
- Booth, J., and Sattayarak, N. (2011). Subsurface Carboniferous-Cretaceous geology of NE Thailand. In: Ridd, M.F., Barber, A.J., Crow, M.J., (eds.). **The Geology of Thailand**. Geological Society of London. pp. 185-222.
- Bordenave, M.J. (1993). **Applied Petroleum Geochemistry**, Éditions Technip, Paris. pp. 352.
- Bordenave, M.L., Combaz, A., and Giraud, A. (1970). Influence de l'origine des matieres organiques et de leur degre d'evolution sur les produits de pyrolyse du kerogene. In: Hobson, G.D., and Speers G.C., (eds.). **Advances in organic geochemistry 1966**. pp. 389-405.
- Bordenave, M.L., Espitalié, J., Leplat, P., and Vandenbroucke, M. (1993). Screening techniques for source rock-evaluation. In: Bordenave, M.L., (ed.). **Applied petroleum geochemistry**. Paris, France, Editions Technip. pp. 217-278.
- Bowker, K.A. (2003a). Recent development of the Barnett Shale play, Fort Worth Basin. **West Texas Geological Society Bulletin**. 42(6): 1-11.
- Bowker, K.A. (2007). Barnett Shale gas production, Fort Worth Basin: Issues and discussion, America. **Assoc. Petrol. Geol. Bull.** 91: 523-533.
- Breit, G.N., and Wanty, R.B. (1991). Vanadium accumulation in carbonaceous rocks: A review of geochemical controls during deposition and diagenesis. **Chem. Geol.** 91: 83-97.
- Brumsack, H.J. (1989). Geochemistry of recent TOC-rich sediments from the Gulf of California and the Black Sea. **Geol. Rundsch.** 78: 851-882.

- Bunopas, S. (1981). Palaeogeographic history of Western Thailand and adjacent parts of South-East Asia: A plate-tectonics interpretation. **Doctoral Thesis**. Victoria University of Wellington, Wellington. (Reprinted in 1982 as Geological Survey Division, Department of Mineral Resources, Geological Survey Paper, No. 5, Special Issue. Bangkok).
- Burnham, A.K. (1989). On the validity of the pristane formation index. **Geochimical et Cosmochimica Acta**. 53: 1693-1697.
- Calvert, S.E., and Pedersen, T.F. (1993). Geochemistry of recent oxic and anoxic marine sediments: Implications for the geological record. **Marine Geology**. 113: 67-88.
- Calvert, S.E., and Piper, D.Z. (1984). Geochemistry of ferromanganese nodules: multiple diagenetic metal sources in the deep sea. **Geochimical et Cosmochimica Acta**, 48: 1913-1928.
- Cardott, B.J. (2012). Hartshorne coal rank applied to Arkoma Basin coalbed methane activity. **International Journal of Coal Geology**, Oklahoma, USA.
- Chalmers, G.R., and Bustin, R.M. (2008). Lower Cretaceous gas shales in northeastern British Columbia, Part II: evaluation of regional potential gas resources. **Bulletin of Canadian Petroleum Geology**. 56 (1): 22-61.
- Chalmers, G.R., Bustin, R.M., and Power, I.M. (2012). Characterization of gas shale pore systems by porosimetry, pycnometer, surface area, and field emission scanning electron microscopy/transmission electron microscopy image analyses: Examples from the Barnett, Wordford, Haynesville, Marcellus, and Doig units. **AAPG Bulletin**. 96: 1099-1119.

- Charusiri, P., Clark, A.H., Farrar, E., Archibald, D., and Charusiri, B. (1993). Granite belts in Thailand: Evidence from the $^{40}\text{Ar}/^{39}\text{Ar}$ geochronological and geological syntheses. **Journal of Southeast Asian Earth Sciences**. 8: 127-136.
- Chen, S., Zhu, Y., Wang, H., Liu, H., Wei, W. and Fang, J. (2011). Shale gas reservoir characterization: A typical case in the southern Sichuan Basin of China. **Energy**. 36: 6609-6616.
- Chinoroje, O., and Cole, M. (1995). Permian carbonate in the Dao Ruang-1 exploration well-implication for petroleum potential, Northeast Thailand. **Proceedings of international conference on Geology, Geotechnology, and Mineral Resources of Indochina** (pp. 563-576), Khon Kaen University, Khon Khaen, Thailand.
- Chonglakmani, C. (2011). Triassic. In: Ridd, M.F., Barber, A.J., Crow, M.J., (eds.). **The Geology of Thailand**. Geological Society of London. pp. 137-150.
- Chonglakmani, C., and Sattayarak, N. (1978). Stratigraphy of the Huai Hin Lat Formation (Upper Triassic) in northeastern Thailand. **Third Reg. Conf. on the Geol. and Min. Res. of SE Asia** (pp. 739-762).
- Clarke, R. (2007). Basin focus: Maverick Basin. **Oil and Gas Investor**. 27: 87-90.
- Clarkson, C.R., Jensen, J.L., Pedersen, P.K., and Freeman, M. (2012). Innovation methods for flow-unit and pore-structure analyses in tight siltstone and shale gas reservoir. **AAPG Bulletin**. 96(2): 355-374.
- Clayton, J.L., and Swetland, P.J. (1978). Subaerial weathering of sedimentary organic matter. **Geochimical et Cosmochimical Acta**. 42(2): 305-312.

- Clementz, D.M., Demaison, G.J., and Daly, A.R. (1979). Well site geochemistry by programmed pyrolysis. **Proceedings of the Eleventh Annual Offshore Technology Conference**. 1: 465-470.
- Cobbing, E.T., and Khin, Z. (2011). Metalliferous Minerals. In: Ridd, M.F., Barber, A.J., Crow, M.J., (eds.). **The Geology of Thailand**. Geological Society of London. pp. 459-492.
- Cohen, A.S. (2003). **Paleolimnology: History and Evolution of Lake Systems**. Oxford University Press. pp. 500.
- Cooper, M.A., Herbert, R. and Hill, G.S. (1989). The structural evolution of Triassic intermontane basins in northern Thailand. In: Thanasuthipak, T., and Ounchanum, P., (eds.). **Symposium on Intermontane Basins; Geology and Resources** (pp. 231-242). Chiang Mai University, Chiang Mai, Thailand.
- Core Laboratories. (1993). **Applications of organic geochemistry**. Western Atlas International Company. pp. 154
- Crusius, J., and Thomson, J. (2000). Comparative behavior of authigenic Re, Mo and U during reoxidation and subsequent long-term burial in marine sediments. **Geochimical et Cosmochimica Acta**. 64: 2233-2243.
- Curtis, J.B. (2002). Fractured shale-gas systems. **AAPG Bulletin**. 86(11): 1921-1938.
- Curtis, J.B. (2009). Shale gas: from onerous child to premier resource. **The Research Partnership to Secure Energy for America (RPSEA) Mid-Continent Gas Shales Forum**, June 4, 2009, Chicago, Illinois, America.
- Dai, H.M., Huang, D., Liu, X.M., Yang, Y., He, X.M., and Peng, H.R. (2008). **Natural Gas Geoscience**. 19(4):503-508.

- Daskaladis, K.D., and Helz, G.R. (1993). The solubility of sphalerite in sulfidic solutions at 25 °C and 1 atm pressure. **Geochimical et Cosmochimica Acta**. 57: 4923-4931.
- Davis, A. (1984). Coal petrology and petrographic analysis. In: Ward, C.R., (ed.). **Coal Geology and Coal Technology**. Blackwell Scientific Publications. pp. 74-112.
- Dewhurst, D.N., Yang, Y., and Aplin, A.C. (1999). Permeability and fluid flow in natural mudstones. In: Aplin, A.C., Fleet, A.J., and Macquaque, J.H.S., (eds.). **Muds and mudstones: Physical and fluid flow properties**. Geological Society (London) Special Publication. 158: 23-43.
- Dill, H. (1986). Metallogenesis of early Palaeozoic graptolite shales from the Graefenthal Horst (northern Bavaria-Federal Republic of Germany). **Econ. Geol.** 81: 889-903.
- Dill, H., Teschner, M., and Wehner, H. (1988). Petrography, inorganic and organic geochemistry of Lower Permian carbonaceous fan sequences (Brandschiefer Series)-Federal Republic of Germany: Constraints to their palaeogeography and assessment of their source rock potential. **Chem. Geol.** 67: 307-325.
- DMF (2014). <http://www.dmf.go.th/index.php?act=epsummary&sec=concession>
- DMR (2007). <http://www.dmr.go.th/download/pdf/NorthEast/korat.pdf>.
- DMR (2008). http://www.dmr.go.th/ewtadmin/ewt/dmr_web.
- DMR. (2012). Huai Hin Lat Stratigraphy. Unpublished report. pp. 63.
- Dunham, R.J. (1962). Classification of carbonate rocks according to depositional texture. In: Ham, W.E., (ed.). Classification of carbonate rocks. **AAPG Memoir**. 1: 108-171.

- Durand, B. (1993). Composition and structure of organic matter in immature sediments. In: Bordenave, M.L., (ed.). **Applied Petroleum Geochemistry**, Paris. pp. 77-100.
- Dymond, J., Suess, E., and Lyle, M. (1992). Barium in deep-sea sediments: A geochemical proxy for paleoproductivity. **Paleoceanography**. 7: 163-181.
- EIA (Energy Information Administration), (1999). **Natural Gas 1998: Issues and Trends**. http://www.eia.doe.gov/pub/oil_gas/natural_gas/analysis_publications/natural_gas_1998_issues_trends/pdf/it98.pdf.
- EIA (Energy Information Administration), (2007). **International Energy Outlook 2007: Natural Gas**. [http://tonto.eia.doe.gov/FTPROOT/forecasting/0484-\(2007\).pdf](http://tonto.eia.doe.gov/FTPROOT/forecasting/0484-(2007).pdf).
- EIA (Energy Information Administration), (2008). **Annual Energy Outlook 2008 with Projections to 2030**. [http://www.eia.doe.gov/oiaf/aeo/pdf/0383\(2008\).pdf](http://www.eia.doe.gov/oiaf/aeo/pdf/0383(2008).pdf).
- Eichhubl, P., and Boles, J. R. (1998). Vein formation in relation to burial diagenesis in the Miocene Monterey Formation, Arroyo Burro Beach, Santa Barbara, California. In: Eichhubl, P., (eds.). **Diagenesis, deformation, and fluid flow in the Miocene Monterey Formation**. Pacific Section SEPM Special Publication, 83: 15-36.
- Embry, A.F., and Klovan, J.E. (1971). A Late Devonian reef tract on Northeastern Banks Island. **Canadian Petroleum Geology Bulletin**. 19: 730-781.
- EPA (Environmental Protection Agency), (2012). **2012 Inventory of U.S. Greenhouse Gas Emissions and Sinks**. U.S. Environmental Protection Agency: Washington, DC.

- Ernst, T.W. (1970). *Geochemical Facies Analysis*. **Amsterdam**, Elsevier. 152 p.
- Espitalié, J., and Bordenave, M.L. (1993). Rock eval pyrolysis. In: Bordenave, M.L., (ed.). **Applied petroleum geochemistry**. 2: 237-272.
- Espitalié, J., Deroo, G., and Marquis, F. (1985). **Rock Eval Pyrolysis and Its Applications**. Preprint; Institut Francais du Petrole, Geologie. 40: 563-579.
- Espitalié, J., Laporte, J.L., Madec, M., Marquis, F., Leplat, P., Paulet, J. and Boutefeu, A. (1977). **Methode rapide de caracterization des roches meres, de leur potential petrolier et de leur degre d'evolution**. Rev. Inst. Franc. du Petr., 32. pp. 23-45.
- Espitalié, J., Madec, M., Tissot, B., Mennig, J.J., and Leplat, P. (1977). Source rock characterization method for exploration. **Proceedings of the Ninth Annual Offshore Technology Conference** (vol. 3, pp. 439-444).
- Espitalié, J., Marquis, F., and Borsony, I. (1984). Geochemical logging. In: Voorhees, K.J., (ed.). **Analytical pyrolysis**, London, Butterworth Co., Ltd. pp. 276-304.
- Espitalié, J., Senga Makada, F., and Trichet, J. (1984). Geochemical logging. In: Butterworth, B. and Co (Publisher). (eds.). **Analytical pyrolysis**. pp. 276-304.
- Esso International Report Non Sung-1, (1985). Geological Completion report, well Non Sung-1. **Internal report on file with Department of Mineral Fuels, Bangkok** (unpublished).
- Fishman, N.S., Hackley, P.C., Lowers, H.A., Hill, R.J., Egenhoff, S.O., Eberl, D.D., and Blum, A.E. (2012). The nature of porosity in organic-rich mudstones of the Upper Jurassic Kimmeridge Clay Formation, North Sea, offshore United Kingdom. **International Journal of Coal Geology**. 19: np.

- Fowler, M., Snowdon, L., and Stasiuk, V. (2005). Applying petroleum geochemistry to hydrocarbon exploration and exploitation. **American Association of Petroleum Geologists Short Course Notes**. June 18-19, 2005, Calgary, Alberta. 224 p.
- Fraser, T.A., Allen, T.L., Lane, L.S., and Reyes, J.C. (2011). Shale gas potential of Devonian shale in north Yukon: Results from a diamond drillhole study in western Richardson Mountains. In: MacFarlane, K.E., and Sack, P.J., (eds.). **Yukon Geological Survey**. pp. 45-74.
- Gale, J.F.W., and Holder, J. (2010). Natural fractures in some U.S. shales and their importance for gas production. **Petroleum Geology Conference Series 7**. (nd): 1131-1140.
- Gehman, H.M. (1962). Organic matter in limestones. **Geochimical et Cosmochimica Acta**. 26: 885-897.
- German, C.R., and Elderfield, H. (1990). Application of the Ce anomaly as a paleoredox indicator: the ground rules. **Paleoceanography**. 5: 823-833.
- Gingele, F., and Dahmke, A. (1994). Discrete barite particles and barium as tracers of paleoproductivity in South Atlantic sediments. **Paleoceanography**. 9: 151-168.
- Giraud, A. (1970). Application of pyrolysis and gas chromatography to the geochemical characterization of kerogen in sedimentary rocks. **Bull. Amer. Assoc. Petrol. Geol.** 54: 439-455.
- Gransch, J.A., and Eisma, E. (1970). Characterisation of the insoluble organic matter of sediments by pyrolysis. In: Hobson, G.D., and Speers G.C., (eds.). **Advances in organic geochemistry 1966**. pp. 407-426.

- Grosjean, E., Adam, P., Connan, P., and Albrecht, P. (2004). Effects of weathering on nickel and vanadyl porphyrins of a Lower Toarcian shale of the Paris basin. **Geochimical et Cosmochimica Acta**. 68: 789-804.
- Ground Water Protection Council, (2009). **Modern Shale Gas Development in the United States: A Primer**. Oklahoma, America. 96 p.
- Gupta L.P., and Kawahata, H. (2006). Downcore diagenetic changes in organic matter and implications for paleoproductivity estimates. **Global and Planetary Change**. 53: 122-136.
- Haile, N.S. (1973). Note on Triassic fossil pollen from Nam Pha Formation, Chulabhon (Nam Phrom) Dam, Thailand. **GST Newsletter**. 6(1): 15-16.
- Hallam, A. (1980). Black shales. **Journal of the Geological Society of London**. 137: 123-124.
- Hallberg, R. O. (1976). A geochemical method for investigation of palaeoredox conditions in sediments. **Ambio, Spec. Rep.** 4: 139-147.
- Hallberg, R.O. (1982). Diagenetic and environmental effects on heavy-metal distribution in sediments: A hypothesis with an illustration from the Baltic Sea. In: Fanning, K. A., Manheim, F. T., (eds.). **The Dynamic Environment of the Ocean Floor**. Lexington, Lexington Books. pp. 305-316.
- Hill, R.J., Zhang, E., Katz, B.J., and Tang, Y. (2007). Modeling of gas generation from the Barnett Shale, Fort Worth Basin, Texas. **AAPG Bulletin**. 91(4): 501-521.
- Hower, J.C., and Davis, A. (1981). Vitrinite reflectance anisotropy as a tectonic fabric element. **Geology**. 9: 165-168.

- Huerta-Diaz, M.A., and Morse, J.W. (1990). A quantitative method for determination of trace metal concentrations in sedimentary pyrite. **Mar. Chem.** 29: 119-144.
- Huerta-Diaz, M.A., and Morse, J.W. (1992). Pyritisation of trace metals in anoxic marine sediments. **Geochimical et Cosmochimica Acta**, 56: 2681-2702.
- Hunt, J.M. (1996). Petroleum geochemistry and geology. New York, Second Edition. 743 p.
- Independent Petroleum Association of Mountain States (IPAMS), (2008). America's independent natural gas producers. **Producing Today's Clean Energy, Ensuring Tomorrow's Innovation.** <http://www.ipams.org/media/docs/Callupdraft10.pdf>.
- International Committee for Coal Petrology (ICCP), (1971). **International Handbook of Coal Petrography, 1st Supplement to 2nd Edition.** CNRS, Paris.
- Iwai, J., Asama, K., Veeraburus, M., and Hongnusunthi, A. (1966). Stratigraphy of the so-called Khorat Series and a note on the fossil planbearing Paleozoic strata in Thailand: Japan. **Journal of Geol. Geogr.** 37(1): 21-38.
- James, R., Cumming, G. V., Mutsamai, S., and Lunwongsa, W. (2008). Tectonic setting of the Chatree epithermal gold-silver deposit, Loei fold belt, Petchabun Province, Central Thailand (abs.). **International Conference on the Tectonic of Northwestern Thailand** (pp. 14-15), 2008, Chiang Mai, Thailand.

- Jarvie, D.M. (2012). Shale resource systems for oil and gas: part 1-shale-gas resource systems. In: Breyer, J. A., (ed.). **Shale reservoirs-giant resources for the 21st century**, AAPG Memoir. 97: 69-87.
- Jarvie, D.M., and Lundell, L.L. (2001). Amount, type, and kinetics of thermal transformation of organic matter in the Miocene Monterey Formation. In: Isaacs, C. M., and Rullkotter, J., (eds.). **The Monterey Formation: From rocks to molecules**. New York. Columbia University Press. chapter 15. pp. 268-295.
- Jarvie, D.M., Claxton, B.L., Henk, F., and Breyer, J.T. (2001). Oil and shale gas from the Barnett Shale, Fort Worth Basin, Texas. **AAPG Annual Meeting Program**. 10: A100.
- Jarvie, D.M., Hill, R.J., and Pollastro, R.M. (2005). Assessment of the gas potential and yields from shales: The Barnett Shale model. In: Cardott, B., (ed.). **Oklahoma Geological Survey Circular 110, Unconventional Gas of the Southern Mid-Continent Symposium**, March 9-10, 2005, Oklahoma City, Oklahoma. pp. 37-50.
- Jarvie, D.M., Hill, R.J., Pollastro, R.M., Wavrek, D.A., Bowker, K.A., Claxton, B.L., and Tobey, M.H. (2003). Evaluation of unconventional natural gas prospects: The Barnett Shale fractured shale gas model (abs.). **21st International Meeting on Organic Geochemistry** (Book of Abstracts, Part II, pp. 3-4), September 8-12, 2003, Krakow, Poland.

- Jarvie, D.M., Hill, R.J., Pollastro, R.M., Wavrek, D.A., Bowker, K.A., Claxton, B.L., and Tobey, M.H. (2004). Geochemical characterization of thermogenic gas and oil in the FortWorth Basin, Texas (abs.). **AAPG Annual Meeting Program**. 13: A71.
- Jarvie, D.M., Hill, R.J., Ruble, T.E., and Pollastro, R.M. (2007). Unconventional shale-gas systems: the Mississippian Barnett Shale of north-central Texas as one model for thermogenic shale-gas assessment. **AAPG Bulletin**. 91: 475-499.
- Jeandel, C., Tachikawa, K., Bory, A., and Dehairs, F. (2000). Biogenic barium in suspended and trapped material as a tracer of export production in tropical NE Atlantic (EUMELI sites). **Mar. Chem.** 71: 125-142.
- Johannes, I., Kruusement, K., Veski, R., Bojesen-Koefoed J.A. (2006). Characterisation of pyrolysis kinetic by rock-Eval basic data. **Oil Shale**, Estonian Academy Publishers. 23(3): 249-257.
- Jones, B., and Manning, D.A.C. (1994). Comparison of geochemical indices used for the interpretation of palaeoredox conditions in ancient mudstones. **Chemical Geology**. 111: 111-129.
- Kakuwa, Y., and Matsumoto, R. (2006). Ceriumnegative anomaly just before the Permian and Triassic boundary event-the upward expansion of anoxia in the water column. **Palaeogeography Palaeoclimatology Paleoecology**. 229: 335-344.

- Kamvong, T., and Khin, Z. (2009). The origin and evolution of skarn-forming fluids from the Phu Lon deposit, northern Loei fold belt, Thailand: Evidence from fluid inclusion and sulphur isotope studies. **Journal of Asian Earth Sciences**. 34: 624-633.
- Khashayar, T., (2010). Application of Rock-Eval6 in Detection Seepage of Yortshah Gas Storage. **World Applied Sciences Journal**. 8 (10): 1193-1199.
- Khositchisri, W.R. (2012). Petroleum geochemistry of Huai Hin Lat Formation in Ampoe Nam Nao, Changwat Petchabun and Ampoe Chumpae, Changwat Khon Kaen, Thailand. **Master Thesis**, Chulalongkorn University, Thailand (unpublished). 127 p.
- Ko, T. (2010). Characterization of gas generated by sequential hydrous pyrolysis of potential gas-prone source rocks for tight-gas reservoir in the Rocky Mountain area. **Master Thesis**. Colorado School of Mines, America.
- Kobayashi, T., and Tokuyama, A. (1959). The Halobiidae from Thailand. **Journal of the Faculty of Science, University of Tokyo, Sect. 2**. 1291: 27-30.
- Kobayasi, T. (1973). Upper Triassic estheriids in Thailand and the conchostracan development in Asia in Mesozoic Era. **Geology and Palaeontology of Southeast Asia**. 16: 57-90.
- Kon'no, E., and Asama, K. (1973). Mesozoic plants from Khorat, Thailand. **Geology and Palaeontology of Southeast Asia**. Tokyo University Press. 12: 149-172.
- Krecji-Graf, K. (1975). Geochemical facies of sediments. **Soil Sci**. 119: 20-23.
- Krinalley, D.H., and Doornkamp, J.C. (1973). **Atlas of Quartz Grain Surface Textures**. Cambridge University Press. Cambridge. 91 p.

- Krokstad, W., Schou, L., Leith, L.T., Vigran, J.O., Due, A., Rendall, H., Andersen, W., Berg, T., Haugen, G., and Vinge, T. (1986). **Source rock evaluation of well 15/12-4, hydrocarbon characterization of oil, cuttings and cores.** Report, IKU Sintkf-Oruppkn. 399 p.
- Kuchinskiy, V., Gentry, K., and Hill, R. (2012). Source Rock Evaluation Technique: A Probabilistic Approach for Determining Hydrocarbon Generation Potential and In-Place Volume for Shale Plays (abstract and presentation). **AAPG Annual Convention and Exhibition**, April 22-25, 2012, Long Beach, California, America.
- Levine, J.R., and Davis, A. (1989). Reflectance anisotropy of Upper Carboniferous coals in the Appalachian foreland basin, Pennsylvania, USA. **International Journal of Coal Geology**. 13: 341-373.
- Levine, J.R., and Davis, A. (1990). Reflectance anisotropy of Carboniferous coals in the Appalachian Foreland Basin, Pennsylvania, U.S.A. **International Journal of Coal Geology**. 16: 201-204.
- Lewan, M.D. (1984). Factors controlling the proportionality of vanadium to nickel in crude oils. **Geochimical et Cosmochimica Acta** 48: 2231-2238.
- Lewan, M.D., and Maynard, J.B. (1982). Factors controlling the enrichment of vanadium and nickel in the bitumen of organic sedimentary rocks. **Geochimical et Cosmochimica Acta**. 46: 2547-2560.
- Lewis, D., and McConchie, D. (1937). **Analytical Sedimentology**. New York, America. 197 p.
- Leythaeuser, D. (1973). Effects of weathering on organic matter in shales. **Geochimical et Cosmochimical Acta**. 37: 113-120.

- Li, H., Zhai, M., Zhang, L., Zhou, Y., Yang, Z., He, J., Liang, J., and Zhou, L. (2013). The Distribution and Composition Characteristics of Siliceous Rocks from Qinzhou Bay-Hangzhou Bay Joint Belt, South China: Constraint on the Tectonic Evolution of Plates in South China. **Scientific World Journal**. 2013: 25.
- Lima, I., Oliveira, M., Da Rocha, P., and Lopes, R.T. (nd). **Characterization of porous reservoir rock systems through Micro-CT**. Published report.
- Liu, L., Zhang, A., Chen, D., Yang, J., Luo, J., and Wang, C. (2007). Implications Based on LA-ICP-MS Zircon U-Pb Ages of Eclogite and Its Country Rock from Jianggalesayi Area, Altyn Tagh, China. **Journal of Earth Science Frontiers**. 14(1): 98-107.
- Lopatin, N.V., Zubairae, S.L., Kos, I.M., Emets, T.P., Romanov, E.A., and Malchikhina, O.V. (2003). Unconventional oil accumulations in the Upper Jurassic Bazhenov black shale formation, West Siberian Basin: a self-sourced reservoir system. **Journal of Petroleum Geology**. 26(2): 225-244.
- Loucks, R.G., and Ruppel, S.C. (2007). Mississippian Barnett Shale: lithofacies and depositional setting of a deep-water shale-gas succession in the Fort Worth Basin, Texas. **AAPG Bulletin**. 91(4): 579-601.
- Loucks, R.G., Reed, R.M., Ruppel, S.C., and Hammes, U. (2012). Spectrum of pore types and networks in mudrocks and a descriptive classification for matrix-related mudrock pores. **American Association of Petroleum Geologist Bulletin**. 96: 1071-1098.

- Loucks, R.G., Reed, R.M., Ruppel, S.C., and Jarvie, D.M. (2009). Morphology, genesis, and distribution of nanometer-scale pore in siliceous mudstones of the Mississippian Barnett Shale. **Journal of Sedimentary Research** 79: 848-861.
- Love, L.G. (1962). Pyrite spheres in sediments. In: Jensen, M.L., (ed.). **Biogeochemistry of sulfur isotopes**. New Haven, Connecticut, Yale University, N.S.F. Symposium. pp. 121-143.
- Mackenzie, F.T., Ver, L.M., Sabine, C., Lane, M., and Lerman, A. (1993). C, N, P, S global biogeochemical cycles and modelling of global change. In: Wollast, R., Mackenzie, F.T., Chou, L., (eds.). **Interactions of C, N, P, and S, Biogeochemical Cycles and Global Changes**. NATO ASI series, 4: 1-61.
- Martini, A.M., Walter, L.M., Ku, T.C.W., Budai, J.M., McIntosh, J.C., and Schoell, M. (2003). Microbial production and modification of gases in sedimentary basins: a geochemical case study from a Devonian shale gas play, Michigan Basin. **AAPG Bulletin**. 87(8): 1355-1375.
- Martin-Puertas, C., Valero-Garces, B.L., Mata, M.P., Moreno, A., and Giralt, S., Martinez-Ruiz, F., and Jimenez-Espejo, F. (2011). Geochemical process in a Mediterinian Lake: a high-rezolution study of the last 4,000 years in Zonar Lake, southern Spain. **Journal of Paleolimnol**, 46: 405-421.
- Matchette-Downes, C. (2009). **Guide to optical microscopy in petroleum geochemistry**, Report, MDOIL Limited, England.
- McCarthy, K., Rojas, K., Niemann, M., Palmowski, D., Peters, K., and Stankiewicz, A. (2011). Basic Petroleum Geochemistry for Source Rock Evaluation. **Oilfield Review Summer 2011**. Schlumberger. 23(2): 31-43.

- McCarthy, M., Beaupre, S. R., Walker, B. D., Voparil, I., Guilderson, T. P., and Druffel, E. R. M. (2011). **Chemosynthetic origin of ^{14}C -depleted dissolved organic matter in a ridge-flank hydrothermal system.** *Nat Geosci.* Vol. 4. (pp. 32-36).
- McManus, J., Berelson, W.M., Klinkhammer, G.P., Hammond, D.E. and Holm, C. (2005). Authigenic uranium: relationship to oxygen penetration depth and organic carbon rain. ***Geochimical et Cosmochimica Acta.*** 69: 95-108.
- Mees, F., Swennen, R., Van Geet, M., and Jacobs, P. (2003). Applications of X-ray Computed Tomography in the Geosciences. **Geological Society**, London, Special Publication. 215: 243.
- Meesook, A., and Saengsrichan, W. (2011). Jurassic. In: Ridd, M.F., Barber, A.J., Crow, M.J., (eds.). **The Geology of Thailand.** Geological Society of London. pp. 151-168.
- Mendonça Filho, J.G., Menezes, T.R., and Mendonça, J.O. (2011c). Organic composition (palynofacies analysis). **ICCP Training Course on Dispersed Organic Matter.** 33-81.
- Metacafe, I. (1984). **Stratigraphy, palaeontology and palaeogeography of the Carboniferous of Souttheast Asia.** *Memories de la Societe Geologique de France.* 147: 107-118.
- Meyers, P.A. (1997). Organic geochemical proxies of paleoceanographic, paleolimnologic and paleoclimatic processes. ***Organic Geochemistry.*** 27: 213-250.

- Meyers, S.R., Sageman, B.B., and Lyons, T.W. (2005). Organic carbon burial rate and the molybdenum proxy: Theoretical framework and application to Cenomanian-Turonian oceanic event 2. **Paleoceanography** 20: 2002.
- Miles, A.J. (1994). Glossary of terms applicable to the petroleum system. In: Magoon, L.B., Dow, W.G., (eds.). *The Petroleum System-From Source to Trap*: **AAPG Memoir**. 60: 643-644.
- Monnin, C., Jeandel, C., Cattaldo, T., and Dehairs, F. (1999). The marine barite saturation state of the world's oceans. **Mar. Chem.**, 65: 253-261.
- Montgomery, S.L., Jarvie, D.M., Bowker, K.A., Pollastro, R.M. (2005). Mississippian Barnett Shale, Fort Worth basin, north-central Texas: gas-shale play with multi-trillion cubic foot potential. **AAPG Bulletin**. 89(2): 155-175.
- Morford, J.L., and Emerson, S. (1999). The geochemistry of redox sensitive trace metals in sediments. **Geochimical et Cosmochimica Acta**. 63: 1735-1750.
- Morse, J.W., and Luther, G.W. (1999). Chemical influences on trace metalsulfide interactions in anoxic sediments. **Geochimical et Cosmochimica Acta**. 62: 3373-3378.
- Mouret, C., Heggemann, H., Gouadain, J., and Krisadasima, S. (1993). Geological history of the siliciclastic Mesozoic strata of the Khorat Group in the Phu Phan Range area, Northern Thailand. **Proceedings of the International symposium on Biostratigraphy of mainland Southeast Asia: Facies and Palaeontology** (vol. 1, pp. 23-31). Chiang Mai, Thailand.

- Murray, R.W., and Leinen, M. (1993). Chemical transport to the seafloor of the equatorial Pacific Ocean across a latitudinal transect at 135 °W: Tracking sedimentary major, trace, and rare earth element fluxes at the Equator and the Intertropical Convergence Zone. **Geochimical et Cosmochimica Acta**. 57: 4141-4163.
- Navigant Consulting, (2008). **North American Natural Gas Supply Assessment**. American Clean Skies Foundation.
- Nelson, D.R. (2001). An assessment of the determination of depositional ages for Precambrian clastic sedimentary rocks by U-Pb dating of detrital zircon. **Sed. Geol.** 141-142: 37-60.
- Nixon, W.C. (1969). **Scanning electron microscopy; Contemporary Physics**. 10: 71-69.
- Norrish, K., and Hutton, J.T. (1969). An accurate X-ray spectrographic method for the analysis of a wide range of geological samples. **Geochim. Cosmochim. Acta**. 33: 431-454.
- O'Brien , N.R. (1971). Fabric of kaolinite and illite floccules. **Clays and Clay Minerals**. 19: 353-359
- O'Brien, N.R. (1972). Microstructure of a laboratory sedimented flocculated illitic sediment. **Canadian Geotechnical Journal**. 9: 120-122
- Paltsev, S., O'Sullivan, F., and Ejaz, Q. (2013). Shale gas in China. Shale gas in China: Can we expect a revolution?. **GTAP Conference on Global Economic Analysis in Shanghai** (pp. 1-18), June 12-14, 2013, China.

- Pashin, J.C. (2008). Coal as petroleum source rock and reservoir rock. In: Ruiz, I. S., Crelling, J. C., (eds.). **Applied Coal Petrology-The Role of Petrology in Coal Utilization**. Elsevier, Amsterdam. pp. 227-262.
- Passey, Q.R., Bohacs, K.M., Esch, W.L., Klimentidis, R., and Sinha, S. (2010). From oil-prone source rock to gas-producing shale reservoir-Geologic and petrophysical characterization of unconventional shale gas reservoirs. **Proceeding of the North American Unconventional Gas Conference and Exhibition, Society of Petroleum Engineers (SPE Paper)**. 131350: 29.
- Patterson, J.H., Ramsden, A.R. and Dale, L.S. and Fardy, J.J. (1986). Geochemistry and mineralogical residences of trace elements in oil shales from Julia Creek, Queensland, Australia. **Chem. Geol.** 55: 1-16.
- Paytan, A., and Kastner, M. (1996). Benthic Ba fluxes in the central Equatorial Pacific, implications for the oceanic Ba cycle. **Earth Planet. Sci. Lett.** 142: 439-450.
- Paytan, A., Cade-Menun, B.J., McLaughlin, K., and Faul, K.L. (2003). Selective phosphorus regeneration on sinking marine particles: evidence from ³¹P-NMR. **Mar. Chem.** 82: 55-70.
- Paytan, A., Moore, W.S., and Kastner, M. (1996). Sedimentation rate as determined by ²²⁶Ra activity in marine barite. **Geochim. Cosmochim. Acta.** 60: 4313-4319.
- Pelet, R. (1985). **Evaluation quantitative des produits formes lors de l'evolution geochimique de la matiere organique**. Revue Institut Franc,ais du Petrole'. 40(5): 551-562.

- Peters, K.E. (1986). Guidelines for evaluating petroleum source rock using programmed pyrolysis. **American Association of Petroleum Geologists Bulletin**. 70(3): 318-329.
- Peters, K.E. , Walters, C.C., and Moldowan, J.M. (2005). The Biomarker Guide, Volume 1. **Biomarkers and Isotopes in the Environment and Human History**. Cambridge University Press, New York. 471 p.
- Peters, K.E., and Cassa, M.R. (1994). Applied source rock geochemistry. In: Magoon, L.B., Dow, W.G., (eds.). **The Petroleum System-From Source to Trap**. AAPG Memoir. 60: 93-120.
- Peters, K.E., Magoon, L.B., Bird, K.J., Valin, Z.C., and Keller, M.A. (2006). North Slope, Alaska: Source rock distribution, richness, thermal maturity, and petroleum charge. **AAPG Bulletin**. 90(2): 261-292.
- Piper, D.Z., and Perkins, R.B. (2004). A modern vs. Permian black shale; the hydrography, primary productivity, and water-column chemistry of deposition. **Chem. Geol.** 206: 177-197.
- Pitman, J.K., Price, L.C., and LeFever, J.A. (2001). Diagenesis and fracture development in the Bakken Formation, Williston Basin: Implications for reservoir quality in the middle member. **U.S. Geological Survey Professional Paper**. 1653: 19.
- Piyasin, S. (1995). The hydrocarbon potential of the Khorat Plateau. In: Wannakao, L., (ed.). **Proceedings of the International Conference on Geology, Geotechnology and Mineral Resources of Indochina Conference** (pp. 551-562), Khon Kaen University, Khon Kaen, Thailand.

- Polachan, S., Srikulwong, S., Yuwanasiri, S., and Tungkaew, T. (1980). Geology of the North-Central Thailand. **Onshore Petroleum Exploration Report, no.1**. Mineral Fuels Division, Department of Mineral Resources (in Thai). 102 p.
- Pollastro, R.M. (2003). Geological and production characteristics utilized in assessing the Barnett Shale continuous (unconventional) gas accumulation, Barnett-Paleozoic total petroleum system. **Fort Worth Basin, Texas, Barnett Shale Symposium** (pp. 1-6). November 12-13, 2003, Ellison Miles Geotechnology, Institute of Brookhaven College, Dallas, Texas.
- Pollastro, R.M., Hill, R.J., Ahlbrandt, T.A., Charpentier, R.R., Cook, T.A., Klett, T. R., Henry, M.E., and Schenk, C.J. (2004b). Assessment of undiscovered oil and gas resources of the Bend arch-Fort Worth basin province of north-central Texas and southwestern Oklahoma, 2003. **U.S. Geological Survey Fact Sheet 2004-3022** (pp. 1-2).
- Pollastro, R.M., Hill, R.J., Jarvie, D.M., and Adams, C. (2004a). Geologic and organic geochemical framework of the Barnett-Paleozoic Total Petroleum System, Bend arch-Fort Worth basin, Texas (abs.). **AAPG Annual Meeting Program** (abstract, vol. 13, pp. A113).
- Pollastro, R.M., Hill, R.J., Jarvie, D.M., and Henry, M.E. (2003). Assessing undiscovered resources of the Barnett–Paleozoic total petroleum system. Bend arch-Fort Worth Basin Province, Texas (abs.). **AAPG Southwest Section Convention, Fort Worth, Texas** (pp. 1-18), March 1-5, 2003.

- Potter, J., Richards, B.C., and Goodarzi, F. (1993). The organic petrology and thermal maturity of lower Carboniferous and Upper Devonian source rocks in the Liard basin, at Jackfish Gap-Yohin Ridge and North Beaver River, northern Canada: implications for hydrocarbon exploration. **Energy Sources**. 15: 289-314.
- Prakash Babu, C., Brumsack, H.J., Schnetger, B., and Bottcher, M.E. (2002). Barium as a productivity proxy in continental margin sediments: a study from the eastern Arabian Sea. **Mar. Geol.** 184: 189-206.
- Public Lands Advocacy, (2008). Energy insecurity. **Public Lands Advocacy NEPA-Permitting Seminar/2008 Annual Meeting**. <http://www.publiclandsadvocacy.org/presentations.htm>.
- Racey, A., and Goodall, J.G.S. (2009). Palynology and stratigraphy of the Mesozoic Khorat Group red bed sequences from Thailand. In: Buffetaut, E., Cuny, G., Le Loeuff, J., and Suteethorn, V., (eds.). **Late Palaeozoic and Mesozoic Ecosystems in SE Asia**, Geological Society, London, Special Publications. 315: 67-81.
- Racey, A., Love, M.A., Canham, A.C., Goodall, J.G.S., Polachan, S., and Jones, P.D. (1996). Stratigraphy and reservoir potential of the Mesozoic Khorat Group, NE Thailand, Part I: stratigraphy and sedimentary evolution. **Journal of petroleum Geology**. 18: 5-39.
- Reolid, M., Rodriguez-Tovar, F. J., Marok, A., and Sebane, A. (2012). The Toarcian oceanic anoxic event in the Western Saharan Atlas, Algeria (North African paleomargin): Role of anoxia and productivity. **Geological Society of America Bulletin**. 124(9-10): 1646-1664.

- Ridd, M.F. (2007). A geological traverse across peninsular Thailand. **Journal of the Geological society of Thailand**. 2006-2007: 1-48.
- Ridd, M.F. (2009a). The Phuket Terrane. A Late Palaeozoic rift at the margin of Sibumasu. **Journal of Asian Earth Science**. 36: 238-251.
- Ridd, M.F. (2009b). Geological history of the Sibumasu Block in Peninsular Thailand: Report of a Geologists' Association field meeting in 2007. **Proceedings of the Geologists Association Conference** (vol. 120, pp. 163-174).
- Ridd, M.F., Barber, A.J., and Crow, M.J. (2011). Introduction to the geology of Thailand. In: Ridd, M.F., Barber, A.J., Crow, M.J., (eds.). **The Geology of Thailand**. Geological Society of London. pp. 1-17.
- Rona, P.A. (1988). Hydrothermal mineralization at oceanic ridges. **Canadian Mineralogist**. 26: 431-465.
- Ross, D.J.K., and Bustin, R.M. (2007). Shale gas potential of the Lower Jurassic Gordondale Member, northeastern British Columbia, Canada. **Bulletin of Canadian Petroleum Geology**. 55(1): 51-75.
- Ross, D.J.K., and Bustin, R.M. (2009). The importance of shale composition and pore structure upon gas storage potential of shale gas reservoirs. **Marine and Petroleum Geology**. 26: 916-927.
- Rutsch, H.J., Mangini, A., Bonani, G., Dittrich-Hannen, B., Kubile, P. W., Suter, M., and Segl, M. (1995). ¹⁰Be and Ba concentrations in western African sediments trace productivity in the past. **Earth Planet. Sci. Lett.** 133: 129-143.

- Salam, A., Zaw, K., Meffre, S., McPie, J., Cumming, G., Suphananthi, S., and James, R. (2008a). Stratigraphy and geochemistry of Permian to Triassic Chatree volcanics, Petchabun Province, Central Thailand (abs.). **International Conference on the Tectonic of Northwestern Thailand** (pp. 37-38). 2008, Chiang Mai.
- Salam, A., Zaw, K., Meffre, S., Golding, S., McPie, J., Suphananthi, S., and James, R. (2008b). Mineralisation and oxygen isotope zonation of Chatree epithermal gold-silver deposit, Petchabun Province, Central Thailand. **PACRIM Congress, 2008** (extend abstract, pp. 123-131). November 24-26, 2008, Australian Institute of Mining and Metallurgy, Gold Coast, Australia.
- Sattayarak, N. (1983). Review of the continental Mesozoic stratigraphy of Thailand. In: Nutalaya, P., (ed.). **Proceedings of a workshop on stratigraphic correlation of Thailand and Malasia** (vol. 1, pp. 127-140).
- Sattayarak, N. (1987). Petroleum geological along Lom Sak-Chumpare highway. **The 4th Department of Mineral Resources Conference, Department of Mineral Resources** (in Thai, pp. 276-300), Bangkok, Thailand.
- Sattayarak, N. (2005). Petroleum potential of the Northeast, Thailand. **Proceedings of the international conference on geology, geotechnology and mineral resources of Indochina** (pp. 21-29), Khon Kaen University, Thailand.
- Sattayarak, N., and Polachan, S. (1990). Rocksalt underneath the Khorat Plaeau. **Proceeding of the Department of Mineral Resources Technical Conference** (pp. 1-14), Bangkok, Thailand (in Thai).

- Sattayarak, N., Polachan, S., and Charusiriawad, R. (1991). Cretaceous rock salt in the NE part of Thailand (abs.). **Proceedings of the GEOSEA VII Conference** (pp. 1-36), November 5-8, 1991, Bangkok, Thailand.
- Sattayarak, N., Polachan, S., Assvarittiprom, V., Sitahirun, S., Chaisilboon, B., and Suppitaya, P. (1996). **Field trip guide to sedimentary and petroleum geology marine Permian and non-marine Mesozoic, rim of the Khorat Plateau**. Department of Mineral Resources. Bangkok. 59 p.
- Sattayarak, N., Srikulwong, S., and Pum-In, S. (1989). Petroleum Potential of the Triassic pre-Khorat intermontane basin in Northeastern Thailand. In: Thanasuthipitak, T., (ed.). **Proceedings of the International symposium on Intermontane Basins: Geology and Resources Conference** (pp. 43-58). Chiang Mai, Thailand.
- Sawaki, Y., Nishizawa, M., Suo, T., Komiya, T., Hirata, T., Takahata, N., Sano, Y., Han, J., Kon, Y., and Maruyama, S. (2008). Internal structures and U–Pb ages of zircons from a tuff layer in the Meishucunian formation, Yunnan Province, South China. **Gondwana Research**. 14: 148-158.
- Schieber, J. (1998). Possible indicators of microbial mat deposits in shales and sandstones-examples from the Mid-Proterozoic Belt Supergroup, Montana, USA. **Sedimentary Geology**. 120: 105-124.
- Schieber J, (1999). Microbial mats in terrigenous clastics: the challenge of identification in the rock record. In: Hagadorn J.W, Pflüger F, Bottjer D.J, (eds.). **Unexplored microbial worlds**. Palaios. 14: 3-13.
- Schieber, J., Southard, J.B., and Thaisen, K. (2007). Accretion of mudstone beds from migrating floccule ripples. **Science**. 318: 1760-1763.

- Schmoker, J.W. (1994). Volumetric calculation of hydrocarbons generated. In: Magoon, L.B., and Dow, W.G., (eds.). The petroleum system-from source to trap. **AAPG Memoir**. 60: 323-326.
- Schmoker, J.W. (1995). **Method for assessing continuous-type (unconventional) hydrocarbon accumulations**. In: Gautier, D.L., Dolton, G.L., Takahashi, K.J., and Varnes, K.L., (eds.). **U.S. Geological Survey Digital Data Series**.
- Schmoker, J.W., Quinn, J.C., Crovelli, R.A., Nuccio, V.F., and Hester, T.C. (1996). Production characteristics and resources assessments of the Barnett Shale continuous (unconventional) gas accumulation, Fort Worth basin, Texas. **U.S. Geological Survey Open-File Report OF-96-254** (pp. 1-20).
- Schneebeili-Hermann, E., Hochuli, P.A., Bucher, H., Goudemand, N., Bruhwiler, T., and Galfetti, T. (2012). Palynology of the Lower Triassic succession of Tulong, South Tibet-Evidence for early recovery of gymnosperms. **Journal of Palaeogeology, Palaeoclimatology, Palaeoecology**. 339: 12-24.
- Selly, R.C. (2000) **Applied sedimentology, second edition**. Academic Press. London. England. pp. 523.
- Selley, R.C. (2005). UK shale-gas resources. Petroleum Geology; North-west Europe and Global Perspectives. **Proceedings of the 6th Petroleum Geology Conference**.
- Senftle, J.T., and Landis, C.R. (1991). Vitrinite Reflectance as a Tool to Assess Thermal Maturity. In: Merrill, R.K., (ed.). Source and Migration Processes and Evaluation Techniques. Tulsa. **AAPG Bulletin**. (nd):119-125.

- Shen, J., Algeo, T.J., Hu, Q., Xu, G., Zhou, L., and Feng, Q. (2012). Volcanic perturbations of the marine environment in South China preceding the latest Permian mass extinction and their biotic effects. **Geobiology**. 10: 82-103.
- Slatt, R.M., and O'Brien, N.R. (2011). Pore types in the Barnett and Woodford gas shales: Contribution to understanding gas storage and migration pathways in fine-grained rocks. **AAPG Bulletin**. 95(12): 2017-2030.
- Slatt, R.M., Philp, P.R., O'Brien, N.R., Abousleiman, Y., Singh, P., Eslinger, E.V., Perez, R., Potas, R., Baruch, E.T., Marfurt, K.J., and Madrid-Arroyo, S., (nd). **Submitted to AAPG book on gas shales**. pp. 24.
- Smart, P., and Tovey, N.K. (1982). **Electron Microscopy of Soils and Sediments**. Clarendon Press. Oxford.
- Smith, N., Turner, P., and Williams, G. (2010). UK data and analysis for shale gas prospectivity. In: Vining, B.A., and Pickering, S.C., (eds.). **Petroleum Geology Conference series 2010: Petroleum Geology: From Mature Basins to New Frontiers-Proceedings of the 7th Petroleum Geology Conference** (pp. 1087-1098).
- Sondergeld, C.H., Ambrose, R.J., Rai, C.S., Moncrieff, J. (2010). Microstructural studies of gas shale. **Society of Petroleum Engineers Unconventional Gas Conference** (SPE Paper, vol. 131771, pp. 1-17), February 23-25, 2010, Pittsburgh, Pennsylvania, America.
- Sone, M., and Metacafe, I. (2008). Parallel Tethyan sutures in mainland Southeast Asia: new insights for Palaeo-Tethys closure and implications for the Indosinian orogeny. **Comptes Rendus Geoscience**. 340: 166-179.

- Stacey, J.S., Kramers, J.D. (1975). Approximation of terrestrial lead isotope evolution by a two-stage model. **Earth and Planetary Science Letters**. 26: 207-221.
- Stach, E., Mackowsky, M-Th., Teichmuller, M., Taylor, G.H., Chandra, D. and Teichmuller, R. (1982). **Coal Petrology**. Gebruder Borntraeger, Berlin-Stuttgart. pp. 535.
- Stanley, R.G. (1987). New estimates of displacement along the San Andreas fault in central California based on paleobathymetry and paleogeography. **Geology**. 15: 171-174.
- Stanley, R.G., Valin, Z.C., and Pawlewicz, M.J. (1992). Rock-Eval pyrolysis and vitrinite reflectance results from outcrop samples of the Rincon Shale (lower Miocene) collected at the Tajiguas Landfill, Santa Barbara County, California. **Open-File Report 92-571**. U.S. Geological Survey. pp. 27.
- Steward, D.B. (2007). The Barnett Shale play: Phoenix of the Fort Worth Basin-A history. **The Fort Worth Geological Society and the North Texas Geological Society** (pp. 1-202).
- Suárez-Ruiz, I., Flores, D., Filho, J.G.M., and Hackley, P.C. (2012). Review and update of the applications of organic petrology: Part 1. **International Journal of Coal Geology**. 99 (2012):54-112.
- Suess, E. (1980). Particulate organic carbon flux in the oceans-surface productivity and oxygen utilization. **Nature**. 288: 260-263.
- Swanson, V.E. (1961). Geology and geochemistry of uranium in marine black shales-a review. **U.S. Geol. Surv. Prof. Pap.** 356-C: 67-112.

- Sweeney, J.J., and Burnham, A.K. (1990). Evaluation of a simple model of vitrinite reflectance based on chemical kinetics. **American Association of Petroleum Geologists Bulletin**. 74: 1559-1570.
- Taiming, L., and Shanfan, L. (1990). A Numerical kerogen type index. **Journal of Petroleum Geology**. 13(1): 87-92.
- Taylor, G.H., Teichmuller, M., Davis, A., Diessel, C.F.K., Littke, R., and Robert, P. (1998). **Organic Petrology**. Gebrüder Borntraeger. Berlin. (pp. 704).
- Taylor, S.R., and McLennan, S.M. (1985). **The Continental Crust: Its Composition and Evolution**. Blackwell Scientific Publication, Oxford.
- Teichmüller, M., and Teichmüller, R. (1982). Fundamentals of coal petrology. In: Stach, E., Mackowsky, M-Th., Teichmuller, M., Taylor, G.H., Chandra, D., and Teichmuller, R., (eds.). **Stach's Textbook of Coal Petrology**. Gebruder Borntraeger, Berlin-Stuttgart. pp. 5-86.
- Thyberg, B., Jahren, J., Winje, T., Bjørlykke, K., and Falcide, J.I. (2009). **From mud to shale; Rock stiffening by micro-quartz cementation, First Break**. 27: 53-57.
- Tian, H., Zhang, S.C., Lui, S.B., and Chen, J.P. (2011). Evolution of pores in organic-rich shales during thermal maturation. **AAPG Headberg Conference: Natural gas geochemistry**, May 9-12, 2011, Beijing, China.
- Tian, H., Zhang, S.C., Lui, S.B., and Chen, J.P. (2011). Evolution of pores in organic-rich shales during thermal maturation. **AAPG Headberg Conference: natural gas geochemistry**. May 9-12, 2011, Beijing, China.

- Tissot B., and Espitalié, J. (1975). **L'évaluation thermique de la matière organique des sédiments: application d'une simulation mathématique.** Rev. Inst. Franc. Petr. 30: 743-777.
- Tissot, B., and Welte, D.H. (1978). Petroleum formation and occurrence. **Springer-Verlag.** 538: np.
- Tissot, B., and Welte, D.H. (1984). **Petroleum Formation and Occurrence, 2nd ed.** Springer-Verlag, Heidelberg. pp. 669.
- Tissot, B., Pelet, R., and Ungerer, P.H. (1987). Thermal history of sedimentary basins, maturation indices and kinetics of oil and gas generation. AAPG Bulletin. 71: 1445-1466.
- Tourtelot, H.A. (1979). Black shale-its deposition and diagenesis. **Clays and Clay Minerals.** 27(5): 313-321.
- Trappe, J. (1998). Phanerozoic phosphorite depositional systems. **Lecture Notes in Earth Sciences.** 76: 316.
- Tribovillard, N., Algeo, T.J., Lyons, T., and Riboulleau, A. (2006). Application of trace metals as paleoredox and paleoproductivity proxies: An update. **Chemical Geology.** 232: 12-32.
- Tyson, R.V. (1993). Palynofacies analysis. In: Jenkins, D.G., (ed.). **Applied Micropaleontology.** Kluwer Academic Publishers, Dordrecht, The Netherlands. pp. 153-191.
- Tyson, R.V. (1995). **Sedimentary Organic Matter: Organic Facies and Palynofacies.** Chapman and Hall, London. pp. 615.

- Ueno, K., and Charoentitirat, T. (2011). Carboniferous and Permian. In: Ridd, M.F., Barber, A.J., Crow, M.J., (eds.). **The Geology of Thailand**. Geological Society of London. pp. 71-136.
- Unfiled report (2011). **Total Organic Carbon of the 29 rock samples from Mali**. Rock Eval™.
- Unocal Thailand Ltd., (1990). Khorat area geochemical study outcrop samples. **Report submitted to Department of Mineral Resources**, Thailand.
- Utha-Aroon, C. (1991). Continental origin of the Maha Sarakham evaporatites, NE Thailand. **Proceedings of the GEOSEA VII Conference**, Bangkok, Thailand.
- Vallentyne, J.R. (1962). A chemical study of pyrite spherules isolated from sediments of Little Round Lake, Ontario. In: Jensen, M.L., (ed.). **Biogeochemistry of sulfur isotopes**. New Haven, Connecticut, Yale University, N.S.F. Symposium. pp. 144-152.
- Van Cappellen, P., and Ingall, E.D. (1994). Benthic phosphorus regeneration, net primary production, and ocean anoxia: A model of the coupled marine biogeochemical cycles of carbon and phosphorus. **Palaeoceanography**. 5: 677-692.
- Vandenbroucke, M., Behar, F., and Rudkiewicz, J. L. (1999). Kinetic modelling of petroleum formation and cracking: implications from the high pressure/high temperature Elgin Field (UK, North Sea). **Organic Geochemistry**. 30: 1105-1125.
- Van der Weijden, C.H. (2002). Pitfalls of normalization of marine geochemical data using a common divisor. **Mar. Geol.** 184: 167-187.

- Veblen, D.R., Guthrie, G.D., and Livi, K.J.T. (1990). High resolution transmission electron microscopy and electron diffraction of mixed-layer illite/smectite: Experimental results. **Clay and Clay Minerals**. 38: 1-13.
- Veto, I., Demeny, A., Hertelendi, E. and Hetenyi, M. (1997). Estimation of primary productivity in the Toarcian Tethys-A novel approach based on TOC, reduced sulphur and manganese contents. **Journal of Palaeogeography, Palaeoclimatology, Palaeoecology**. 132: 355-371.
- Walters, C.C. (2006). The origin of petroleum. In: Hsu, C.S., and Robinson, P.R., (eds.). **Practical Advances in Petroleum Processing**. pp 79-101.
- Wang, Z. and Krupnick, A. (2013). A retrospective review of shale gas development in the United States: What led to the boom?. **Resources for the Future**, Washington, DC. 39 p.
- Waples, D.W. (1985). *Geochemistry in petroleum exploration*: Boston, International Human Resources Development Corporation. 232 p.
- Waples, D.W., and Marzi, R.W. (1998). The universality of the relationship between vitrinite reflectance and transformation ratio. **Organic Geochemistry**. 28(6): 383-388.
- Wehrly, B., and Stumm, W. (1989). Vanadyl in natural waters: Adsorption and hydrolysis promote oxygenation. **Geochimical et Cosmochimica Acta**, 53: 69-77.
- Wongprayoon, T., and Sangsrichan, W. (2008). **Geological Report (in Thai)**. Department of Mineral Resources. 121 p. <http://khonkaengeopark.com/index.php>.

Yamamoto, K. (1987). Geochemical characteristics and depositional environments of cherts and associated rocks in the Franciscan and Shimanto terranes. **Sedimentary Geology**. 52: 65-108.

Yarincik, K.M., Murray, R.W., and Peterson, L.C. (2000). Climatically sensitive eolian and hemipelagic deposition in the Cariaco Basin, Venezuela, over the past 578,000 years: Results from Al/Ti and K/Al. **Paleoceanography**. 15: 210-228.

Zaw, K., Rodmanee, T., Khositqnot, S., and Ruamkid, S. (2008). Mineralogy and genesis of Phu Thap Fah gold skarn deposit, Northeast Thailand: Implications for reduced gold skarn formation. **International Geological Congress (IGC)**. Norway, August, 2008.

http://www.dmf.go.th/dmfweb/index.php?option=com_content&view=article&id=184&Itemid=11&lang=th

